

Portland State University

PDXScholar

Dissertations and Theses

Dissertations and Theses

2-9-2009

Synthesis of Aptamer-Porphyrin Conjugate for Photodynamic Therapy & Synthesis and stability of mixed thiol/lipid coated Gold Nanoparticles

Sarita Sitaula

Portland State University

Follow this and additional works at: https://pdxscholar.library.pdx.edu/open_access_etds

 Part of the [Chemistry Commons](#)

Let us know how access to this document benefits you.

Recommended Citation

Sitaula, Sarita, "Synthesis of Aptamer-Porphyrin Conjugate for Photodynamic Therapy & Synthesis and stability of mixed thiol/lipid coated Gold Nanoparticles" (2009). *Dissertations and Theses*. Paper 6132.

This Dissertation is brought to you for free and open access. It has been accepted for inclusion in Dissertations and Theses by an authorized administrator of PDXScholar. Please contact us if we can make this document more accessible: pdxscholar@pdx.edu.

SYNTHESIS OF APTAMER-PORPHYRIN CONJUGATE FOR PHOTODYNAMIC
THERAPY
&
SYNTHESIS AND STABILITY OF MIXED THIOL/LIPID COATED GOLD
NANOPARTICLES

by
SARITA SITLAULA

A dissertation submitted in partial fulfillment of the
requirements for the degree of

DOCTOR OF PHILOSOPHY
in
CHEMISTRY

Portland State University
2009

DISSERTATION APPROVAL

The abstract and dissertation of Sarita Sitaula for the Doctor of Philosophy in Chemistry were presented February 9, 2009, and accepted by the dissertation committee and the doctoral program.

COMMITTEE APPROVALS:



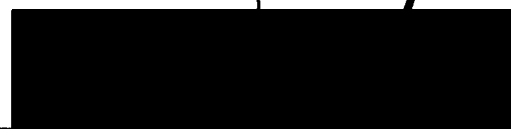
Scott M. Reed, Chair



Carl C. Wamser



Niles Lehman



Andres La Rosa



John Rueter
Representative of the Office of Graduate Studies

DOCTORAL PROGRAM APPROVAL:



Kevin A. Reynolds, Director
Chemistry Ph.D. Program

ABSTRACT

An abstract of the dissertation of Sarita Sitaula for the Doctor of Philosophy in Chemistry presented February 9, 2009.

Title: Synthesis of Aptamer-Porphyrin Conjugate for Photodynamic Therapy & Synthesis and Stability of Mixed Thiol/Lipid Coated Gold Nanoparticles

An underlying problem in Photodynamic Therapy (PDT) is low selectivity of photosensitizers currently being used for the treatment of tumors. This thesis is focused on developing new PDT drugs and is divided into two parts. The first chapter describes a method for selective delivery of the photosensitizers to the tumor site by conjugating porphyrins to an aptamer for the targeted PDT. To achieve this, a novel synthesis of 2'-porphyrin-modified uridine was developed. The 3'-H-phosphonate derivatives of both 2'-porphyrin and 2'-dithiaporphyrin modified uridine were also synthesized. The 3'-H-phosphonate derivative of 2'-porphyrin-modified uridine was conjugated to a 19-mer DNA and to a 31-mer aptamer that binds to under-glycosylated mucin 1 (uMUC1) glycoprotein, a well known tumor marker. The uMUC1 aptamer-porphyrin conjugate has potential applications for various tumor-targeted PDT. Potential applications of internally modified 2'-porphyrin 3'-H-phosphonate could be in the synthesis of various other aptamer-porphyrin conjugates or in creating porphyrin arrays on DNA scaffold by using automated solid phase synthesis.

The second part of the thesis describes the functionalization of gold nanoparticles with phospholipids. The idea behind this effort is to pave the way for future applications for the functionalization of bilayer gold nanoparticles with aptamer-porphyrin conjugates that could play dual roles for selective delivery of drugs and PDT. Both natural and synthetic phospholipids were used to synthesize gold nanoparticles coated with various types of phospholipid bilayers. Bilayer gold nanoparticles were converted to hybrid bilayer gold nanoparticles by partial thiol exchange. TEM image analysis showed only small changes in size by varying phospholipids in hybrid bilayer gold nanoparticles. The stabilities of bilayer and hybrid bilayer gold nanoparticles were tested with potassium cyanide and iodine. Results showed that the stability of various types of phospholipid-coated bilayer gold nanoparticles can be tuned by using partial alkanethiol exchange. Stable gold nanoparticles were obtained by exchanging hydrophobic alkanethiol for various types of phospholipid-coated bilayers gold nanoparticles, which forms a submonolayer on the gold surface with a gold: 1-decanethiol ratio of 21:1. The stable hybrid bilayer gold nanoparticles could find applications in micropatterning and formation of solid supported lipid bilayers for biosensor design.

ACKNOWLEDGEMENTS

I am very thankful for the privilege to work on my graduate studies at Portland State University. During the time, I have gotten to know many people and I am truly indebted to the people who have helped me get this far along. I would like to express my sincere gratitude to the individuals who accompanied me in this adventure. I am grateful to my research advisor Dr. Scott M. Reed for his guidance, support and effort to make me successful in research. I would like to express my sincere thanks to committee member Professor Carl C. Wamser for his encouragement, help, and support. Furthermore, I am very thankful to Professor Andres La Rosa, Department of Physics, Portland State University; Professor Niles Lehman, Department of Chemistry, Portland State University; and Professor John Rueter, Department of Environmental Science, Portland State University, for their enthusiasm, comments and useful suggestions in dissertation in spite of their busy schedule. My special thanks goes to my former research advisor Professor Kyung il Choi from the Korean Institute of Science and Technology (KIST) for his guidance and continuous support during my year at KIST and for letting me fly to the USA to join this program without any restrictions. I am grateful to my former research advisor Professor Sarbanja M. Tuladhar (RECAST, Kirtipur, Nepal) for encouraging education abroad.

I would like to thank Professor Albert S. Benight, Department of Chemistry, Portland State University and his group specially Fidelis Manyanga for letting me use their lab to get electrophoresis and helping me with my research. My thanks go to

Professor David Peyton for helping me with the NMR instrument. I am grateful to Jeff More (OSU) for mass spectrometry. I really appreciate Dr. Andrea DeBarber and Jenny Luo (OHSU) for their help in mass spectrometry. I should also not forget to thank Dr. Aoife O' Brine for training me to use DNA synthesizer and HPLC, and Dr. Marilyn R. Mackiewicz for her help with the TEM instrument. I also want to thank the PSU Writing Center and its staff for helping me with English language.

A special thank goes to Professor Dirk Iwata-Reuyl, Department of Chemistry, Portland State University for his kind suggestions and for helping me in the beginning. A special word of thanks goes to my labmates Whacko (Benjamin R. Ayers) and Paul J. Rencit for their help and for keeping my spirits high whenever I felt stressed in the lab. My thanks go to My-Trinh Do for always caring me.

I would like to thank Papa (Dick Cordell) for his love of international students and for introducing me to many beautiful places in Portland. I am grateful to Claire and Russ, Cathy Varis, Andy Peloquin, and Greg Steward from FOCUS group for praying for my success and for their friendship and letting me join them for outdoor activities. Thanks to Dr. Vern Bissel for encouraging me and praying for my success. Many people that I came to know from FOCUS group really helped feel at home at a foreign land. I would like to thank them all as well.

I am grateful to Dennis B. Plies (Professor of music, Warner Pacific College) and Barbara Plies and their family for their support, encouragement and for

introducing me to many friends, and for making my stay comfortable at their home when I first arrived in Portland. I miss book reading every Sunday at their home.

I would like to thank Andy Nelson and Carol Nelson (Corvallis) for their invitations over Christmas, Thanksgiving break, and other occasions, along with providing me with constant encouragement.

My thanks goes to my friends Nazeen Ahmad (Assistant Professor of Economic, Weber State University, UTAH), Suman Parajuli (Chemistry Department, University of Southern Mississippi Eastern), Santosh K. Mahato (Chemistry Department, Wayne State University), Sujit Suwal (Chemistry Department, Wayne State University), Sunil Hamal (Chemistry Department, University of Reno), Basant Giri (Chemistry Department, Oregon State University), Babita Thapa and Dr. Sabita Thapa for their love, support and encouragement. Moreover, I would like to thank my former roommates Tang Lan (China), Junhong (China) for always taking care of me and Dr. Rosalina S. Topalova (Department of Botany, Sofia, Bulgaria) for encouraging me and for helping me during deteriorating situations when I was frustrated. My thanks go to my uncle Dr. Prem Lohani and my aunt Shyama Lohani and Bijaya Lohani for their continuous support and care.

Lastly, I would like to mention my family members who have been a source of constant inspiration. I would not have completed my degree without their continuous support. I would like to thank my mother Sita D. Sitaula for always being there for me, trusting what I was doing, always smiling when I talked to her and making me relaxed

when I was stressed out. Thanks to my elder brother Madhab Sitaula for supporting, encouraging, and teaching me values of hard work. My sister Geeta Sitaula is a great inspiration and I thank her for making me laugh during tough times.

Thanks to my sister in-laws Anju Sitaula and Sarita Sitaula (we share the same name) and brothers Saroj Thapaliya and Yadav Sitaula for encouraging me while I was disappointed. Many, many thanks to my younger brother Sunil Sitaula for his continuous encouragement, suggestions, financial support, and for sharing all my pain throughout my time in the US. Thanks for “If” by Rudyard Kipling; it was of great help. I want to also thank my nieces and nephews Ashima Sitaula, Nishima Sitaula, Gimasis Tripathee and Anima Sitaula for making me laugh with all their comments every time I talked to them. Thanks everyone. I really appreciate your help.

TABLE OF CONTENTS

	Page
Acknowledgements.....	i
List of Figures.....	x
List of Schemes.....	xvii
List of Tables.....	xviii
List of Abbreviations and Symbols.....	xix
CHAPTER 1 SYNTHESIS OF APTAMER-PORPHYRIN CONJUGATE FOR PHOTODYNAMIC THERAPY	
1.1 INTRODUCTION.....	1
1.1.1 Porphyrin.....	1
1.1.2 Construction of Porphyrin Array.....	2
1.1.3 Photosensitizers.....	7
1.1.3.1 Second Generation Photosensitizers.....	9
1.1.3.2 Antibodies-Photosensitizers.....	11
1.1.4 Aptamers	14
1.1.4.1 Aptamer Conjugated to Photosensitizers.....	16
1.1.5 Approaches to Automated Synthesis of DNA.....	17
1.1.5.1 Phosphoramidite Approach.....	18
1.1.5.2 H-phosphonate Approach.....	24
1.1.6 Oligonucleotide-Porphyrin Conjugates.....	29
1.1.7 Terminal Modification.....	29
1.1.8 Internal Modification.....	30
1.1.9 Cancer Target Mucin 1 Glycoprotein (MUC1).....	36

	Page
1.2 GOALS AND OBJECTIVES OF THESIS (PART 1).....	39
1.3 EXPERIMENTAL.....	41
1.3.1 General Synthetic Methods.....	41
1.3.1.1 Chemicals.....	41
1.3.1.2 Instrument.....	42
1.3.2 Synthesis of Monocarboxy Porphyrin.....	43
1.3.3 Aminouridine Porphyrin Coupling Reactions.....	45
1.3.4 Synthesis of 3' H-phosphonate Salt of Internally Porphyrin-Modified Uridine.....	48
1.3.5 Synthesis of Porphyrin-uMUC1 Aptamer Conjugate (24).....	49
1.3.5.1 Precipitation of uMUC1 Aptamer-Porphyrin Conjugate (24).....	51
1.3.5.2 Gel Analysis of Porphyrin-uMUC1 Aptamer Conjugate (24).....	51
1.4 RESULTS AND DISCUSSION.....	53
1.4.1 Synthesis of Photosensitizer-Nucleotide Monomers.....	53
1.4.1.1 2'-Amino-2'-doxyuridine (5'-Hydroxyl Protected with DMT)	56
1.4.1.2 2'-Porphyrin-modified Uridine.....	56
1.4.1.3 2'-Dithiaporphyrin-modified Uridine.....	57
1.4.1.4 2'-Pyropheophorbide a-modified Uridine.....	60
1.4.2 Synthesis of Photosensitizer-Nucleic Acid Conjugates.....	62

	Page
1.4.2.1 Phosphoramidite Chemistry.....	62
1.4.2.2 3' H-phosphonate Chemistry.....	65
1.4.3 Benefits of Internal Modification Approach.....	70
1.4.4 Porphyrin-uMUC1 Aptamer Conjugate.....	71
1.4.4.1 Applications of uMUC1 Aptamer-Porphyrin Conjugate.....	77
1.5 CONCLUSIONS.....	79
1.6 FUTURE DIRECTIONS.....	80
1.7 REFERENCES.....	81
CHAPTER 2 SYNTHESIS AND STABILITY OF MIXED THIOL/LIPID COATED GOLD NANOPARTICLES	
2.1 INTRODUCTION.....	100
2.1.1 Metal Nanoparticles.....	100
2.1.1.1 Optical Properties of Metal Nanoparticle.....	101
2.1.2 Gold Nanoparticles.....	106
2.1.2.1 Bilayer Gold Nanoparticles.....	109
2.1.3 Phospholipids.....	111
2.1.3.1 Lipid Curvature.....	114
2.1.3.2 Application of Phospholipid-Coated Gold Nanoparticles in Formation of Solid Supported Lipid Bilayers.....	118
2.1.4 Stability of Gold Nanoparticles in Potassium Cyanide.....	121

	Page
2.1.5 Stability of Gold Nanoparticles in Iodine.....	123
2.2 GOALS AND OBJECTIVES OF THESIS (PART 2).....	125
2.3 EXPERIMENTAL.....	127
2.3.1 Materials and Methods.....	127
2.3.2 Transmission Electron Microscopy (TEM).....	128
2.3.3 General Procedures.....	128
2.3.3.1 Preparation of Liposome.....	128
2.3.3.2 Synthesis of Various Types of Phospholipid-Coated Bilayer Gold Nanoparticle.....	129
2.3.3.3 General Procedure for Synthesis of Hybrid Bilayer Gold Nanoparticles.....	130
2.3.3.4 General Procedure for Stability Tests of Bilayer and Hybrid Bilayer Gold Nanoparticles in KCN.....	130
2.3.3.5 General Procedure for Iodine Stability Tests of Bilayer and Hybrid Bilayer Gold Nanoparticles.....	130
2.4 RESULTS AND DISCUSSION.....	132
2.4.1 Phospholipid-Coated Bilayer Gold Nanoparticles.....	132
2.4.2 TEM Images of POPC and Soy PC-Coated Bilayer Gold Nanoparticles.....	143
2.4.3 Hybrid Bilayer Gold Nanoparticles.....	147
2.4.3.1 TEM Images of Various Types of Phospholipid- Coated Hybrid Bilayer Gold Nanoparticles.....	149
2.4.3.2 Estimation of Thiol in Hybrid Bilayer Gold Nanoparticles.....	161

	Page
2.4.4 Stability of Hybrid Bilayer Gold Nanoparticles in KCN.....	163
2.4.4.1 Stability of Different Acyl Chain Phospholipid-Coated Hybrid Bilayer Gold Nanoparticles in KCN....	163
2.4.4.2 Stability of Different Headgroups in Phospholipid-Coated Hybrid Bilayer Gold Nanoparticles in KCN....	169
2.4.5 Iodine Stability Tests of Various Types of Hybrid Bilayer Gold Nanoparticles	175
2.4.5.1 Stability of Different Acyl Chain Phospholipid-Coated Gold Nanoparticles in Iodine.....	175
2.4.5.2 Stability of Different Headgroups in Phospholipid-Coated Gold Nanoparticles in Iodine.....	180
2.5 CONCLUSIONS.....	186
2.6 FUTURE DIRECTIONS.....	188
2.7 REFERENCES.....	189
TERMINAL REFERENCES.....	200
APPENDICES (CHAPTER 1).....	230
Appendix A: Synthesis of Mono-carboxy Dithia Core-modified Porphyrin (18).....	230
Appendix B: Synthesis of 2'-Amino-2'-deoxyuridine (21).	238
Appendix C: Recepte for 16% Polyacrylamide Gel (25 mL).....	241

LIST OF FIGURES

Figures	Page	
1.1	Porphyrin arrays. (A) A linear porphyrin array, ²⁹ (B) porphyrin array on a growing DNA scaffold. CPG stands for Control Pore Glass	6
1.2	Role of photosensitizers in singlet oxygen production. S_0 = ground state of photosensitizers, A = absorption of light of specific wavelength, S_1 = excited state of photosensitizers, E = emission, K_{isc} = intersystem crossing, T_1 = triplet state of photosensitizers.....	7
1.3	Haematoporphyrin derivative II (Photofrin).....	8
1.4	Second generation photosensitizers. (A) Mono-L-aspartyl chlorine e6, (B) protoporphyrin IX, (C) benzoporphyrin derivatives, (D) m-tetrahydroxyphenylchlorine (m-THPC), (E) bis aminosilicon (IV) phthalocyanine (BAM-SiPC), and (F) dithiaporphyrin	10
1.5	Schematic diagram showing antibody-photosensitizer conjugate. Orange ovals are photosensitizers (e.g., BPD) attached to the antibody (7 BPD/Ab>1).....	13
1.6	Starting base in DNA synthesis attached to the solid support (CPG) by long spacer and 5'-hydroxyl protected with DMT. Base1 could be Adenine, Guanine, Cytosine, and Thymine. Amines protected with benzoyl or isobutyryl group.....	18
1.7	Schematic diagram of removal of DMT by TCA. Right side of arrow shows free trityl cation and free 5'-hydroxyl nucleoside	20
1.8	Activation of phosphoramidite nucleoside by tetrazole and coupling of activated phosphoramidite to growing oligonucleotide attached to a solid support.....	21

Figures	Page
1.9 Capping of failure base in DNA synthesis with acetic anhydride.....	22
1.10 Oxidation of phosphorus (III) to the phosphorus (V) in DNA synthesis.....	22
1.11 Automated DNA synthesis cycle using phosphoramidite method.....	23
1.12 Commercially available monomers of H-phosphonate. Bu = isobutyryl and Bz = benzoyl protecting groups.....	25
1.13 DNA synthesis cycle using H-phosphonate method.....	27
1.14 Porphyrin-modified DNA. (A) 5'-terminal porphyrin-modified DNA, (B) internally 2'-porphyrin-modified DNA, X = NH or S.	35
1.15 MUC1 showing 20 amino acid sequences. Green and orange are tandem repeats in MUC1. Orange is the most immunogenic sequence within the tandem repeats. ¹⁹⁷	37
1.16 UV-vis of 2'-photosensitizers-modified uridine in CH ₂ Cl ₂ , a – 2'-pyropheophorbide-a, b – 2'-porphyrin, c – 2'-dithiaporphyrin.....	61
1.17 ³¹ P NMR spectra of compound 8 (162 MHz, CDCl ₃). Proton decoupled (black), and ³¹ P and proton coupled (pink).....	68
1.18 UV-vis spectrum of uMUC1 aptamer-porphyrin conjugate 24 in NH ₄ OH, porphyrin Soret band absorption at λ _{max} 421 nm.....	75
1.19 (A) Polyacrylamide gel of the uMUC1 aptamer-porphyrin conjugate after scanned in HP Photo Scanner. Lane 1 – ladder DNA and Lane 2 – uMUC1 aptamer (fast moving band) and uMUC1 aptamer-porphyrin conjugate (slower moving band). (B) Fluorescence emission spectrum of gel (lane 2 – slower moving band)excitation at 410 nm and emission at 648 nm.....	77

Figures	Page
2.1 A scheme showing dipole oscillations of electrons in nanoparticles surface. (A) An electric field of an incoming light, (B) polarization of electrons and creation of the ionic and electronic clusters ²³	102
2.2 Size dependent surface plasmon resonance of gold nanoparticles ³⁵	104
2.3 Schematic diagram of gold nanoparticles. (A) Thiol functionalized, (B) Polymer-coated, and (C) TOAB-coated	108
2.4 A bilayer assembly of phospholipids in water. (A) A typical phospholipid, (B) liposome.....	111
2.5 Lipid curvature (cartoon). ⁹⁰ (A) Positive, (B) zero, and (C) negative....	116
2.6 Formation of solid-supported lipid bilayer. (A) Deposition of the liposome on solid support, (B) rearrangement of liposome to form bilayer on solid support ¹⁰⁰	120
2.7 Structures of phospholipids with different chain lengths and degrees of saturation. (A) Soy PC, (B) POPC, (C) HyPC, and (D) DLPC.....	134
2.8 Structures of phospholipids with different headgroups. (A) PG, (B) sphingomyelin, (C) PS, and (D) DPPE	135
2.9 UV-vis spectra of bilayer gold nanoparticles in water (normalized) (A) Different in tail lipid stabilized bilayer AuNPs. Green – DLPC, red – HyPC, purple – POPC and blue – Soy PC. (B) Different head groups stabilized bilayer AuNPs. Maroon – sphingomyelin, blue – PS, and green – PG.....	141
2.10 (A) TEM images of the Soy PC-coated bilayer gold nanoparticles without TG. Scale bar = 20 nm. (B) Histogram for size distribution of 98 particles of Soy PC-coated bilayer gold nanoparticles (bin size = 2 nm).....	144
2.11 (A) TEM images of 1% TG added Soy PC-coated bilayer gold nanoparticles after partial 1-decanethiol exchange (hybrid bilayer AuNPs). Scale bar = 20 nm. (B) The histogram for size distribution of 101 particles of Soy PC-coated bilayer nanoparticles (bin size = 2 nm).....	145

Figures	Page
2.12 (A) TEM of POPC-coated bilayer gold nanoparticles. Scale bar = 20 nm. (B) Histogram for size distribution of 100 particles (bin size = 2 nm).....	147
2.13 (A) TEM images of PG-coated hybrid bilayer gold nanoparticles. Scale bar = 20 nm. (B) Histogram for size distribution of 106 particles (bin size = 2 nm).....	150
2.14 (A) TEM images of PS-coated hybrid bilayer gold nanoparticles. Scale bar = 20 nm. (B) Histogram for size distribution of 114 particles (bin size = 2 nm).....	151
2.15 (A) TEM images of sphingomyelin-coated hybrid bilayer gold nanoparticles. Scale bar = 20 nm (left image) and scale bar = 0.2 μ m (right image). (B) Histogram for size distribution of 109 particles (bin size = 2 nm).....	152
2.16 (A) TEM images of POPC-coated hybrid bilayer gold nanoparticles. Scale bar = 20 nm. (B) Histogram for size distribution of 71 POPC-coated hybrid bilayer gold nanoparticles (bin size = 2 nm).....	154
2.17 (A) DLPC-coated triangle shaped hybrid gold nanoparticles seen in a few fields of the grid. Scale bar = 20 nm. (B) TEM images of DLPC-coated hybrid bilayer gold nanoparticles. Scale bar = 20 nm (left image) and scale bar = 0.2 μ m (right image). (C) Histogram for size distribution of 107 hybrid bilayer gold nanoparticles (bin size = 2 nm).....	156
2.18 (A) TEM images of HyPC-coated hybrid bilayer AuNP. Scale bar = 20 nm. (B) Histogram for size distribution of 107 hybrid bilayer nanoparticles (bin size = 2 nm).....	158
2.19 TEM images of DPPE-coated hybrid bilayer gold nanoparticles. Scale bar = 20 nm. Left image (showing aggregation of particles), right image (both aggregated and free spherical nanoparticles).....	159

Figures	Page
2.20 UV-vis “absorbance vs. time” experiments for 20 nmol 1-decanethiol exchanged hybrid bilayer gold nanoparticles for one hour in KCN (6 mM final concentration. (A) POPC-coated hybrid bilayer nanoparticles (blue), POPC-coated bilayer nanoparticles (orange); (B) HyPC-coated hybrid bilayer nanoparticles (blue) (KCN added after 5 min data collection in UV-vis), HyPC-coated bilayer nanoparticles (orange); (C) DLPC-coated hybrid bilayer nanoparticles (blue), DLPC-coated bilayer nanoparticles (orange); (D) Soy PC-coated hybrid bilayer (blue), Soy PC-coated bilayer nanoparticles (orange).....	164
2.21 UV-vis “absorbance vs. time” experiments (normalized) of different acyl chain phospholipid-coated hybrid bilayer gold nanoparticles for one hour in KCN (final concentration 6 mM); (A) 5 nmol thiol exchanged bilayer gold nanoparticles. POPC-coated hybrid bilayer nanoparticles (purple), DLPC-coated hybrid bilayer nanoparticles (green), HyPC-coated hybrid bilayer nanoparticle (red), Soy PC-coated hybrid bilayer nanoparticles (blue); (B) 1 nmol thiol changed hybrid bilayer nanoparticles. HyPC-coated hybrid bilayer nanoparticles (purple), Soy PC-coated hybrid bilayer nanoparticles (blue), DLPC-coated hybrid bilayer nanoparticles (red), POPC-coated hybrid bilayer nanoparticles (green).....	166
2.22 UV-vis “absorbance vs. time” experiments of different headgroups in phospholipid-coated gold nanoparticles for one hour in KCN final concentration (6 mM). Hybrid bilayer nanoparticles formed by exchange of 20 nmol 1-decanethiol in nanoparticle solution of an optical density 1.2. (A) PS-coated hybrid bilayer nanoparticles (blue), PG-coated bilayer nanoparticles (red); (B) PG-coated bilayer nanoparticles (blue), PG-coated hybrid bilayer nanoparticles (red); (C) sphingomyelin-coated bilayer nanoparticles (blue), sphingomyelin-coated hybrid bilayer (red).....	169

Figures	Page	
2.23	UV-vis “absorbance vs. time” graphs (normalized) of different headgroups in phospholipid-coated hybrid bilayer gold nanoparticles at final concentration of KCN (6 mM) for one hour. (A) Hybrid bilayer nanoparticles formed after 5 nmol 1-decanethiol exchanged for bilayer nanoparticle solutions of an optical density 1.2; sphingomyelin-coated hybrid bilayer nanoparticles (blue), PS-coated hybrid bilayer nanoparticles (red), PG-coated hybrid bilayer nanoparticles (green). (B) Hybrid bilayer nanoparticles formed after 1 nmol 1-decanethiol exchange for bilayer nanoparticles solution of an optical density 1.2. Sphingomyelin-coated hybrid bilayer nanoparticles (blue), PS-coated hybrid bilayer nanoparticles (red), PG-coated hybrid bilayer nanoparticles (green).....	171
2.24	UV-vis of Soy PC-coated hybrid bilayer gold nanoparticles before and after iodine final concentration 1 μ M. a – Soy PC-coated hybrid bilayer before iodine, b – scattering of Soy PC-coated hybrid bilayer AuNP 4 min in iodine, c – Soy PC-coated hybrid bilayer gold nanoparticles one hour in iodine.....	176
2.25	(A) TEM images of Soy PC-coated hybrid bilayer nanoparticles with iodine (1 μ M final concentration). Scale bar = 20 nm. (B) Histogram of 101 nanoparticles in iodine (bin size = 2 nm).....	177
2.26	Stability of different acyl chain phospholipid-coated hybrid bilayer gold nanoparticles at 1 μ M final concentration of iodine for one hour. HyPC-coated hybrid bilayer nanoparticles (blue), HyPC-coated bilayer nanoparticles (red); (B) DLPC-coated hybrid bilayer nanoparticles (red), DLPC-coated bilayer nanoparticles (blue); (C) POPC-coated hybrid bilayer nanoparticles (red), POPC-coated bilayer nanoparticles (blue); (D) Soy PC-coated hybrid bilayer nanoparticles (blue), Soy PC-coated bilayer nanoparticles (red).....	178
2.27	UV-vis spectra of hybrid bilayer gold nanoparticles. a – before iodine, b – 2 min in iodine, c – one hour in iodine. (A) DLPC-coated hybrid bilayer gold nanoparticles, (B) HyPC-coated hybrid bilayer gold nanoparticles.....	180

Figures	Page
2.28 UV-vis time experiments. “Absorbance vs. time” graph of different headgroups in phospholipid-coated bilayer and hybrid bilayer gold nanoparticles at 1 μ M final concentration of iodine. (A) PG-coated bilayer gold nanoparticles (blue), PG-coated hybrid bilayer nanoparticles (red); (B) PS-coated hybrid bilayer nanoparticles (red), PS-coated bilayer nanoparticles (blue); (C) sphingomyelin-coated hybrid bilayer nanoparticles (red), sphingomyelin-coated bilayer nanoparticles (blue).....	181
2.29 UV-vis spectra of different headgroups in phospholipid-coated hybrid bilayer gold nanoparticles formed at 20 nmol thiol exchange. a – before iodine, b – 2 min in iodine final concentration 1 μ M, c – one hour in iodine final concentration 1 μ M; (A) PG-coated hybrid nanoparticles, (B) PS-coated hybrid nanoparticles, and (C) sphingomyelin-coated hybrid nanoparticles.....	183

LIST OF SCHEMES

Schemes	Page
1.1 Synthesis of mono acid functionalized porphyrin. i) Microwave 10 min, ii) KI/K ₂ CO ₃ , iii) DMF/CH ₂ Cl ₂ , iv) ClCH ₂ COOC ₂ H ₅ , v) 10% KOH (1:1 Ethanol/water), 16 h reflux	55
1.2 Synthesis of 2'-porphyrin-modified uridine. i) EDCI/DMAP, CH ₂ Cl ₂ /12 h at room temperature.....	57
1.3 Synthesis of 2'-dithiaporphyrin-modified uridine. i) EDCI/DMAP, CH ₂ Cl ₂ /12 h at room temperature	59
1.4 Synthesis of 2'-pyropheophorbide-a modified uridine. i) EDCI/DMAP, CH ₂ Cl ₂ /12 h at room temperature.....	60
1.5 Solid phase synthesis of porphyrin-DNA conjugates by using 3'-phosphoramidite of 2'-porphyrin-modified uridine. i) DIPEA/EtOAc , ii) ETT/Tetrazole, iii) CPG-3'GAAGGGCCCTTG-OH 5', and iv) I ₂ /pyridine/H ₂ O (trace), v) 30% NH ₄ OH 12 h at 4 °C.....	64
1.6 Synthesis of 3' H- phosphonate of 2'-porphyrin-modified uridine. i) Pyridine/30 min at room temperature, ii) Et ₃ N/H ₂ O (1:1), iii) 20 min at room temperature, X = NH (7), X = S (8).....	67
1.7 Synthesis of porphyrin-uMUC1 aptamer conjugates. i) Pyridine/acetonitrile (1:1), ii) 1-adamantane carboxylic acid chloride, iii) CPG attached uMUC1 aptamer, iv) I ₂ in pyridine/water (trace), v) 30% NH ₄ OH.....	74
2.1 Systematic scheme of bilayer gold nanoparticles synthesis. (A) Liposome, i) HAuCl ₄ in H ₂ O, ii) Sodium citrate in H ₂ O (5 equiv), (B) bilayer gold nanoparticles.....	138
2.2 Synthesis of hybrid bilayer gold nanoparticles. (A) Phospholipid-coated bilayer gold nanoparticles, (B) hybrid bilayer gold nanoparticles.....	148

LIST OF TABLES

Tables		Page
2.1	Self assemble structures for different head and acyl chain of lipids ⁷⁹	113
2.2	Phospholipids with different headgroups and acyl chain lengths.....	137
2.3	λ_{\max} of various types of phospholipid-coated bilayer AuNPs with TG (1 mol % of phospholipid).....	142
2.4	Average size and λ_{\max} of various types of phospholipid-coated hybrid bilayer AuNPs.....	160
2.5	Comparative stability of various types of hybrid bilayer AuNPs at different concentrations of 1-decanethiol exchange in solution of bilayer AuNPs of an optical density 1.2 in KCN final concentration 6 mM.....	173
2.6	Stability of various types of phospholipid-coated bilayer AuNPs and hybrid bilayer AuNPs one hour in iodine final concentration 1 μ M at their λ_{\max} . Hybrid bilayer AuNPs of an optical density 1.2 was formed after 20 nmol 1-decanethiol exchange.....	184

LIST OF ABBREVIATIONS/SYMBOLS

A, T, G, C	Adenine, Guanine, Thymine and Cytosine
A, P, D, T, R, V, G, H, S	Alanine, Proline, Aspartic acid, Threonine, Arginine, Valine, Glycine, Histidine, Serine
BPD	Benzoporphyrin derivative
BAM-SiPc	Bis-amino silicon (IV) phthalocyanine
CCD	Charge Coupled Detector
CPG	Control Pore Glass
DCA	Dichloroacetic acid
DMF	<i>N,N</i> -Dimethylformamide
DNA	Deoxyribonucleic acid
DLPC	1,2-Dilauroyl- <i>sn</i> -glycero-3-phosphocholine
DPPE	1,2-Dipalmitoyl- <i>sn</i> -glycero-3-phosphoethanolamine
DMAP	4-(Dimethylamino)pyridine
DMT	4, 4' Dimethoxy trityl
DIPEA	<i>N, N'</i> -diisopropylethylamine
EDCI	1-Ethyl-3-(3-dimethylaminopropyl) carbodiimide) hydrochloride
EDTA	Ethylenediaminetetraacetic acid
equiv	Equivalent(s)
ETT	5-(Ethylthio)-1 <i>H</i> -tetrazole

FDA	US Food and Drug Administration
FRET	Förster Resonance Energy Transfer
HepG2	Hepatocyte Growth Factor 2
HyPC	L- α -phosphatidylcholine, hydrogenated
HER3	Human Epidermal Growth Factor Receptor 3
HPLC	High Performance Liquid Chromatography
kDa	Kilo dalton
mer	Nucleotide units in RNA or DNA
m	Multiplet
mL	Mililitre(s)
mmol	Milimole(s)
MHz	Megahertz (unit of frequency)
mM	Milimolar
m-THPC	<i>meta</i> Tetrahydroxyphenyl chlorine
NMR	Nuclear Magnetic Resonance
nmol	nanomole(s)
nm	Nanometer(s)
n	Total number of particles
PDGF	Platelet Derived Growth Factor
PDT	Photodynamic therapy
PC	Phosphatidylcholine

PG	L- α -phosphatidyl-DL-glycerol or Phosphatidylglycerol
PE	Phosphatidylethanolamine
PS	1,2-diacyl- <i>sn</i> -glycero-phospho-L-serine or Phosphatidylserine
PSMA	Prostate Specific Membrane Antigen
POPC	1-Palmitoyl-2-Oleoyl- <i>sn</i> -Glycero-3-phosphocholine
rpm	Rotations per minute
RNA	Ribonucleic acid
SELEX	Systematic Evolution of Ligands by Exponential Enrichment
SPR	Surface Plasmon Resonance
Soy PC	L- α -phosphatidylcholine (soybean)
TBAF	Tetrabutylammonium fluoride
TCBQ	Tetrachloro-1,4-benzoquinone
TCA	Trichloroacetic Acid
TAMRA	Carboxytetramethylrhodamine
TBE	Tris/Boric acid/EDTA buffer
TBDMS	tert-Butyldimethylsilyloxy group
TBDMSCl	tert-Butyldimethylsilyl chloride
TEM	Transmission Electron Microscopy
TEMED	N,N,N',N'-tetramethylethylenediamine
TG	Glycerol trioleate

THF	Tetrahydrofuran
TLC	Thin Layer Chromatography
TOAB	Tetraoctylammonium bromide
uMUC1	Under-glycosylated mucin 1
UV-vis	Ultraviolet-Visible Spectrophotometry
VEGF	Vascular Endothelial Growth Factor
vs.	Versus
3-D	Three dimensional
d	Doublet
h	Hour(s)
g	Gram(s)
<i>J</i>	Coupling constant
M	Molar (mol L ⁻¹)
min	Minute(s)
nm	Nanometer(s)
nmol	Nanomole(s)
pKa	Acid dissociation constant
q	Quartet
s	Singlet
t	Triplet
v/v	Volume per volume
w/v	Weight to volume

μL	Microlitre(s)
μM	Micromolar
μmol	Micromole(s)
λ	Wavelength
δ	Chemical shift
σ	Standard deviation
\bar{x}	Average size

CHAPTER 1

SYNTHESIS OF APTAMER-PORPHYRIN CONJUGATE FOR PHOTODYNAMIC THERAPY

1.1 INTRODUCTION

In the introductory section of Chapter 1, first the porphyrin and construction of porphyrin arrays are briefly described. Second, the section covers porphyrin based photosensitizers and their roles in Photodynamic Therapy (PDT), followed by antibody and aptamer target for a selective delivery of photosensitizers to the tumor site. General procedures of different approaches of solid phase DNA synthesis, porphyrin-DNA conjugates, and internal modification of bases are described in brief. Furthermore, this section gathers information on the underglycosylated-mucin 1 glycoprotein (uMUC1), and also addresses the question of why aptamers to these proteins are selected for a tumor target. Finally, this thesis describes why uMUC1 aptamer was chosen for these studies.

1.1.1 Porphyrin

Porphyrins are common structures in Nature and are found in such systems as chlorophyll and hemoglobin. Porphyrins such as myoglobin and hemoglobin play important roles in many biochemical functions including oxygen storage and oxygen transport.^{1,2} In many enzymatic reactions, porphyrins transport electrons³ (cytochrome b and c). They are also involved in oxygen activation and utilization in cytochrome P450 and cytochrome oxidase.^{4,5} Porphyrins are the major structural units in light harvesting antennae used in natural photosynthesis.⁶

In the laboratory, these structures can be molecularly designed and constructed to mimic the natural photosynthetic system,⁶⁻¹⁰ and enzymic processes.¹¹ Porphyrins are attractive building blocks for the construction of supramolecular structures because they show interesting properties in optoelectronics,¹² light-energy conversion,^{13,14} and catalysis.¹⁵⁻¹⁷ Further, porphyrins have been shown to have potential application in information storage¹⁸ and as semiconductors.¹⁹ Recently, the non-covalent assemblies of porphyrins have been used to develop photoactive nanodevices.^{20,21}

Porphyrins can be designed and synthesized to obtain various desirable properties. For example, synthetic metalloporphyrin arrays are used in sensors²² in artificial olfaction.^{23,24} Oligomer-conjugated porphyrin polymers show non-linear optical properties.^{25,26} Anderson and co-workers have developed conjugated porphyrin polymers that show increase in non-linear optical properties.²⁷ Therefore, these molecules have potential applications in optical communications and electro-optical signal processing. In recent years, synthetic supramolecular porphyrin arrays have received an enormous attention among scientists, and are described in following section.

1.1.2 Construction of Porphyrin Array

Various methodologies have been employed for creating porphyrin arrays for applications in electronics and molecular photonics devices. Lindsey and Wagner²⁸ designed and created a covalently linked linear porphyrin array for the construction of molecular photonic wires. In this array, an excited state of porphyrin first results from light absorption by one end of the array, followed by

the transfer of excitation energy from the light-absorbed end to the opposite end of the array. Recently, Kim and co-workers have developed covalently linked cyclic porphyrin arrays, which can be used in modeling the photosynthetic reaction center.²⁹ Kobuke and co-workers have developed a method for creating a multiporphyrin array which could enable transfer of excitation energy.³⁰ Eventually, these arrays could substitute the photophysical properties of chlorophyll. The electronic structure of porphyrin arrays is very similar to π -conjugated systems; when a π -conjugated system is conjugated with porphyrin, it exhibits nonlinear optical properties.^{25,27,31} Consequently, porphyrin arrays have potential applications in creating novel opto-electronic materials. Such arrays can also serve as models for the study of energy and electron transfer processes in artificial photosynthetic systems.

A large number of covalently linked cyclic and linear supramolecular porphyrin arrays have already been constructed for the purpose of modeling and adopting light-harvesting, as well as for charge transfer studies in natural photosynthetic systems^{6,29,32-35}; these structures have potential applications in various molecular devices. Furthermore, covalently linked linear multiporphyrin arrays (shown in Fig 1.1(A)) transfer electron and energy efficiently upon irradiation with light.²⁹ Therefore, these arrays could be used as electronic and photonic wires. Changes in a porphyrin's substitution pattern and metalation influence their physical as well as chemical properties.³⁶ Photo-physical properties of synthetic porphyrins can be altered by co-coordinating different metals in the core.³⁷⁻³⁹ In addition, the heterogeneous combinations of porphyrin derivatives have been applied to energy-transfer, and electron-transfer systems.⁴⁰ When

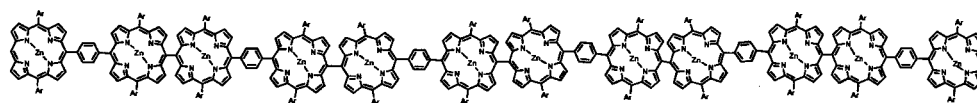
different substituted porphyrin units are covalently linked, electronic interaction between the porphyrin units changes,⁴¹⁻⁴³ which is crucial in the design of electronic gradients for effective energy or electron transfer in various devices. A large number of publications have demonstrated that the covalently-linked supramolecular porphyrin arrays are versatile building blocks for the design of electronics, sensors, optical devices, and solar energy conversions. However, replacement of porphyrin building blocks along the array is cumbersome and requires the redesign and reconstruction of the complete supramolecular array.

Recently, DNA has been exploited as supramolecular scaffold to produce nanoscale molecular photonic wires.^{44,45} In particular, Garca-Paraj and co-workers demonstrated that chromophores attached on a DNA-scaffold transferred energy at high efficiency.⁴⁴ The DNA-based photonic wires have received a great deal of attention for their applications in nanobiotechnology. For example, AuNPs can be selectively attached to the DNA in a DNA chip which leads to precise micropatterning of gold.⁴⁶ Moreover, functional molecules assembled on DNA scaffold can be used in creating nano mechanical devices which have biological applications.^{26,47,48} Co-ordination of functional molecules on DNA scaffold is a promising approach for the development of structurally controlled precise nanostructures. Kool and co-workers have developed a library of chromophore arrays on DNA-like scaffold that mimics the properties of natural DNA.⁴⁹ Furthermore, they demonstrated that single-chromophore labeled deoxyribosides exhibit different fluorescence properties compared to multiple-chromophore labeled deoxyribosides. Recently, Yamana and co-workers created pyrene arrays on an RNA scaffold, and reported that RNA- and DNA-based chromophore arrays

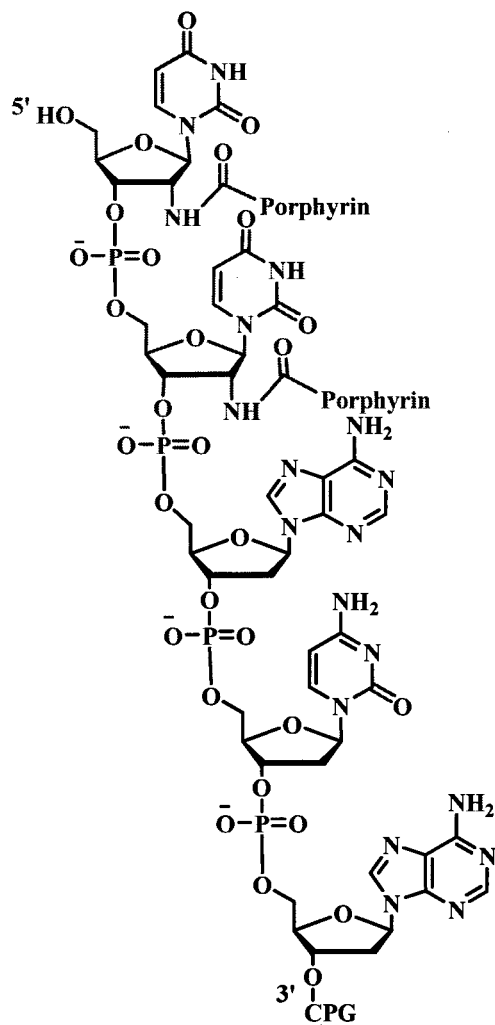
could find applications in molecular recognition due to the unique helical structure.⁴⁰

Various research groups have reported that multichromophore assembled supramolecular systems exhibit significantly different photophysical properties from the monomeric chromophore unit.^{31,50-52} Therefore, the number of chromophores and their arrangements play important roles in optimization of electron transfer in self-assembled systems.^{31,51} Porphyrins are one of the most attractive chromophores, and possess unique photochemical properties including the ability to absorb red light. By employing a DNA scaffold, supramolecular porphyrin arrays (Fig 1.1(B)) can be created, and their photonic and electronic properties can be explored. Later in this thesis, a method has been developed which can be used for creating porphyrin arrays on a DNA scaffold (Section: 1.4.3).

Apart from the aforementioned applications of porphyrins, they have also been employed in phototherapy.⁵³ Porphyrins absorb and transfer energy with high efficiency in natural systems.^{54,55} Due to their high energy absorption and transfer properties, porphyrins are used as photosensitizer in PDT, which is the focus of the current research. Various types of porphyrin based photosensitizers and their roles in PDT will be described next.



(A)



(B)

Figure 1.1 Porphyrin arrays. (A) A linear porphyrin array,²⁹ (B) porphyrin array on a growing DNA scaffold. CPG stands for Control Pore Glass.

1.1.3 Photosensitizers

Porphyrins and porphyrin-based photosensitizers have been extensively studied for their application in PDT^{53,56,57} because of their beneficial properties. These include high singlet oxygen quantum yield, a lack of dark toxicity, and strong absorption with a high molar extinction coefficient in the red region.^{58, 59} PDT is a localized treatment of tumors that uses a photosensitizer, light, and oxygen. Upon absorption of light of a specific wavelength, the photosensitizers are changed into an excited singlet state, and via intersystem crossing excited singlet state changes to the triplet state. The triplet state of photosensitizers transfers energy to the ground state molecular oxygen present in tissue surrounding it, which

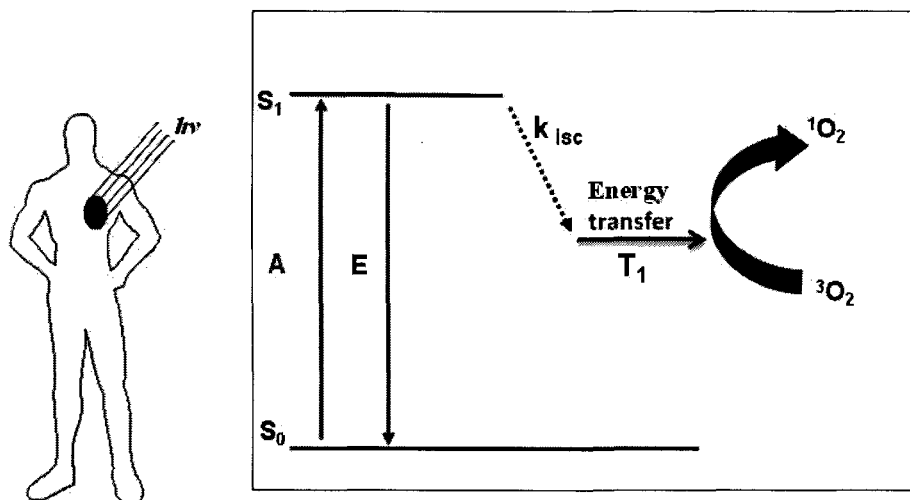


Figure 1.2 Role of photosensitizers in singlet oxygen production. S₀ = ground state of photosensitizers, A = absorption of light of specific wavelength, S₁ = excited state of photosensitizers, E = emission, K_{isc} = intersystem crossing, and T₁ = triplet state of photosensitizers.

results in the production of reactive oxygen species such as singlet oxygen ($^1\text{O}_2$) (as shown in Fig 1.2.) which kills tumor cells.^{58,60}

The Food and Drug Administration (FDA) approved the photosensitizer, Photofrin (Fig 1.3), a derivative of hematoporphyrins, which has been used in PDT in various countries.^{58,61,62} However, there are several drawbacks to the drug, such as low selectivity and low molar absorptivity at 630 nm.^{56,61} Higher doses of the drug are therefore required, as well as a more intense light for the effective treatment of tumor in PDT. Additionally, a major disadvantage of Photofrin is the side effects involved with treatment. The remnant of the drug causes the post-treatment photosensitization effect on patients.^{61,62} To overcome these side effects, effort has been directed towards the development of photosensitizers that have fewer or no side effects after treatment. A few of the second generation photosensitizers that have high molar absorptivity and high phototoxicity have been developed and are discussed in the following section.

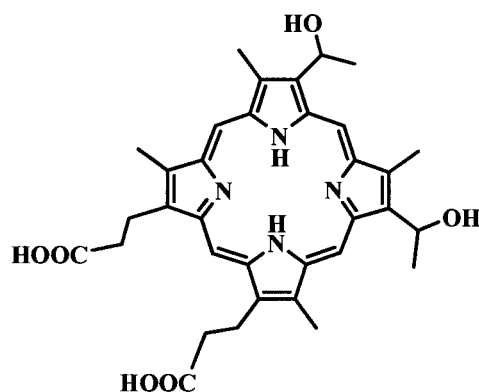


Figure 1.3 Haematoporphyrin derivative II (Photofrin).

1.1.3.1 Second Generation Photosensitizers

An ideal photosensitizer should have the following attributes: absorbs light strongly in the red region (600 – 800 nm), where light has maximum penetration into deep tissue; produces enough singlet oxygen and kills tumor cells efficiently; be tumor specific, and finally; should rapidly clear from the system soon after treatment.^{58,63,64} Some of the second generation photosensitizers possess a few properties of an ideal photosensitizer. Mono-L-aspartyl chlorine e6 at 654 nm ($40,000 \text{ M}^{-1}\text{cm}^{-1}$), Benzoporphyrin Derivatives (BPD) at 690 nm ($36,000 \text{ M}^{-1}\text{cm}^{-1}$), phthalocyanine at 650 – 700 nm ($200,000 \text{ M}^{-1}\text{cm}^{-1}$), *meta*-tetrahydroxyphenyl chlorine (m-THPC) at 652 nm ($22,400 \text{ M}^{-1}\text{cm}^{-1}$),⁵⁶ pyropheophorbide-a derivatives at 665 nm ($47,500 \text{ M}^{-1}\text{cm}^{-1}$),⁶⁵ which all have high molar absorption coefficient, are promising second generation photosensitizers (Fig 1.4 (A) – (F)) for PDT. Another class of photosensitizer is dithia core-modified porphyrins. These porphyrins absorb in the near infrared region of light, and have high molar absorptivity at 690 – 717 nm ($7500 \text{ M}^{-1}\text{cm}^{-1}$)^{66,67} compared to Photofrin at 630 nm ($1170 \text{ M}^{-1}\text{cm}^{-1}$),⁶² which make them amenable candidates for the treatment of tumors in a near infrared region. Recently, Leung and co-workers have reported that the Bis-Amino Silicon (IV) Phthalocyanine (BAM-SiPc) that has significantly high phototoxicity against HepG2 tumor tissue but biodistribution of BAM-SiPc was found to be nonspecific.⁶⁸

Although many promising photosensitizers have been developed, none of them are effective on PDT unless they are specifically targeted to tumor cells. The

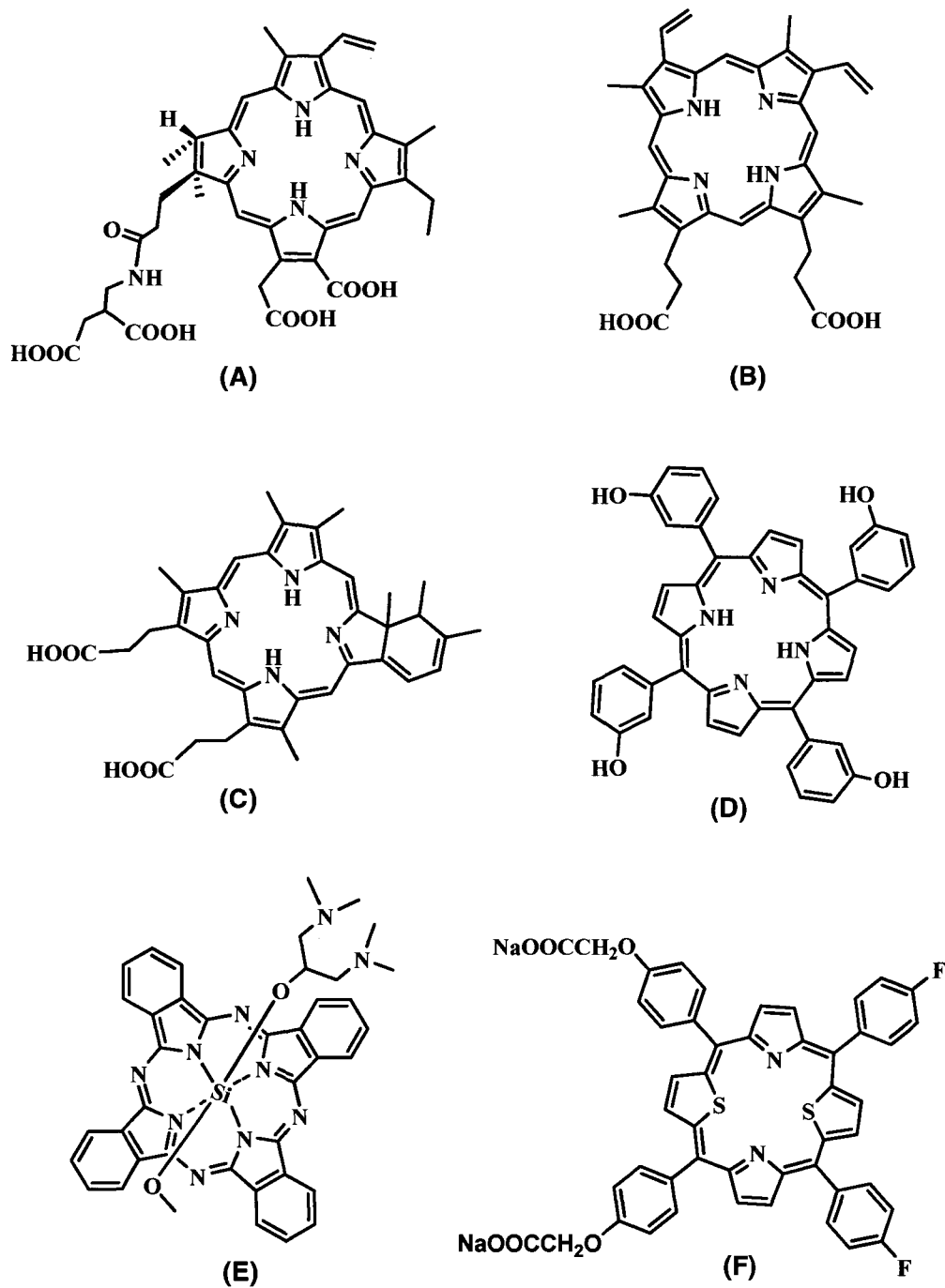


Figure 1.4 Second generation photosensitizers. (A) Mono-L-aspartyl chlorin e6, (B) protoporphyrin IX, (C) benzoporphyrin derivatives, (D) m-tetrahydroxyphenyl chlorin (m-THPC), (E) bis aminosilicon(IV) phthalocyanine (BAM-SiPC), and (F) dithiaporphyrin.

main drawback of all photosensitizers is a low selectivity for tumor over normal tissue.⁴⁷ This may result in damage to normal tissue after PDT due to photosensitization effect. Another challenge is that photosensitizers are hydrophobic in nature, which makes them difficult to dissolve in aqueous and biological fluid.⁶⁹ Recently, the synthesis of glycosylated porphyrin dimers and their potential application in PDT has been reported.⁴⁹ Progress has been made in developing the third generation of photosensitizers, and will be discussed next.

1.1.3.2 Antibodies-Photosensitizers

Recent progress in the development of a third generation of photosensitizers involves conjugation of photosensitizers to the biomolecules. This provides specificity to targeting cancerous cells. By conjugating photosensitizers to monoclonal antibodies, photosensitizers can be selectively delivered to the tumor associated antigen.⁵⁶ Levy and co-workers conjugated porphyrin to antibodies for the first time in the 1980s.⁷⁰ Conjugation of haematoporphyrin with albumin,⁷¹ phthalocyanine with monoclonal antibodies⁷² and porphyrin with antibodies^{73,74} were all studied for targeted PDT. Toluidine Blue O (TBO) conjugated to an antibody specifically targeted against the cell surface of *Porphyromonas gingivalis*.⁷⁵ In particular, TBO-antibodies conjugates were found more effective compared to non-conjugated TBO. Various research groups have demonstrated that antibody-targeted photosensitizers provide high specificity.^{56,76-81}

Because hydrophobic photosensitizers tend to aggregate in an aqueous medium, conjugation of photosensitizers to antibodies is cumbersome.^{76,82} Therefore, photosensitizer immunoconjugates employed in past studies were contaminated with free photosensitizer impurities.^{58,83} Recently, a novel and simple method for producing functional high purity photosensitizer immunoconjugates have been developed by Hasan and co-workers.^{83,84} In that work, they first modified an antibody with two branched polyethylene glycol before conjugation of photosensitizers to the antibody. Hasan's group also demonstrated that photosensitizer-antibody immunoconjugates selectively targeted and killed Epidermal Growth Factor Receptor (EGFR) over expressing tumor cells in PDT.⁸³ Further, the quantum yield of conjugated photosensitizer to antibody (Fig 1.5) was found to be sufficient to kill cancer cells. Particularly, they demonstrated that BPD-C225 conjugate targeted and killed the EGFR while free BPD did not show specificity. However, the binding affinity of conjugated antibodies decreased compared to native antibodies. Furthermore, these studies explained that the binding affinity of antibody depends on the number of photosensitizers loaded per antibody. In particular, for seven photosensitizers (e.g., BPD) loaded per antibody, the binding affinity decreased by 50%. On the other hand, the authors also reported that the photosensitizer labeled immunoconjugate was found less effective than the free photosensitizer due to changes in the photophysical and photochemical properties of the photosensitizer.⁸³

Antibodies are an attractive target for selective treatment of tumors in PDT. However, there are several problems associated in the development of high

quality antibody-photosensitizer conjugates that do not alter the antibody's photophysical and biological properties. Due to the poor solubility of the photosensitizer in water, a serious problem occurs when coupling of the photosensitizer to the antibody.^{56,85} As mentioned earlier, a major problem is the aggregation of photosensitizers in an aqueous media. Therefore, prior to the conjugation of photosensitizers to the antibodies, a modification of photosensitizers with a suitable functional group is required for linking the lysine,^{86,87} thiol,^{77,88} dextran⁸⁹ or polyvinyl alcohol group⁸⁷ of a monoclonal antibody.⁵⁶

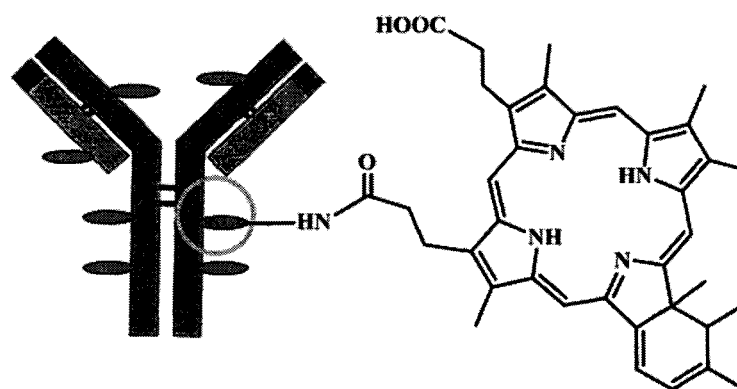


Figure 1.5 Schematic diagram showing antibody-photosensitizer conjugate. Orange ovals are photosensitizers (e.g., BPD) attached to the antibody (7 BPD/antibody).

Furthermore it has been reported, particularly *in vivo*, that the large size of a monoclonal antibody limits the ability of the conjugate to penetrate large solids such as deep-seated and poorly vascularized tumors.⁹⁰ Options for selective drug delivery includes aptamers targeting. Conjugating a therapeutic agent (e.g., a photosensitizer) to the aptamer is becoming a common method of creating targeted therapeutic treatment. In the next section, recent studies in aptamers, their advantages over antibodies, and their applications will be described.

1.1.4 Aptamers

Aptamers are 3-D structures of artificial single stranded DNA, RNA or modified nucleic acids that have high binding affinity to a target protein,⁹¹⁻⁹³ whole cell^{94, 95} or small molecules targets (i.e., cocaine).⁹⁶⁻⁹⁹ These structures fold and bind to the target with very high specificities at nanomolar,^{91,100} and micromolar quantities.^{101,102} Aptamers were discovered in the early 1990s,^{103,104} and since then have been extensively studied for their applications in detection reagents,¹⁰⁵ pharmaceuticals,¹⁰⁶ and proteomic tools.^{107,108} The unique binding properties and synthetic versatility of aptamers have provided an additional route for the development of novel therapeutics and molecular biological tools.^{109,110} This has been demonstrated by increasing number of research that use aptamers in target validation, biomarkers, therapeutics, and drug discovery.^{91,111-114} Aptamers have a distinct advantage over the antibodies in that they have a small size (8 – 15 kDa)

relative to antibodies (150 kDa).^{114,115} The stability and small size of aptamers make them superior to antibodies for *in vivo* applications.

Aptamers are typically generated by a process called Systematic Evolution of Ligand by Exponential Enrichment (SELEX).¹⁰³ SELEX is a combinatorial library in which specific oligonucleotides sequences that bind with high affinities toward a target can be rapidly screened.¹¹⁶ SELEX can be performed in both automated systems^{116,117} as well as manually at the bench top. This method uses a large ($10^{14} - 10^{15}$ sequences) oligonucleotide pool to select potential binding species, i.e., aptamers to molecular targets.^{115,118} In addition to generating aptamers against purified proteins and small molecules, cell-SELEX technology can also be applied to generate aptamers that are specific to cells^{94,95,119,120} and tissues.¹²¹

The unique binding features of aptamers have made them particularly interesting. Okahata and co-workers have selected RNA-aptamers for the sensing of arginine-rich-motif peptide *in vitro*.¹²² Recently, the selection of DNA aptamers that bind with high affinity and selectivity to tumor markers present in a variety of malignant tissues known as under-glycosylated mucin 1 glycoprotein (uMUC1) were generated.^{90,123} In another study, aptamers were employed to identify new tumor markers with a potential application in the diagnosis of glioblastoma brain tumors.^{124,125} Aptamers have been selected against various cancer specific proteins such as Platelet Derived Growth Factor (PDGF),¹²⁶⁻¹²⁸ PSMA,^{129,130} VEGF,^{131,132} and Tenascin-C,^{125,133,134} the oligomeric form of HER3 that are found in cancer cells.^{135,136} Even though aptamers are selective for binding, they do not usually possess an innate therapeutic property. Aptamers can be efficiently used to produce

specific molecular probes to differentiate diseased cells.¹³⁷ They can distinctly recognize the molecular level differences between healthy cells and diseased cells.^{120,138} Aptamers can be also applied in distinguishing between conformational states of proteins, and can also be exploited in selection of regulatory sites of the protein.^{136,139} In such sites, they either inhibit protein function or change an active form of protein to stable form. Recently, a general strategy for designing aptamer-fluorophore conjugate that functions by switching structures from DNA/DNA duplex to DNA/target complex has been reported by Nutiu and co-workers.¹⁴⁰ From their study, aptamers form defined tertiary structures for specific target binding, which results in release of the quencher attached to complementary oligonucleotides. Eventually, aptamers are useful in the design of a biological switch.

Some major advantages afforded by aptamers are that they are small, stable, adaptable to organic solvent, and easy to handle. Because of their small size, they can easily penetrate large deep-seated tumors.^{90,141} In addition, they rapidly clear from the system due to their high hydrophilicity, and lower molecular weight.^{142,143} This project has focused on the use of DNA aptamer for targeted PDT. A recent study that uses aptamer target is presented next.

1.1.4.1 Aptamer Conjugated to Photosensitizers

Recently, aptamers have been used to improve imaging and radiotherapy with reduced side effects. Missailidis and co-workers¹⁴¹ have generated mono and

multi-aptamer complexes around a porphyrin chelator. In their work, a commercially available tetra(carboxy-phenyl)porphyrin bearing four carboxyl groups was coupled with selected 5'-amine modified aptamer to the MUC1 tumor marker followed by radiolabeling. Further, the radiolabel multi-aptamer complexes were used in a targeted radiopharmaceutical. These complexes were found to increase the retention time of the complex in circulation, without affecting its superior tumor penetration properties.

The experiments in this thesis have developed a general method of conjugating porphyrin to aptamers in an efficient way for specific tumor targeting. For this, a 2'-internally porphyrin-modified nucleoside has been created which can be conjugated to DNA (as shown in Fig 1.1(A)) using solid phase automated synthesis. Further, a goal of the research – to employ a solid phase automated DNA synthesis to conjugate porphyrin to the aptamer – was achieved by using a 2'-porphyrin-modified H-phosphonate derivative of uridine. In addition, using a solid phase method, a porphyrin can be conjugated multiple times along an aptamer strand attached to a solid support. General procedures of different approaches in automated solid phase DNA synthesis will be described next.

1.1.5 Approaches to Automated Synthesis of DNA

DNA synthesis uses multiple approaches in generating the oligonucleotides including: phosphotriester,^{144,145} phosphoramidite,^{146,147} and H-phosphonate¹⁴⁸ methods. Generally, the phosphotriester method is common in

solution phase synthesis.¹⁴⁹ However, phosphoramidite and H-phosphonate chemistry are most commonly used in automated solid phase synthesis.

1.1.5.1 Phosphoramidite Approach

The phosphoramidite method is the most widely used synthetic approach in DNA synthesis. The 3'-phosphoramidite derivatives of nucleosides are most commonly used in automated DNA synthesis.^{150,151} This method adds one nucleotide per synthesis cycle to the 5' end of the sequence. The DNA synthesis cycle begins with a 3'-hydroxyl nucleoside attached to a solid support Control Pore Glass (CPG) through a long spacer arm (as shown in Fig 1.6). The support-bound nucleoside has a 5'-DMT protecting group (DMT = 4,4'-dimethoxytrityl) and a

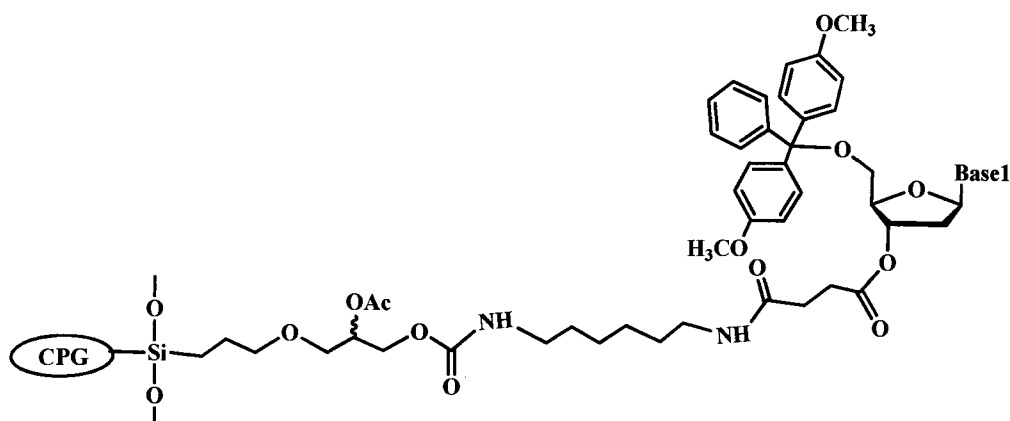


Figure 1.6 Starting base in DNA synthesis attached to the solid support (CPG) by long spacer. 5'-hydroxyl protected with DMT. Base1 could be Adenine, Guanine, Cytosine, and Thymine. Amines protected with benzoyl or isobutyryl group.

base protected with benzoyl or isobutyryl group. Using this solid supported DNA synthesis allows the filtration of excess reagent, thus eliminating further purification steps between the consecutive base additions.

The phosphoramidite cycle involves the four different steps:

- **Detritylation**
- **Activation/coupling of the bases**
- **Capping**
- **Oxidation**

Detritylation

The first step, called detritylation (also called deblocking), is the removal of DMT group with trichloroacetic acid (TCA) which frees the 5'-hydroxyl for the coupling reaction (Fig 1.7). DMT protection is commonly used in DNA synthesis since it is easily removed with mild acid. Another benefit of the of trityl groups is that carbocations have a distinctive orange color which can be used as diagnostic tool on a DNA synthesis. The efficiency of each cycle can be followed by using the absorbance reading of trityl (4,4'-dimethoxytrityl) removed in UV-vis spectroscopy.

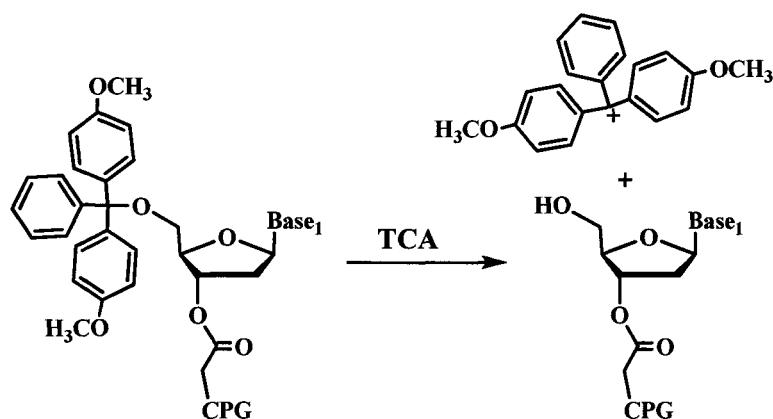


Figure 1.7 Schematic diagram of the removal of DMT by TCA. Right side of arrow shows free trityl cation and 5'-hydroxyl free nucleoside.

Activation and coupling

In the second step, the activation is followed by the coupling of 3'-phosphoramidite base (as shown in Fig 1.8). The phosphoramidite derivative of the sequential nucleotides is activated using tetrazole. Tetrazole is a secondary amine so the donation of proton allows formation of a thermodynamically stable anionic aromatic ring, which does not affect the DMT group. Tetrazole protonates the diisopropylamino group of a nucleoside's phosphoramidite, making it susceptible to the nucleophilic attack. The resulting intermediate is very reactive, leading to the complete coupling step in less than 30 seconds.

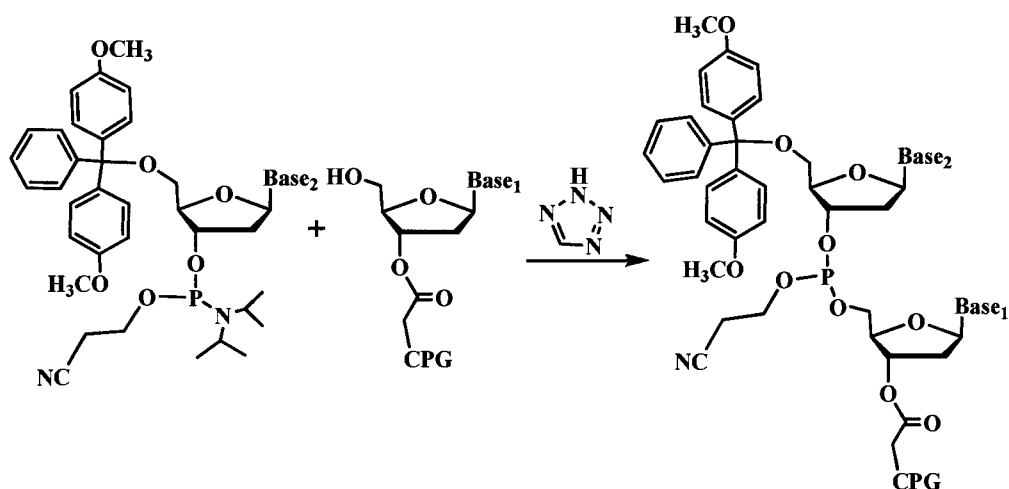


Figure 1.8 Activation of 3'-phosphoramidite of nucleoside by tetrazole, and coupling of activated phosphoramidite to growing oligonucleotide attached to a solid support.

Capping

The third step is called capping, and this step terminates any chain that did not undergo coupling (Fig 1.9). The unreacted chain has a free 5'-hydroxyl which can be terminated or coated by acetylation to become "failure products" while the DMT group of a successful coupling step protect the 5'-hydroxyl end from being coated. This is achieved with acetic anhydride and 1-methylimidazole. This step minimizes the impurities and facilitates purification of trityl-on (4,4'-dimethoxytrityl) DNA showing different retention time in HPLC.

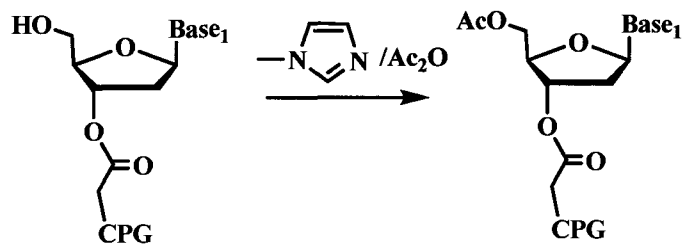


Figure 1.9 Capping of failure base in DNA synthesis with acetic anhydride.

Oxidation

The fourth step is oxidation. In this step, the internucleotide linkage is oxidized from the less stable phosphotriester P(III) to the more stable phosphate P(V) as shown in Fig 1.10. Upon oxidation, the DMT moiety is removed using

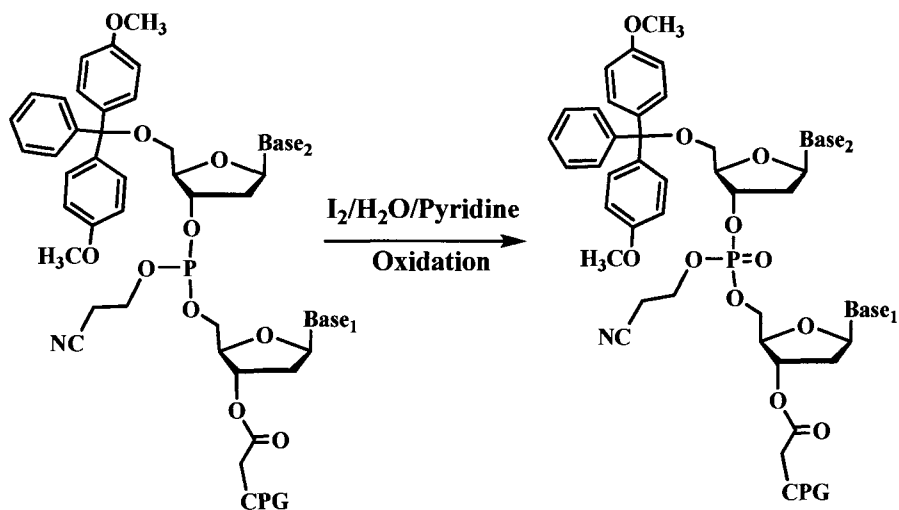


Figure 1.10 Oxidation of phosphorus (III) to the phosphorus (V) in DNA synthesis.

TCA, and the cycle can be repeated until the desired chain elongation is complete. The complete solid phase automated DNA synthesis cycle using 3'-phosphoramidite nucleoside is illustrated (Fig 1.11).

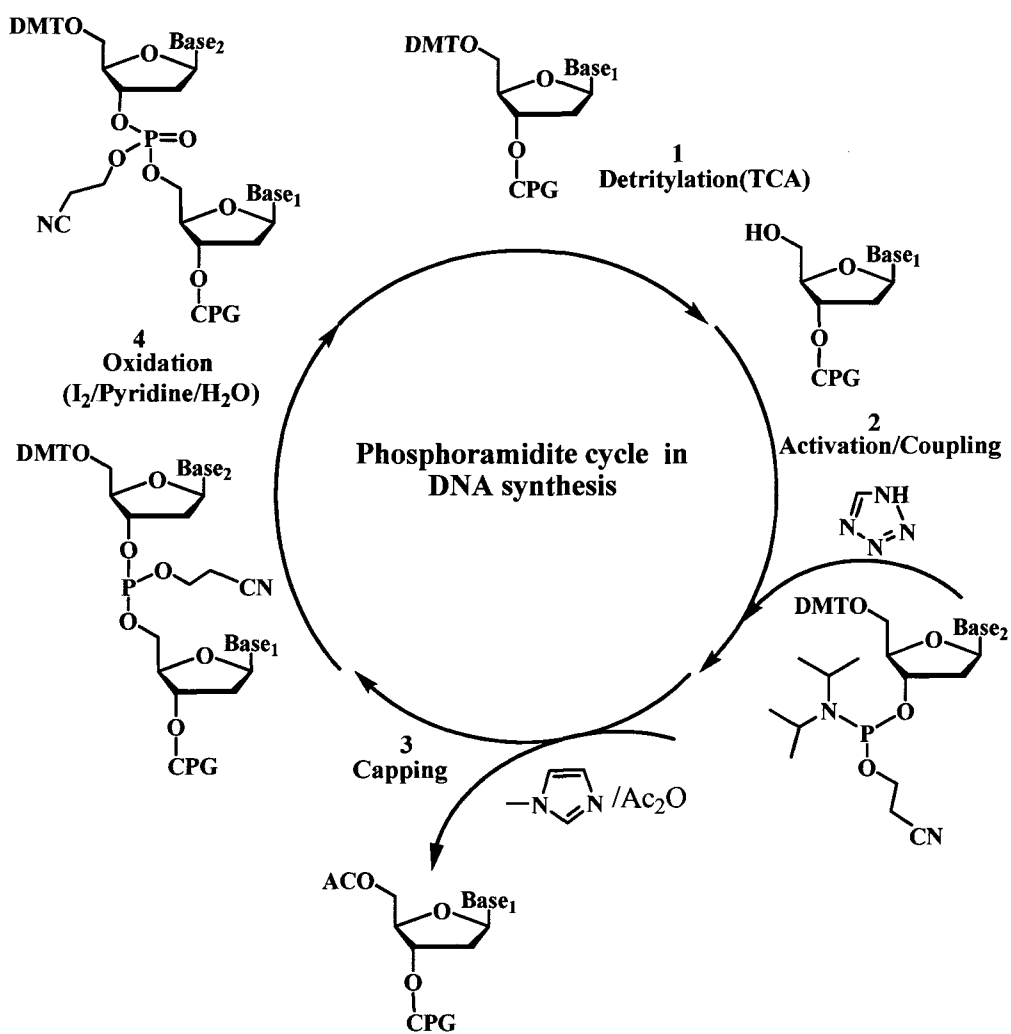


Figure 1.11 Automated DNA synthesis cycle using a phosphoramidite method

In this project, the H-phosphonate approach was used to conjugate porphyrin to an aptamer that is attached to a solid support. While the phosphoramidite method is effective, it is time consuming because oxidation and capping steps are required after each condensation reaction. Despite widespread use of the phosphoramidite coupling method, certain functional groups are not compatible, and the H-phosphonate method discussed in the following section remains a viable alternative synthetic approach.

1.1.5.2 H-Phosphonate Approach

H-phosphonate chemistry¹⁵² uses the same solid support (CPG) as the phosphoramidite cycle, and the chemistry is very similar to that of the phosphoramidite approach. Differences result from the properties of the monomers utilized and from a simpler synthetic cycle. The 3'-H-phosphonate monomers (as shown in Fig 1.12) are used instead of the 3'-phosphoramidite derivatives. In this method, the monomer that is able to be activated is a 5'-hydroxyl protected 3'-H-phosphonate salt form of nucleosides. A different activating agent is used such as pivaloyl chloride, and 1-adamantoyl chloride.¹⁵³ Because H-phosphonates nucleosides are stable and resistant to air oxidation, the phosphate protection is unnecessary.¹⁵³ In addition Rogers and co-workers reported that amine protection is also not required in H-phosphonate nucleosides.¹⁵⁴ The H-phosphonate diesters generated by the coupling reactions are stable to the normal reaction conditions,^{153, 155} so oxidation at every step is not required. Instead, a single oxidation step is

performed at the end of the chain elongation. This single oxidation step makes it easy to produce modified DNA. For instance, if an elemental sulfur is used as the oxidizing agent, all of the internucleotide bonds will then contain sulfur instead of oxygen attached to the phosphorous atom.¹⁵⁶ Further, the H-phosphonate approach is of value when the internucleotide linkage required is other than the standard phosphodiester linkage. The most popular use of H-phosphonate chemistry is for the radioactive labeling of all phosphodiester linkages to phosphorothioate by using radioactive sulfur.¹⁵⁷ However, H-phosphonate chemistry is used in this research only for conjugation of porphyrin to the DNA and aptamers.

The H-phosphonate monomers

The H-phosphonate monomers (Fig 1.12) are protected at the 5'-hydroxyl position with a DMT. In commercially available H-phosphonate nucleosides, the exocyclic amines on the bases are protected by the benzoyl or isobutyryl groups as

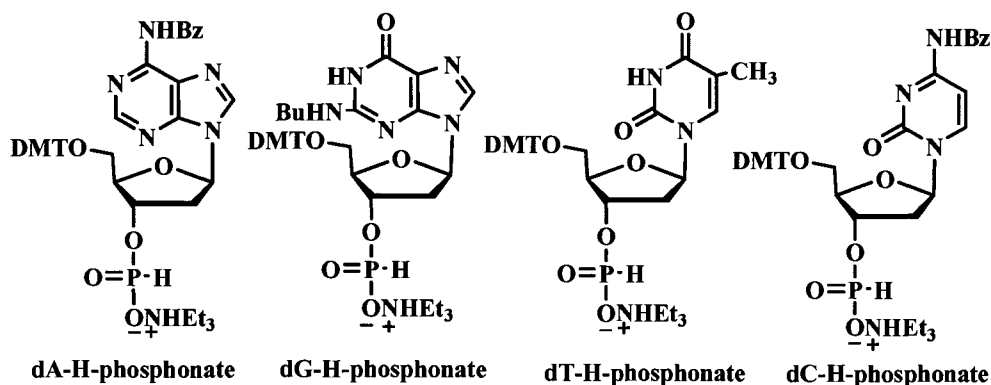


Figure 1.12 Commercially available monomers of H-phosphonate. Bu = isobutyryl and Bz = benzoyl protecting groups.

in the β -cyanoethyl phosphoramidites. The H-phosphonate group is attached to the 3'-position of the nucleoside. The steps involved in H-phosphonate cycle are described below.

Detritylation

This step is similar to the phosphoramidite cycle as described for phosphoramidites. Residual TCA from the detritylation step should be neutralized with a solution of pyridine in acetonitrile. Neutralization also provides the proper solvent medium for the coupling reaction in H-phosphonate cycle.

Coupling

After detritylation and neutralization, the second step is the delivery of base protected H-phosphonate derivatives of nucleoside to the reaction column. Adamantoyl carboxyl acid chloride is used to activate the H-phosphonate. First, adamantoyl carboxyl acid chloride is added to the 3'-H-phosphonate nucleoside monomer. The coupling occurs through a nucleophilic attack by the free 5'-hydroxyl group on the phosphorous of the incoming activated monomer and completes in 1 – 2 min. For this reason, it is important that the environment be hydroxyl-free. The phosphonate diester linkages generated by this coupling are stable. Therefore, an oxidation step is not necessary in each step, and is performed at the end of the synthesis.

Following the coupling step, the cycle of reactions is repeated, beginning with the detritylation step, until chain elongation is complete.

Oxidation

The oxidation step is normally omitted during cyclic chain elongation, and a single oxidation is performed later with the required oxidizer. In the oxidation step, the hydrogen atom which is bound to the phosphorous is replaced with an oxygen atom. Oxidation is accomplished with a mixture of two solutions. One solution contains iodine in tetrahydrofuran (THF), and the other N-methylmorpholine in water and THF. If required, the DNA can be modified at this step. The complete solid phase DNA synthesis cycle by using 3'-H-phosphonate nucleoside is presented (Fig 1.13).

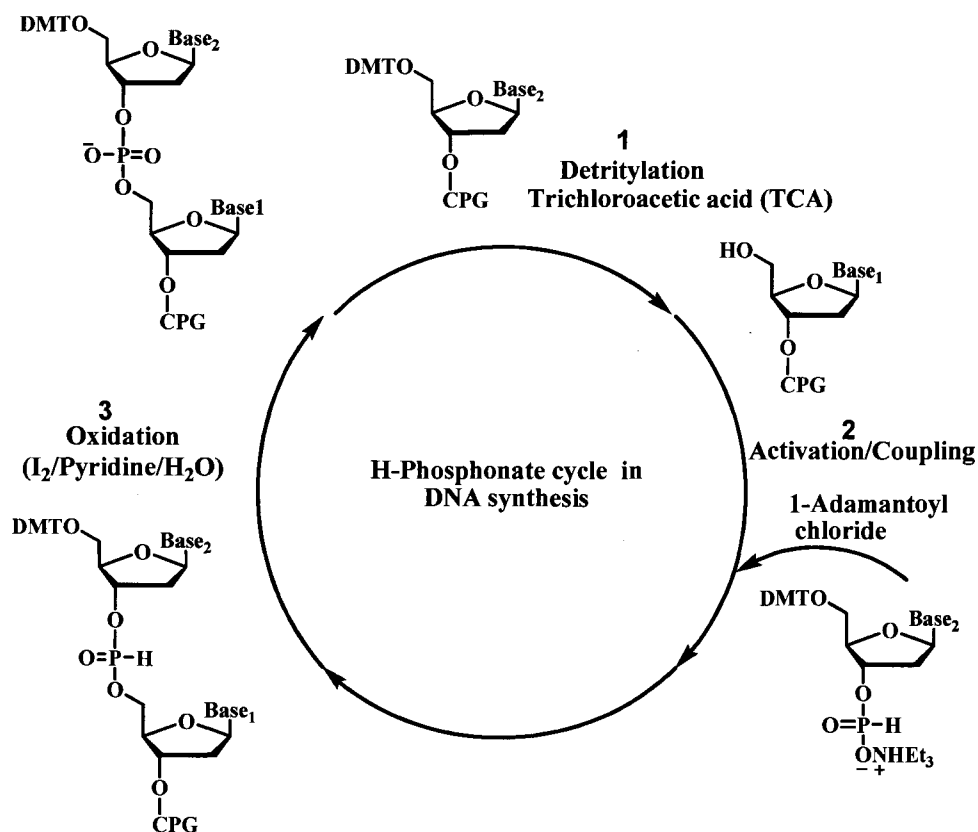


Figure 1.13 Automated DNA synthesis cycle using H-phosphonate method.

Final detritylation

The regular detritylation cycle is used unless reverse phase purification is required. When final DMT remains coordinated, it exhibits higher retention time than truncated DNA, and assists purification by a reverse phase cartridge or by HPLC.

Oligonucleotide deprotection

Upon completion of the synthesis, concentrated aqueous ammonia solution deprotects a solid support attached to the DNA as well as the benzoyl protecting group of the oligonucleotide. Isobutyryl protecting groups can be removed by heating the ammonia solution at 55 °C for an hour. After deprotection, DNA and modified DNA can be purified by HPLC and gel electrophoresis.

This research has used an internally 2'-porphyrin-modified base, and the H-phosphonate approach to synthesize a porphyrin-DNA conjugate using a solid phase automated synthesis. Methods of synthesis of porphyrin-DNA conjugates have already been reported, and literature review on synthesis of porphyrin-DNA conjugate will be presented next.

1.1.6 Oligonucleotide-Porphyrin Conjugates

The interaction of porphyrins with DNA has been an area of interest for its potential applications in cancer therapy.¹⁵⁸⁻¹⁶⁰ Free porphyrins and metalloporphyrins are known for site selective cleavage of DNA.¹⁶⁰⁻¹⁶² In addition, porphyrin covalently conjugated to oligonucleotides has received a greater attention to get insight of electron transfer phenomena and conformational analysis of DNA. Muenier and co-workers have covalently attached tetracationic manganese porphyrins to oligonucleotides and were found efficient site selective DNA cleaving molecules.^{163,164} Berova and co-workers have conjugated porphyrin derivatives to DNA for the study of DNA conformations.^{165, 166} Further, porphyrin-DNA conjugates have also been extensively explored in electron transport studies by this group. Porphyrin-modified oligonucleotides exhibited a lower melting temperature than their unmodified analogues.^{167,168} The method for conjugating porphyrins to DNA includes terminal and internal modification. Terminal modification is commonly used in porphyrin modified DNA synthesis, and recent work in terminal porphyrin modified DNA is described next.

1.1.7 Terminal Modification

Modified synthetic oligonucleotides have been synthesized by various methods. DNA can be modified at terminal ends or at various internal positions of nucleoside. Terminal modification of DNA includes the modification at 3'- or 5'-position (Fig 1.14(A)). These modifications can be carried during DNA synthesis

or post-DNA synthesis. Modification at 5'- and 3'-ends of the nucleosides is the most common, and has been widely used in the synthesis of modified oligonucleotides. Porphyrins have been conjugated at 5'-end^{167,168} and 3'-end¹⁶⁵ of DNA, and have also been embedded in between DNA.¹⁶⁹ These instances have been reported and their roles in electron transport studied. Recently, water-soluble 5'-modified porphyrin and metalloporphyrin-DNA conjugates with a short 5'-amide linker between porphyrin chromophore and nucleobase were reported.¹⁶⁸

Exclusively, DNA modification has employed both 5'-and 3'-ends; however, modification at these ends terminates the synthesis of DNA. In order to conjugate porphyrins at either the 5' or 3' end of DNA, prior modification at those positions with an amine or other functional groups is required. An efficient way of conjugating porphyrins without terminating the DNA synthesis is of a subject interest in this project. Internal modification, where the modifier is located on or in place of an internal base is another route to introduce porphyrins in DNA. Literature review on internal modification of nucleosides, and the recent work on internally porphyrin-modified DNA will be introduced next.

1.1.8 Internal Modification

Modified oligonucleotides are widely used in diagnostic probes, therapeutic candidates, and artificial enzymes.¹⁷⁰⁻¹⁷² The 5'-position of deoxyuridine is the most common for introducing structural diversity in oligonucleotides. The structural modification of biopolymers such as DNA and

RNA provides these molecules to be used in sensors, aptamers and molecule recognitions as well as in various other biological applications.

Recently, internal modification has gained interest for modifying synthetic oligonucleotides. For example, an internally fluorophore-modified oligonucleotide probe is advantageous for Fluorescence Resonance Energy Transfer (FRET) studies. DNA-based probes with longer sequences that have fluorophore and quencher separated by 4-5 nucleotides resulted in best FRET signal implying that internally fluorophore label DNA could exhibit better performance.^{173,174} FRET occurs within 1 nm to 10 nm of donor and acceptor.¹⁷⁵ DNA-based FRET study has useful biological applications in real time monitoring *in vivo* as well as *in vitro*.¹⁷⁵ By using internal modification, two identical fluorophores can be efficiently inserted in close proximity along a DNA strand. Watanabe and co-workers have demonstrated that two identical fluorophores inserted in a DNA-based donor probe increased the fluorescence signal intensity and minimized the background noise.¹⁷⁶ In another study, Watanabe's group have detected a RNA molecule selectively from the identical sequences under similar conditions by using intramolecular FRET study.¹⁷⁷

Modification of nucleosides using phosphoramidite or H-phosphonate moieties is one way of internal modification. The phosphorus backbone modification is another approach to modify DNA internally. Recently, Majima and co-workers synthesized porphyrin-DNA conjugate by introducing porphyrin to the phosphorus atom via a linker which is diastereochemically pure phosphoramidate.⁵² By modifying the phosphorus backbone, oligonucleotides

become resistant to enzymatic cleavage.¹⁷⁸ However, this affects the internucleotidic linkages between nucleotides. In addition these modifications require either special synthetic steps or special modified nucleoside monomer, other than phosphoramidite derivatives.

Modification at various positions of nucleobases is an established method of internal modification. Internal modification has been reported for adenine,¹⁷⁹ thymine,¹⁸⁰ guanine and cytosine with 1-ethynyl pyrene,¹⁸¹ and at various positions of uridine. Tetramethyl rhodamine (TAMRA) labeled at the 5-position¹⁸² of base as well as various molecules such as iodine, fluorine label at bases were reported for various purposes. Recently, 7-fluoro substituted adenine and guanine monomers were found to increase the stability of DNA duplexes.¹⁸³ The quencher dye, TAMRA, labeled at the 5-position of the uridine, and at the 4-position of the thymidine has been used for FRET study.¹⁷⁴ Porphyrin labeled at the 5-position of uridine¹⁸⁴ was recently reported for creating porphyrin arrays in DNA molecules. The porphyrin array at the 5-position in 10-mer and 20-mer DNA strands with rigid acetylene spacers showed a significant drop in the melting temperatures of duplex DNA. Further, every additional porphyrin added into the strand displayed a noticeable disruption in the base pairing by the porphyrin. This study revealed that the modification at bases on nucleoside interfere with the base pairing of DNA.

Recently reported methods of internal modification include at the 2'-position of sugar ring. Various lengths of the amine linker modified bases are commercially available for internal modification of oligonucleotides. The 2'-modified bases have been an important tool for the introduction of molecules of the

desired interest into oligonucleotides. The 2'-selenium modified uridine was also found to crystallize DNA well.¹⁸⁵ Methyl, methoxy and the alcohols¹⁸⁶ modified at the 2'-position of uridine have been reported. The 2'-amine-modified uridine, synthesized by McGee and co-workers,¹⁸⁷ is a well established method that has received enormous attention in the modification of oligonucleotides. Shohda and co-workers¹⁸⁸ have reported the synthesis of 2'-O-methyl-2-thiouridine modified oligonucleotides and have demonstrated enhanced selectivity of modified bases. Oligonucleotide-anthraquinone conjugates via one carbon linker at the 2'-position of sugar were reported by Yamana and co-workers.¹⁸⁹ 2'-anthraquinone modified oligonucleotides were found to be excellent electrochemical probes for measuring long range charge coupling through DNA duplexes.^{189,190} Wagenknecht and co-worker developed the 2'-pyrene-modified uridine.¹⁹¹ Further, Yamana and co-workers synthesized 2'-pyrene-modified RNA and demonstrated that the multiple 2'-pyrene-modified RNA duplexes found to have slightly different melting temperature (T_m) within the range of 0 – 3 °C.⁴⁰ Furthermore, the stability of 2'-pyrene modified RNA did not significantly change in T_m corresponding to its unmodified RNA. Therefore, fluorophores such as pyrene, dansyl¹⁹² and anthraquinone etc. modified at the 2'-position of a nucleoside does not interfere with base pairing.

Even though internal modifications at the phosphorous-backbone and various other positions of the nucleobases have been established, these modifications still have a few drawbacks. These include the need for phosphorus backbone modification of each new modified nucleoside while modification of the

nucleobase interferes with the base pairing of the DNA. On the other hand, 2'-modified nucleosides has interference with base pairing and do not terminate the synthesis of DNA. A method of synthesis of internally 2'-porphyrin-modified DNA (Fig 1.14(B)) and aptamer was developed. For this purpose, 5'-hydroxyl protected with DMT and 2'-amine-modified uridine was employed, and porphyrin was conjugated at the 2'-position of uridine via an amido linker.

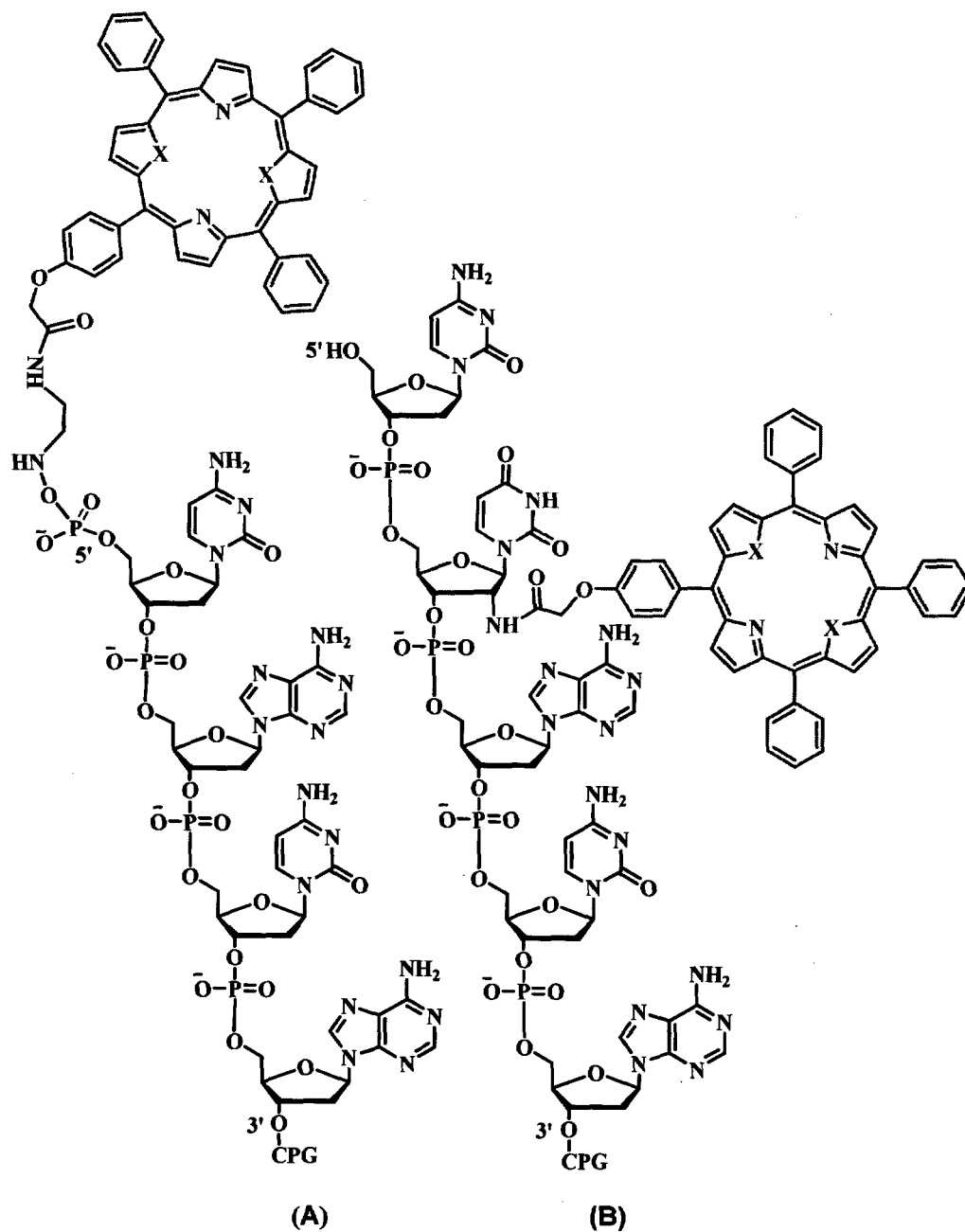


Figure 1.14 Porphyrin modified DNA. (A) 5'-terminal porphyrin-modified DNA, (B) internally 2'-porphyrin-modified DNA, X = NH or S.

1.1.9 The Cancer Target Mucin 1 (MUC1) Glycoprotein

Type I transmembrane mucin glycoprotein MUC1 is a well known marker for tumor diagnostics and treatment.^{90,193} MUC1 is expressed at the apical surfaces of normal ductal, glandular and some haematological lineages of almost all human epithelia.¹⁹⁴ In normal epithelial cells, MUC1 are involved in protection from microorganism, lubrication, adhesion, as well as hydration of cell surfaces.^{195,196} Furthermore, MUC1 is also known to interact with signal transducing molecules such as erbB and β -catenin.¹⁹⁶ The extracellular domain of the MUC1 consists of a variable number of O-glycosylated multiple tandem repeats of the 20 amino acid (aa) peptides.¹⁹⁷ The tandem repeats is a highly conserved amino acid sequences (VTSAPDTRPAPGSTAPPAHG) as seen in Fig 1.15.^{197,198} In healthy tissues, MUC1 is heavily-glycosylated (50 – 90% of its molecular mass is due to carbohydrates); in neoplastic (tumor) tissues, MUC1 is under-glycosylated.¹⁹⁹ In cancerous tissues, early termination of the oligosaccharide chains of MUC1 proteins occurs by the addition sialic acids, which results in under-glycosylated truncated sequences.^{195,200} The tumor associated under-glycosylated MUC1 antigen (uMUC1) is overexpressed on epithelial cell surfaces of many human tumors, including > 90% of human breast,^{201,202} ovarian,²⁰³ pancreatic,^{204,205} lung,²⁰⁶ gastric,²⁰⁷ colorectal, prostate cancer as well as hematological malignancies.^{193,202,208,209} The under-glycosylation permits the immune system access the peptide core of the tumor associated uMUC1 antigen, and exposed this antigen to immune recognition.²¹⁰ However, in normal cells this antigen is masked due to heavy glycosylation of protein. Cancer affected MUC1 is known to be poorly glycosylated compared to mucin from various healthy sources

such as milk^{211,212} and urine.²¹³ The APDTRPA sequence within the tandem repeats has been found to be the most immunogenic sequence of MUC1 protein, which responds with almost all anti-MUC1 monoclonal antibodies.¹⁹⁸ However, majority of anti-MUC1 monoclonal antibodies specifically allocated to the PDTR sequences within the tandem repeats.^{214,215}

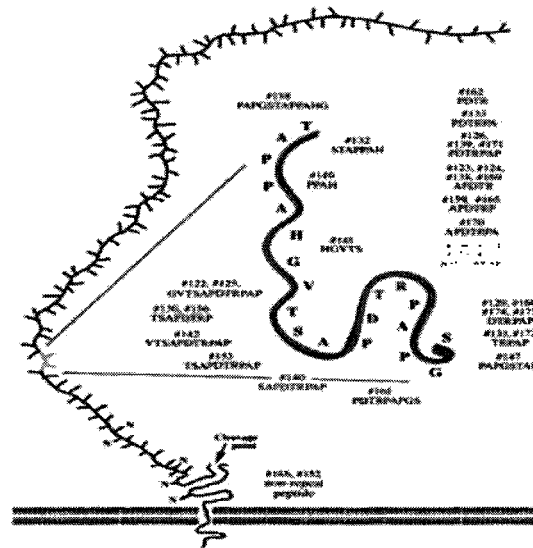


Figure 1.15 MUC1 showing 20 amino acid sequences. Green and orange are tandem repeats in MUC1. Orange is the most immunogenic sequence within the tandem repeats.¹⁹⁷

In breast adenocarcinoma and a number of epithelial tumors, MUC1 is upregulated with an unusual expression over the epithelia surfaces.^{198,216} The MUC1

is exceptionally overexpressed on breast cancer cells in an under-glycosylated form compared to normal tissues,²¹⁶ and is therefore a target for cancer therapy.

A model tumor antigen MUC1 is overexpressed in a wide range of cancer cells with variable glycosylation and can be exploited for the characterization and treatment of various types of cancer cells. By targeting the tumor marker (core peptide of uMUC1), various types of tumors can be selectively treated. The aptamers of uMUC1 have been already developed by Ferreira and co-workers,¹²³ which was discussed in a previous section. This project has developed a method of the conjugation of uMUC1 aptamer to porphyrin by using solid phase DNA synthesis. The uMUC1 aptamer-porphyrin conjugate can selectively deliver porphyrin to a tumor site, and upon irradiation of light of a specific wavelength, porphyrin can transfer energy to molecular oxygen present in the surrounding tissue, producing $^1\text{O}_2$. This is cyto-toxic substance which can selectively destroy the tumor in PDT. The method and procedures involved in conjugation of uMUC1 aptamer to porphyrin are described in the following section.

1.2 GOALS AND OBJECTIVES OF THESIS (PART 1)

Porphyrin-based photosensitizers are used as drugs for localized treatment of tumors in PDT. Current photosensitizers have shown low selectivity toward tumors and a post-treatment long-term photosensitization effect. The problems associated with current photosensitizers have spurred researchers to develop novel types of tumor-targeted photosensitizers. Recently, aptamers: the RNA, DNA and modified nucleic acids with high binding specificity, have been employed in drug targeting. MUC1 is found in epithelia of various types of tissues, and is known to be overexpressed in an under-glycosylated form in a variety of tumor tissues. Most recently, the aptamers have been selected through a SELEX process that binds an under-glycosylated MUC1 tumor marker. The goal of this project is to develop an efficient method for synthesizing aptamer-porphyrin conjugates to a MUC1 tumor marker for targeted PDT. This goal is achieved through the following objectives.

The main objectives of this project are:

1. To synthesize internally 2'-photosensitizer-modified uridine (5'-hydroxyl protected with DMT and 3'-hydroxyl free).
2. To develop a method for synthesizing (5'-hydroxyl protected with DMT) 2'-porphyrin-modified 3'-H-phosphonate or phosphoramidite derivatives that can undergo solid phase automated DNA synthesis.
3. To conjugate porphyrin to DNA without terminating DNA synthesis.

The project started with design and synthesis of mono acid functionalized porphyrin with a single carbon spacer and chosen to conjugate 2'-amino-2'-deoxyuridine (5'-hydroxyl protected with DMT). To achieve the goal and objectives of this project various compounds were synthesized and the synthetic procedures and their results are presented in the following sections.

1.3 EXPERIMENTAL

This section describes a general method for synthesis, including the corresponding procedures and equipment used, followed by the procedures for synthesis of various porphyrins. Next, the synthetic procedure of photosensitizers-modified uridine, and the 3'-H-phosphonate of 2'-porphyrin-modified uridine will be described in detail. Finally, the procedure for conjugation of uMUC1 aptamer to the porphyrin and gel analysis of crude product will be described.

1.3.1 General Synthetic Methods

1.3.1.1 Chemicals

Tetrahydrofuran (THF) (Aldrich) was distilled over sodium and benzophenone. Dichloromethane (VWR) and ethyl acetate (Mallinkrodt) were distilled over calcium hydride and stored over 4 Å molecular sieves. N, N'-diisopropylethylamine (DIPEA) (Acros) and pyridine (Sigma) were distilled over potassium hydroxide. Pyrrole was filtered through basic aluminum oxide just before use. Silica gel (60-200 mesh) and basic aluminum oxide (60 mesh) (Fischer Scientific) were used for column chromatography. Pyropheophorbide-a (Fischer Scientific), boron tribromide (Acros), and *n*-BuLi (Strem Chemical) were used as received. All other reagents were bought from Aldrich and used as received. Diphenylphosphite (Fluka), 1-adamantane carboxylic acid chloride (Acros) and dT-H-phosphonate (Glen Research) were also used as received. Silica gel TLC grade 7749 (Aldrich) was used for purifications by Chromatotron. The 2,5-

bis(phenyl(1*H*-pyrrol-2-yl)methyl)thiophene was prepared as described in the literature.⁶⁷

1.3.1.2 Instrument

¹H NMR spectra were obtained at the operating frequency 90 MHz on an Eft NMR, at 500 MHz on a Tecmag Nicolet, and at 400 MHz on a BZH 400/52 Bruker spectrometer. ¹H NMR spectra were referenced to an internal TMS standard. ¹³C NMR spectra were recorded at 22.5 and 166 MHz. The ¹³C NMR spectra were referenced to CDCl₃. ³¹P NMR were recorded at 162 MHz and referenced to an external 85% H₃PO₄. Mass spectra were obtained from JEOL MS and Thermo Feningan LCQ positive ion trap. UV-vis spectra were collected with an Ocean Optics USB 2000 Spectrometer. The synthesis of oligonucleotide was performed on a Beckman Oligo 1000 DNA synthesizer, using cyanoethyl-phosphoramidite chemistry. DNA synthesis columns (empty) were from Applied Biosystems. The phosphoramidite of all four bases (Transgenomic) were dissolved in anhydrous acetonitrile with 3 Å molecular sieves and attached directly to the DNA synthesizer. The synthesizer was operated under an atmosphere of helium gas (99.99% pure). DNA (12-mer) was synthesized in Beckman Oligo 1000 DNA synthesizer and the DNAs (19-mer and 31-mer) with CPG were from Biosynthesis. Orbital Shaker was from Mandel Technology Group (Ontario, Canada). HP Scanjet 4800 series Photo Scanner (Hewlett-Packard Company, Houston, TX) was used for gel scan. Chromatotron was from Harrison Research (Model 7924T, Ser. no Q13, USA). Photon Technology International (PTI) fluorimeter with 814 photomultiplier detection system was used in excitation and emission study of gel.

1.3.2 Synthesis of Monocarboxy Porphyrin.

(a) Synthesis of 5-(4-hydroxyphenyl)-10,15,20-triphenylporphyrin (1)

4-Hydroxybenzaldehyde (244 mg, 2 mmol) was dissolved in CH₂Cl₂, added to silica (1.7 g), and stirred until CH₂Cl₂ was completely evaporated. Subsequently, benzaldehyde (212 mg, 2 mmol) was added to the silica. Next, pyrrole (1.3 mL, 4 mmol) was added to silica (11 g). The samples were combined and heated in a conventional microwave for 10 min (5 × 2 min). The mixture was heated for 2 min, cooled down for 5 min and again heated. This process was repeated for 5 times. The black mass formed was extracted with CH₂Cl₂ in a Soxhlet extractor. The crude material was separated on a silica column eluting with CH₂Cl₂. The second fraction obtained from the column was further purified by Chromatotron using ethyl acetate/hexanes (1:4). After the removal of solvent, a purple solid was obtained (5 mg, 0.9%). ¹H NMR (500 MHz, CDCl₃): δ - 2.82 (s, 2H), 5.00 (s, 1H), 7.15 (d, 2H, *J* = 10 Hz), 7.75-7.69 (m, 9H), 8.03 (d, 2H, *J* = 10 Hz), 8.17 (d, 4H, *J* = 5 Hz), 8.80 (s, 6H), 8.83 (d, 4H, *J* = 5 Hz).

(b) Synthesis of ethyl-5-(4-carboxylatomethoxyphenyl)-10,15,20-triphenylporphyrin (2)

Compound **1** (30 mg, 0.047 mmol) was dried *in vacuo* in a 100 mL flask and flushed with nitrogen. Potassium carbonate (315 mg, 0.704 mmol) and potassium iodide (44 mg, 0.261 mmol) were added to the flask and it was fitted with a rubber septum and flushed with nitrogen. DMF (1.5 mL) and CH₂Cl₂ (4 mL) were added. 2-Chloroethyl acetate (100 μL, 0.704 mmol) was injected into the

flask under nitrogen, the flask was fitted with a condenser, and refluxed for 5 h. The solvent was removed *in vacuo*. After removal of DMF, the reaction mixture was extracted with CH₂Cl₂ and washed with water several times, dried over MgSO₄, and the solvent evaporated to yield a purple solid (32.3 mg, 97.8%). ¹H NMR (500 MHz, CDCl₃): δ -2.79 (s, 2H), 4.4 (q, 2H), 4.91 (s, 2H), 7.29 (d, 2H, *J* = 10 Hz), 7.48 (t, 3H), 7.7 (m, 9H), 8.13 (d, 2H, *J* = 10 Hz), 8.2 (d, 6H, *J* = 10 Hz), 8.83 (s, 6H).

(c) **Synthesis of 5-(4-carboxylatomethyloxyphenyl)-10,15,20-triphenylporphyrin (3)**

Compound 2 (50 mg, 0.069 mmol) was added to a flask followed by 10% potassium hydroxide in 1:1 ethanol: water (30 mL) and refluxed for 18 h. The mixture was cooled to room temperature and diluted with water (10 mL). HCl (0.1M) was added gradually with a dropper until the reaction mixture changed to neutral. Subsequently, CH₂Cl₂ was added and the organic layer was separated, washed with water, and dried with MgSO₄. After evaporation of the solvent, a purple solid was obtained (33 mg, 69.4%). ¹H NMR (500 MHz, CDCl₃) : δ -2.78 (s, 2H), 5.0 (s, 1H), 7.33-7.35 (m, 10H), 7.36 (s, 2H), 7.73-7.76 (m, 7H), 8.15 (d, 2H, *J* = 5 Hz), 8.82 (d, 4H, *J* = 5 Hz), 8.84 (s, 6H).

1.3.3 Aminouridine Porphyrin Coupling Reactions

(a) Synthesis of Aminouridine-Porphyrin Conjugate (4)

5-(4-Carboxylatomethoxyphenyl)-10,15,20-triphenylporphyrin (**3**) (13 mg, 0.018 mmol), **21** (9 mg, 0.018 mmol), EDCI (4.8 mg, 0.027 mmol) and DMAP (< 1 mg) were added to a 25 mL flask. The flask was fitted with rubber septum and flushed with nitrogen. The reaction mixture was dissolved in dry CH₂Cl₂ and stirred at room temperature for 12 h. After the consumption of compound **3**, the reaction mixture was washed with water (10 mL × 3) and dried over MgSO₄. The crude product was purified in a silica column by eluting with CH₂Cl₂/diethyl ether (1:4). After evaporation of solvent, the second fraction was a purple solid (6 mg, 33.3%). Further purification was obtained by repeated recrystallization in ethyl acetate/hexanes. The crystals were dissolved in benzene and dried *in vacuo*. The UV-vis spectrum showed the absorption at 260 nm, 415 nm (Soret band), and at 511, 548, 588 and 644 nm (Q bands)). ¹H NMR (500 MHz, CDCl₃): δ -2.79 (s, 2H), 2.33 (s, 1H), 3.47 (s, 2H), 3.79 (s, 6H), 4.25 (s, 1H), 4.63 (d, 1H, *J* = 5 Hz), 4.81-4.83 (m, 2H), 5.53 (d, 1H, *J* = 5 Hz), 6.26 (d, 1H *J* = 10 Hz), 6.87 (d, 4H, *J* = 10 Hz), 7.31-7.33 (m, 8H), 7.43 (d, 2H, *J* = 10 Hz), 7.62 (d, 1H, *J* = 5 Hz), 7.71-7.78 (m, 10H), 8.07 (s, 1H), 8.18 (d, 1H, *J* = 5 Hz), 8.21 (d, 8H, *J* = 10 Hz), 8.85 (s, 8H). ¹³C NMR (100 MHz, CDCl₃): 169.22, 162.53, 158.79, 158.94, 150.82, 144.07, 142.14, 139.94, 136.30, 135.76, 135.20, 135.07, 130.12, 129.34, 128.17, 128.11, 127.73, 127.24, 126.69, 120.19, 119.23, 113.41, 113.15, 103.36, 102.97, 102.92, 87.31, 86.79, 85.58, 77.33, 77.01, 76.69, 67.57,

63.59, 56.35, 55.27, 55.23, 53.40. The calculated mass was 1216.34 and the observed mass 1216.98.

(b) Synthesis of Aminouridine-Dithiaporphyrin Conjugate (5)

To compound **18** (3 mg, 0.004 mmol), **21** (2 mg, 0.004 mmol), EDCI (1 mg, 0.005 mmol) and DMAP (<1 mg) were added in a 10 mL flask, and it was gently flushed with nitrogen. The reaction mixture was dissolved in dry CH₂Cl₂ (1mL) and stirred at room temperature for 12 h. After the complete consumption of **18**, the reaction mixture was washed with water (10 mL × 3) and dried over MgSO₄. The solvent was evaporated *in vacuo* with benzene. An orange solid was obtained (3 mg, 60.0%). UV-vis (260 nm, 434 nm (Soret band), at 511, 542, 634 and 691 nm (Q bands). ¹H NMR (500 MHz, CDCl₃): δ 3.45 (s, 2H), 3.79 (s, 6H), 4.21 (s, 1H), 4.57 (br s, 1H), 4.82 (m, 3H), 5.52 (d, 1H, *J* = 10 Hz), 6.24 (d, 1H, 10 Hz), 6.86 (d, 4H, *J* = 10 Hz), 7.4-7.2 (m, 10H), 7.61 (d, 1H, *J* = 5 Hz), 7.7 (d, 1H), 7.8 (m, 9H), 8.2-8.1 (m, 8H), 8.49 (s, 1H), 8.6 (m, 4H), 9.68 (s, 4H). The calculated mass was 1250.44 and the observed mass 1250.38.

(c) Synthesis of 2'-pyropheophorbide-a-Modified Uridine (6)

Pyropheophorbide-a (15 mg, 0.028 mmol) and 2'-amino-2'-deoxyuridine (22.9 mg, 0.042 mmol), EDCI (6.3 mg, 0.033 mmol) and DMAP (0.343 mg, 0.0028 mmol) were dissolved in CH₂Cl₂ (5 mL) and stirred at room temperature for 12 h. The progress of reaction was monitored by TLC, and after the complete consumption of pyropheophorbide-a, the crude product was diluted with CH₂Cl₂ (10 mL) and washed with water (3 mL × 4) and dried over MgSO₄. Solvent was

removed in a rotary evaporator. The crude product was then purified in a silica column using 5% MeOH/ethyl acetate. The first faint band was discarded, the second major dark band was collected, the solvent was evaporated and the product was dried *in vacuo*. A dark green solid was obtained (28 mg, 78.4% yield). UV-vis (260 nm, 415 (Soret band), 501, 534, 605, 666 (Q bands)). ¹H NMR (400 MHz, CDCl₃): δ -1.52 (s, 2H), 1.37-1.33 (t, 3H), 1.78-1.70 (m, 5H), 2.57-2.52 (m, 2H), 3.16-3.12 (m, 1H), 3.25 (s, 3H), 3.38 (s, 1H), 3.42 (s, 3H), 3.76 (s, 6H), 4.21-4.17 (m, 2H), 4.38 (d, 1H, *J* = 4 Hz), 4.58-4.56 (q, 1H), 4.76-4.74 (q, 1H), 4.86 (d, 1H, *J* = 20 Hz), 5.36 (d, 1H, *J* = 20 Hz), 5.56 (d, 1H, *J* = 8 Hz), 6.22 (d, 1H, *J* = 8 Hz), 6.31-6.29 (m, 1H), 6.36 (s, 1H), 6.84-6.82 (dd, 4H), 7.23 (d, 2H, *J* = 20 Hz), 7.31-7.28 (m, 6H), 7.42-7.40 (d, 2H, *J* = 8 Hz), 7.68 (d, 1H, *J* = 8 Hz), 7.98 (d, 1H, *J* = 8 Hz), 8.03 (d, 1H, *J* = 8 Hz), 8.50 (s, 1H), 9.34 (s, 1H), 9.98 (s, 1H). ¹³C NMR (400 MHz, CDCl₃): δ 197.54, 174.26, 172.43, 163.71, 160.63, 158.84, 155.60, 151.99, 150.40, 148.80, 145.30, 144.39, 142.09, 140.15, 136.72, 135.56, 135.42, 135.37, 132.04, 130.35, 129.39, 128.41, 128.235, 127.26, 127.06, 122.71, 105.56, 103.45, 97.08, 93.15, 87.23, 86.10, 85.78, 72.16, 64.10, 57.14, 55.39, 52.04, 49.98, 47.72, 34.16, 31.56, 22.96, 19.04, 17.32, 14.40, 12.31, 11.45, 10.05. The calculated mass was 1062.22 and mass observed 1062.20.

1.3.4 Synthesis of Internally 2'-Porphyrin-Modified 3'-H-phosphonate Salt of Uridine

(a) Synthesis of 2'-Porphyrin-Modified 3'-H-phosphonate Salt of Uridine (7)

Compound 4 (20 mg, 0.016 mmol) was dissolved in pyridine (0.5 mL) under nitrogen. Diphenylphosphite (30 μ L, 0.192 mmol) was added gradually with a syringe and stirred at room temperature for 30 min. The progress of the reaction was monitored by TLC (1:1 ethyl acetate/MeOH). Subsequently, Et₃N/H₂O (1:1, 1 mL) was added and stirred under nitrogen for 30 min. The reaction mixture was evaporated in a rotary evaporator to dryness, and the residue was dissolved in CH₂Cl₂ (10 mL), and washed with 5% NaHCO₃ (2 mL \times 2). The CH₂Cl₂ layer was dried over MgSO₄. The solvent was evaporated and the solid residue was dissolved in a minimum quantity of CH₂Cl₂ and precipitated with 1:1 (diethyl ether/hexane). The precipitate was filtered, washed with 1:1 (diethyl ether/hexane), and the precipitate was collected by adding CH₂Cl₂. The solvent was evaporated again and the purple solid was dried *in vacuo* overnight. The dry purple solid weighed (16 mg, 72.3%). ³¹P NMR, ¹H NMR, and mass were as reported previously.²¹⁷

(b) Synthesis of 2'-Dithiaporphyrin 3'-H-phosphonate Salt of Uridine (8)

Compound 5 (10 mg, 0.008 mmol) was vacuum dried and dissolved in pyridine (1 mL) under nitrogen. Subsequently, diphenylphosphite (38 μ L, 0.158

mmol) was added to the solution of compound **5** and stirred for 30 min. To this reaction mixture, Et₃N/H₂O (1:1, 1 mL) was added, and the mixture was stirred under nitrogen for 20 min. The solvent was removed in a rotary evaporator and the crude solid was dissolved in CH₂Cl₂ (5 mL). Then, it was washed with 5% NaHCO₃ (2 mL × 2). Next, CH₂Cl₂ was evaporated in the rotary evaporator. Orange solid was dissolved in minimum quantity of CH₂Cl₂ and precipitated with diethyl ether/hexane (1:1). After the overnight drying *in vacuo*, the precipitate was weighed (8 mg, yield 72.1%). ¹H NMR (400 MHz, CDCl₃): δ 1.26-1.22 (t, 9H), 1.35 (d, 1H, *J* = 8 Hz), 3.01-3.95 (q, 6H), 3.48-3.45 (m, 1H), 3.56 (m, 1H), 3.73 (s, 6H), 4.52 (t, 1H), 4.78 (s, 2H), 5.05-5.01 (m, 1H), 5.17-5.13 (m, 1H), 5.39 (d, 1H, *J* = 8 Hz), 6.28 (s, 1H), 6.47 (d, 1H, *J* = 8 Hz) 7.26 (s, 6H), 7.33-7.29 (m, 6H), 7.81-7.79 (m, 11H), 7.84 (d, 1H, *J* = 8 Hz), 8.17 (d, 2H, *J* = 8 Hz), 8.24-8.22 (m, 7H), 8.29 (d, 1H, *J* = 8 Hz), 8.70-8.67 (m, 4H), 6.69-9.67 (m, 4H), 9.73 (d, 1H, *J* = 4 Hz), 12.00 (s, 1H); (³¹P NMR (162 MHz, CDCl₃) Proton coupled δ_p 4.44 (*J*_{P,H} = 626.94 Hz) and δ_{p-H} 4.38 (*J*_{P,H} = 628.56 Hz) and the proton decoupled δ_p 4.41. The calculated mass for an anion C₇₆H₅₉N₅O₁₁PS₂⁻ was 1313.41 and observed mass for an anion C₇₆H₅₉N₅O₁₁PS₂⁻ 1313.90.

1.3.5 Synthesis of uMUC1 Aptamer- Porphyrin Conjugate (**24**)

First, the DMT moiety was removed from a CPG attached 31-mer uMUC1 aptamer (5' HO-GCTCAAGCAGTTGATCCTTTGGATACCCTGG-CPG 3') (600 nmol) in column using 2% dichloroacetic acid (DCA) in CH₂Cl₂ in a DNA

synthesizer. Next, the column was rinsed with pyridine/acetonitrile (1:1) (1 mL). The 3'-H-phosphonate salt **7** (5 mg, 0.003 mmol) was dissolved in pyridine/acetonitrile (1:1, 200 μ L). Subsequently, the 1-adamantyl carboxylic acid chloride (10 μ L, 0.1M) was mixed with the 3'-H-phosphonate salt **7** of 2'-porphyrin modified uridine solution. Immediately, after activation, the 3'-H-phosphonate salt of 2'-porphyrin-modified uridine was injected with a syringe into the column with the 5'-hydroxyl free 31-mer uMUC1 aptamer. It was allowed to react for 20 – 25 min by circulating the reaction mixture in and out carefully of the column using two syringes. This column was manually rinsed with pyridine/acetonitrile (1:1, 2 mL) followed by CH_2Cl_2 . Afterwards, the column was washed thoroughly with CH_2Cl_2 in a DNA synthesizer to remove unreacted 3'-H-phosphonate derivative of 2'-porphyrin-modified uridine. The CPG-attached uMUC1 aptamer-porphyrin conjugate was injected with NH_4OH (1 mL), and left to precipitate in the refrigerator overnight. Next day, NH_4OH was collected, and again the column was rinsed with NH_4OH (2 mL). The diluted uMUC1 aptamer-porphyrin conjugate showed absorbance for porphyrin at 415 nm ($A_{\text{obs}} = 0.03$) in UV-vis spectrum. The ammonia solution of conjugate was incubated at 55 $^{\circ}\text{C}$ for 3 h. Subsequently, NH_4OH was evaporated in a speed vacuum. The purple residue obtained was resuspended in water (1.2 mL). The UV-vis spectrum of water soluble product showed the porphyrin Soret band at 415 nm.

1.3.5.1 Precipitation of uMUC1 Aptamer-Porphyrin Conjugate (24)

The crude product uMUC1 aptamer-porphyrin conjugate solution (60 μL) was taken in two different microcentrifuge tubes. Sodium acetate (6 μL) (3M 1/10th of crude product sample) and ethanol (1.25 mL) were added respectively in each microcentrifuge tube. Afterwards, the tubes were left inside the freezer overnight. Then, the product was centrifuged at 14,000 rpm for 5 min to form a pellet, and the pellet was dried in a speed vacuum followed by the resuspension in water (500 μL).

1.3.5.2 Gel Analysis of uMUC1 Aptamer-Porphyrin Conjugate (24)

Acrylamide gel 25 mL (16%) was prepared by mixing 28% Bis-acrylamide (14.3 mL), 10 \times Tris-Borate-EDTA (TBE) buffer of pH 8.1 – 8.3 (2.5 mL), glycerol (2.5 mL), and freshly prepared ammonium persulfate (1.6% (w/v), 1.63 mL). The total volume was adjusted to 25 mL and a catalytic amount TEMED (20 μL) was added prior to pouring the gel. After, the gel was poured, it was allowed to polymerize for at least one hour before loading sample. Gel loading indicator solution (Blue JuiceTM) 1/10th of sample volume was added to the resuspended product **24** in water after precipitation with ethanol without further concentration. Lane 1 was loaded with ladder DNA (5 μL) and the compound **24** sample (20 μL) was loaded in lane 2 of gel by using micropipette. The gel was run at 150 V for 10 h using a Hoeffer MiniVE, vertical electrophoresis mini gel system. Stains-All 100 mL was prepared by mixing Stains-AllTM of 0.005% (w/v),

formamide of 10% (v/v), isopropanol of 25% (v/v), trizma HCl (pH 8.8, 15 mL) and nanopure water 65% (v/v). Then, the gel was stained in Stains-All overnight with continuous shaking in Orbital Shaker. Afterwards, the gel was exposed to air, washed with water, and scanned in HP-Scanjet 4800 series Photo Scanner with resolution of 3600 dpi (Fig 1.19(A)). Two bands were visible in lane 2. The first dark band and a second faint band were sliced into small pieces by razor blade (sterilized in Bunsen flame) and used for fluorescence study. The fast moving dark band did not show any fluorescence emission for porphyrin. The second faint band when excited at 410 nm showed an emission spectrum for porphyrin at 648 nm. The band that showed an emission spectrum was cut and crushed into pieces by the razor blade. Subsequently, pieces of gel were soaked into 2 mL crush and soak solution (3M NaCl) in a microcentrifuge tube, and vortexed overnight at room temperature. After vortexing, liquid was transferred into a Nanosep column and spun at 13,200 rpm for 3 min, and the supernant was collected and transferred to another Nanosep MW (3 kD) and was spun at 6000 rpm until the volume was decreased to 100 μ L. Then, the total volume was diluted to 1000 μ L and the emission of porphyrin was measured in a fluorimeter but no emission was observed. The crushed gel was transferred into the cuvette, and excited at 410 nm in fluorimeter. The emission spectrum at 648 nm for porphyrin was observed in crushed gel.

1.4 RESULTS AND DISCUSSION

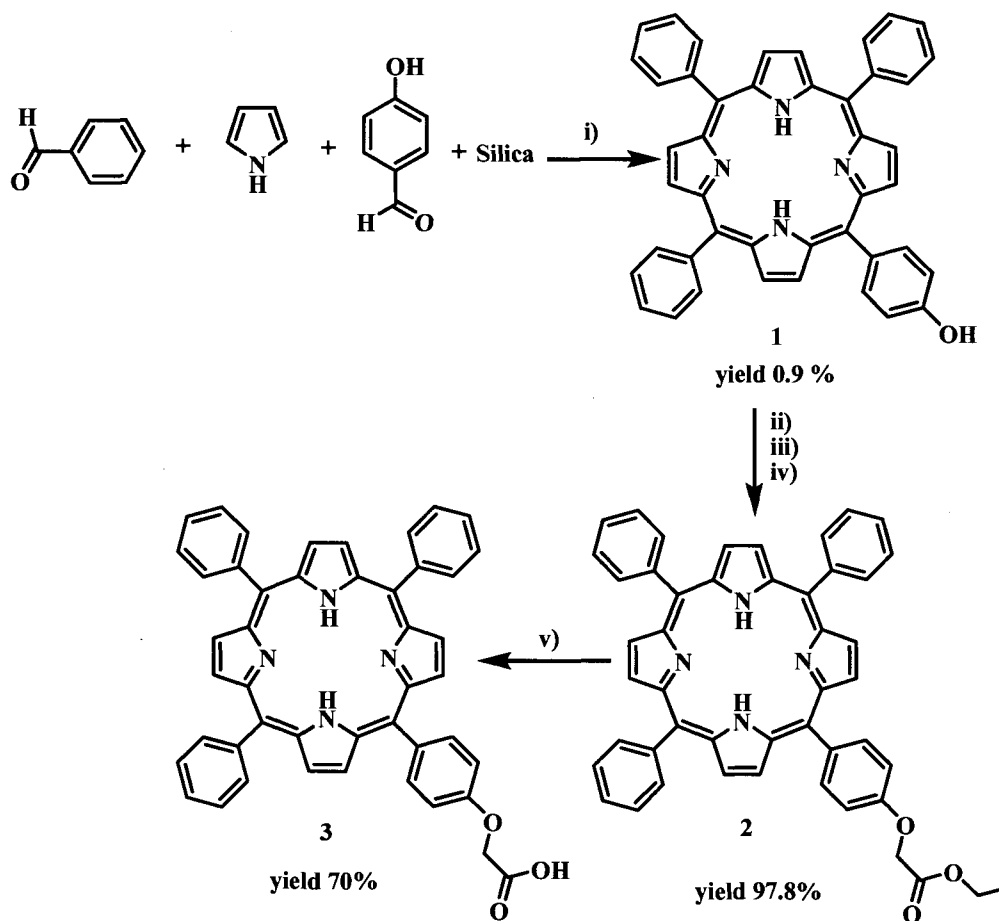
In this section, the results of synthesis of three different types of photosensitizer-nucleoside monomers are described, followed by a discussion of the synthesis of 3'-H-phosphonate derivatives of 2'-porphyrin-modified uridine. Next, the discussion of the synthesis of photosensitizer-oligonucleotide conjugate by using phosphoramidite chemistry, and why it was switched to H-phosphonate method will be described. Synthesis of 3'-H-phosphonate derivative followed by conjugation of 2'-porphyrin-modified 3'-H-phosphonate derivative to a solid support attached oligonucleotide, and the results will be discussed. Finally, benefits of internal modification will be described in brief prior to the result and discussion of synthesis of uMUC1 aptamer-porphyrin conjugates.

1.4.1 Synthesis of Photosensitizer-Nucleoside Monomers

Carboxylic acid functionalized porphyrin **3** was synthesized by modifying a literature procedure²¹⁸ as shown in Scheme 1.1. Aid functionalized porphyrin **3** efficiently coupled with 2'-amino-2'-deoxyuridine minimizing side products. A one-step microwave synthesis of 5-(4-hydroxyphenyl)-10,15,20 triphenyl porphyrin **1** was successfully carried out by modifying the literature procedure.²¹⁹ A microwave synthesis was preferred over the stepwise synthesis of porphyrin **1**, which is expensive and time consuming. Benzaldehyde and p-hydroxybenzaldehyde (3:1 mole ratio) resulted in major product tetraphenylporphyrin. Benzaldehyde and p-hydroxybenzaldehyde 1:1 resulted in

0.9% yield of **1**, and minimized the formation of the tetraphenylporphyrin. In the first trial purification, a Cromatotron was used to purify **1**, but later purification of **1** was easily obtained by using CH₂Cl₂ and a silica column. The second band from the column was collected, and after evaporation of CH₂Cl₂, the purple solid obtained was **1** and showed impurities on TLC. Compound **1** along with the impurities that came off from the column purification were dried overnight *in vacuo*. These impurities were found to be very soluble in methanol while **1** is insoluble in methanol. Thus, impurities were washed with methanol until **1** showed a single spot in TLC. Purified **1** was obtained in 0.9 – 1% yield. Afterwards, compounds **2** and **3** were synthesized by the modification of the literature procedures.²¹⁸ Synthesis of compound **2** required reflux at a high temperature (150 °C), and the synthesis of compound **3** needed careful neutralization of the reaction mixture before purification. Very dilute HCl (0.1M) was used with constant pH checks while reaction mixture was neutralized. Loss of the product resulted when excess of acid was added. The purified compound **3** was obtained in 55 – 70% yield.

Scheme 1.1



Scheme 1.1 Synthesis of mono acid functionalized porphyrin. i) Microwave 10 min, ii) KI/K₂CO₃, iii) DMF/CH₂Cl₂, iv) ClCH₂COOC₂H₅, v) 10% KOH (ethanol/water 1:1), 16 h reflux.

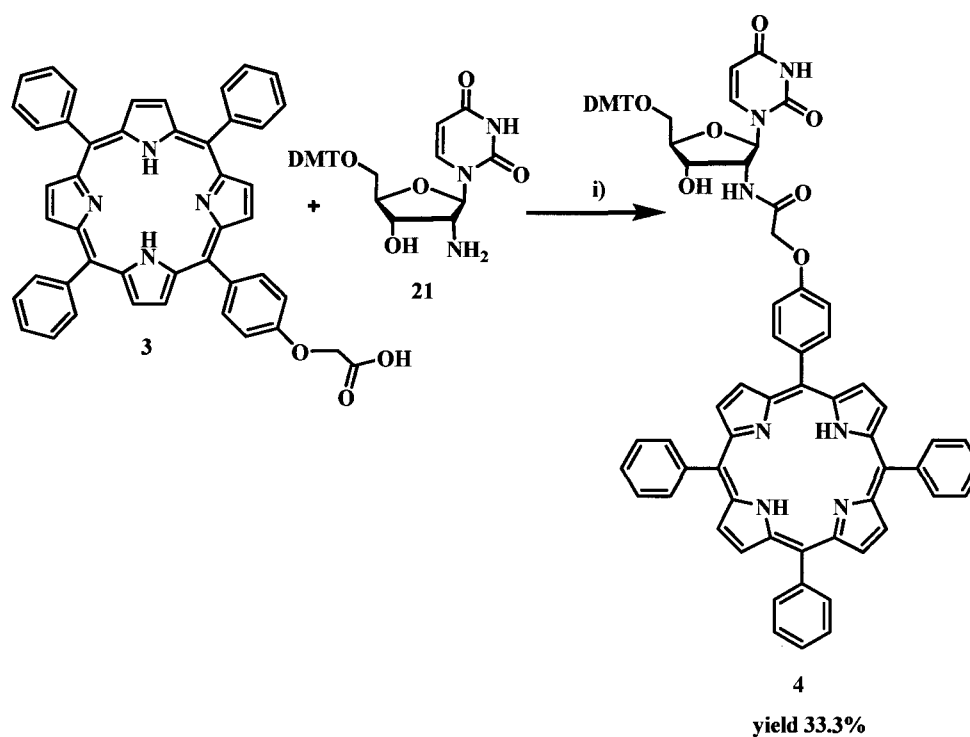
1.4.1.1 2'-Amino-2'-doxyuridine (5'-Hydroxyl Protected with DMT)

The 5'-DMT protected 2'-amino-2'-deoxyuridine **21** was synthesized following the literature procedure¹⁸⁷ as shown in Appendix B (details in Appendix).

1.4.1.2 2'-Porphyrin-Modified Uridine

Compound **4** was synthesized by EDCI coupling in a 33.3% yield, as shown in Scheme 1.2. Column purification was used to separate a large amount of side product that formed and excess of mono acid functionalized porphyrin. Diethyl ether/CH₂Cl₂ (1:4) separated compound **4** on a silica column very well. The mass of **4** showed a molecular ion peak at 1279.31 along with molecular ion peaks at 1280.32 and 1281.32 for possible isotopes of the compound. The UV-vis spectra of different porphyrin conjugated to aminouridine are shown in Fig 1.15. The conjugated product **4** showed a) absorption at 260 nm for uridine, b) intense Soret band at 415 nm and Q bands at 511, 548, 588, and 644 nm for porphyrin.

Scheme 1.2



Scheme 1.2 Synthesis of 2'-porphyrin-modified uridine. i) EDCI/DMAP, CH_2Cl_2

1.4.1.3 2'-Dithiaporphyrin-Modified Uridine

Dithiaporphyrins are potential photosensitizers for PDT since they produce enough singlet oxygen and absorb in near infrared.⁶⁷ This project worked on synthesis of dithiaporphyrin-modified uridine which can be conjugated to aptamer. Compound 5 was synthesized from 18 and 21 by the EDCI coupling

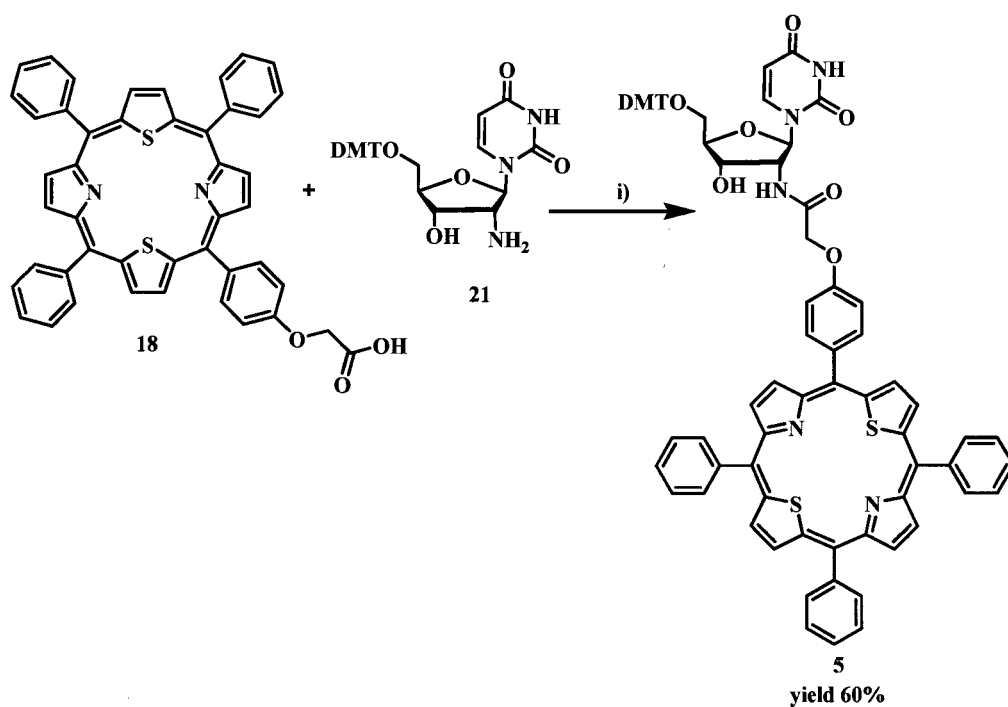
method, and the purified product was obtained in 60% yield as shown in Scheme 1.3. Dithia core-modified porphyrins are known to absorb at longer wavelengths of light as compared to typical porphyrin.^{66,67} Mono acid functionalized dithia core-modified porphyrin was synthesized using a stepwise method by following the modifications of literature procedure⁶⁷ as shown in appendix A.

Compound **9** [4-methoxy-phenyl-1-hydroxymethyl]thiophene was synthesized from thiophene (Appendix A). The hydroxyl group of [4-methoxy phenyl-1-hydroxymethyl]thiophene was protected with TBDMS, compound **10** (detail in Appendix A). Compound **11** was synthesized from compound **10** and from benzaldehyde (detail in Appendix A). Unsymmetrical diol 2-(1-(4-methoxyphenyl)-1-hydroxymethyl)-5-(1-phenyl-1-hydroxymethyl)thiophene **12** was synthesized from compound **11** ((tert-butyldimethylsilyloxy)(4-methoxyphenyl)methyl)thiophene-2-yl)(phenyl)methanol by removal of TBDMS protecting group (detail in appendix A). Symmetrical diol **13** was synthesized from thiophene and benzaldehyde (detail in Appendix A). After the synthesis of symmetrical diol, it was converted to half core-modified porphyrin **14** (Appendix A). Synthesis of dithia-core-modified-mono-methoxy functionalized porphyrin **15** was synthesized from compound **14** and compound **12** (as described in Appendix A). Compound **16**, compound **17**, and compound **18** were synthesized (detail in Appendix A) by following the literature procedure.⁶⁷

Compound **5** was synthesized from compound **18** and compound **21** by EDCI coupling as shown in Scheme 1.3. Compound **5** was purified by using a silica column as in compound **4**. The purified 2'-dithiaporphyrin-uridine conjugate

was prepared in 60% yield. The UV-vis spectrum (Fig 1.16 green trace) of compound **5** showed a Soret band at 434 nm, and Q bands at 511, 542, 633, and 691 nm, indicating longer wavelength absorbance for dithiaporphyrin. A mass spectrum of **5** showed a molecular ion peak at 1250.38, along with possible isotope peaks at 1251.39, 1252.39, 1253.39, and 1254.39 (mass spectrum is not shown here).

Scheme 1.3

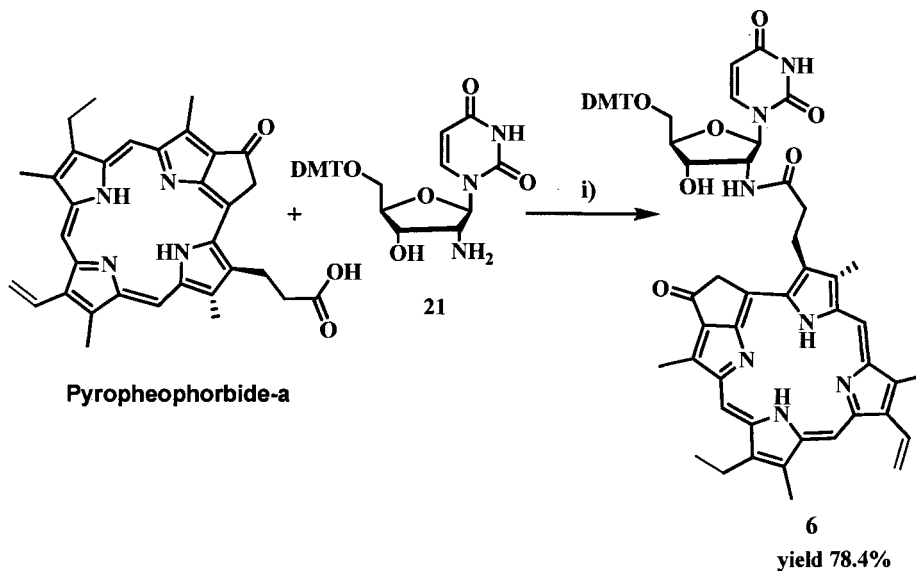


Scheme 1.3 Synthesis of 2'-dithiaporphyrin-modified uridine. i) EDCI/DMAP, CH₂Cl₂/12 h at room temperature.

1.4.1.4 2'-Pyropheophorbide-a-Modified Uridine

Commercially available pyropheophorbide-a was conjugated with **21** by EDCI coupling, as shown in Scheme 1.4. Purification of compound **6** was successfully carried out in a silica column using the same solvent as for compound **4**, and exposure to light was minimized during purification. The purified product **6** was dark green, formed in 78.4% yield. Upon exposure to light, **6** decomposed, and TLC of the purified product showed new spots.

Scheme 1.4



Scheme 1.4 Synthesis of 2'-pyropheophorbide-a-modified uridine. i) EDCI/DMAP, CH_2Cl_2 /12 h at room temperature.

UV-vis spectrum of conjugate **6** (Fig 1.16 blue trace) showed absorption at 260, 415 (Soret band), 501, 534, 605, and 666 nm (Q bands). The UV-vis spectra showed minimal absorbance for uridine at 260 nm and an intense Soret band for porphyrin in all conjugates. A mass spectrum of **6** showed a molecular ion peak at 1062.20 which is equivalent to the calculated mass. The molecular ion peaks for possible isotopes of compound **6** at 1061.20, 1063.20, and 1064.20 also appeared in the spectrum.

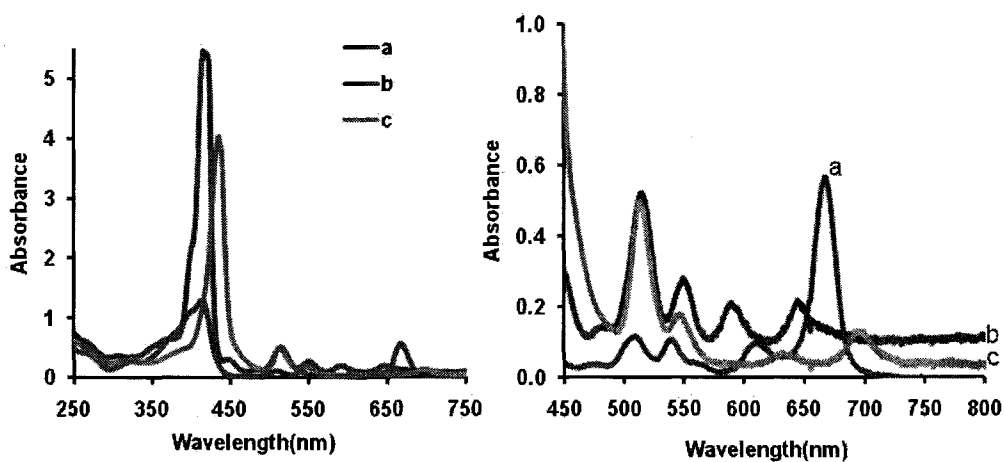


Figure 1.16 UV-vis of 2'-photosensitizers-modified uridine in CH_2Cl_2 . a – 2'-pyropheophorbide-a, b – 2'-porphyrin, c – 2'-dithiaporphyrin.

1.4.2 Synthesis of Photosensitizer-Nucleic Acid Conjugates

Internally 2'-photosensitizers-modified nucleosides, as shown earlier in this section, have 5'-hydroxyl protected with DMT and 3'-hydroxyl free. The 3'-hydroxyl of these nucleosides can be converted into 3'-phosphoramidite or 3'-H-phosphonate derivatives which can be undertaken in a solid phase automated DNA cycle. Thus, the first attempt was to synthesize the 3'-phosphoramidite derivative of compound **4**, as described next.

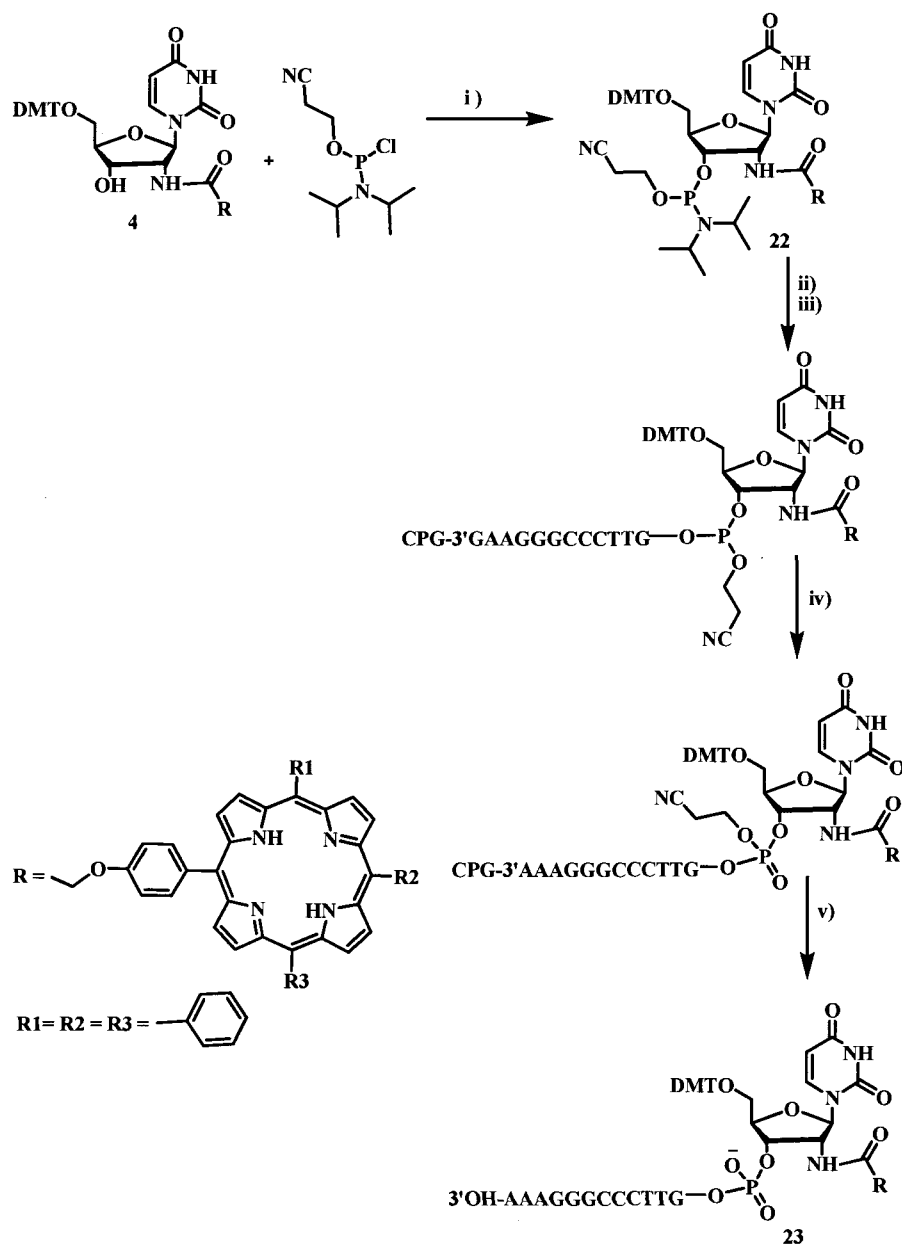
1.4.2.1 Phosphoramidite Chemistry

Synthesis of porphyrin-DNA conjugates most commonly uses phosphoramidite chemistry. The synthesis of phosphoramidite of compound **4** was attempted a few times, as in Scheme 1.5. The formation of compound **22** (step i) was monitored by TLC. The starting compound **4** changed to a new compound with higher R_f than compound **4**. However, purification of the product **22** was found to be challenging and was not achieved. Excess DIPEA added was removed *in vacuo* before the coupling (step ii). Phosphoramidite **22**, on exposure to air changed to a more polar compound as observed in TLC. The coupling of crude phosphoramidite with DMT off 12-mer DNA (3' CPG-GAAGGGCCCTTG-OH 5') attached to CPG (step iii) was performed in a DNA synthesizer as well as in a separate flask. Iodination (step iv) was continued in the DNA synthesizer. Then, the DNA was removed from CPG (step v), and the deprotection of β -cyanoethyl group was performed by incubation at 55 °C for 2 h. After a butanol wash and

drying over a speed vacuum, compound **23** was found to be slightly purple. The compound **23** was dissolved in water for HPLC analysis. The HPLC did not show a peak in a chromatogram for Soret band at 417 nm of porphyrin but there was an intense peak for uncoupled DNA at 260 nm. It was expected that the crude product would have interfered in coupling, or the concentration of phosphoramidite **22** was too low to yield compound **23**. It was also expected that a very small amount of compound **23** had coupled since the slightly purple color of porphyrin was observed after cleavage of CPG and speed vacuum drying. The repeated experiment after cleavage from CPG was followed by UV-vis absorption. The UV-vis spectrum did not reveal any absorption for porphyrin at 417 nm. The remaining crude product after exposure to air was found to have a lower R_f than compound **23**. Then, an attempt was made to separate the crude product in a silica column, but the product after the column showed a few different R_f spots in the TLC. Since unreacted starting material was present in the crude product, NMR was not helpful to analyze the product.

The 3'-H-phosphonate derivatives of the compound **4** is another route of synthesis of porphyrin-modified DNAs on solid phase support. This project has synthesized the 3'-H-phosphonate derivative of compound **4**, in order to use it in an automated DNA synthesis cycle.

Scheme 1.5



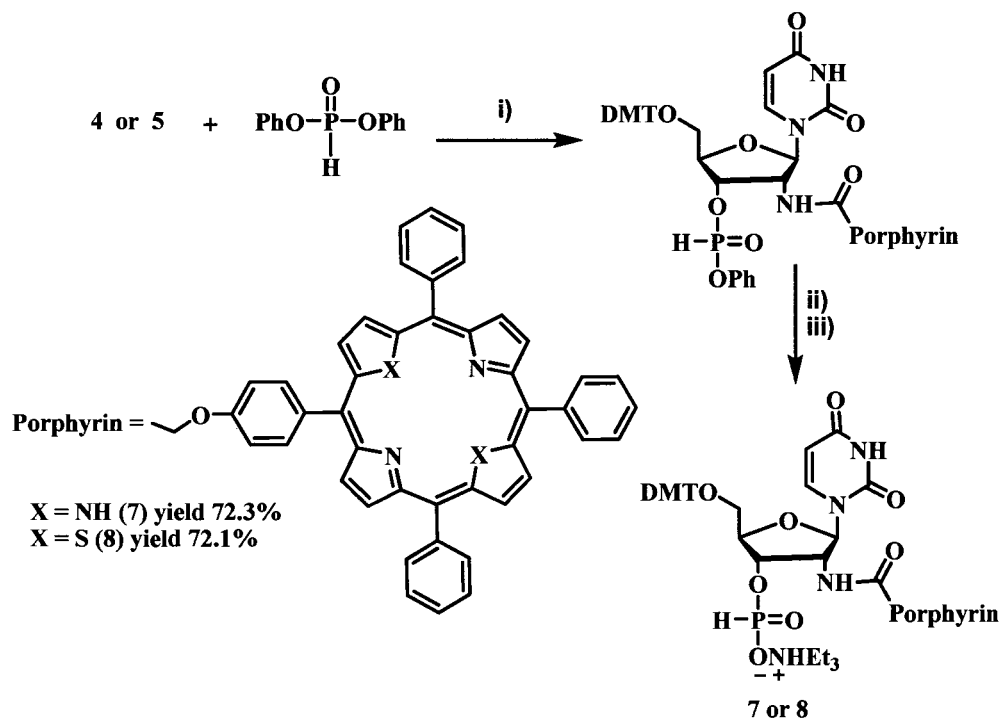
Scheme 1.5 Solid phase synthesis of porphyrin-DNA conjugate by using 3'-phosphoramidite of 2'-porphyrin-modified uridine. i) DIPEA/ethyl acetate, ii) ETT/tetrazole, iii) CPG-3'GAAGGGCCCTTG-OH 5', iv) I₂/pyridine/H₂O (trace), v) 30% NH₄OH 12 h at 4 °C.

1.4.2.2 3'-H-phosphonate Chemistry

Since phosphoramidite **22** was prone to oxidation, it was challenging to conjugate porphyrin with DNA. An alternative for phosphoramidite is 3'-H-phosphonate method. The coupling efficiency of H-phosphonate monoester to diester is known to be high and is more stable compared to corresponding phosphoramidite derivative;^{153,220} and can be recovered after experiment.²²¹ Therefore, the 3'-H-phosphonate method was chosen to accomplish the coupling of DNA with 2'-porphyrin-modified 3'-H-phosphonate salt of uridine as described in reference.²¹⁷ The 3'-H-phosphonate salt **7** was synthesized as in Scheme 1.6. The conversion of compound **4** to **7** was monitored by TLC and the appearance of a new spot with lower R_f than the compound **4** and disappearance of compound **4** was an indication of formation of an intermediate product. Further identification of the intermediate was not carried out at this step and was converted to salt form compound **7** by addition of triethylamine/water (1:1) as mentioned in literature.²²¹ TLC of the salt form of compound **7** did not show any change in R_f compared to intermediate compound. After work up (detail in experimental section), the product was precipitated with diethyl ether/hexane (1:1). Excess diphenylphosphite (8 – 10 equiv) was added in order to achieve complete conversion of starting compound to **4**. More than 30 min reaction time did not result in a high yield of product. Rather it resulted in oxidation of H-phosphonate which was disadvantageous. ¹H NMR of the oxidized product did not show a peak for proton at δ 12 ppm. After synthesis, crude product was precipitated by diethyl ether/hexane (1:1) and after vacuum drying, the product was directly used in coupling to a CPG attached DNA and

aptamer. Further purification of H-phosphonate salt **7** in a silica column destroyed the properties of 3'-H-phosphonate. After silica column, the purified product showed a single spot in TLC. Even though the R_f value of product was not changed before and after silica column, the ^1H NMR showed a missing peak at δ 12 ppm, and ^{31}P NMR did not show coupled signal of phosphorus with hydrogen indicating that the product no longer has hydrogen attached to the phosphorus. The 2'-dithiaporphyrin-modified H-phosphonate salt **8** was synthesized as in Scheme 1.6 by following the procedures of compound **7**. However, excess of diphenylphosphite was added in compound **5**. Removal of excess diphenylphosphite was found difficult and it showed up in ^{31}P NMR.

Scheme 1.6



Scheme 1.6 Synthesis of 3'-H-phosphonate of 2'-porphyrin-modified uridine. i) Pyridine/30 min at room temperature, ii) $\text{Et}_3\text{N}/\text{H}_2\text{O}$ (1:1), iii) 20 min at room temperature, X = NH (**7**), X = S (**8**)

^{31}P NMR spectra of compound **8** are as shown in Fig 1.17. Proton decoupled and proton coupled spectra of compound **8** showed a small amount of diphenylphosphite present in the product. The signals at δ 1.07 present in proton decoupled spectrum and δ_{P} 1.08 ($\delta_{\text{P,H}} = 636 \text{ Hz}$) in proton coupled spectrum are due to diphenylphosphite present in the product. ^1H NMR of both compound **7** and

8 showed peaks for triethylammonium salt at δ 1.32 (t) and δ 3.72 (q) and H-phosphonate at δ 12.00 (s). The 3'-H-phosphonate salt of **6** was also synthesized following the procedure used for **7** and **8**. Formation of 3'-H-phosphonate salt of compound **6** was monitored by the TLC. ^{31}P NMR spectra of H-phosphonate salt of **6** showed signal at δ_{P} 4.4 ($J_{\text{P,H}} = 640$ Hz) and δ_{P} 4.34 ($J_{\text{P,H}} = 638$ Hz) for proton coupled and at δ_{P} 4.37 for decoupled.

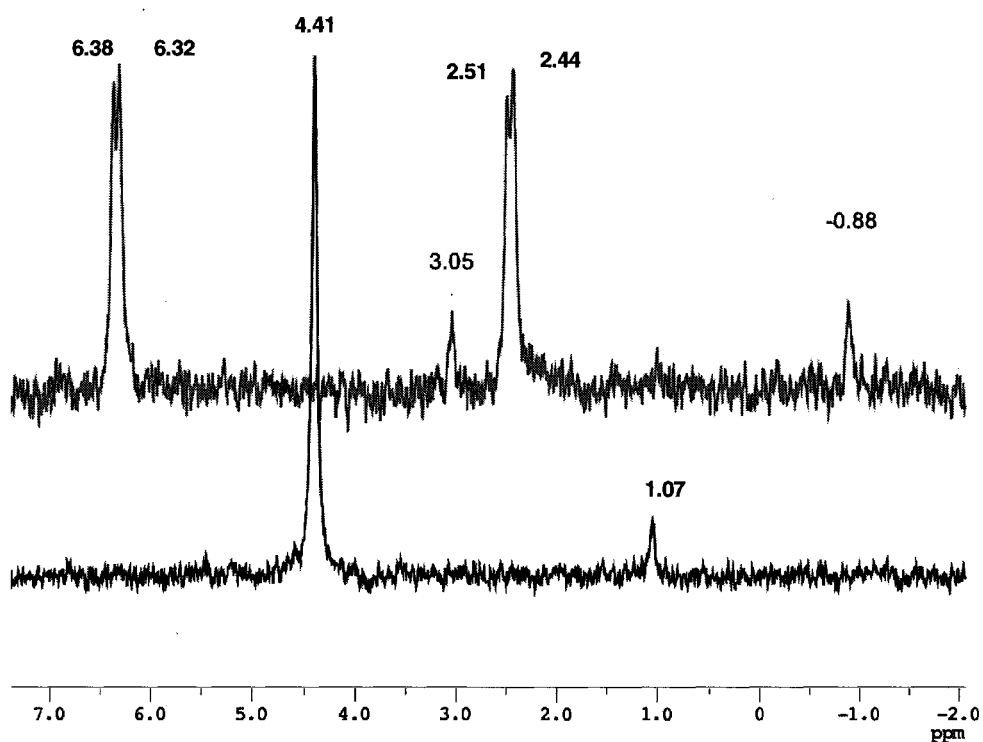


Figure 1.17 ^{31}P NMR spectra of compound **8** (162 MHz, CDCl_3). Proton decoupled (black), and ^{31}P and proton coupled (pink).

When ^{31}P NMR of 3'-H-phosphonate of compound **6** was integrated, it was found that diphenylphosphite was four times as compared to 3'-H-phosphonate salt of compound **6** (^{31}P NMR spectra are not shown here). Excess of diphenylphosphite present in product decreased the stability of 2'-pyropheophorbide-a-modified H-phosphonate derivative. A continuous shift in signals in proton coupled and decoupled ^{31}P NMR spectra were observed indicating that 2'-pyropheophorbide-a-modified H-phosphonate salt of compound **6** was not as stable as compound **7** and **8**. Finally, after three days of synthesis of product, only one signal in the proton-coupled ^{31}P NMR spectrum was observed suggesting that the product had oxidized.

In a trial experiment, H-phosphonate salt **7** was coupled with a single guanine nucleoside (3' CPG-G-OH 5') attached to a solid support. In coupling step, the H-phosphonate salt **7** (pyridine/acetonitrile 1:1) in the presence of coupling reagent 1-adamantane carboxylic acid chloride (0.5 equiv of compound **7** in pyridine/acetonitrile 1:1) was manually injected in a column with solid support attached DMT-off G (guanine nucleoside). After coupling time (20 min), the column was washed with pyridine (2 mL) followed by CH_2Cl_2 (10 mL) several times until the wash showed no absorbance for porphyrin in UV-vis spectra. Subsequently, a mild deblocking reagent, 2% DCA in CH_2Cl_2 was injected into the column. The orange color of DMT cation came off from the column indicating that compound **7** had coupled to guanine nucleoside. After cleavage of solid support with NH_4OH , the UV-vis spectrum in NH_4OH solution was checked. The NH_4OH solution showed absorption in UV-vis spectrum only at 260 nm, indicating that

there was no porphyrin-oligonucleotide conjugate present in NH_4OH solution. However, it was suspected that the number of nucleotides in the conjugate was only two so the porphyrin conjugated product is more hydrophobic and must be insoluble in water and NH_4OH . Subsequently, the column was washed with methanol and the UV-vis spectrum of the collected methanol was checked, and it showed very small absorption for both porphyrin and nucleotides in UV-vis spectrum (spectrum not shown). Negligible product (dinucleotide-porphyrin conjugate) had formed and further characterization was not carried out. After successful result of coupling of H-phosphonate **7** with a single nucleoside, the 19-mer DNA was coupled with compound **7** and additional three bases were added as described in reference.²¹⁷

1.4.3 Benefits of Internal Modification Approach

Internally modified bases have been commonly used for modifying DNAs. Such bases, for example a 3'-H-phosphonate of 2'-porphyrin-modified uridine is as shown in Scheme 1.6, can undergo solid phase automated DNA synthesis cycle. By using internally 2'-porphyrin-modified nucleosides, the DNA cycle can be continued and additional commercially available bases, as well as the 2'-porphyrin-modified nucleoside itself can be repeatedly added along the growing DNA scaffold. In this way, a variety of modifications can be introduced in both DNA and RNA. Another benefit of an internally modified nucleoside is that the terminal modification of DNA with an amine and other functional groups prior to the coupling step is not required. Furthermore, internally modified nucleosides

undergo solid phase automated synthesis so the purification of product from the rest of reactant used in synthesis is simplified. In addition modification at the 2'-position of nucleoside does not disrupt base pairing of DNA (described in internal modification section). Moreover, another advantage of an internally porphyrin-modified base is that it can be used to create supramolecular porphyrin arrays on DNA scaffold by using solid phase synthesis as shown in Fig 1.1(B). The H-phosphonate derivatives of 2'-porphyrin- and dithiaporphyrin-modified uridine developed in this research can be efficiently positioned along a DNA strand for the construction of supramolecular arrays so that their interesting photophysical properties can be studied. In this project, internally 2'-porphyrin-modified 3'-H-phosphonate nucleoside has been used to conjugate uMUC1 aptamer to the porphyrin by using solid phase synthesis.

1.4.4 uMUC1 Aptamer-Porphyrin Conjugate

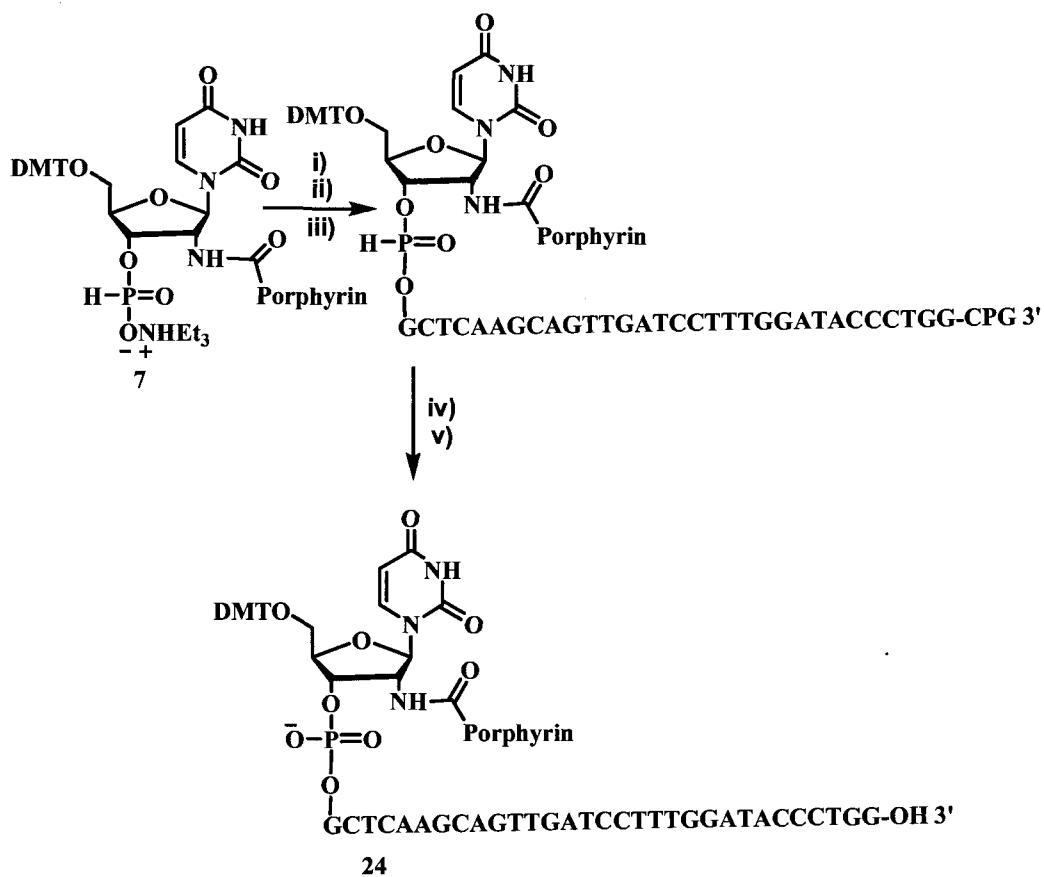
Recently, uMUC1 aptamer was selected for its affinity to bind to the core peptide APDTRPAPG, which can be expressed in epithelial cells of various cancer tissues (section 1.1.9). Most recently, Tan and co-workers have conjugated the TD05 aptamer to the Chlorine-e₆ (Ce₆) photosensitizer by using the 5'-amine modified aptamer.⁶⁹ In their work, TD05 aptamer-Ce₆ conjugate has shown specific binding to Ramos cell and its binding efficiency did not decrease after conjugation with the photosensitizer. At the same time, the properties of the photosensitizer were also conserved after conjugation with the aptamer.²²² In another work, the same group investigated aptamer-photosensitizer conjugate

absorbed onto the single-walled carbon nanotubes (SWNT) surface. Afterwards, the target was applied onto the surface of SWNT, which resulted in significant increase in fluorescence intensity of conjugate. Their results indicated that aptamer-photosensitizer conjugate can selectively trigger the target and enhance the effectiveness of PDT.

In contrast to the synthesis of 5'-photosensitizer-aptamer conjugate as described in the literature, this project succeeded in conjugating porphyrin to both 2'-position of DNA and uMUC1 aptamer by using the H-phosphonate approach in solid phase. In one experiment, 19-mer DNA was conjugated to the porphyrin as described in reference 217. After successful coupling of 19-mer DNA to the 3'-H-phosphonate salt **7**, the synthesis of uMUC1 aptamer-porphyrin conjugate was performed. The 31-mer uMUC1 aptamer (5' HO-GCTCAAGCAGTTGATCCTTTGGATACCCTGG-CPG 3') attached to a solid support (5'-hydroxyl protected with DMT) was bought from Biosystems and was packed in a DNA synthesis column. Conjugation of uMUC1 aptamer to 3'-H-phosphonate salt **7** was carried as shown in Scheme 1.7. After the removal of DMT from uMUC1 aptamers, 3'-H-phosphonate salt **7** in pyridine/acetonitrile (1:1) was activated by 1-adamantane carboxylic acid chloride and immediately coupled to uMUC1 aptamers in order to obtain 2'-porphyrin-modified uMUC1 aptamer **24**. The 3'-H-phosphonate and 1-adamantane carboxylic acid chloride (4:1) in excess mole ratio was used and the coupling time was increased to 20 min. Typically, coupling time in automated DNA synthesizer is 1 – 2 min for H-phosphonate but it was increased in this experiment to increase coupling efficiency of 2'-porphyrin-

modified H-phosphonate. During the coupling time light was avoided. After coupling, the column was washed with pyridine and acetonitrile until the absorption of porphyrin of the last wash was not observed in UV-vis spectrum. Subsequently, the column was washed by using CH_2Cl_2 in the DNA synthesizer and the washing was repeated several times in order to confirm that the excess of porphyrin-modified H-phosphonate **7** was washed from the column. Since porphyrin is slightly soluble in acetonitrile, washing the column needs either pyridine or CH_2Cl_2 in order to remove the excess of porphyrin modified **7** used in synthesis. The solid support of the uMUC1 aptamer was deprotected by using 30% NH_4OH at 4 °C overnight.

Scheme 1.7



Scheme 1.7 Synthesis of uMUC1 aptamer-porphyrin conjugates. i) Pyridine/acetonitrile (1:1), ii) 1-adamantane carboxylic acid chloride, iii) CPG attached uMUC1 aptamer, iv) I₂ in pyridine/water (trace), and v) 30% NH₄OH.

The UV-vis spectrum of collected NH₄OH solution showed absorption of an optical density 0.03 for the Soret band of porphyrin at 421 nm (as shown in Fig 1.18). However, absorption for Q bands and nucleotides were not clearly visible.

As compared to the 31-mer nucleotide, only one porphyrin unit was conjugated to the aptamer. Thus, porphyrin absorption was very small in ratio compared to DNA absorption in the UV-vis spectrum. Conjugate **24** was precipitated by ethanol precipitation method (detail in experimental section). After precipitation, it was speed vacuumed and the precipitate was solubilized in water while UV-vis was checked again. Absorbance for porphyrin Soret band (similar to that shown in Fig 1.18) was observed, indicating that a water-soluble uMUC1-porphyrin conjugate had formed.

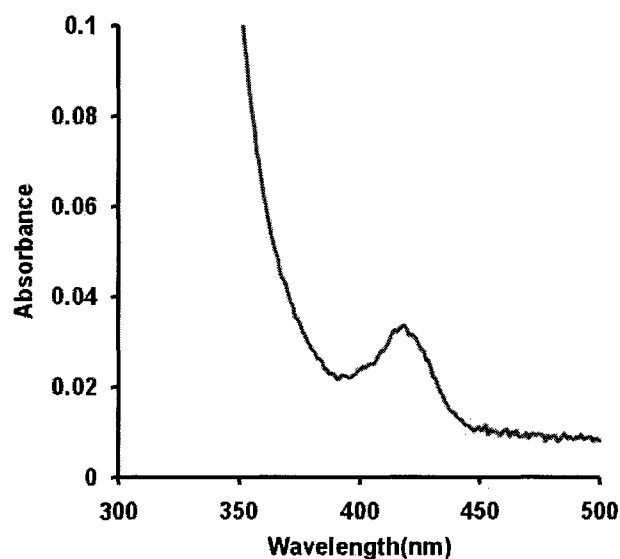


Figure 1.18 UV-vis spectrum of uMUC1 aptamer-porphyrin conjugate **24** in NH_4OH , porphyrin Soret band absorption at λ_{max} 421 nm.

Further purification of the uMUC1 aptamer-porphyrin was carried out by gel electrophoresis. Polyacrylamide gel (16%) was run for uMUC1 aptamer porphyrin **24** for 10 h at 150 V. After 5 h in Stains-All, the stained gel showed two visible bands for DNA as shown in Fig 1.19(A) (lane 2). The slow moving band was cut and the gel was directly scanned in a fluorimeter. Excitation was carried at 410 nm and emission of gel was observed at 648 nm as shown in Fig 1.19(B), which is similar to the emission of porphyrin (spectrum not shown here). However, the fast moving band scanned in the fluorimeter did not show any emission for porphyrin indicating that there is no porphyrin present. The slow moving band (lane 2 in Fig 1.19(A)) was soaked in crush-and-soak solution (3M NaCl) at room temperature and vortexed overnight. The solution after filtration through a nanosep MF column, was spun at 13,200 rpm for 3 min. The supernant collected was transferred to another nanosep MF of molecular weight (3 kD), and was spun at 6200 rpm until volume decreased to 100 μ L. The 50 μ L of this was diluted to 1000 μ L and emission of porphyrin was checked in fluorimeter but no emission was observed (spectrum not shown here). However, crushed gel itself showed emission at 648 nm for porphyrin. Aptamer-porphyrin conjugate was not easily released from polyacrylamide gel.

The control experiment of the gel without loading any sample was also performed. The gel was excited at 410 nm, but this gel did not show any emission (spectrum not shown here). The control experiment of porphyrin was also performed, and it showed emission at 648 nm similar to that of uMUC1 aptamer-porphyrin conjugate (spectrum not shown here).

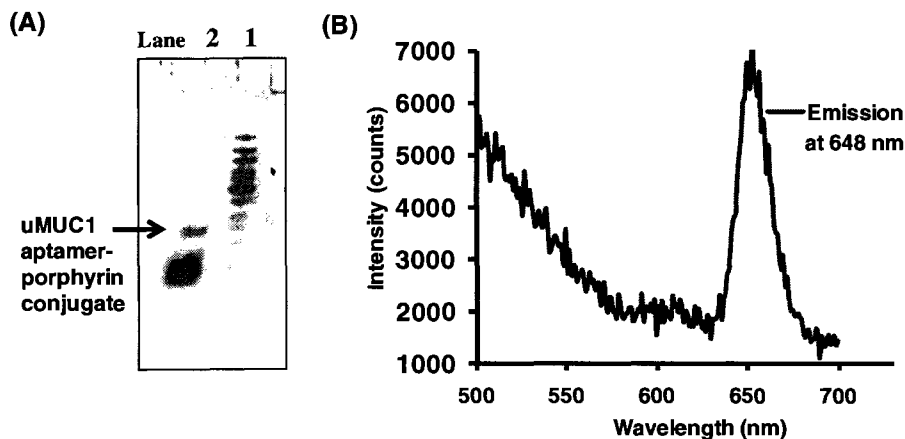


Figure 1.19 (A) Polyacrylamide gel of the uMUC1 aptamer-porphyrin conjugates after scanned in HP Photo Scanner. Lane 1 – ladder DNA and Lane 2 – uMUC1 aptamer (fast moving band) and uMUC1 aptamer-porphyrin conjugate (slower moving band) (B) Fluorescence emission spectrum of gel (lane 2 – slower moving band) excitation at 410 nm and emission at 648 nm.

From gel analysis, it was observed that coupling efficiency of porphyrin to uMUC1 aptamer was not high. Since coupling efficiency was observed to be low in gel analysis, it was a challenge to purify compound **24** by HPLC and gel.

1.4.4.1 Applications of Porphyrin-uMUC1 Aptamer Conjugate

An uMUC1 is a common tumor marker expressed in various types of cancer such as breast, bladder, colorectal, prostate, lung, and gastric (as detailed in the introductory section). A recent study tested radiolabeled uMUC1 target for

imaging, and the targeted radiotherapy *in vitro* and *in vivo*. The study has shown the high potential of radiolabeled uMUC1 aptamer to penetrate the solid tumor as compared to radiolabeled antibodies. The antibodies have poor tumor penetration and have long circulation time. Thus, photosensitization is still a problem for antibodies-targeted PDT. Presumably, the uMUC1 aptamer-porphyrin conjugate could be the most efficient third-generation photosensitizer. Porphyrin uMUC1 aptamer synthesized in this project has the potential application in treatment of various tumors in PDT.

1.5 CONCLUSIONS

Three different types of photosensitizers were successfully conjugated at the 2'-position of uridine via EDCI coupling. The 3'-H-phosphonate derivative of the 2'-photosensitizers-modified (5'-hydroxyl protected with DMT) uridine was synthesized. The 2'-porphyrin-modified 3'-H-phosphonate derivative of uridine was used in the synthesis of oligonucleotide-porphyrin and aptamer-porphyrin conjugates. The solid support attached to a 19-mer DNA was conjugated with a 2'-porphyrin-modified 3'-H-phosphonate derivative of uridine. After the addition of the 2'-porphyrin-modified 3'-H-phosphonate derivative of uridine, a commercially available monomer of H-phosphonate derivative of thymidine (dT-H-phosphonate) was successfully added. The goal of this project was to conjugate aptamer to the porphyrin by the solid phase automated synthesis. This was achieved by conjugating an uMUC1 aptamer to a 2'-porphyrin-modified 3'-H-phosphonate derivative of uridine, but this resulted in a low coupling efficiency. However, improving the reaction conditions and repeating the process could increase the coupling efficiency, and provide a better yield.

1.6 FUTURE DIRECTIONS

This project offers many opportunities for future research. First, the project can be continued to develop an appropriate method for purifying aptamer-porphyrin conjugates. Furthermore, the uMUC1 peptide binding assay with purified anti-MUC1 aptamer-porphyrin conjugate will be an interesting area of research to pursue. In another case, the 2'-dithiaporphyrin-modified 3'-H-phosphonate derivative of uridine (synthesized in this project) could be utilized for coupling aptamers of interest. For example, an aptamer-dithiaporphyrin conjugate could be a more efficient photosensitizer in PDT compared to an aptamer-porphyrin conjugate; further, the quantum yield of a dithiaporphyrin conjugated aptamer is also of interest. On another front, the 3'-H-phosphonate derivatives of 2'-porphyrin and 2'-dithiaporphyrin modified uridine can be used in creating both porphyrin arrays, dithiaporphyrin arrays, or mixed porphyrin and dithiaporphyrin arrays in the DNA scaffold, and their properties will be a fascinating area of research to be pursued.

1.7 REFERENCES

1. Matera, M. K.; Takahashi, S.; Fujii, H.; Hong, Z.; Ishikawa, K.; Yoshimura, T.; Rousseau, D. L.; Yoshida, T.; Ikeda-Saito, M. *J. Biol. Chem.* **1996**, *271*, 6618-6624.
2. Meunier, B. *Chem. Rev.* **1992**, *92*, 1411-1456.
3. Fuller, S. D.; Darley-Usmar, V. M.; Capaldi, R. A. *Biochemistry* **1981**, *20*, 7046-7053.
4. Nam, W.; Han, H. J.; Oh, S.-Y.; Lee, Y. J.; Choi, M.-H.; Han, S.-Y.; Kim, C.; Woo, S. K.; Shi, W. *J. Am. Chem. Soc.* **2000**, *122*, 8677-8684.
5. Sono, M.; Roach, M. P.; Coulter, E. D.; Dawson, J. H. *Chem. Rev.* **1996**, *96*, 2841-2888.
6. Wagner, R. W.; Johnson, T. E.; Lindsey, J. S. *J. Am. Chem. Soc.* **1996**, *118* (45), 11166-11180.
7. Gust, D.; Moore, T. A.; Moore, A. L. *Acc. Chem. Res.* **2001**, *34* (1), 40-48.
8. Holten, D.; Bocian, D. F.; Lindsey, J. S. *Acc. Chem. Res.* **2002**, *35* (1), 57-69.
9. Wasielewski, M. R. *Chem. Rev.* **1992**, *92* (3), 435-461.
10. van der Boom, T.; Hayes, R. T.; Zhao, Y.; Bushard, P. J.; Weiss, E. A.; Wasielewski, M. R. *J. Am. Chem. Soc.* **2002**, *124* (32), 9582-9590.
11. Murakami, Y.; Kikuchi, J.-i.; Hisaeda, Y.; Hayashida, O. *Chem. Rev.* **1996**, *96* (2), 721-758.
12. Ambroise, A.; Wagner, R. W.; Rao, P. D.; Riggs, J. A.; Hascoat, P.; Diers, J. R.; Seth, J.; Lammi, R. K.; Bocian, D. F.; Holten, D.; Lindsey, J. S. *Chem. Mater.* **2001**, *13* (3), 1023-1034.

13. Hasobe, T.; Imahori, H.; Kamat, P. V.; Fukuzumi, S. *J. Am. Chem. Soc.* **2003**, *125* 14962-1496.
14. Hasobe, T.; Kamat, P. V.; Troiani, V.; Solladie, N.; Ahn, T. K.; Kim, K.; Kim, D.; Kongkanand, A.; Kuwabata, S.; Fukuzumi, S. *J. Phys. Chem. B* **2005**, *109*, 19-23.
15. Collman, J. P.; Anson, F. C.; Barnes, C. E.; Bencosme, C. S.; Geiger, T.; Evitt, E. R.; Kreh, R. P.; Meier, K.; Pettman, R. B. *J. Am. Chem. Soc.* **1983**, *105* (9), 2694-2699.
16. Collman, J. P.; Bencosme, C. S.; Barnes, C. E.; Miller, B. D. *J. Am. Chem. Soc.* **1983**, *105* (9), 2704-2710.
17. Collman, J. P.; Tyvoll, D. A.; Chng, L. L.; Fish, H. T. *J. Org. Chem.* **1995**, *60* (7), 1926-1931.
18. Yu, J.; Mathew, S.; Flavel, B. S.; Johnston, M. R.; Shapter, J. G. *J. Am. Chem. Soc.* **2008**, *130* (27), 8788-8796.
19. Liu, Z.; Yasseri, A. A.; Lindsey, J. S.; Bocian, D. F. *Science* **2003**, *302* (5650), 1543-1545.
20. Wang, Z.; Li, Z.; Medforth, C. J.; Shelnut, J. A. *J. Am. Chem. Soc.* **2007**, *129* (9), 2440-2441.
21. Kanayama, N.; Kanbara, T.; Kitano, H. *J. Phys. Chem. B* **2000**, *104* (2), 271-278.
22. Rakow, N. A.; Suslick, K. S. *Nature* **2000**, *406* (6797), 710-713.
23. Zimmerman, S. C.; Wendland, M. S.; Rakow, N. A.; Zharov, I.; Suslick, K. S. *Nature* **2002**, *418* (6896), 399-403.

24. Suslick, K. S.; Rakow, N. A.; Kosal, M. E.; Chou, J.-H. *J. Porphyrins Phthalocyanines* **2000**, *4* (4), 407-413.
25. Anderson, H. L. *Chem. Commun.* **1999**, (23), 2323-2330.
26. Lin, V. S. Y.; DiMugno, S. G.; Therien, M. J. *Science* **1994**, *264* (5162), 1105-1111.
27. Screen, T. E. O.; Thorne, J. R. G.; Denning, R. G.; Bucknall, D. G.; Anderson, H. L. *J. Am. Chem. Soc.* **2002**, *124* (33), 9712-9713.
28. Wagner, R. W.; Lindsey, J. S. *J. Am. Chem. Soc.* **1994**, *116* (21), 9759-9760.
29. Park, M.; Yoon, M.-C.; Yoon, Z. S.; Hori, T.; Peng, X.; Aratani, N.; Hotta, J.-i.; Uji-i, H.; Sliwa, M.; Hofkens, J.; Osuka, A.; Kim, D. *J. Am. Chem. Soc.* **2007**, *129* (12), 3539-3544.
30. Ogawa, K.; Kobuke, Y. *Angew. Chem. Int. Ed.* **2000**, *39* (22), 4070-4073.
31. Schenning, A. P. H. J.; Meijer, E. W. *Chem. Commun.* **2005**, (26), 3245-3258.
32. Ambroise, A.; Li, J.; Yu, L.; Lindsey, J. S. *Org. Lett.* **2000**, *2* (17), 2563-2566.
33. Kozaki, M.; Uetomo, A.; Suzuki, S.; Okada, K. *Org. Lett.* **2008**, *10* (20), 4477-4480.
34. Yu, L.; Lindsey, J. S. *J. Org. Chem.* **2001**, *66* (22), 7402-7419.
35. Kuciauskas, D.; Liddell, P. A.; Lin, S.; Johnson, T. E.; Weghorn, S. J.; Lindsey, J. S.; Moore, A. L.; Moore, T. A.; Gust, D. *J. Am. Chem. Soc.* **1999**, *121* (37), 8604-8614.

36. Aratani, N.; Cho, H. S.; Ahn, T. K.; Cho, S.; Kim, D.; Sumi, H.; Osuka, A. *J. Am. Chem. Soc.* **2003**, *125* (32), 9668-9681.
37. Liu, Z.-X.; Mu, L.-J.; Shi, S.-Q.; Zhou, Y.-Q.; Shen, P.-W. *Gaodeng Xuexiao Huaxue Xuebao* **1996**, *17* (10), 1504-1508.
38. Sun, X.; Chen, G.; Zhang, J. *Dyes Pigm.* **2008**, *76* (2), 499-501.
39. Clayton, R. K., *IUPAB Biophysics Series, Vol. 4: Photosynthesis: Physical Mechanisms and Chemical Patterns*. **1980**; pp 281.
40. Nakamura, M.; Ohtoshi, Y.; Yamana, K. *Chem. Commun.* **2005**, (41), 5163-5165.
41. Flamigni, L.; Marconi, G.; Dixon, I. M.; Collin, J.-P.; Sauvage, J.-P. *J. Phys. Chem. B* **2002**, *106* (26), 6663-6671.
42. Flamigni, L.; Dixon, I. M.; Jean, J.-P. C.; Sauvage, P. *Chem. Commun.* **2000**, 2479-2480.
43. Dixon, I. M.; Collin, J.-P.; Sauvage, J.-P.; Barigelletti, F.; Flamigni, L. *Angew. Chem. Int. Ed.* **2000**, *39*, 1292-1295.
44. Sanchez-Mosteiro, G.; van Dijk, E. M. H. P.; Hernando, J.; Heilemann, M.; Tinnefeld, P.; Sauer, M.; Koberlin, F.; Patting, M.; Wahl, M.; Erdmann, R.; van Hulst, N. F.; Garcia-Parajo, M. F. *J. Phys. Chem. B* **2006**, *110* (51), 26349-26353.
45. Heilemann, M.; Kasper, R.; Tinnefeld, P.; Sauer, M. *J. Am. Chem. Soc.* **2006**, *128* (51), 16864-16875.
46. Kannan, B.; Kulkarni, R. P.; Majumdar, A. *Nano Lett.* **2004**, *4* (8), 1521-1524.

47. Eckardt, L. H.; Naumann, K.; Pankau, W. M.; Rein, M.; Schweitzer, M.; Windhab, N.; von Kiedrowsk, G. *Nature* **2002**, *417*, 286.
48. Yan, H.; Park, S. H.; Finkelstein, G.; Reif, J. H.; LaBean, T. H. *Science* **2003**, *301* (5641), 1882-1884.
49. Gao, J.; Strassler, C.; Tahmassebi, D.; Kool, E. T. *J. Am. Chem. Soc.* **2002**, *124* (39), 11590-11591.
50. Osuka, A.; Nakajima, S.; Maruyama, K.; Mataga, N.; Asahi, T.; Yamazaki, I.; Nishimura, Y.; Ohno, T.; Nozaki, K. *J. Am. Chem. Soc.* **1993**, *115* (11), 4577-4589.
51. Hoeben, F. J. M.; Jonkheijm, P.; Meijer, E. W.; Schenning, A. P. H. J. *Chem. Rev.* **2005**, *105* (4), 1491-1546.
52. Endo, M.; Fujitsuka, M.; Majima, T. *J. Org. Chem.* **2008**, *73* (3), 1106-1112.
53. Dougherty, T. J.; Kaufman, J. E.; Goldfarb, A.; Weishaupt, K. R.; Boyle, D.; Mittleman, A. *Cancer Res.* **1978**, *38* (8), 2628-2635.
54. Pullerits, T.; Sundstrom, V. *Acc. Chem. Res.* **1996**, *29* (8), 381-389.
55. Clayton, R. K., *Photosynthesis: Physical Mechanism and Chemical Patterns*. Cambridge University Press, N. Y., Ed. **1980**.
56. van Dongen, G. A. M. S.; Visser, G. W. M.; Vrouenraets, M. B. *Adv. Drug Delivery Rev.* **2004**, *56* (1), 31-52.
57. Moreira, L. M.; dos Santos, F. V.; Lyon, J. P.; Maftoum-Costa, M.; Pacheco-Soares, C.; da Silva, N. S. *Aust. J. Chem.* **2008**, *61* (10), 741-754.
58. Sternberg, E. D.; Dolphin, D.; Brückner, C. *Tetrahedron* **1998**, *54* (17), 4151-4172.

59. Ochsner, M. J. *Photochem. Photobiol. B* **1997**, *39* (1), 1-18.
60. Weishaupt, K. R.; Gomer, C. J.; Dougherty, T. J. *Cancer Res.* **1976**, *36* (7_Part_1), 2326-2329.
61. Olemick, N. L.; Evans, H. H. *Rad. Res.* **1998**, *150*, 5146-5156.
62. Triesscheijn, M.; Baas, P.; Schellens, J. H. M.; Stewart, F. A. *Oncologist* **2006**, *11* (9), 1034-1044.
63. Sharman, W. M.; Allen, C. M.; van Lier, J. E. *Drug Discov. Today* **1999**, *4* (11), 507-517.
64. Detty, M. R.; Gibson, S. L.; Wagner, S. J. *J. Med. Chem.* **2004**, *47* (16), 3897-3915.
65. Henderson, B. W.; Bellnier, D. A.; Greco, W. R.; Sharma, A.; Pandey, R. K.; Vaughan, L. A.; Weishaupt, K. R.; Dougherty, T. J. *Cancer Res.* **1997**, *57* (18), 4000-4007.
66. Hilmey, D. G.; Abe, M.; Nelen, M. I.; Stilts, C. E.; Baker, G. A.; Baker, S. N.; Bright, F. V.; Davies, S. R.; Gollnick, S. O.; Oseroff, A. R.; Gibson, S. L.; Hilf, R.; Detty, M. R. *J. Med. Chem.* **2002**, *45* (2), 449-461.
67. You, Y.; Gibson, S. L.; Hilf, R.; Davies, S. R.; Oseroff, A. R.; Roy, I.; Ohulchanskyy, T. Y.; Bergey, E. J.; Detty, M. R. *J. Med. Chem.* **2003**, *46* (17), 3734-3747.
68. Leung, S. C. H.; Lo, P. C.; Ng, D. K. P.; Liu, W. K.; Fung, K. P.; Fong, W. *P. Br. J. Pharmacol.* **2008**, *154* (1), 4-12.
69. Mallikaratchy, P.; Tang, Z.; Tan, W. *Chem. Med. Chem.* **2008**, *3* (3), 425-428.

70. Mew, D.; Lum, V.; Wat, C. K.; Towers, G. H. N.; Sun, C.-H.; Walter, R. J.; Wright, W.; Berns, M. W.; Levy, J. G. *Cancer Res.* **1985**, *45*, 4348.
71. Hamblin, M. R.; Newman, E. L. *J. Photochem. Photobiol. B* **1994**, *26* (1), 45-56.
72. Savitskii, A. P.; Lopatin, K. V.; Golubeva, N. A.; Poroshina, M. Y.; Chernyaeva, E. B.; Stepanova, N. V.; Solovieva, L. I.; Lukyanets, E. A. *J. Photochem. Photobiol., B* **1992**, *13* (3-4), 327-333.
73. Papkovskii, D. B.; Savitskii, A. P.; Egorova, S. G.; Sukhin, G. M.; Chisov, V. I.; Krasnovskii, A. A.; Egorov, S. Y.; Ponomarev, G. V.; Kirillova, G. V. *Biomed. Sci.* **1990**, *1* (4), 401-406.
74. Egorov, S. Y.; Krasnovskii, A. A.; Papkovskii, D. B.; Ponomarev, G. V.; Savitskii, A. P. *Byull. Eksp. Biol. Med.* **1990**, *109* (4), 349-351.
75. Bhatti, M.; MacRobert, A.; Henderson, B.; Shepherd, P.; Cridland, J.; Wilson, M. *Antimicrob. Agents Chemother.* **2000**, *44* (10), 2615-2618.
76. Savellano, M. D.; Pogue, B. W.; Hoopes, P. J.; Vitetta, E. S.; Paulsen, K. D. *Cancer Res.* **2005**, *65* (14), 6371-6379.
77. Goff, B. A.; Blake, J.; Bamberg, M. P.; Hasan, T. *Br. J. Cancer* **1996**, *74* (8), 1194-1198.
78. Lei, H.; Zhao, F.; Xin, H.; Zhang, F. *Huaxue Jinzhan* **2007**, *19* (4), 527-534.
79. Hasan, T.; Savellano, M. D.; Skobe, M. Photoimmunotherapies for cancer using photosensitizer immunoconjugates and combination therapies. 2002-US137762002100326, 20020501, **2002**.

80. Hamblin, M. R.; Del Governatore, M.; Rizvi, I.; Hasan, T. *Br. J. Cancer* **2000**, *83* (11), 1544-1551.
81. Bhatti, M.; Yahioğlu, G.; Milgrom, L. R.; Garcia-Maya, M.; Chester, K. A.; Deonarain, M. P. *Int. J. Cancer* **2008**, *122* (5), 1155-1163.
82. Aveline, B. M.; Hasan, T.; Redmond, R. W. *J. Photochem. Photobiol. B* **1995**, *30* (2-3), 161-169.
83. Savellano, M. D.; Hasan, T. *Clin. Cancer Res.* **2005**, *11* (4), 1658-1668.
84. Savellano, M. D.; Hasan, T. *Photochem. Photobiol.* **2003**, *77* (4), 431-439.
85. Brasseur, N.; Langlois, R.; La Madeleine, C.; Ouellet, R.; Van Lier, J. E. *Photochem. Photobiol.* **1999**, *69* (3), 345-352.
86. Hamblin, M. R.; Miller, J. L.; Hasan, T. *Cancer Res.* **1996**, *56* (22), 5205-.
87. Jiang, F. N.; Jiang, S.; Liu, D.; Richter, A.; Levy, J. G. *J. Immunol. Methods* **1990**, *134* (1), 139-149.
88. Marco Del Governatore; Hamblin, M. R.; Shea, C. R.; Rizvi, I.; Molpus, K. G.; Tanabe, K. K.; Hasan, T. *Cancer Res.* **2000**, *60* (15), 4170-4175.
89. Rakestraw, S. L.; Tompkins, R. G.; Yarmush, M. L. *Bioconjug. Chem.* **1990**, *1* (3), 212-221.
90. Missailidis, S.; Gariépy, J.; Ferreira, C. S. M. Aptamers against MUC1 and their uses in cancer diagnosis and therapy. 2006-87782437727, 20060504, 2007.
91. Baines, I. C.; Colas, P. *Drug Discov. Today* **2006**, *11* (7 & 8), 334-341.
92. Jenne, A. *Innovations Pharm. Technol.* **2005**, (16), 44-47.
93. Egli, M. *Angew. Chem. Int. Ed.* **1997**, *36* (5), 480-482.

94. Xiao, Z.; Shangguan, D.; Cao, Z.; Fang, X.; Tan, W. *Chem.--Eur. J.* **2008**, *14* (6), 1769-1775, S1769/10S1769/2.
95. Tang, Z.; Parekh, P.; Turner, P.; Moyer, R. W.; Tan, W. *Clin. Chem.* **2009**, *55* (4), 813-822.
96. Stojanovic, M. N.; Landry, D. W. *J. Am. Chem. Soc.* **2002**, *124* (33), 9678-9679.
97. Stojanovic, M. N.; Landry, D. W. *Abstracts of Papers, 222nd ACS National Meeting, Chicago, IL, United States, August 26-30, 2001* **2001**, BIOL-005.
98. Green, L. S.; Bell, C.; Janjic, N. *Biotechniques* **2001**, *30* (5), 1094-1096.
99. Shi, C.; Ma, C.; Zhang, S.; Kong, J. Method for detecting target molecules using nucleic acid aptamer and PCR. 2008-10160859101368209, 20080912, **2009**.
100. Bayer, T. S.; Booth, L. N.; Knudsen, S. M.; Ellington, A. D. *Rna* **2005**, *11* (12), 1848-1857.
101. Lin, C. H.; Patel, D. J. *Chem. Biol.* **1997**, *4* (11), 817-832.
102. Low, S. Y.; Hill, J. E.; Peccia, J. *Biochem. Biophys. Res. Commun.* **2009**, *378* (4), 701-705.
103. Ellington, A. D.; Szostak, J. W. *Nature* **1990**, *346* (6287), 818-822.
104. Tuerk, C.; Gold, L. *Science* **1990**, *249* (4968), 505-510.
105. Haes, A. J.; Giordano, B. C.; Collins, G. E. *Anal. Chem.* **2006**, *78* (11), 3758-3764.
106. Feng, H.; Hu, K.-h. *Virol. Sin.* **2008**, *23* (5), 315-320.
107. Gold, L. *Comb. Chem. Technol.* **1999**, 389-403.

108. Yang, X.; Wang, L.; Wang, K.; Tan, W.; Tang, H.; Meng, X.; Guo, Q. *Chin. Sci. Bull.* **2008**, *53* (2), 204-208.
109. Burgstaller, P.; Girod, A.; Blind, M. *Drug Discov. Today* **2002**, *7* (24), 1221-1228.
110. Burgstaller, P.; Jenne, A.; Blind, M. *Curr. Opin. Drug Discov. & Dev.* **2002**, *5* (5), 690-700.
111. Guo, K.-T.; Schaefer, R.; Paul, A.; Ziemer, G.; Wendel, H. P. *Mini-Rev. Med. Chem.* **2007**, *7* (7), 701-705.
112. Pendergrast, P. S.; Epstein, D. M. *Aptamer Handb.* **2006**, 265-279.
113. Proske, D.; Blank, M.; Buhmann, R.; Resch, A. *Appl. Microbiol. Biotechnol.* **2005**, *69* (4), 367-374.
114. Dua, P.; Kim, S.; Lee, D.-K. *Recent Pat. DNA Gene Sequences* **2008**, *2* (3), 172-186.
115. Hicke, B. J.; Stephens, A. W. *J. Clin. Invest.* **2000**, *106* (8), 923-928.
116. Cox, J. C.; Rajendran, M.; Riedel, T.; Davidson, E. A.; Sooter, L. J.; Bayer, T. S.; Schmitz-Brown, M.; Ellington, A. D. *Comb. Chem. High Throughput Screening* **2002**, *5* (4), 289-299.
117. Cox, J. C.; Hayhurst, A.; Hesselberth, J.; Bayer Travis, S.; Georgiou, G.; Ellington Andrew, D. *Nucleic Acids Res.* **2002**, *30* (20), e108.
118. Shamah, S. M.; Healy, J. M.; Cload, S. T. *Acc. Chem. Res.* **2008**, *41* (1), 130-138.
119. Chen, H. W.; Medley, C. D.; Sefah, K.; Shangguan, D.; Tang, Z.; Meng, L.; Smith, J. E.; Tan, W. *Chem. Med. Chem.* **2008**, *3* (6), 991-1001.

120. Tang, Z.; Shangguan, D.; Wang, K.; Shi, H.; Sefah, K.; Mallikratchy, P.; Chen, H. W.; Li, Y.; Tan, W. *Anal. Chem.* **2007**, *79* (13), 4900-4907.
121. Keefe, A. D.; Wilson, C.; Wang, C. Selection of oligonucleotides through SELEX. 2008-US89212009014705, 20080721, **2009**.
122. Fukusho, S.; Furusawa, H.; Okahata, Y. *Chem. Commun.* **2002**, (1), 88-89.
123. Ferreira, C. S. M.; Garipey, J. Aptamers that recognize the carbohydrate N-acetylgalactosamine for diagnosis and treatment of cancer. 2007-CA7572007128109, 20070504, **2007**.
124. Liu, Y.; Kuan, C.-T.; Mi, J.; Zhang, X.; Clary, B. M.; Bigner, D. D.; Sullenger, B. A. *Biol. Chem.* **2009**, *390* (2), 137-144.
125. Hicke, B. J.; Marion, C.; Chang, Y.-F.; Gould, T.; Lynott, C. K.; Parma, D.; Schmidt, P. G.; Warren, S. *J. Biol. Chem.* **2001**, *276* (52), 48644-48654.
126. Pietras, K.; Ostman, A.; Rubin, K.; Heldin, C.-H. Method for treatment of tumors using nucleic acid ligands to PDGF. 2001-US160782001087351, 20010517, **2001**.
127. Fang, X.; Cao, Z.; Beck, T.; Tan, W. *Anal. Chem.* **2001**, *73* (23), 5752-5757.
128. Sennino, B.; Falcon, B. L.; McCauley, D.; Le, T.; McCauley, T.; Kurz, J. C.; Haskell, A.; Epstein, D. M.; McDonald, D. M. *Cancer Res.* **2007**, *67* (15), 7358-7367.
129. Lupold, S. E.; Hicke, B. J.; Lin, Y.; Coffey, D. S. *Cancer Res.* **2002**, *62* (14), 4029-4033.

130. Diener, J. L.; Hatala, P.; Killough, J. R.; Wagner-Whyte, J.; Wilson, C.; Zhu, S. Stabilized aptamers to PSMA and their use in diagnosis and treatment of prostate cancer. 2006-US81932006096754, 20060307, **2006**.
131. Ruckman, J.; Green, L. S.; Beeson, J.; Waugh, S.; Gillette, W. L.; Henninger, D. D.; Claesson-Welsh, L.; Janjic, N. *J. Biol. Chem.* **1998**, *273* (32), 20556-20567.
132. Adamis, A. P.; Shima, D.; Wincott, F.; Calias, P. VEGF-binding aptamers capped with inverted nucleotides and sustained release compositions for use in pharmaceuticals. 2004-US254222005014814, 20040806, **2005**.
133. Daniels, D. A.; Chen, H.; Hicke, B. J.; Swiderek, K. M.; Gold, L. *Proc. Natl. Acad. Sci. U. S. A.* **2003**, *100* (26), 15416-15421.
134. Foerster, C.; Brauer, A. B. E.; Brode, S.; Schmidt, K. S.; Perbandt, M.; Meyer, A.; Rypniewski, W.; Betzel, C.; Kurreck, J.; Fuerste, J. P.; Erdmann, V. A. *Acta Crystallogr., Sect. F: Struct. Biol. Cryst. Commun.* **2006**, *F62* (7), 665-668.
135. Chen, C.-H. B.; Landgraf, R. Inhibition of heregulin signaling by aptamers to human epidermal growth factor receptor-3 and their use in cancer therapy. 2004-US230392005040339, 20040716, 2005.
136. Chen Chi-Hong, B.; Chernis George, A.; Hoang Van, Q.; Landgraf, R. *Proc. Natl. Acad. Sci. U.S. A.* **2003**, *100* (16), 9226-9231.
137. Phillips, J. A.; Lopez-Colon, D.; Zhu, Z.; Xu, Y.; Tan, W. *Anal. Chim. Acta* **2008**, *621* (2), 101-108.

138. Shangguan, D.; Li, Y.; Tang, Z.; Cao, Z. C.; Chen, H. W.; Mallikaratchy, P.; Sefah, K.; Yang, C. J.; Tan, W. *Proc. Natl. Acad. Sci. U. S. A.* **2006**, *103* (32), 11838-11843.
139. Becker, K. C. D.; Becker, R. C. *Curr. Opin. Mol. Therap.* **2006**, *8* (2), 122-129.
140. Nutiu, R.; Li, Y. *J. Am. Chem. Soc.* **2003**, *125* (16), 4771-4778.
141. Borbas, K. E.; Ferreira, C. S. M.; Perkins, A.; Bruce, J. I.; Missailidis, S. *Bioconjug. Chem.* **2007**, *18* (4), 1205-1212.
142. Lee, J. F.; Stovall, G. M.; Ellington, A. D. *Curr. Opin. Chem. Biol.* **2006**, *10* (3), 282-289.
143. Brody, E. N.; Gold, L. *J. Biotechnol.* **2000**, *74* (1), 5-13.
144. Rajendrakumar, G. V.; Sundari, N. S.; Ganesh, K. N. *Proc. - Indian Acad. Sci., Chem. Sci.* **1985**, *95* (4), 357-368.
145. Li, B. F. L.; Reese, C. B.; Swann, P. F. *Biochemistry* **1987**, *26* (4), 1086-1093.
146. Beaucage, S. L. *Methods Mol. Biol.* **1993**, *20*, 33-61.
147. Beaucage, S. L.; Iyer, R. P. *Tetrahedron* **1993**, *49* (46), 10441-10488.
148. Froehler, B. C. *Methods Mol. Biol. (Totowa, N. J.)* **1993**, *20* (Protocols for Oligonucleotides and Analogs), 63-80.
149. Reese, C. B.; Song, Q. *J. Chem. Soc., Perkin Trans. I* **1999**, (11), 1477-1486.
150. Herdewijn, P.; Editor, *Oligonucleotide Synthesis: Methods and Applications. [In: Methods Mol. Biol. (Totowa, NJ, U. S.); 2005, 288].* **2005**; 435 pp.

151. Khudiyakov, Y. E.; Fields, H. A.; Editors, *Artificial DNA: Methods and Applications*. **2003**; 417 pp.
152. Stawinski, J.; Stroemberg, R. *Trends Org. Chem.* **1993**, *4* (1), 31-67.
153. Stawinski, J. *Handb. Organophosphorus Chem.* **1992**, 377-434.
154. Kung, P. P.; Jones, R. A. *Tet. Lett.* **1992**, *33* (40), 5869-5872.
155. Froehler, B. C.; Ng, P. G.; Matteucci, M. D. *Nucleic Acids Res.* **1986**, *14* (13), 5399-5407.
156. Andrus, A.; Zon, G. *Nucleic Acids Symp. Ser.* **1988**, *20*, 121-122.
157. Stein, C. A.; Iversen, P. L.; Subasinghe, C.; Cohen, J. S.; Stec, W. J.; Zon, G. *Anal. Biochem.* **1990**, *188* (1), 11-16.
158. Grand, C. L.; Han, H.; Munoz, R. M.; Weitman, S.; Von Hoff, D. D.; Hurley, L. H.; Bearss, D. J. *Mol. Cancer Therap.* **2002**, *1* (8), 565-573.
159. Ma, H.-m.; Chen, X.; Sun, S.-t.; Zhang, L.-n.; Wu, D.; Zhu, P.-h.; Li, Y.; Du, B.; Wei, Q. *Guangpuxue Yu Guangpu Fenxi* **2009**, *29* (2), 423-427.
160. Schneider, H.-J.; Wang, M. *J. Org. Chem.* **1994**, *59* (24), 7473-7478.
161. Ward, B.; Skorobogaty, A.; Dabrowiak, J. C. *Biochemistry* **1986**, *25* (22), 6875-6883.
162. Lipscomb, L. A.; Zhou, F. X.; Presnell, S. R.; Woo, R. J.; Peek, M. E.; Plaskon, R. R.; Williams, L. D. *Biochemistry* **1996**, *35* (9), 2818-2823.
163. Mestre, B.; Jakobs, A.; Pratviel, G.; Meunier, B. *Biochemistry* **1996**, *35* (28), 9140-9149.
164. Casas, C.; Lacey, C. J.; Meunier, B. *Bioconjug. Chem.* **1993**, *4* (5), 366-371.

165. Balaz, M.; Holmes, A. E.; Benedetti, M.; Proni, G.; Berova, N. *Bioorg. Med. Chem.* **2005**, *13* (7), 2413-2421.
166. Balaz, M.; Holmes, A. E.; Benedetti, M.; Rodriguez, P. C.; Berova, N.; Nakanishi, K.; Proni, G. *J. Am. Chem. Soc.* **2005**, *127* (12), 4172-4173.
167. Balaz, M.; Steinkruger, J. D.; Ellestad, G. A.; Berova, N. *Org. Lett.* **2005**, *7* (25), 5613-5616.
168. Mammana, A.; Asakawa, T.; Bitsch-Jensen, K.; Wolfe, A.; Chaturantabut, S.; Otani, Y.; Li, X.; Li, Z.; Nakanishi, K.; Balaz, M.; Ellestad, G. A.; Berova, N. *Bioorg. Med. Chem.* **2008**, *16* (13), 6544-6551.
169. Berlin, K.; Jain, R. K.; Simon, M. D.; Richert, C. *J. Org. Chem.* **1998**, *63* (5), 1527-1535.
170. Reed, M. W.; Wald, A.; Meyer, R. B. *J. Am. Chem. Soc.* **1998**, *120* (38), 9729-9734.
171. Lukhtanov, E. A.; Kutuyavin, I. V.; Gorn, V. V.; Reed, M. W.; Adams, A. D.; Lucas, D. D.; Meyer, R. B., Jr. *J. Am. Chem. Soc.* **1997**, *119* (27), 6214-6225.
172. Robles, J.; McLaughlin, L. W. *J. Am. Chem. Soc.* **1997**, *119* (26), 6014-6021.
173. Cardullo, R. A.; Agrawal, S.; Flores, C.; Zaacetoneitrileik, P. C.; Wolf, D. E. *Proc. Natl. Acad. Sci. U. S. A.* **1988**, *85* (23), 8790-8794.
174. Walton, T. A.; Lyttle, M. H.; Dick, D. J.; Cook, R. M. *Bioconjug. Chem.* **2002**, *13* (5), 1155-1158.
175. Didenko, V. V. *Biotechniques* **2001**, *31* (5), 1106-1121.

176. Okamura, Y.; Kondo, S.; Sase, I.; Suga, T.; Mise, K.; Furusawa, I.; Kawakami, S.; Watanabe, Y. *Nucleic Acids Res.* **2000**, *28* (24), E107.
177. Okamura, Y.; Watanabe, Y. *Methods Mol. Biol.* **2006**, *335*, 43-56.
178. Eckstein, F. *Antisense Nucleic Acid Drug Dev.* **2000**, *10* (2), 117-121.
179. Major, D. T.; Laxer, A.; Fischer, B. *J. Org. Chem.* **2002**, *67* (3), 790-802.
180. Alzeer, J.; Schaerer, O. D. *Nucleic Acids Res.* **2006**, *34* (16), 4458-4466.
181. Wagner, C.; Rist, M.; Mayer-Enthart, E.; Wagenknecht, H.-A. *Org. Biomol. Chem.* **2005**, *3* (11), 2062-2063.
182. Giller, G.; Tasara, T.; Angerer, B.; Muhlegger, K.; Amacker, M.; Winter, H. *Nucleic Acids Res.* **2003**, *31* (10), 2630-2635.
183. Seela, F.; Xu, K. *Org. Biomol. Chem.* **2008**, *6* (19), 3552-3560.
184. Fendt, L.-A.; Bouamaied, I.; Thoni, S.; Amiot, N.; Stulz, E. *J. Am. Chem. Soc.* **2007**, *129* (49), 15319-15329.
185. Salon, J.; Chen, G.; Portilla, Y.; Germann, M. W.; Huang, Z. *Org. Lett.* **2005**, *7* (25), 5645-5648.
186. Li, N.-S.; Piccirilli, J. A. *J. Org. Chem.* **2004**, *69* (14), 4751-4759.
187. McGee, D. P. C.; Vaughn-Settle, A.; Vargeese, C.; Zhai, Y. *J. Org. Chem.* **1996**, *61* (2), 781-785.
188. Shohda, K.; Okamoto, I.; Wada, T.; Seio, K.; Sekine, M. *Bioorg. Med. Chem. Lett.* **2000**, *10* (16), 1795-1798.
189. Kumamoto, S.; Watanabe, M.; Kawakami, N.; Nakamura, M.; Yamana, K. *Bioconjug. Chem.* **2008**, *19* (1), 65-69.

190. Whittemore, N. A.; Mullenix, A. N.; Inamati, G. B.; Manoharan, M.; Cook, P. D.; Tuinman, A. A.; Baker, D. C.; Chambers, J. Q. *Bioconjug. Chem.* **1999**, *10* (2), 261-270.
191. Mayer-Enthart, E.; Wagenknecht, H.-A. *Angew. Chem. Int. Ed.* **2006**, *45* (20), 3372-3375.
192. Yamana, K.; Ohashi, Y.; Nunota, K.; Nakano, H. *Tetrahedron* **1997**, *53* (12), 4265-4270.
193. Henderikx, P.; Kandilogiannaki, M.; Petrarca, C.; von Mensdorff-Pouilly, S.; Hilgers, J. H. M.; Krambovitis, E.; Arends, J. W.; Hoogenboom, H. R. *Cancer Res* **1998**, *58* (19), 4324-4332.
194. von Mensdorff-Pouilly, S.; Snijdewint, F. G. M.; Verstraeten, A. A.; Verheijen, R. H. M.; Kenemans, P. *Int. J. Biol. Markers* **2000**, *15* (4), 343-356.
195. Burdick, M. D.; Harris, A.; Reid, C. J.; Iwamura, T.; Hollingsworth, M. A. *J. Biol. Chem.* **1997**, *272* (39), 24198-24172.
196. Brayman, M.; Thathiah, A.; Carson, D. D. *Reprod. Biol. Endocrinol.* **2004**, *2*, No pp given.
197. Price, M. R.; Rye, P. D.; Petrakou, E.; Murray, A.; Brady, K.; Imai, S.; Haga, S.; Kiyozuka, Y.; Schol, D.; Meulenbroek, M. F.; Snijdewint, F. G.; von Mensdorff-Pouilly, S.; Verstraeten, R. A.; Kenemans, P.; Blockzijl, A.; Nilsson, K.; Nilsson, O.; Reddish, M.; Suresh, M. R.; Koganty, R. R.; Fortier, S.; Baronic, L.; Berg, A.; Longenecker, M. B.; Hilgers, J.; et al. *Tumour Biol.* **1998**, *19 Suppl 1*, 1-20.

198. Adluri, S.; Gilewski, T.; Zhang, S.; Ramnath, V.; Ragupathi, G.; Livingston, P. *Br. J. Cancer* **1999**, *79* (11/12), 1806-1812.
199. Moore, A.; Medarova, Z.; Potthast, A.; Dai, G. *Cancer Res* **2004**, *64* (5), 1821-1827.
200. Barratt-Boyes, S. M. *Cancer Immunol. Immunother.* **1996**, *43* (3), 142-151.
201. Girling, A.; Bartkova, J.; Burchell, J.; Gendler, S.; Gillett, C.; Taylor-Papadimitriou, J. *Int J Cancer* **1989**, *43* (6), 1072-6.
202. Rowse, G. J.; Tempero, R. M.; VanLith, M. L.; Hollingsworth, M. A.; Gendler, S. J. *Cancer Res.* **1998**, *58* (2), 315-321.
203. Fujii, K.; Okamoto, S.; Sasaki, N.; Takano, M.; Kudoh, K.; Kita, T.; Tsuda, H.; Kikuchi, Y. *Trends Cancer Res.* **2005**, *1*, 133-138.
204. Swanson, B. J.; McDermott, K. M.; Singh, P. K.; Eggers, J. P.; Crocker, P. R.; Hollingsworth, M. A. *Cancer Res.* **2007**, *67* (21), 10222-10229.
205. Zhang, H.; Lu, H.; Kong, G. *Xiandai Zhongliu Yixue* **2005**, *13* (6), 756-758.
206. Jarrard, J. A.; Linnoila, R. I.; Lee, H.; Steinberg, S. M.; Witschi, H.; Szabo, . *Cancer Res.* **1998**, *58* (23), 5582-5589.
207. Nan, Z.; Ji, W. *Shanxi Yiyao Zazhi* **2007**, *36* (10), 879-881.
208. Rubinstein, D. B.; Karmely, M.; Ziv, R.; Benhar, I.; Leitner, O.; Baron, S.; Katz, B.-Z.; Wreschner, D. H. *Cancer Res.* **2006**, *66* (23), 11247-11253.
209. Yu, Y.; Li, H.; Wang, L. Recombinant fusion proteins comprising BCG heat shock protein 65 and the epitope of MUC1. 2003-6352112005031649, 20030806, **2005**.
210. Agrawal, B.; Krantz, M. J.; Reddish, M. A.; Longenecker, B. M. *Nat. Med.* **1998**, *4* (1), 43-49.

211. Berry, N.; Jones, D. B.; Smallwood, J.; Taylor, I.; Kirkham, N.; Taylor-Papadimitriou, J. *Br. J. Cancer* **1985**, *51* (2), 179-186.
212. Hilkens, J.; Buijs, F.; Hilgers, J.; Hageman, P.; Calafat, J.; Sonnenberg, A.; van der Valk, M. *Int. J. Cancer* **1984**, *34* (2), 197-206.
213. Bhavanandan, V. P.; Zhu, Q.; Yamakami, K.; Dilulio, N. A.; Nair, S.; Capon, C.; Lemoine, J.; Fournet, B. *Glycoconjug. J.* **1998**, *15* (1), 37-49.
214. Fontenot, J. D.; Tjandra, N.; Bu, D.; Ho, C.; Montelaro, R. C.; Finn, O. J. *Cancer Res.* **1993**, *53* (22), 5386-5394.
215. Ryuko, K.; Schol, D. J.; Snijdwint, F. G. M.; Von Mensdorff-Pouilly, S.; Poort-Keesom, R. J. J.; Karuntu-Wanamarta, Y. A.; Verstraeten, R. A.; Miyazaki, K.; Kenemans, P.; Hilgers, J. *Tumor Biol.* **2000**, *21* (4), 197-210.
216. Hilkens, J.; Vos, H. L.; Wesseling, J.; Boer, M.; Storm, J.; van der Valk, S.; Calafat, J.; Patriarca, C. *Cancer Lett.* **1995**, *90* (1), 27-33.
217. Sitaula, S.; Reed, S. M. *Bioorg. & Med. Chem. Lett.* **2008**, *18* (2), 850-855.
218. Syrbu, S. A.; Semelkin, A. S.; Berezin, B. D.; Koifman, O. I. *Chem. Heterocyclic Comp.* **1980**, *25*, 1149-1153.
219. Chauhan, S. M. S.; Sahoo, B. B.; Srinivas, K. A. *Synth. Commun.* **2001**, *31* (1), 33-37.
220. Stawinski, J.; Kraszewski, A. *Acc. Chem. Res.* **2002**, *35* (11), 952-960.
221. Iyer, P. C.; Yagi, H.; Sayer, J. M.; Jerina, D. M. *Chem. Res. Toxicol.* **2007**, *20* (2), 311-315.
222. Zhu, Z.; Tang, Z.; Phillips, J. A.; Yang, R.; Wang, H.; Tan, W. *J. Am. Chem. Soc.* **2008**, *130* (33), 10856-10857.

CHAPTER 2

SYNTHESIS AND STABILITY OF MIXED THIOL/LIPID COATED GOLD NANOPARTICLES

2.1 INTRODUCTION

The introductory section of Chapter 2 describes the optical properties of metal nanoparticles, followed by a description of various types of phospholipids used in these experiments, including the concept of lipid curvature. A literature survey on solid-supported lipid bilayers is described in brief. Finally, this section presents information found in the literature on the stability of gold nanoparticles in potassium cyanide and iodine solutions.

2.1.1 Metal Nanoparticles

Over the last decade, metal nanoparticles ranging from 1 nm to 100 nm have received a great deal of attention for their diverse applications in various fields of science. In particular, colloidal metal nanoparticles are of great interest because of their use in catalysis,¹⁻⁶ bio-labeling,⁷⁻¹⁰ sensors,¹¹⁻¹³ optoelectronics and electronics,^{14,15} and magnetic devices.¹⁶ Metal nanoparticles can be easily synthesized in the laboratory, and their surfaces can be functionalized with various types of functional molecules for a variety of applications. These metal nanoparticles have been shown to exhibit optical and chemical properties that are different from those of bulk solids of the same kind.¹⁷⁻¹⁹ Nevertheless, their electrical properties are typically similar to corresponding bulk metals.²⁰ In

particular, optical properties of nanoparticles are usually influenced by the particle size and shape; these are described in the following section.

2.1.1.1 Optical Properties of Metal Nanoparticles

Metal nanoparticles often exhibit unique optical properties derived from collective oscillations of conduction electrons upon interaction with electromagnetic radiation.²¹⁻²⁴ As shown in Fig 2.1, the electric field of an incoming light wave causes polarization of the free electrons on the surface of the nanoparticles, which results in an “electronic cluster” with respect to the heavier ionic core known as “ionic cluster”. The difference in net charge at the surface of nanoparticles creates the dipolar oscillations known as Surface Plasmon Resonance (SPR).²³ The SPR of metal nanoparticles depends on size,²⁵ shape,^{26,27} surface modification of the particle,²⁸⁻³⁰ and temperature.³¹

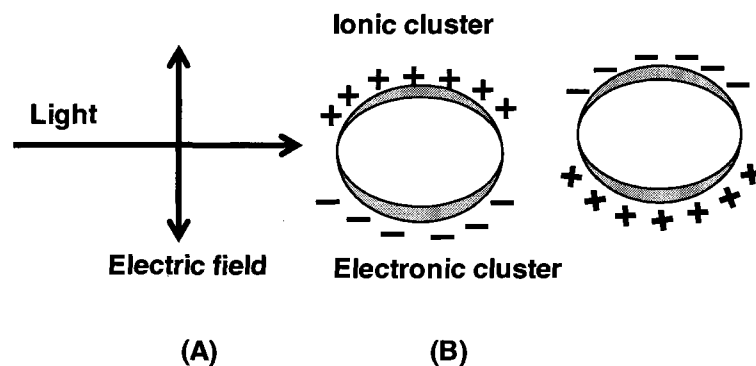


Figure 2.1 A scheme showing dipole oscillations of electrons in nanoparticle surfaces. (A) An electric field of an incoming light, (B) polarization of electrons and creation of the ionic and electronic clusters.²³

Metal nanoparticles usually show plasmon resonance extinction bands in the visible region and possess strong colors like that of molecular dyes.²⁰ The optical properties of nanoparticles can be tuned gradually with particle size and shape.^{23,32} Such properties provide nanoparticles' unique advantages over organic dye molecules, making nanoparticles more interesting than organic dye molecules. The molar extinction coefficient of nanoparticles is of the order of $10^5 - 10^6 \text{ M}^{-1} \text{ cm}^{-1}$ for small particles ($< 20 \text{ nm}$) and increases with increasing particle sizes.²⁴ In particular, 20 nm nanoparticles' extinction coefficient is $10^9 \text{ M}^{-1} \text{ cm}^{-1}$.²³ As the nanoparticles size increases, the wavelength of SPR related absorption shifts to longer wavelengths.^{23,32} For metal nanoparticles with the same composition, extinction maxima of SPR can also be shifted hundreds of nanometers by changing

its shape.²⁰ The SPR also depends on the surface properties of the nanoparticle. The surface of the particles determines the boundary properties of the metal.

The lambda maximum (λ_{\max}) absorption of the SPR also depends on the nanoparticle size. A decrease in size and dimension of the nanomaterial changes the density and the spatial length scale of the electronic motion.^{24, 33, 34} However, of the nanoparticles much smaller than the wavelength of absorbing light (about 25 nm for gold), only the dipole term is assumed to contribute to SPR.^{22,23} Mie theory for nanoparticles much smaller than wavelength of absorbing light ($\lambda \gg 2R$ (R = particle radius)) changed for the dipole dependent relationship as shown in the equation [1] below.^{24,37,128}

$$\sigma_{ext} = \frac{9V\epsilon_m^{3/2}}{C} \cdot \frac{\omega\epsilon_2(\omega)}{[\epsilon_1(\omega)+2\epsilon_m]^2 + \epsilon_2(\omega)^2} \quad [1]$$

where

σ_{ext} = extinction cross section of nanoparticles

V = volume of spherical particles and depends on radius of particles

C = speed of light

ω = angular frequency of the exciting radiation

ϵ_m = dielectric constant of the medium

$\epsilon_2(\omega)$ = real dielectric function of particles

$i\epsilon_2(\omega)$ = imaginary dielectric function of particles

The resonance in particles occurs when $\epsilon_1(\omega) \approx -2\epsilon_m$ in equation [1] if ϵ_2 is small.³⁷ V is dependent on the radius of spherical particles so it varies only in intensity of absorption maxima within the dipole approximation. The modification in Mie theory assumes that for small metal nanoparticles dielectric function depends on the size [$\epsilon = \epsilon(\omega, R)$]. Therefore, size-dependent absorption within the dipole approximation occurs which is known as intrinsic size effects.^{27,37} As shown in Fig 2.2, metal particles of nanometer sizes, most significantly ranging from 1 nm to 10 nm diameter, show size-dependent properties.³⁵

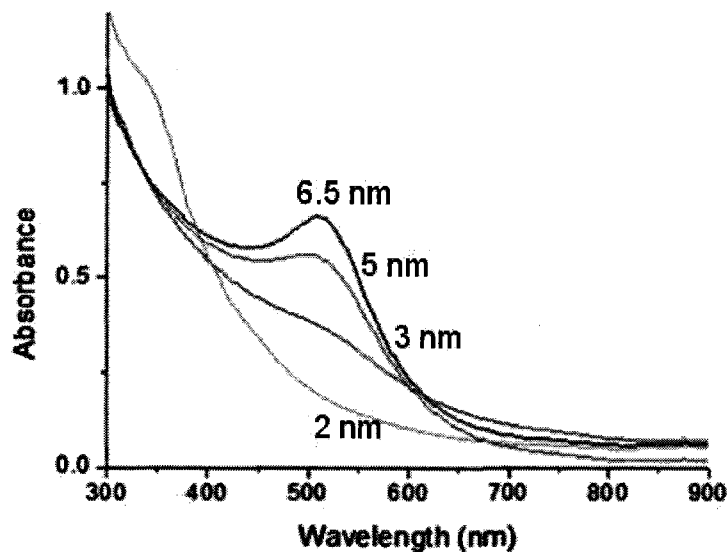


Figure 2.2 Size dependent surface plasmon resonance of gold nanoparticles.³⁵

For larger nanoparticles (>25 nm for gold particles) the extinction coefficient of SPR exclusively depends on the particle size.^{36,37} The larger the particles' size, the more important the SPR's higher order modes.²⁴ The higher order peak is at a lower energy, so the plasmon resonance of larger particles shifts to the red. The SPR bandwidth increases with increasing diameter of the nanoparticle because the wavelength of the interacting light leads to an inhomogeneous polarization of the large particles in an electromagnetic field. The broadening of the SPR is usually attributed to retardation effects.^{22,23} The optical absorption spectra of nanoparticles strongly depend on the size of particles. The size dependent property of these particles is known as an extrinsic size effect, which is explained by Mie's theory.²²

Among metal nanoparticles, gold nanoparticles (AuNPs) exhibit unique shape and size dependent optical properties. The AuNPs have an extremely high surface areas compared to its volume than the bulk gold (two million times more surface area).²³ The shape of AuNPs has a pronounced effect in the optical absorption spectrum. When the nanoparticles elongate to form a rod-like shape along one axis, the plasmon resonance of these particles splits into two bands.^{23,24} The band that absorbs at around 520 nm corresponds to the oscillations of electrons perpendicular to the short axis and is known as the transverse plasmon band.²⁴ The other band is caused by oscillations of electrons along the long axis of a particle and is known as a longitudinal plasmon band and appears in the near infrared region.^{24,38} The value obtained from long axis divided by short axis of the rod shaped particles is known as aspect ratio. As the aspect ratio increases, the energy

separation between resonance frequencies of the two plasmon bands increases.^{23,38,39}

Spherical AuNPs exhibit only one strong plasmon resonance band²⁷ in the visible spectrum that ranges from 400 nm to 700 nm.²³ The unique plasmon resonance of AuNPs has made it superior among metal nanoparticles. In this project, various types of phospholipid-coated spherical bilayer AuNPs that absorbed between 528 nm to 549 nm in UV-vis spectra have been synthesized. The classic method of AuNP synthesis and capping reagents used by various research groups in synthesis of AuNPs will be described next.

2.1.2 Gold Nanoparticles

AuNPs have been intensively studied for their potential application in various fields of science. Synthesis and characterization of AuNPs has attracted interest among scientists for its promising applications in catalysis,⁴⁰ biological labeling and sensing.^{21,41} A cell culture study of spherical AuNPs with various surface modifiers showed that these particles are biocompatible and nontoxic to human cells.⁴²

Various methods have been developed for synthesis of AuNPs. The classic method of synthesis of AuNPs involves the reduction of Au(III)Cl₃ with trisodium citrate, a method pioneered by Turkevitch in 1951,²¹ which was later modified by Frens in the 1970s.⁴³ In the classic method, citrate salt initially acts as a reducing agent and reduces Au(III) salt to Au(0), and later it also stabilizes the

AuNPs forming a layer of citrate ions on the AuNP surface. Another popular method of AuNP synthesis involves the two phase Brust-Schiffrin method⁴⁴ in which one phase is usually an organic solvent. The AuNPs synthesis in an organic solvent uses a capping agent, usually a thiol with a sodium borohydride reducing agent, which results in uniform size. Nanoparticles possess high surface electron density and are unstable, agglomerating during synthesis.⁴⁵ For this reason, nanoparticles are usually synthesized in the presence of stabilizing reagents. Spherical AuNPs have been synthesized by using various stabilizer such as surfactants,⁴⁶ polymers,⁴⁷ thiols,³⁰ dendrimers,^{48,49} and ionic liquids.⁵⁰ Thiols are the most common ligands in AuNP synthesis because the thiol protected AuNPs (Fig 2.3A) are highly stable and can be isolated and handled easily.⁵¹ However, thiols strongly interact with nanoparticle surfaces and form a densely packed monolayer on the surface, thus they are less useful for catalytic and biological applications.⁵² Tetraalkylammonium bromide-protected AuNPs (Fig 2.3(C)) are also known for long term stability.⁴⁶ However, this capping reagent also restricts AuNPs for their technological applications.⁵³ Citrate is commonly used as a capping as well as reducing reagent in AuNPs synthesis. AuNPs are synthesized by using the citrate reduction method that results in nanoparticles ranging from 2 nm to 100 nm. The size of particles can be tuned by changing the gold to citrate ratio during synthesis.⁴³

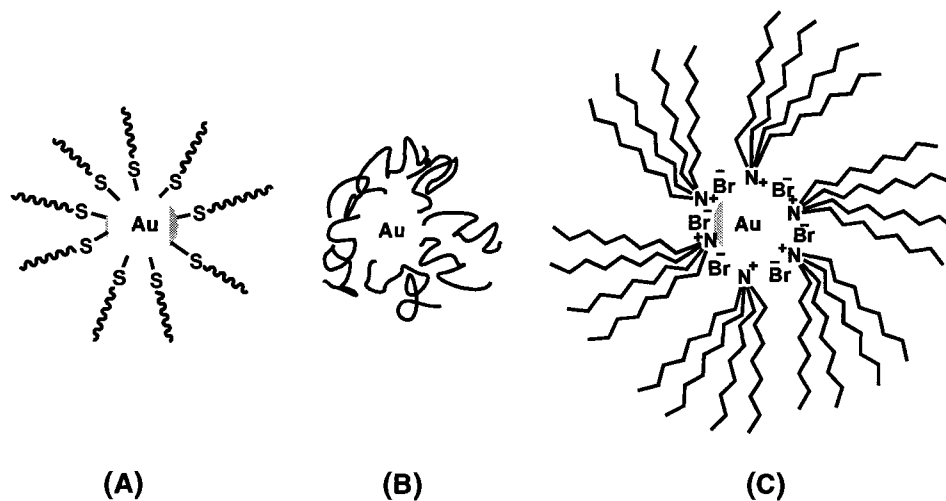


Figure 2.3 Schematic diagram of gold nanoparticles. (A) Thiol functionalized, (B) polymer-coated, and (C) TOAB-coated.

AuNPs have been widely used in interdisciplinary fields of science such as electronics,⁵⁴ catalysis,^{55,56} biotechnology,^{57,58} and material science.⁵⁹ Their increasing applications in various fields attracted scientists to develop nanoparticles of specific size, shape, and with variable functional groups. In fact, solubility and stability of nanoparticles have limited their applications in various fields. Surfactants or protecting reagents self assemble to form a monolayer onto the surface of the nanoparticle, which results in formation of Monolayer Protected Clusters (MPCs) nanoparticles.^{60,61} Further, Mixed Monolayer-Protected Clusters (MMPCs) nanoparticles have been synthesized by ligand exchange reaction in MPC. These particles are known to have increased solubility and stability and to be easy to handle,⁵¹ and they are reported to have wide applications in catalysis,^{62,63}

heavy-metal detection,⁶¹ and chemical recognition.^{64,65} Although a variety of MPCs and MMPCs AuNPs have been synthesized and used in various devices, the stability and solubility of these clusters have restricted them for long term applications. Recently, stabilities of AuNPs with structural variations in the capping reagents have been studied by different groups. Murray and co-workers⁵¹ have synthesized MPCs of gold by varying the chain lengths of alkanethiol and studied their stability in KCN. Various capping reagents such as xanthate,⁶⁶ dendrimers^{2,67} and peptide,^{68,69} have been used to tune the stability of AuNPs.

Nanoparticles' functionalization, solubility, and stability play critical roles in their use in biotechnology. The synthesis of bilayer AuNP has broadened the applications of AuNP for various purposes. Recent studies on bilayer AuNP and capping reagents used in synthesis of these particles will be described next.

2.1.2.1 Bilayer Gold Nanoparticles

In recent years, phospholipid-coated bilayer AuNPs have attracted an enormous interest with respect to their solubility, biocompatibility, and the potential applications in various fields of science. Sastry and coworkers have developed a simple one-step preparative method of cetyltrimethyl ammonium bromide bilayer protected gold nanocrystals with various morphologies.⁷⁰ AuNPs have been synthesized in the presence of cationic lipids and cholesterol.⁷¹ Further, various cationic lipids have been immobilized through disulfide onto AuNP with the aim of biological studies. He and co-worker have synthesized 1,2-dipalmitoyl-

sn-glycero-3-phosphothio-ethanol phospholipid modified AuNPs.⁷² They also have used different phospholipids to control the size of AuNPs. Recently, Zhu and coworkers have synthesized L- α -dipalmitoyl phosphatidylcholine (DPPC) monolayer-coated AuNPs at a water/toluene interface by a one-step process. Zhang and co-workers have synthesized stable and hydrophilic dimethyldioctadecylammonium bromide (DDAB) cationic lipid bilayer-protected AuNP in situ by reduction with NaBH₄.⁷³ DDAB has also been used as a capping reagent for the formation of monolayer-protected AuNPs in an organic medium.⁷⁴ Another group has reported that an increase in the concentration of DDAB in the synthesis of AuNPs changes the shape and size of the AuNPs.⁷⁵ Recently, Reed and co-workers have used L- α -phosphatidylcholine (95% Soy PC) in bilayer AuNP synthesis.⁷⁶ In this work, transfer of 95% Soy PC-coated monolayer AuNPs to bilayer AuNPs was achieved in the absence of a phase transfer reagent. More recently, Nakashima and co-workers have used 1,2-dipalmitoyl-*sn*-glycero-3-phosphothioethanol (DPPTE) for synthesis of gold nanorods.⁷⁷

Phospholipids are environmentally benign ligands for the synthesis of bilayer AuNPs. This research has used various types of synthetic and natural phospholipids for synthesis of bilayer AuNPs. A brief introduction of phospholipids and their self assembly in aqueous medium is described next.

2.1.3 Phospholipids

Phospholipids are a major structural component in biological membranes. A typical structure of a phospholipid is presented in Fig 2.4(A). Phosphatidylcholine is also known as lecithin, the most common phospholipid in which a hydrophilic polar headgroup links to a pair of hydrophobic acyl hydrocarbon chains. In aqueous media, molecules of phospholipids self assemble in a bilayer vesicle known as a liposome (Fig 2.4(B)) in order to minimize unfavorable interactions between hydrophilic bulk aqueous phase and the long hydrocarbon fatty acid chains.⁷⁸

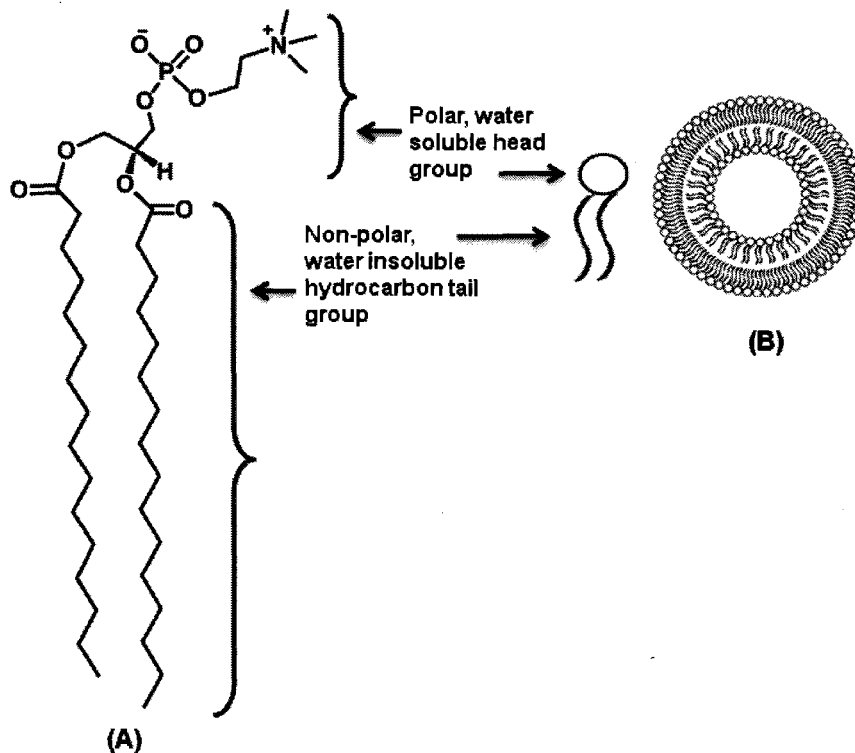


Figure 2.4 A bilayer assembly of phospholipids in water. (A) A typical phospholipid, (B) liposome.

Phospholipids can be derived from natural sources such as plants and animals or derived synthetically from the laboratory. Natural sources of these are in fact a mixture of phosphatidylcholines, with acyl chains of different lengths and varying degrees of unsaturation. Phospholipids from plant sources have a high level of polyunsaturation in the fatty acyl chains and from animal source contains a higher proportion of fully saturated chains.⁷⁸ Lecithin derived from soybean contains various phospholipid compositions. As listed in Avanti Polar Lipids catalog, phosphatidylcholine (95% Soy PC) used in this research consists of 97.2% L- α -phosphatidylcholine including numerous other lipids such as phosphatidylethanolamine, phosphatidylinositol, phosphatidic acid and 2.8% various lipid phosphatidylcholine (LPC). Furthermore, sphingomyelin derived from animal sources, in particular from egg and chicken, consists of a few saturated phospholipids with different acyl chains.

Self assembly of lipids in aqueous media varies with the type of headgroups and tail lengths of lipids. Self assembled structures formed by lipids of different headgroups and acyl chain lengths are shown in Table 2.1.

Table 2.1 Self assembled structures for different headgroups and acyl chain of the lipids.⁷⁹

Lipids	Type of self assembled structure formed in water
Single-chained lipids with large headgroups (e.g., detergents, lysolipid)	Spherical micelles
Double-chained lipids with large headgroup areas and fluid chains (e.g., sphingomyelin, phosphatidylcholine, phosphatidylglycerol, phosphatidylserine)	Bilayer membranes
Double-chained lipids with small headgroups (e.g., phosphatidylethanolamine)	Hexagonal II (H _{II}) or inverted micelles

This project has used various types of phospholipids in AuNP synthesis and tested the stability of these particles. For this study, various types of phospholipids which differ in headgroups, tail lengths, and tail saturation were used. The fluidity of the phospholipid bilayer depends on headgroups, tail length and tail saturation. In the following section, the effect of changing headgroup and acyl chain in phospholipid bilayer curvature will be described.

2.1.3.1 Lipid Curvature

Biological membranes are known to exist in bilayer curvature stress. The functions of biomembranes are controlled by spontaneous curvature of the membrane's monolayer.⁸⁰ Anderson and coworkers reported that the hydrophobic interactions of the lipid bilayer and membrane protein cause bilayer curvature stress, which can play a crucial role in protein conformation and structural change.⁸¹ This phenomenon modulates protein functions.

Biological membranes consist of a wide variety of phospholipids of various compositions.^{79,82} Further, individual constituents of the membranes' monolayer change the packing in the monolayer, which contributes to the equilibrium curvature of the monolayer resulting in bilayer curvature frustration. The bilayer membranes also include small size headgroup phospholipids present in the monolayer that do not self-assemble into a bilayer assembly; these are known as non-bilayer lipids.^{80,83} The small size headgroup phospholipids, for example, phosphatidylethanolamine, have a cone shape and prefer inverted hexagonal (H_{II}) or nonlamellar phase upon hydration.⁸⁰ When these non-bilayer phospholipids, in appropriate proportion, are combined with the other bilayer forming phospholipids, they cause spontaneous negative curvature in the monolayer.^{80,84} The flat lamellar $L\alpha$ phases are formed by the assembly of the cylindrical phospholipids with large headgroup lipids as in phosphatidylcholines.^{84,85} Moreover, the small headgroup lipids that form non-bilayer structures are believed to be important in membrane fusion and control activity of membranes associated proteins.⁸⁶ Another type of

phospholipid are the conical lipids with large polar headgroups such as lysolipids that form either micelles or the hexagonal H_{II} phase.⁸⁷

The equilibrium curvature of a membrane's monolayer could be positive, zero, or negative depending on the shape and size of headgroups of phospholipids compared to their acyl chain area.^{88,89} The monolayer prefer positive curvature as seen in Fig 2.5(A), if the effective shape of the polar headgroup of the phospholipid is greater compared to the acyl chains. The monolayer of a membrane changes to negative curvature (Fig 2.5(C)) if the effective shape and size of the phospholipid headgroup is smaller compared to the acyl chains. Phospholipids with a cylindrical shape form planar monolayers with zero equilibrium curvature (Fig 2.5(B)).^{84,88,89} Further, Anderson's group reported that the equilibrium curvature can be changed by the addition of amphipathic molecules that differ in the shape of the polar headgroup.⁸¹

The change in a membrane's curvature stress could be due to change in packing of the monolayer which may result in density change.⁹⁰ As a consequence, membrane lipids exert a force on membrane protein to perturb the conformation and structure of the protein. Eventually, change in conformation changes the activities of protein in biological membranes.^{83,90}

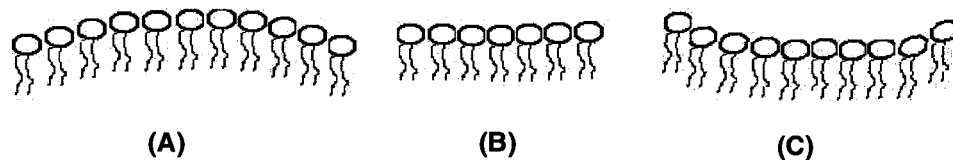


Figure 2.5 Lipid curvature (cartoon).⁸⁷ (A) Positive, (B) zero, and (C) negative.

Gruner proposed the idea of spontaneous curvature ($1/R_0$), where R_0 is defined as the radius of monolayer curvature that minimizes the bending elastic free energy and is a property of the individual lipid species.⁸⁴ The elastic free energy, μ_E , is expressed by

$$\mu_E = k (1/R - 1/R_0)^2 \quad [2]$$

where

k = elastic constant,

R = radius of the curvature of lipid/water interface, and

R_0 = equilibrium radius of curvature

$R_0 = R$ is in an elastically relaxed state in monolayer. R_0 is a property of a lipid, which does not depend on shape of lipid. However, factors such as temperature or unsaturation decrease the R_0 . A charge on a headgroup also increases the effective headgroup area, which increases the R_0 . If other energies do not compete with μ_E , the lipid monolayer will have lower elastic energy.⁸⁴

Charge on the headgroup of a phospholipid, hydration, and temperature changes the lipid fluidity of bilayer membrane.^{81,91} In one study, Gruner and Kirk have found that addition of hydrophobic alkane in a phospholipid bilayer changes it from lamellar to hexagonal phases.⁹² A change in lipid shape in monolayer results in curvature of membranes, which could be due to change in the molecular packing in the membrane.⁸⁷ The lipid bilayer environment affects the characteristic of several types of channels, including membrane protein channels, such as sodium and potassium channels.⁹³

Based on the references mentioned above, lipid curvature can be altered by the addition of lipids that differ in shape and size of the polar headgroups and acyl chains. The stable mixed thiol/phospholipid-coated bilayer AuNPs prepared in this project can be applied in the formation of solid-supported lipid bilayer and is described next.

2.1.3.2 Application of Phospholipid-Coated Gold Nanoparticles in of Solid-Supported Lipid Bilayer

Solid-supported phospholipid bilayers are simple and versatile model of biological membranes for biotechnological applications.^{94,95} Phospholipid membranes have intrinsic properties to fuse and self organize into a planar bilayer membrane onto various solid substrates.⁹⁶ The electrostatic interactions between positively charged solid support and negatively charged or zwitterionic lipid vesicles play a vital role in the adsorption of lipids on solid substrates.⁹⁷ The solid bound membranes mimic one property of cellular membranes: maintaining lateral fluidity.^{98,99} Therefore, such membranes are excellent models for investigation of cell signaling,¹⁰⁰ membrane-protein interactions^{101,102} and pathogenic attack.⁹⁸ Further, solid bound bilayer membranes possess unique physical properties, and the two-dimensional fluidity of individual lipid molecules is maintained by a film of water trapped between the solid substrate and the bilayer.^{103,104} Typically, the ultrathin film of water between the solid support and the lipid bilayer is around 10 Å.¹⁰⁵

Various methods have been used to form solid supported lipid bilayers. One of the methods of formation of solid-supported lipid bilayers is the adsorption and fusion of vesicles from an aqueous solution to the solid substrate, for example, glass or silica¹⁰⁶ as shown in Fig 2.6(A).⁹⁸ The spontaneous fusion of lipid bilayer vesicles takes place with an appropriate hydrophilic solid surface, such as oxidized Si, resulting in a surface bound bilayer.^{107,108} The membrane

deposition models on solid support have been widely exploited for mimicking cell membranes as well as for their potential biotechnological applications.¹⁰⁹

Solid support bound lipid bilayer and hybrid lipid bilayer have been intently studied for their potential applications in nanotechnology and for understanding the role of cell membranes.⁹⁸ Further, the solid-bound hydrated lipid bilayer (Fig 2.6(B)) has attracted interests in biosensor design. Recently, Boxer and Cremer have reported that phospholipid membranes in combination with microfluidic devices can be applied in sensor platforms.¹¹⁰ The amphiphilic phospholipid membrane can coordinate closely associated proteins or nanoparticles either on surfaces or inside the membrane.⁹⁸ Furthermore, solid supported bilayers are an attractive model in biotechnology because they possess mechanical stability and thus accessibility to various analytical techniques (e.g., internal reflection, SPR, and atomic force microscopy (AFM)) that can detect interfacial events with high sensitivity.^{96,98,111} Further, they can be used to generate micropatterned membranes on a solid support. For example, a bilayer membrane can be micropatterned onto a glass or suitable solid substrate by standard microfabrication or microcontact printing.¹¹² The hybrid bilayer containing both thiol and natural lipids provides an insight into understanding membrane protein activity.¹¹³ Further, a hybrid membrane is one approach of stabilizing a lipid bilayer membrane on a solid support, which conserve structural and physical properties of the lipid bilayer.¹¹³ For example, a hybrid bilayer with a bottom self-assembled hydrophobic thiol monolayer on a solid surface and a top lipid layer can be formed and then hydrated.^{104,114} The solid supported

hydrophobic thiol and thiolipid monolayer are shown to have better electrical conductivity and thermal stability compared to lipid monolayers.¹¹⁵ Further, SPR can be applied to the hybrid lipid bilayer assembled with gold film or glass substrate in specific protein-membrane binding study.¹¹⁴ In addition, this approach provides hydrophobicity to metal support, which is accessible to electrochemical techniques.¹¹⁶

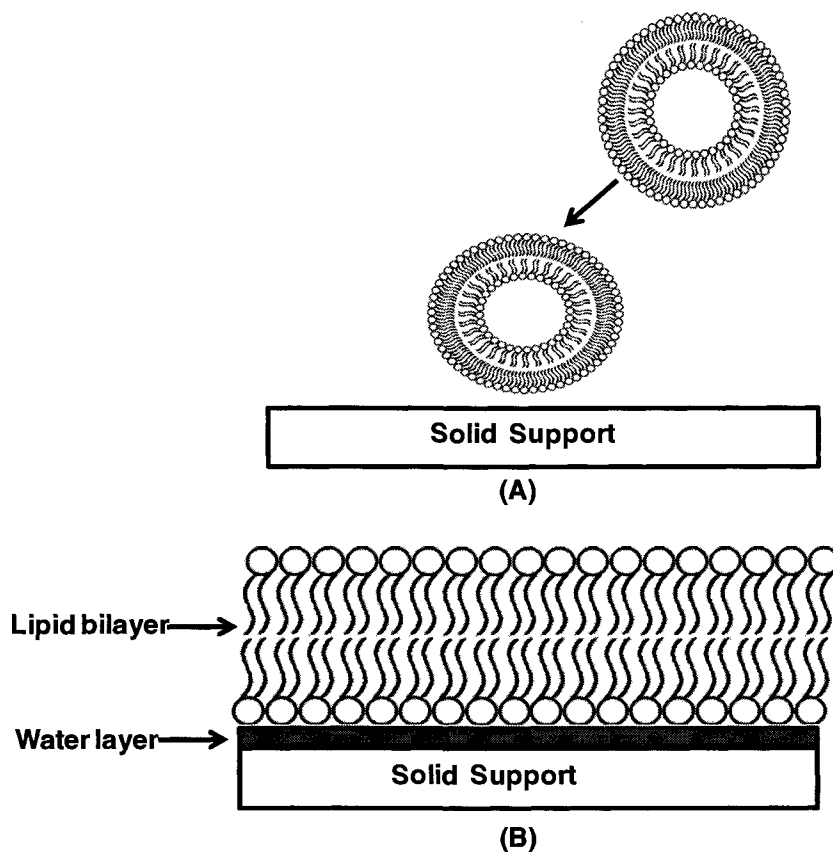
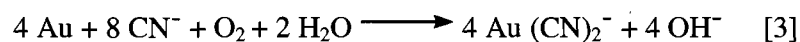


Figure 2.6 Formation of solid-supported lipid bilayer. (A) Deposition of the liposome on solid support, (B) rearrangement of liposome to form bilayer on solid support.⁹⁸

Phospholipid-coated bilayer AuNPs and mixed thiol/phospholipid-coated bilayer AuNPs could find applications in the formation of solid-supported bilayers for the development of biological sensors. This research has developed a method for the formation of various types of mixed thiol/phospholipid coated bilayer AuNPs that are remarkably stable towards potassium cyanide (KCN). Variation in the stability of AuNPs has been reported by different research groups. The stability of AuNPs in KCN varies depending upon the capping reagent used in synthesis of nanoparticles and is described next.

2.1.4 Stability of Gold Nanoparticles in Potassium Cyanide

Cyanide is known to dissolve gold to form a soluble gold complex in the presence of oxygen. In a cyanide solution, oxygen oxidizes gold (0), and cyanide ions form a complex with gold ions (III). Elsner's equation¹¹⁷ for cyanide etching of gold is expressed as:



Cyanide etching is frequently employed to characterize the ligands adsorbed on the gold surface. AuNPs in the presence of cyanide and oxygen decrease in size.¹¹⁸ The stability of monolayer protected AuNPs in cyanide has been studied by Murray and co-workers.⁵¹ This study showed an increase in

stability with the increase in carbon chain lengths of the alkanethiol. The stability of the thiol-coated AuNPs in KCN increases gradually from 2 – 12 carbons in the thiol.¹¹⁹ The rate of decomposition correlates with a protective barrier that the thiolated monolayer provides to the gold surface. The Monolayer Protected Cluster (MPC) exhibiting strong hydrogen bonding showed the slowest decomposition rate with KCN.¹²⁰ The decomposition rate increased up to 9-fold for the MPC with the weakest hydrogen bonding. Similarly, the stability test of the monolayer protected nanoparticles in KCN was also studied by Knoll and co-workers.¹²¹ This study showed that surface-modified AuNPs are more resistant to cyanide etching. However, the stability of these particles lasts less than an hour. The strength of the intramolecular hydrogen bond was correlated with resistance of the AuNPs to cyanide-mediated oxidative etching.¹²⁰ The distance dependent correlation of dendron-coated AuNPs showed an increase in stability of particles in cyanide.¹²² The stability test of the AuNPs coated with cross-linked block copolymers was sensitive to the structure of the cross-linker and distance of cross-link from the nanoparticle surface.¹²³ Chen and co-workers¹²⁴ observed enhanced chemical and physical stability of AuNPs in KCN by cross linking amphiphile block co-polymer with an increase of UV-irradiation time.

The stability of different ligand-coated AuNPs changes depending upon the types of ligands used in the AuNPs. The stability and solubility of nanoparticles has a significant impact in their potential application in biomedicine. Stable AuNPs can also be useful in micropatterning since KCN-mediated washing of these particles does not dissolve the protected AuNPs in the micropattern. In the second project of this thesis, I succeeded in synthesizing various types of

remarkably stable mixed thiol/phospholipid-coated AuNPs in the presence of excess KCN compared to the AuNPs previously described in the literature.

2.1.5 Stability of Gold Nanoparticles in Iodine

Iodine is also known to etch gold. Iodide ions form a strong bond with gold.¹²⁵ The iodine adsorption on a gold surface is expressed in the equation below:



Finklea described that a monolayer of iodide forms spontaneously upon immersing a bulk gold in dilute iodine solution.¹²⁶ Recently, Wang and co-workers reported the aggregation of AuNPs in the presence of iodine.¹²⁷ Further, they mentioned that the adsorbed iodine on AuNPs lowers the surface potential, and as a result, increases van der Waal's attractive forces between iodide-coated nanoparticles that resulted in the aggregation of particles. Generally, a saturated iodine solution in the presence of KI can oxidize gold nanoparticle into Au³⁺ ions. Sastry and Rautaray performed leaching experiment of the AuNPs coated on membrane in iodine solution.¹²⁸ Their study showed complete disappearance of gold color from the membrane. Iodine forms the most stable complexes with gold,¹²⁶ and it has been used to quantify ligands adsorbed on the surface of AuNP. Murray and co-workers have used iodine to determine the amount of ligand in a ligand-exchange reaction.¹²⁹ In this work, the decomposition of MPCs gold with

iodine quantitatively liberated the alkanethiolate monolayers as dialkyl disulfide compounds, but liberation of ligand was found difficult compared to cyanide exposed decomposition. Iodide ions exert a major influence over the evolution of the shape of a gold nanocrystal. Recently, Weaver and Wasileski have reported that iodine has a strong affinity to chemisorb on the gold surface.¹²⁵ Further, their study showed that iodine brings rapid reconstruction on the adsorbed faces of gold surface. Sastry and co-workers predicted that iodine binds strongly on the surface of gold and the mismatch between the gold surface and adsorbed iodide leads to the change in morphology of AuNPs.¹³⁰ More recently, Prasad and co-workers have shown that the addition of iodine brings changes to the shape and size of monolayer protected AuNPs.¹³¹ In their work, 1 nmol of iodine is sufficient to aggregate 9000 nmol of AuNPs.

As reported in the literature, iodine causes a change of shape, aggregation, and a shift in plasmon resonance of AuNPs as described above. This project has tested stability of various types of phospholipids-coated bilayer and mixed thiol/phospholipid coated bilayer AuNPs in iodine solution. Unlike instability of AuNPs in iodine described in the references, this project has shown no significant change in the shape and size of hybrid bilayer AuNPs in excess of iodine.

2.2 GOALS AND OBJECTIVES OF THESIS (PART 2)

AuNPs have been employed in various fields of science. The shape, size, stability, and solubility of AuNPs has limited their use in biomedicine and other fields of science. Phospholipids are major components of biomembranes and constitute an environmentally benign source of ligand to functionalize AuNPs, providing solubility in water. The goal of this project is to develop various types of phospholipid-functionalized hybrid bilayer AuNPs, tune the size of the particles by varying the phospholipid types, and test their stability.

The main objectives of this project are:

1. To synthesize various types of phospholipid-coated bilayer AuNPs and hybrid bilayer AuNPs by using phospholipids that differs in headgroups and acyl chains.
2. To analyze TEM images of various types of phospholipid-coated hybrid bilayer AuNPs to verify any change in size or shape with variation of phospholipids.
3. To test the stabilities of various types of phospholipid-coated hybrid bilayer AuNPs in KCN and iodine solutions.

The hypothesis made in this project was that variation of phospholipids in the synthesis of AuNPs changes the size and stability of AuNPs. To test this hypothesis, the project started with selection of various types of natural and synthetic phospholipids that differ in headgroup, acyl chain length, and degree of

saturation. To achieve the goals and objectives of this project the following sections described synthetic procedures for phospholipid-coated bilayer AuNPs and hybrid bilayer AuNPs and their size analysis and stability tests.

2.3 EXPERIMENTAL

This section describes the general materials and methods for the synthesis of seven types of phospholipid-coated AuNPs and the preparation of these particles for TEM analysis. The general procedures leading to the formation of hybrid bilayer AuNP, and their stability tests are also described.

2.3.1 Materials and Methods

HAuCl₄ (Strem Chemicals), 95% L- α -phosphatidylcholine (95% Soy PC), 1-palmitoyl-2-oleoyl-*sn*-glycero-3-phosphocholine (POPC), L- α -phosphatidylcholine hydrogenated (HyPC) (egg), 1,2-dilauroyl-*sn*-glycero-3-phosphocholine (DLPC), 1,2-dipalmitoyl-*sn*-glycero-3-phosphoethanolamine (DPPE), and sphingomyelin were bought from Avanti Polar and used as received. L- α -phosphatidyl-DL-glycerol sodium salt (PG) (egg yolk), 1,2-diacyl-*sn*-glycero-phospho-L-serine (PS) (brain), and glycerol trioleate (TG) were bought from Sigma/Aldrich and used as received. Chloroform (VWR) was filtered through basic alumina before use. All other chemicals were purchased from Sigma/Aldrich and were used as received. Nanopure water was from Milli-Q ultra-pure system. The optical absorbances of dilute solutions of nanoparticles were measured with an Ocean Optics USB 2000 UV-vis spectrometer and Agilent 8453 UV-vis spectrophotometer with a diode array using a 1 cm path length quartz cell.

2.3.2 Transmission Electron Microscopy (TEM)

Samples for TEM were prepared by drop-casting dilute solutions of nanoparticles onto carbon-coated (300 Å) Formvar films on copper grids (Ted Pella). For dilute samples of an optical density 1.2, 5 μL of sample was loaded on the grid repeatedly, followed by allowing the sample to dry in air for a few minutes. For more concentrated samples only 5 μL were loaded. Subsequently, the samples were dried in air for one day before the TEM images were obtained. Transmission electron micrographs were acquired on a TEM FEI Tecnai F-20 at an acceleration voltage of 150 kV using a CCD detector. The size of the nanoparticles were analyzed by using ImageJ Software, after applying a bandpass filter to the images and adjusting the filters' threshold. The histograms were obtained with a window bin size of 2 nm. Each histogram presented in this thesis shows the x-axis center value of the bin that ranged from +1 to -1.

2.3.3 General Procedures

2.3.3.1 Preparation of Liposomes

The eight different types of phospholipids in 9.9 μmol quantities were dissolved in chloroform and transferred into labeled scintillation vials. Subsequently, TG (0.1 μmol , 1 mol % of phospholipids) was dissolved in Chloroform, added to each vial, and swirled until the phospholipids dissolved. Sphingomyelin was not completely soluble in Chloroform so a drop of methanol

was added. DPPE was not soluble in Chloroform at room temperature so it was sonicated at 55 °C for an hour. The solvent was carefully evaporated under a stream of nitrogen until it formed a thin film. Subsequently, the film was dried *in vacuo* for one day. Water (4 mL) was added to the dried, thin lipid film, and sonicated for 45 min. The transparent liposome obtained after sonication was used in the synthesis of bilayer AuNPs, immediately.

2.3.3.2 Synthesis of Various Types of Phospholipid-Coated Bilayer Gold Nanoparticles

Liposomes (10 μmol , 4 mL) of each phospholipid, including TG, were transferred into labeled vials. An aqueous solution of HAuCl_4 (10 μmol , 3.4 mL) of concentration 2.94 mM and sodium citrate (25 μmol , 0.98 mL) were added to the vials with liposome solutions. The combined mixture was stirred at room temperature. After an hour the solution in the vial slowly changed to a bluish color. Stirring was continued for another 6 h, and the solution was stored at room temperature overnight. The solubility of these AuNPs slowly increased in one to two days. Vials containing PG, PS, and phosphatidylcholine (PC) became detectably purple in 30 min, and an intense purple in 2 h. The UV-vis spectra were recorded for seven types of bilayer AuNPs at the same dilution after one day of synthesis at room temperature.

2.3.3.3 General Procedure for Synthesis of Hybrid Bilayer Gold

Nanoparticles

Different concentrations of thiol-exchanged hybrid bilayer AuNPs were obtained by varying the amount of thiol. 1-Decanethiol (1 mM) in ethanol, 20 nmol (20 μ L), 5 nmol (5 μ L), and 1 nmol (1 μ L) were added separately to the phospholipid-coated bilayer AuNPs solutions (1 mL) of an optical density of 1.2, and stirred for 2 h at room temperature.

2.3.3.4 General Procedure for Stability Tests of Bilayer and Hybrid Bilayer Gold Nanoparticles in KCN

A KCN solution in water (20 μ L, 307 mM) was added to the aqueous solutions of various types of phospholipid-coated bilayer and hybrid bilayer AuNPs (1 mL) of an optical density of 1.2. Subsequently, the spectra were collected every 30 seconds, with constant stirring for one hour.

2.3.3.5 General Procedure for Stability Tests of Bilayer and Hybrid Bilayer Gold Nanoparticles in Iodine

Iodine solution in ethanol (10 μ L, 0.1 mM) was added to the aqueous solution of various types of phospholipid-coated bilayer and hybrid bilayer AuNPs solutions (1 mL) of an optical density of 1.2, making the total concentration of the

solutions 1 μM . UV-vis spectra were collected every 30 seconds for one hour with constant stirring.

2.4 RESULTS AND DISCUSSION

In this section, synthesis of various types of phospholipid-coated bilayer AuNPs and different concentrations of thiol exchange in various types of phospholipid-coated bilayer AuNPs to form hybrid bilayer AuNPs will be discussed. TEM image analysis of various types of hybrid bilayer AuNPs will be shown. Finally, the results of stability tests of various types of hybrid bilayer (mixed thiol/phospholipid) AuNPs and bilayer AuNPs in the presence of KCN and iodine will be presented.

2.4.1 Phospholipid-Coated Bilayer Gold Nanoparticles

Eight different types of phospholipids, as listed in Table 2.2, were used in the synthesis of bilayer AuNPs. Among these lipids DPPE, DLPC, and POPC are synthetic phospholipids while 95% Soy PC, HyPC, sphingomyelin, PG, and PS are from natural sources. As shown in Table 2.2, these phospholipids vary in pK, depending upon the headgroups on the lipids.^{78,132,133} Quaternary amine headgroup in phospholipids showed higher pK compared to ethanolamine headgroup in phospholipids. PS has three pK values for phosphate, amine, carboxyl ionic species and PG has only one pK for phosphate ion.¹³² Phospholipids with a negative charge in headgroup, such as PS and PG are more acidic while the phospholipids with choline headgroups are more basic. The basicity of phospholipids decreases for different headgroup in order of choline > ethanoamine > serine.¹³⁴ Further, phospholipids with high basicity also exhibited high melting points. For example,

phosphatidylethanolamines, sphingomyelin, and phosphatidylcholines show melting point of about 197, 210 and 230 °C respectively.¹³⁴ The difference in acidity of these lipids is expected to change the reduction potential in AuNPs synthesis.

The structures of natural and synthetic phospholipids of different chain lengths with different degrees of saturation used in the synthesis of bilayer AuNPs are shown in Fig 2.7. POPC and 95% Soy PC have different degrees of unsaturation with the same chain lengths, whereas DLPC and HyPC are saturated but have different chain lengths. DLPC and POPC are synthetic lipids with a high degree of purity, while 95% Soy PC is derived from soybeans and HyPC is derived from egg yolk and both consist of other lipids as impurities.

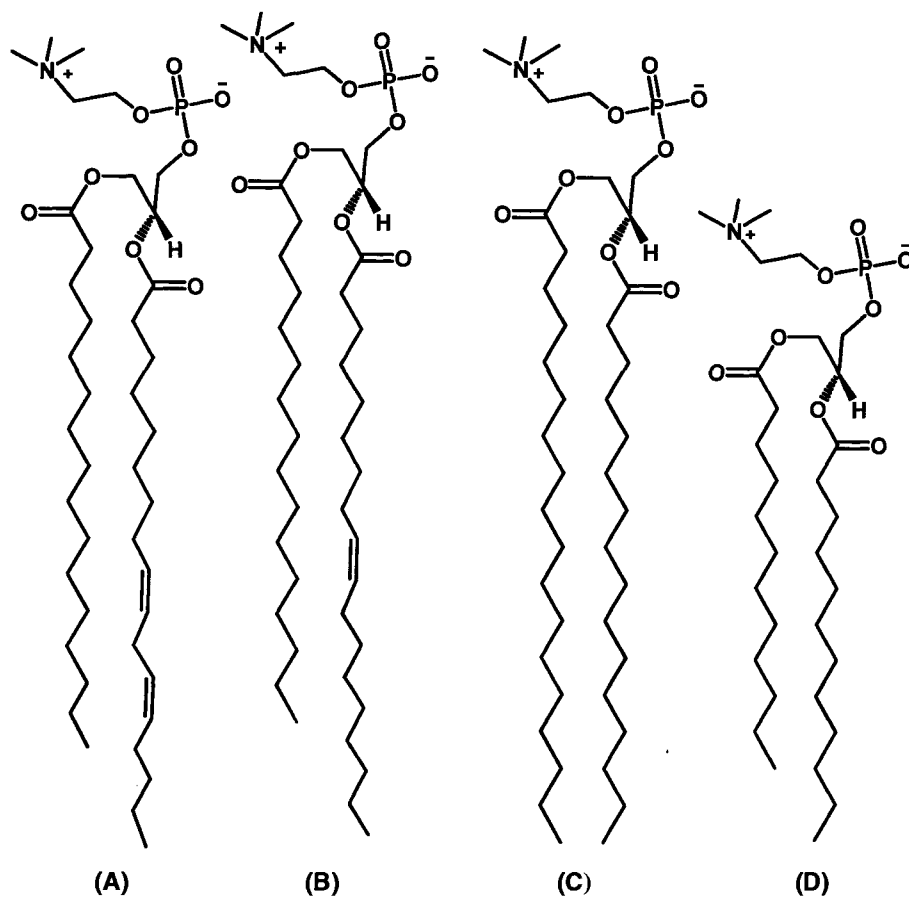


Figure 2.7 Structures of phospholipids with different acyl chain lengths and degrees of saturation. (A) 95% Soy PC, (B) POPC, (C) HyPC, and (D) DLPC.

The structures of phospholipids with different headgroups which were used in the synthesis of bilayer AuNPs are shown in Fig 2.8. DPPE has a smaller headgroup as compared to sphingomyelin. PG and PS have a negative charge on the headgroup. The DPPE used in the synthesis of bilayer AuNP is a synthetic lipid with a high degree of purity.

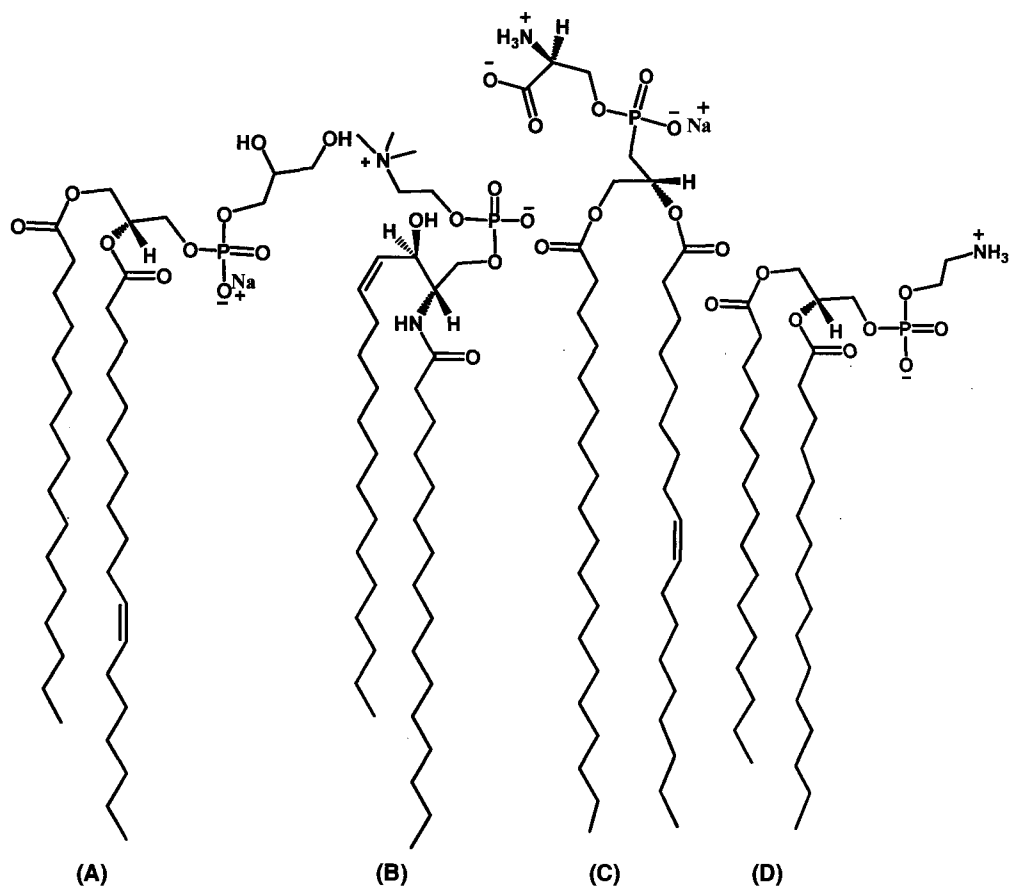




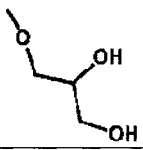
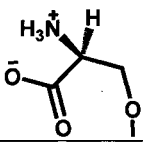
Figure 2.8 Structures of phospholipids with different headgroups. (A) PG, (B) sphingomyelin, (C) PS and (D) DPPE.

Liposomes consisting of various types of phospholipids, as listed in Table 2.2, were prepared as shown in Scheme 2.1 before the synthesis of AuNP. The molecular weight of each phospholipid listed in Table 2.2 was used in the calculation of the amount of phospholipids utilized in preparing the liposomes. However, natural phospholipids also include a large amount of other lipids as impurities and correction for variable molecular weights was not done. For the

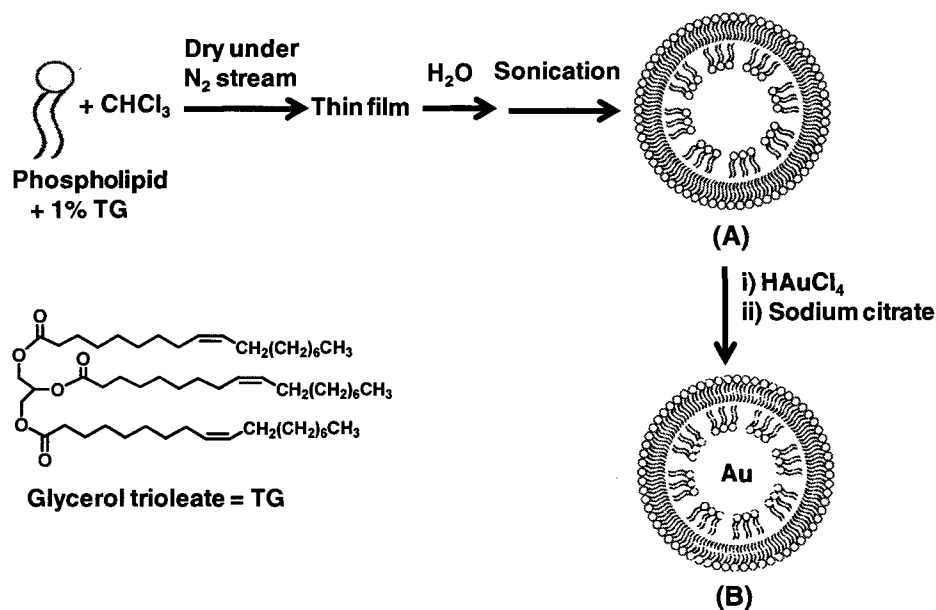
natural phospholipids molecular weight of abundant species was used in calculation of amount of lipid. After 45 min of sonication in water, clear liposome solutions were obtained with choline, serine, and glycerol headgroup phospholipids. However, DPPE did not form a clear liposome solution, and some precipitates of DPPE were observed after 45 min of sonication.

Various types of phospholipid-coated bilayer AuNPs were synthesized by the monophasic method as shown in Scheme 2.1. A gold to liposome ratio of 1: 1 was reduced by aqueous sodium citrate (2.5 equiv). The solution of gold salt (HAuCl_4) in water absorbs with peaks at 315 nm (maxima) and 270 nm (minima) in its UV-vis spectrum.¹³⁵ The disappearance of absorption maxima for gold (III) at 315 nm (spectrum not shown) and the appearance of plasmon resonance in the visible region as shown in UV-vis spectra (Fig 2.9) are an indication of the transformation of gold (III) into gold (0). Synthesis of AuNPs was also attempted under similar conditions using sodium citrate (5 equiv). AuNPs generated from 5 equiv of sodium citrate also showed similar SPRs in the UV-vis spectra compared to AuNPs made using 2.5 equiv of sodium citrate. All AuNPs discussed for UV-vis spectra, TEM analysis, and stability tests were made by using 2.5 equiv of sodium citrate.

Table 2.2 Phospholipids with different headgroups and acyl chain lengths

Phospholipids	Hydrophobic tail	pK ¹³²	M.W.	Headgroups
L- α -phosphatidylcholine (95% Soy PC)	Unsaturated	13 (quaternary amine)	758	
1-palmitoyl-2-oleoyl- <i>sn</i> -glycero-3-phosphocholine (POPC)	Unsaturated	2.5 (PO ₄ ⁻)	760	
1,2-dilauroyl- <i>sn</i> -glycero-3-phosphocholine (DLPC)	Saturated		621	
L- α -phosphatidylcholine, hydrogenated (HyPC) (egg)	Saturated		762	
Sphingomyelin (egg, chicken)	Unsaturated		703	
1,2-dipalmitoyl- <i>sn</i> -glycero-3-phosphoethanolamine (DPPE)	Saturated	9 (amine) 2.5 (PO ₄ ⁻)	691	
L- α -phosphatidyl-DL-glycerol (PG) (egg yolk)	Unsaturated	3 (PO ₄ ⁻)	768	
1,2-diacyl- <i>sn</i> -glycero-phospho-L-serine (PS) (brain)	Unsaturated	10.3 (amine) 2.5 (PO ₄ ⁻) 4.5 (COO ⁻)	790	

Scheme 2.1



Scheme 2.1 Systematic scheme of bilayer gold nanoparticles synthesis (A) Liposome, i) HAuCl_4 in H_2O , ii) sodium citrate in H_2O (2.5 equiv), and (B) bilayer gold nanoparticles.

TG (1 mol % of phospholipid) was added to all phospholipids before the formation of liposome in order to obtain a better solubility of the nanoparticles. The phospholipid-coated bilayer AuNPs that were synthesized in the absence of TG showed scattering in the UV-vis spectra. In the presence of 1 mol % TG, only small scattering was observed. In fact, the TG higher than 1 mol % of the phospholipid that was added in the synthesis of AuNPs showed more scattering in the UV-vis spectra (spectra are not shown here). However, in the absence of TG the AuNPs solubility slowly increased over time.

A negative spontaneous curvature (as seen in Fig 2.5(C)) is common for phospholipids with small headgroups.⁸³ In aqueous solution, these lipids may aggregate to form hexagonal II phase structures. Since DPPE has a smaller headgroup compared to other phospholipids, liposomes of DPPE were found to be unstable because they did not form a clear liposome solution. Indeed, the DPPE-coated bilayer AuNPs showed precipitation of AuNPs as evidenced in UV-vis scattering (spectrum not shown here). Both the negatively charged PG and neutral charged PC have zero spontaneous curvature. The location of sodium ion has a larger effect on the bilayer fluidity properties than the lipid's headgroup size.⁷⁸ In this research, the PG-coated bilayer AuNPs formed easily, and were found more soluble compared to other phospholipid-coated nanoparticles. The color of the glycerol headgroup in phospholipid-coated bilayer AuNP started to develop within 30 min and reached an intense reddish purple after an hour of stirring at room temperature. The mixture was continuously stirred for 2 h and later stored at room temperature. As compared to other phospholipid-coated AuNPs, the glycerol headgroup in phospholipid-coated bilayer AuNP formed much faster and became very soluble. The higher solubility of the glycerol headgroup in phospholipid-coated AuNPs compared to other phospholipids could be due to the sodium ion present.

The UV-vis spectra for all bilayer AuNPs were recorded after one day of synthesis. For all seven different types of phospholipids, water soluble bilayer AuNPs formed and solubility of AuNPs increased slowly over time, which showed increase in absorbance in UV-vis spectra (comparative spectra are not shown). The

UV-vis spectra of these nanoparticles (as shown in Fig 2.9) showed λ_{\max} ranging from 529 nm to 549 nm. The λ_{\max} of SPR of various types of phospholipid-coated bilayer AuNPs with TG (1 mol % of phospholipid) are listed in Table 2.3. Citrate reduced bilayer AuNPs of PS and sphingomyelin initially formed a black color, and over time changed to a reddish-purple indicating that small particles had formed first. Sphingomyelin-coated bilayer AuNP showed λ_{\max} at 536 nm, while PS-coated bilayer AuNP absorbed at λ_{\max} 534 nm with no sharp SPR. The broad SPR in sphingomyelin-coated bilayer AuNP could be due to the broader size of distribution of these particles, as described in image analysis of these particles. Even though SPRs of these particles shifted by a few nanometers, only a small change in size was observed in the TEM image analysis.

Sodium citrate reduced bilayer AuNPs of POPC, 95% Soy PC, HyPC, and DLPC formed more slowly compared to the negatively charged headgroup (glycerol or serine) coated nanoparticles. Negative headgroups in phospholipids resulted in highly water-soluble bilayer AuNPs with narrow size distribution (detail in TEM image analysis). In addition, these nanoparticles showed less scattering in UV-vis spectra (as shown in Fig 2.9(A)) as compared to other phospholipids. Initially, all phospholipids, except PG, showed a black color in one hour and after 4 h these particles turned purple. The UV-vis spectra of these particles showed small scattering (as shown in Fig 2.9(B)). In particular, the UV-vis spectrum of DLPC-coated bilayer AuNP showed less scattering compared to 95% Soy PC-coated bilayer AuNPs. DLPC-coated bilayer AuNPs showed λ_{\max} at 536 nm and 95% Soy PC-coated bilayer AuNPs showed λ_{\max} at 531 nm.

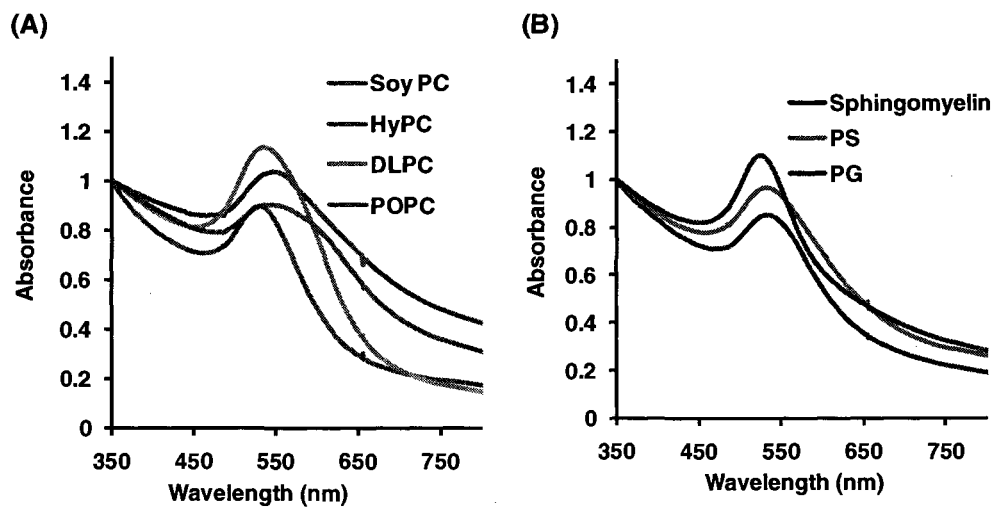


Figure 2.9 UV-vis spectra of bilayer gold nanoparticles in water (normalized at 350 nm). (A) Phospholipid-coated bilayer gold nanoparticles with different acyl chain. Green – DLPC, red – HyPC, purple – POPC and blue – 95% Soy PC. (B) Phospholipid-coated bilayer gold nanoparticles with different headgroups. Maroon – sphingomyelin, blue – PS, and green – PG.

The sharpness of intensity of SPR in the UV-vis spectra indicated that the glycerol headgroup in phospholipid and DLPC-coated nanoparticles have a narrow size distribution. PG-coated bilayer AuNPs showed λ_{max} at 529 nm with sharp SPR.

Table 2.3 λ_{max} of various types of phospholipid-coated bilayer AuNPs with TG (1 mol % of phospholipid)

Types of phospholipids in bilayer AuNPs	λ_{max} (nm) of bilayer AuNPs
95% Soy PC	531
POPC	542
HyPC	549
DLPC	536
PG	529
PS	534
Sphingomyelin	536

As mentioned earlier (introductory section 2.1.1.1), the SPR of AuNP is very sensitive to size, shape, and inter-particle distance. In an aggregated state, the individual nanoparticles can interact with each other and give rise to oscillations that are combinations of oscillations of individual nanoparticles.⁸² The SPR of POPC-coated bilayer AuNPs is broad when compared to other phospholipid-coated bilayer AuNPs and showed λ_{max} at 542 nm. The POPC-coated bilayer AuNP was bluish purple. It could be due to the aggregation of particles and broader size distribution. TEM image analysis of POPC and 95% Soy PC-coated bilayer AuNPs will be discussed next.

2.4.2 TEM Images of POPC and 95% Soy PC-Coated Bilayer Gold Nanoparticles

The 95% Soy PC-coated bilayer AuNPs both with TG and without TG were synthesized under similar conditions and TEM images were analyzed. TEM images of 95% Soy PC-coated bilayer AuNPs in the absence of TG are shown in Fig 2.10(A). The size analysis of 98 particles of 95% Soy PC-coated bilayer AuNP without TG showed an average size of $15 \text{ nm} \pm 4.6 \text{ nm}$. Further TEM images of 1 mol % TG added 95% Soy PC-coated bilayer AuNPs were also analyzed (images and histogram are not shown here). The results obtained from TEM image analysis of 95% Soy PC-coated bilayer AuNPs in the presence of 1 mole % TG was similar to that of bilayer AuNPs in the absence of TG; the addition of TG in phospholipids during synthesis of AuNP did not show significant changes in the size and distribution of particles.

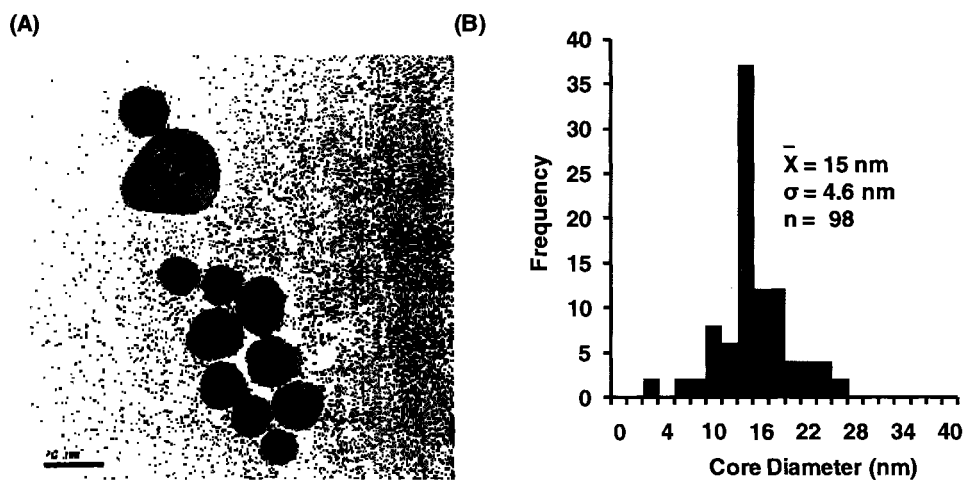


Figure 2.10 (A) TEM images of the 95% Soy PC-coated bilayer gold nanoparticles without TG. Scale bar = 20 nm. (B) Histogram for size distribution of 98 particles of 95% Soy PC-coated bilayer gold nanoparticles (bin size = 2 nm).

Furthermore, TEM images of 1 mole % TG added 95% Soy PC-coated bilayer AuNPs after partial 1-decanethiol exchange were also obtained and are shown in Fig 2.11(A). The size analysis of a total of 101 particles showed an average size of $14.4 \text{ nm} \pm 4.2 \text{ nm}$ which is similar to the average size of bilayer AuNPs before thiol exchange. Later in this project, TEM images of various types of 1 mole % TG added various types of phospholipid-coated bilayer AuNP were analyzed after 1-decanethiol was exchanged. In particular, both SPR and size of 95% Soy PC-coated bilayer AuNPs before and after partial 1-decanethiol exchange did not change. For this reason, TEM images of various other types of

phospholipid-coated bilayer AuNPs before thiol exchange were not studied separately.

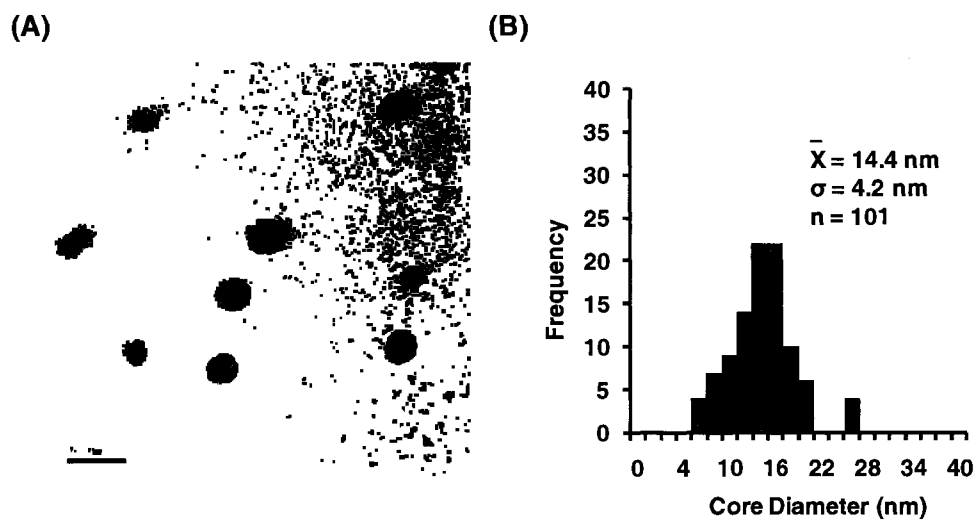


Figure 2.11 (A) TEM images of 1% TG added 95% Soy PC-coated bilayer gold nanoparticles after partial 1-decanethiol exchange (hybrid bilayer AuNPs). Scale bar = 20 nm. (B) The histogram for size distribution of 101 particles of 95% Soy PC-coated bilayer nanoparticles (bin size = 2 nm).

However, POPC-coated bilayer AuNP was noticeably different in color from POPC-coated hybrid bilayer AuNPs that formed after the addition of 1-decanethiol. The SPR of POPC-coated bilayer AuNPs after thiol exchange increased in intensity compared to POPC-coated bilayer AuNPs. After partial thiol exchange, a few nanometers blue shift of plasmon resonance in UV-vis spectrum was observed (spectrum not shown here). For this reason, TEM images of POPC-

coated bilayer AuNP and POPC-coated hybrid bilayer AuNPs were studied separately.

TEM images of POPC-coated bilayer AuNPs are shown in Fig 2.12(A). A few fields in the grid of POPC-coated bilayer AuNPs showed a small size particles which were not analyzed. From the size analysis of clearly visible 100 particles, an average size found was $12.2 \text{ nm} \pm 4.0 \text{ nm}$. In the histogram, the majority of particles were found in between 6 nm and 20 nm. When compared with TEM images of POPC-coated hybrid bilayer AuNPs, POPC-coated bilayer AuNPs showed a small increase in size which indicates that POPC-coated bilayer AuNPs aggregate to form larger particles over time in the absence of 1-decanethiol. One explanation for the broadening of plasmon resonance of POPC-coated bilayer AuNPs in UV-vis spectrum is aggregation of particles.

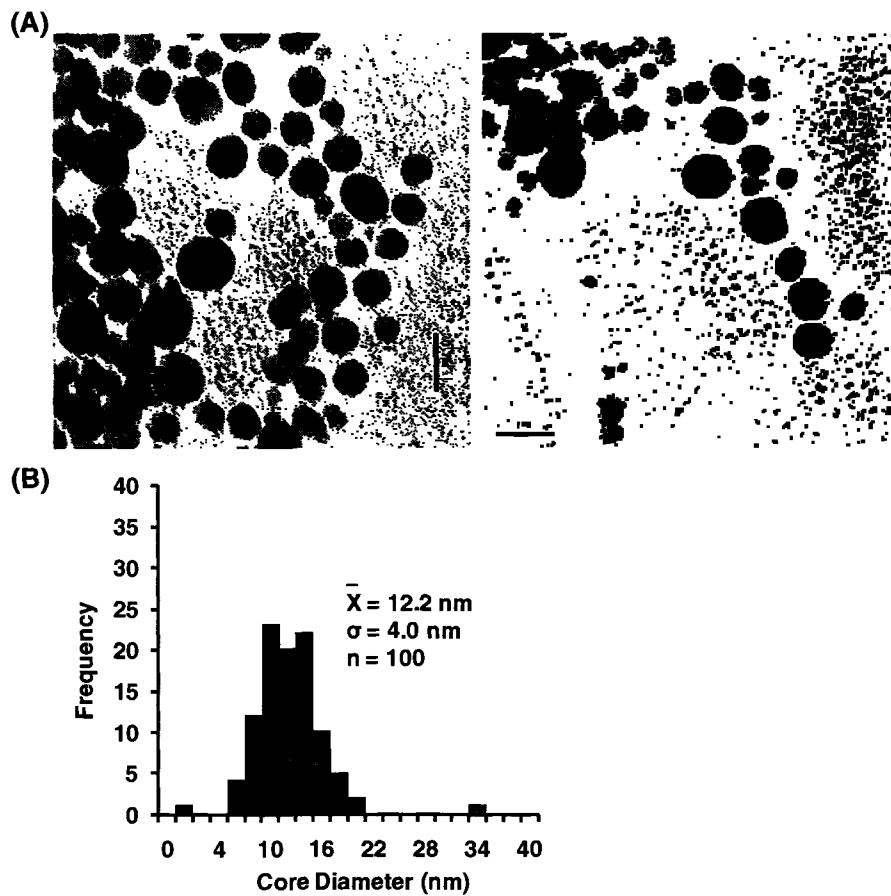


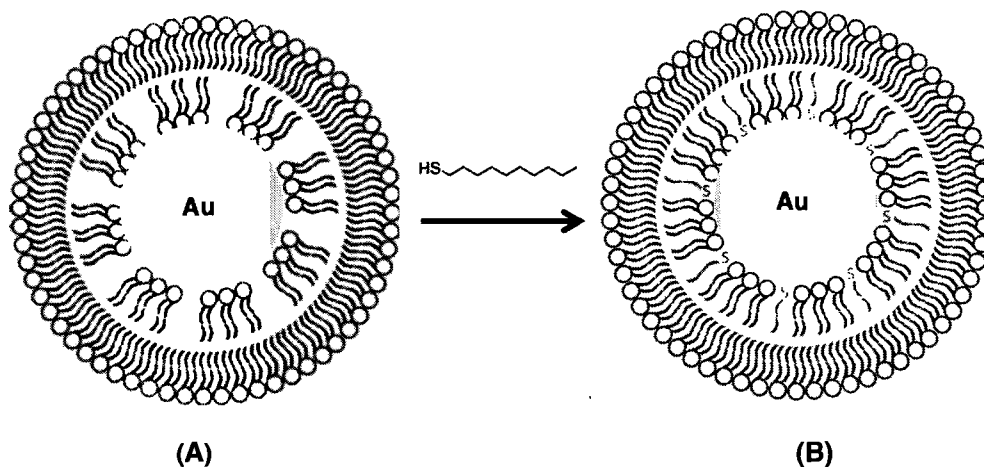
Figure 2.12 (A) TEM images of POPC-coated bilayer gold nanoparticles. Scale bar = 20 nm. (B) Histogram for size distribution of 100 particles (bin size = 2 nm).

2.4.3 Hybrid Bilayer Gold Nanoparticles

Various types of phospholipid-coated hybrid bilayer AuNPs were synthesized by partial exchange of phospholipid with 1-decanethiol as shown in Scheme 2.2 by following the established procedure as described in reference.¹³⁶ The number of gold atoms per 1-decanethiol used in synthesis of hybrid bilayer

AuNPs was also estimated by using the procedure described previously.¹³⁶ The moles of lipids used in the synthesis of bilayer AuNPs is equal to the molar equivalent of gold (III) salt. The number of lipids exchanged per thiol was not calculated since AuNPs were not purified after synthesis. The illustration shown in Scheme 2.2 represents that multiple gold atoms stabilized inside liposome.

Scheme 2.2



Scheme 2.2 Synthesis of hybrid bilayer gold nanoparticles. (A) Phospholipid-coated bilayer gold nanoparticles, B) hybrid bilayer.

2.4.3.1 TEM Image Analysis of Various Types of Phospholipid-Coated Hybrid Bilayer Gold Nanoparticles

TEM images of 1 mole % TG added samples of various types of phospholipid-coated bilayer AuNPs after 1-decanethiol (20 nmol) exchange with an optical density of 1.2 were studied. Particle size was analyzed by using software imageJ. The histogram was obtained at window bin size 2 nm. The λ_{max} of SPR of various types of phospholipid-coated hybrid bilayer AuNPs used for TEM sample preparation is as shown in Table 2.4. The TEM images of PG-coated hybrid bilayer AuNPs did not show any aggregation in the grid (Fig 2.13(A)). After partial 1-decanethiol exchange for PG-coated bilayer AuNPs, size analysis of 106 nanoparticles showed an average particle size of $6.9 \text{ nm} \pm 2.6 \text{ nm}$. As shown in the histogram (Fig 2.13(B)), the size distribution of these nanoparticles ranged from 2 nm to 14 nm and was narrow compared to other phospholipids-coated hybrid bilayer AuNPs. The sharp plasmon resonance of PG-coated bilayer AuNPs in UV-vis matched narrower size distribution as shown in histogram (Fig 2.13(B)).

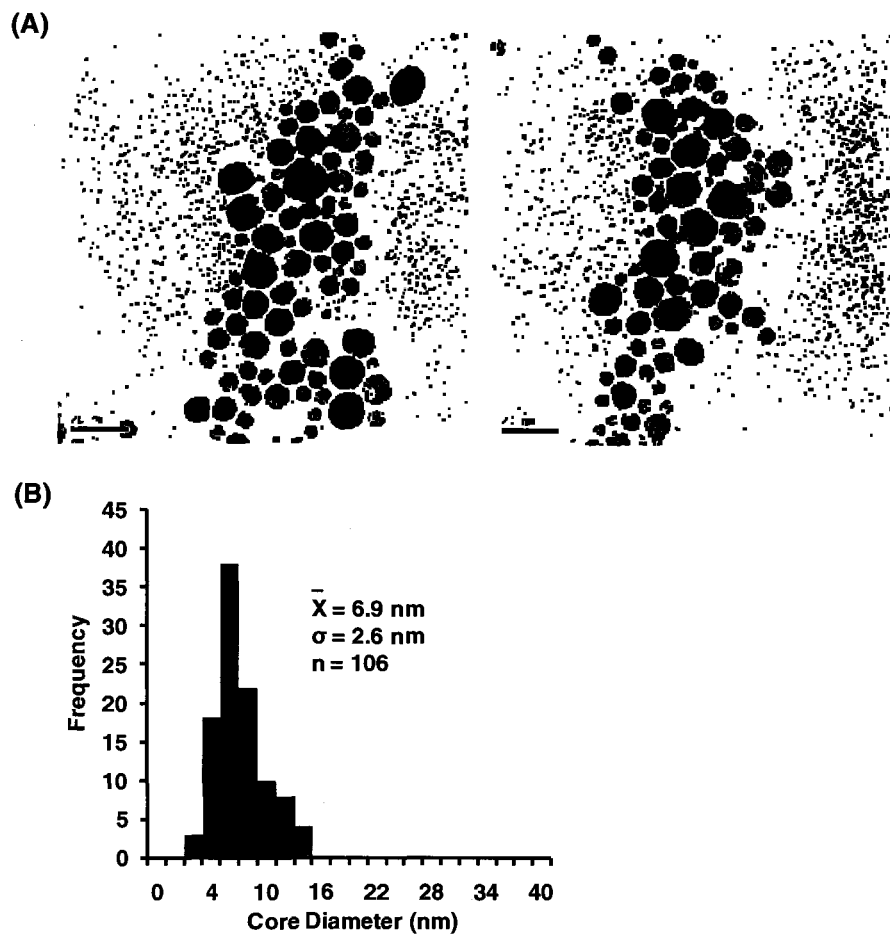


Figure 2.13 (A) TEM images of PG-coated hybrid bilayer gold nanoparticles. Scale bar = 20 nm. (B) Histogram for size distribution of 106 particles (bin size = 2 nm).

TEM images of 20 nmol 1-decanethiol exchanged of serine headgroup in phospholipid-coated bilayer AuNPs were studied. The average particle size after 1-decanethiol exchange in PS-coated hybrid bilayer AuNP was $9.9 \text{ nm} \pm 3.7 \text{ nm}$ in diameter (Fig 2.14(A)). The histogram of 114 serine headgroup in phospholipid-coated hybrid bilayer AuNPs ranges from 3 nm to 33 nm (Fig 2.14(B)). However,

a majority of the particle sizes were between 6 nm and 14 nm and were spherical. A few pyramidal nanoparticles were also observed in a few fields of the grid. These images are not shown here.

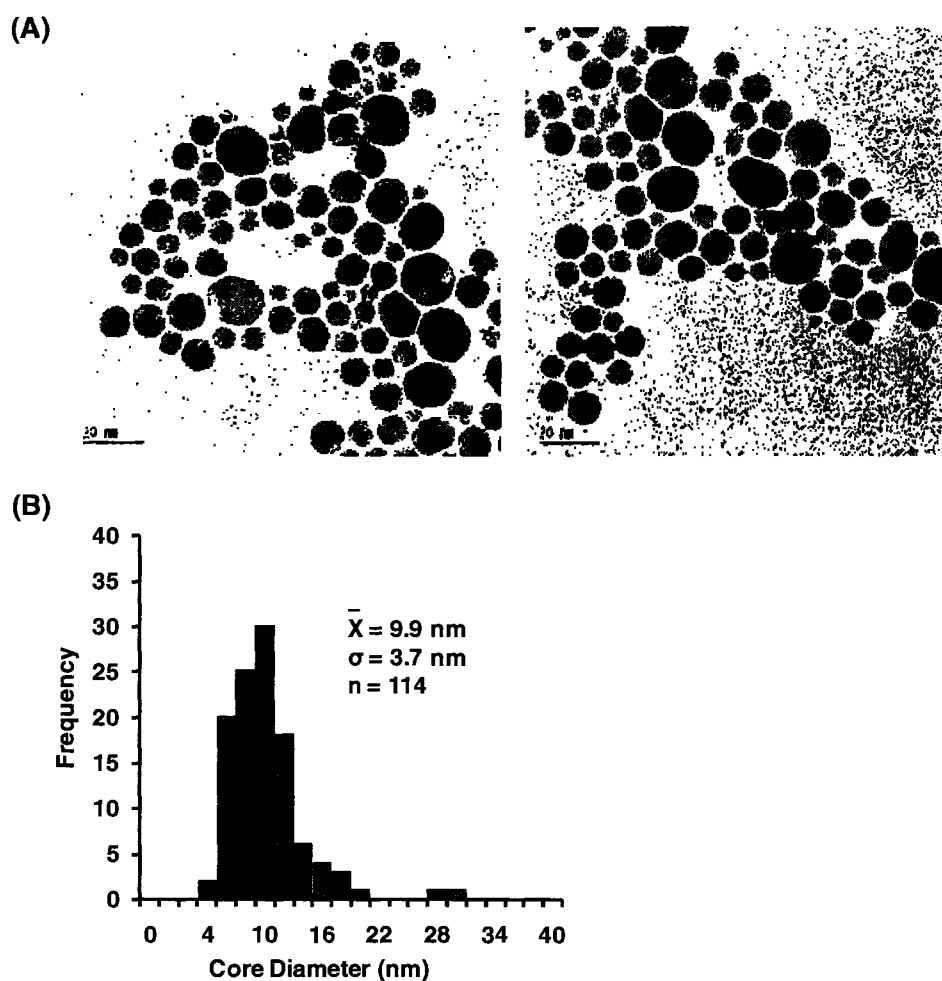


Figure 2.14 (A) TEM images of PS-coated hybrid bilayer gold nanoparticles. Scale bar = 20 nm. (B) Histogram for size distribution of 114 particles (bin size = 2 nm).

TEM images of sphingomyelin-coated hybrid bilayer AuNPs (Fig 2.15(A)) showed spherical particles of average size $10.1 \text{ nm} \pm 3.5 \text{ nm}$. The

histogram of 109 sphingomyelin-coated hybrid bilayer AuNPs showed a broad range of size distribution that ranged from 1 nm to 34 nm (Fig 2.15(B)). A few triangles were also observed in some fields of the grid. Larger liposomes were also

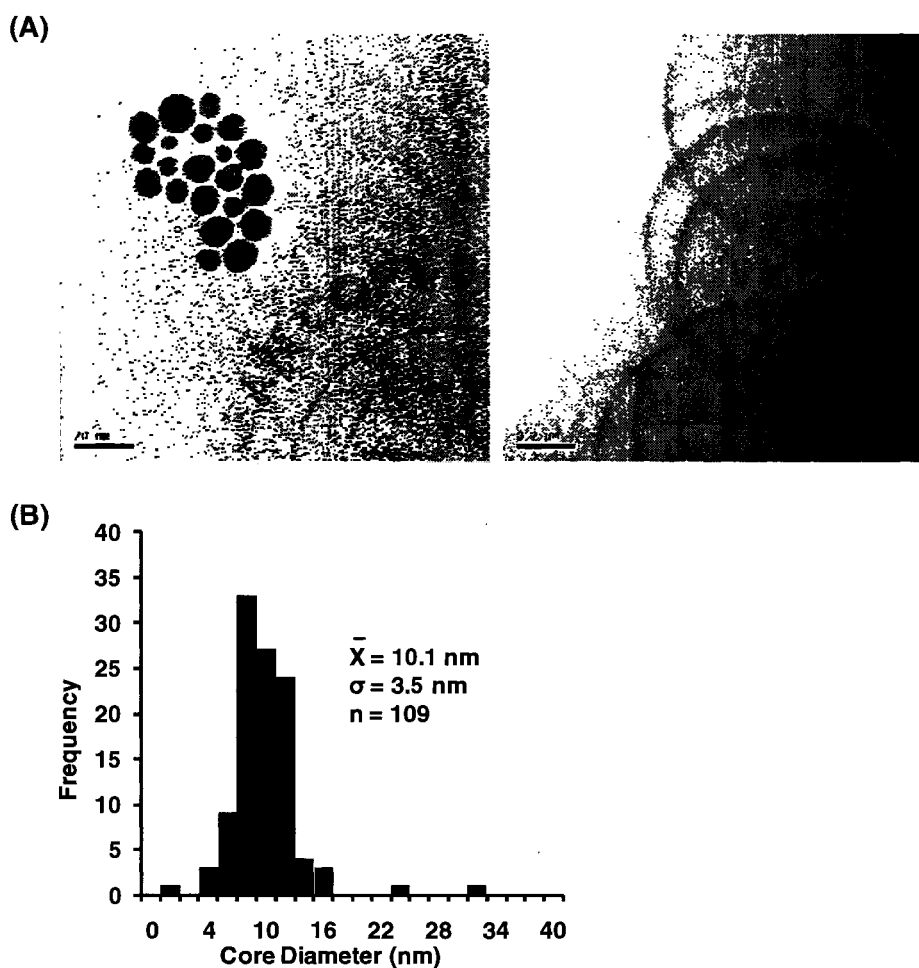


Figure 2.15 (A) TEM images of sphingomyelin-coated hybrid bilayer gold nanoparticles. Scale bar = 20 nm (left image) and scale bar = 0.2 μm (right image). (B) Histogram for size distribution of 109 particles (bin size = 2 nm).

visible in some fields of the grid and nanoparticles were visible inside the liposomes (Fig 2.15(A) right image).

After converting to hybrid bilayer AuNPs by partial thiol exchange, POPC-coated bilayer AuNPs changed from lilac to reddish purple, and they were found to be more soluble in water. The SPR and color of nanoparticles are very sensitive to particle aggregation.⁴⁷ The SPR of POPC-coated hybrid bilayer AuNPs was sharp and plasmon resonance shifted to the blue region, indicating that the hybrid bilayer AuNP is more soluble and no aggregation of nanoparticles occurred compared to POPC-coated bilayer AuNPs. TEM images of POPC-coated hybrid bilayer AuNPs (Fig 2.16(A)) were obtained under similar conditions as for other hybrid bilayer AuNPs. After the analysis of TEM images of 71 POPC-coated hybrid bilayer AuNPs, the histogram (Fig 2.16(B)) of particles showed a narrow size distribution compared to the POPC-coated bilayer AuNP (as shown in Fig 2.12(B)). The average size of POPC-coated hybrid bilayer AuNPs was found to be $9.9 \text{ nm} \pm 2.6 \text{ nm}$. When compared the standard deviation of TEM images of POPC-coated bilayer AuNP ($12.2 \text{ nm} \pm 4 \text{ nm}$), the hybrid bilayer AuNPs of POPC showed high precision in size analysis and no aggregation in the TEM grid. The plasmon resonance of POPC-coated hybrid bilayer AuNPs also shifted to a lower wavelength ($\lambda_{\text{max}} = 534 \text{ nm}$) compared to POPC-coated bilayer AuNPs ($\lambda_{\text{max}} = 542 \text{ nm}$), indicating that no aggregation of particles occurred after formation of hybrid bilayer AuNPs.

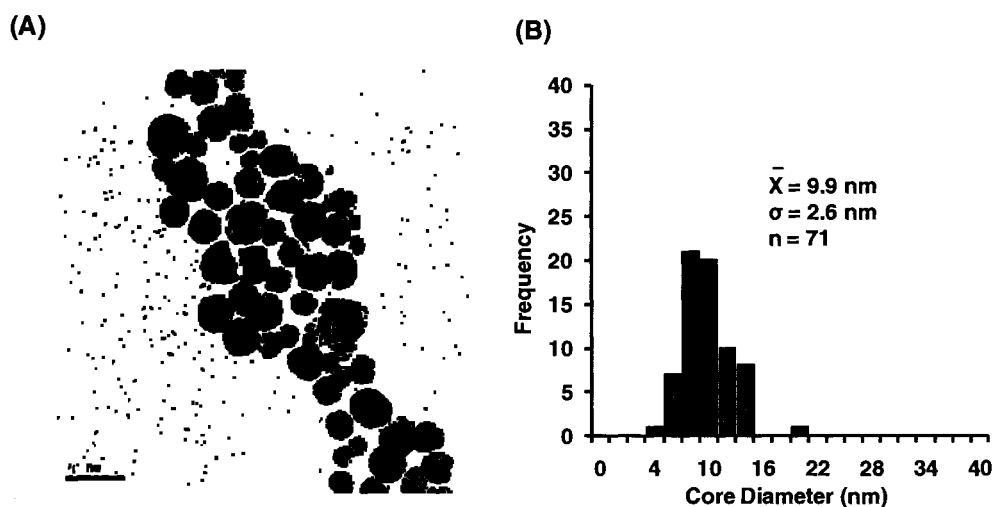


Figure 2.16 (A) TEM image of POPC-coated hybrid bilayer gold nanoparticles. Scale bar = 20 nm. (B) Histogram for size distribution of 71 POPC-coated hybrid bilayer gold nanoparticles (bin size = 2 nm).

TEM images of DLPC-coated hybrid bilayer AuNPs showed a majority of the small size particles in many fields of the TEM grid. The DLPC-coated hybrid bilayer AuNPs showed a small number of flat rods and prisms in a few fields of the TEM grid (Fig 2.17(A)). Small size particles were not analyzed because of quality of TEM grid being used. Only the distinctly visible spherical particles (Fig 2.17(B)) were picked for size analysis. Because a few prisms and flat rods were seen in the TEM grid, these were not included in size analysis. Prism and rod shape AuNPs usually shift plasmon resonance to longer wavelengths compared to plasmon resonance of spherical AuNPs. However, a few prisms and rod shaped nanoparticles seen in DLPC-coated hybrid bilayer nanoparticles did not show any shift in SPR. Size analysis of 107 particles showed an average size of

9.9 nm \pm 3.9 nm in histogram (Fig 2.17(C)) and the size distribution ranged from 2 nm to 25 nm. Nanoparticles were seen in a chain around the small liposome (Fig 2.17(B) right image). Interestingly, TEM images of liposomes of DLPC were visible without any stain, and small liposomes were surrounded by many large liposomes (these TEM images are not shown). Multilamellar liposome-like structures were visible in TEM images and were found larger than 2000 nm in size (images are not shown).

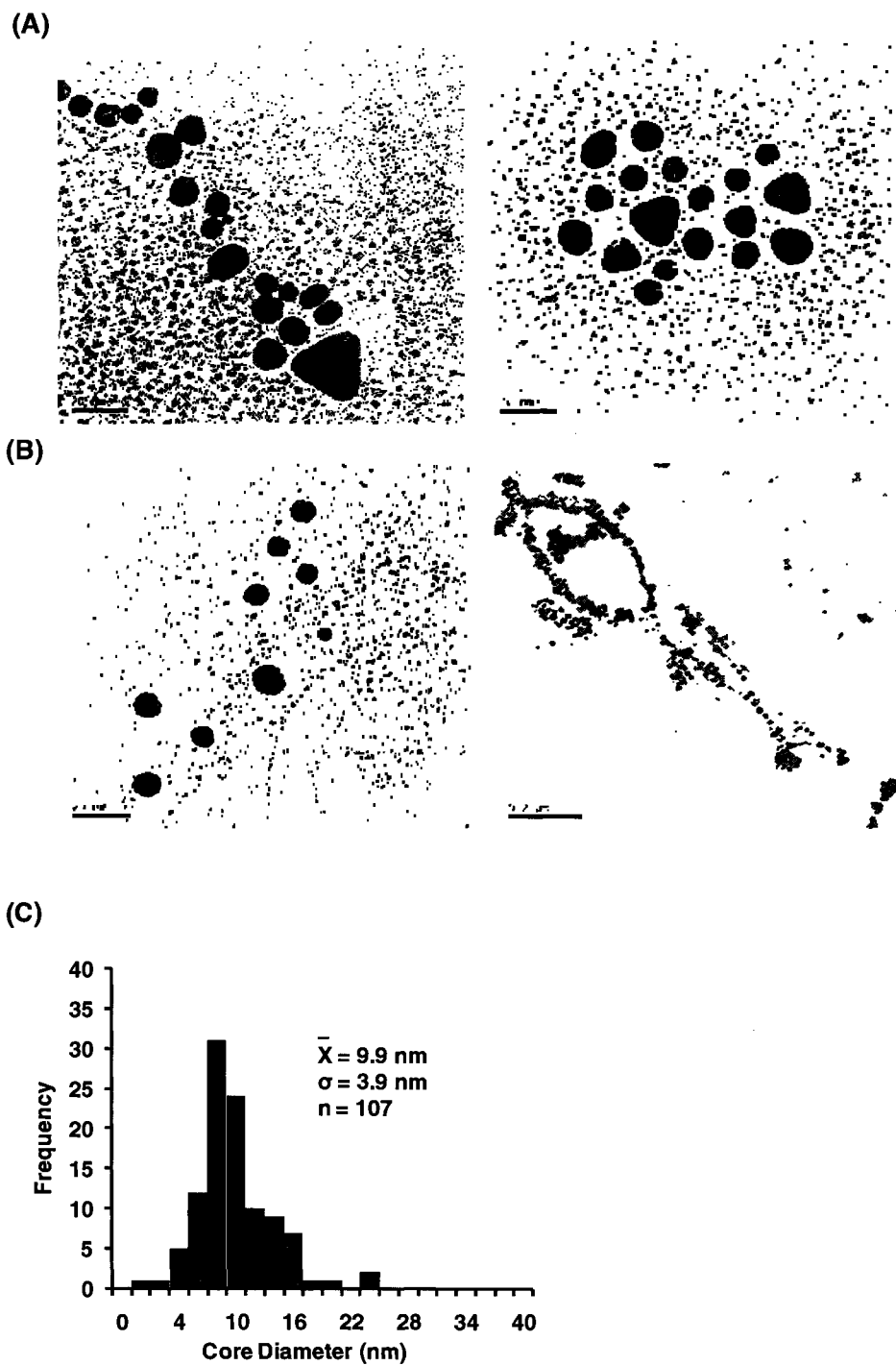


Figure 2.17 (A) DLPC-coated triangle shaped hybrid gold nanoparticles seen in a few fields of the grid. Scale bar = 20 nm. (B) TEM images of DLPC-coated hybrid bilayer gold nanoparticles. Scale bar = 20 nm (left image) and scale bar = 0.2 μm (right image). (C) Histogram for size distribution of 107 hybrid bilayer gold nanoparticles (bin size = 2 nm).

TEM images of the HyPC-coated hybrid bilayer AuNPs showed that the majority of the particles were of smaller size (Fig 2.18(A)) and could not be analyzed by the quality of the TEM grid being used. The analysis of larger and clearly visible 107 particles showed an average size of $7.3 \text{ nm} \pm 3.7 \text{ nm}$ and a broader size distribution in the histogram (Fig 2.18(B)). The broad SPR of the HyPC-coated hybrid bilayer AuNPs in the UV-vis spectrum is possibly due to the distribution of both small and large particles as seen in TEM images. Some triangles and asymmetric particles were also observed in a few fields of the grid (images are not shown).

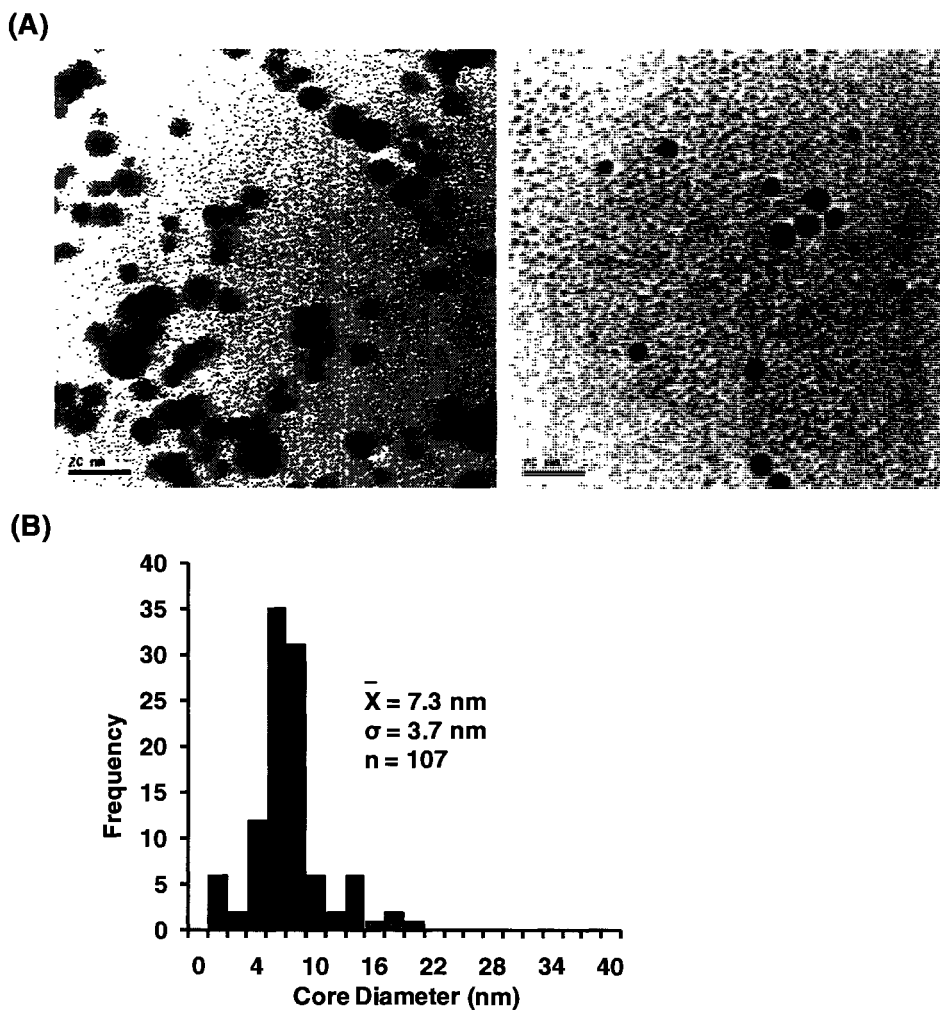


Figure 2.18 (A) TEM images of HyPC-coated hybrid bilayer gold nanoparticles. Scale bar = 20 nm. (B) Histogram for size distribution of 107 hybrid bilayer nanoparticles (bin size = 2 nm).

Phosphatidylethanolamine (PE) has a small headgroup, where only three hydrogen atoms are attached to the nitrogen atom compared to bulkier headgroup in PC. The small headgroup of PE prefers the non-lamellar inverted hexagonal

phase.^{83,89,137} Therefore, the small headgroup lipids do not tilt to form the stable liposomes. The TEM images of DPPE-coated hybrid bilayer AuNPs showed an asymmetric irregular shape and some spherical shaped nanoparticles (Fig 2.19). The unusual shape in TEM could be due to the aggregation of particles or precipitated liposome. Because of the aggregation of the particles, the size analysis would be less accurate; for that reason, size analysis of DPPE-coated nanoparticles was not implemented.

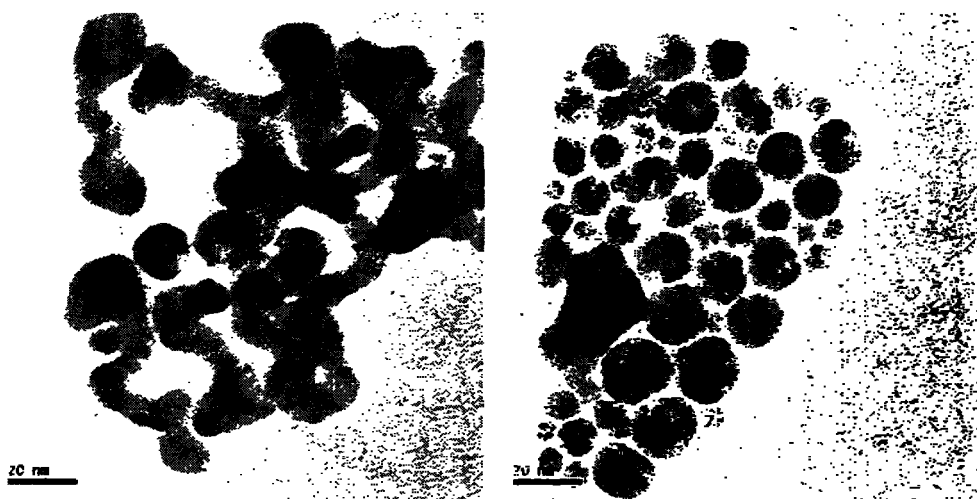


Figure 2.19 TEM images of DPPE-coated hybrid bilayer gold nanoparticles. Scale bar = 20 nm. Left image (showing aggregation of particles), right image (both an aggregated and free spherical nanoparticles).

The size analysis of TEM images of various types of phospholipid-coated hybrid bilayer AuNPs showed small changes in size depending on the type of phospholipids used in the AuNPs synthesis as shown in Table 2.4.

Table 2.4 Average size and λ_{\max} of various types of phospholipid-coated hybrid bilayer AuNPs

Types of phospholipids in hybrid bilayer AuNPs	Average particle size (nm)	λ_{\max} (nm)
95% Soy PC	14.4 ± 4.2	530
POPC	9.9 ± 2.6	534
HyPC	7.3 ± 3.7	547
DLPC	9.9 ± 3.9	531
PG	6.9 ± 2.6	528
PS	9.9 ± 3.7	529
Sphingomyelin	10.1 ± 3.5	533

By varying the types of phospholipids in the synthesis of bilayer AuNPs small changes in particle size were observed. In addition to the analysis of size of the different types of phospholipid-coated hybrid bilayer AuNPs, the stability of these particles was also of interest in this project and was tested in the presence of KCN solution and is presented in section 2.4.4.

2.4.3.2 Estimation of Thiol in Phospholipid-Coated Hybrid Bilayer Gold

Nanoparticles

Phospholipid-coated AuNPs were synthesized in aqueous medium. HAuCl₄ (10 μmol) was dissolved in 3.4 mL water. Then, liposome (10 μmol in 4 mL) and sodium citrate (25 μmol in 0.98 mL) were prepared in water. The aqueous solutions were combined and stirred. Initially, the solution was colorless and after one hour transformation of gold salt to AuNPs was observed by the color change of the solution. After one day of synthesis UV-vis spectra were recorded. The total volume of AuNPs solution in water is 8.38 mL. Without further purification, 0.35 mL of the AuNPs solutions were diluted to 1 mL. At this dilution, absorbances of an optical density 1.2 were recorded for most of phospholipid-coated bilayer AuNPs synthesized in this research. Assuming total conversion of gold salt to AuNPs, 0.35 mL of AuNPs solution is equivalent to 417 nmol of AuNPs.

A gold to lipid ratio is 1:1 during synthesis. The alkanethiol added to AuNPs solutions is very small amount compared to phospholipid. Therefore partial thiol exchange is expected for phospholipid. The 1-decanethiol (1 nmol, 5 nmol or 20 nmol) were added to the solution of phospholipid-coated bilayer AuNPs (417 nmol) of an optical density 1.2 and the total gold to thiol ratio in hybrid bilayer AuNPs is as shown below.

For 1 nmol thiol exchanged, total gold: thiol ratio is 417:1.

For 5 nmol thiol exchanged, total gold: thiol ratio is 83:1.

For 20 nmol thiol exchanged, total gold: thiol ratio is 21:1.

The total number of gold atoms in the nanoparticles can be calculated by using the equation ($N = 283.7 r^3$),^{136,138,139} where r is radius of nanoparticles and for an average size (diameter) of 10 nm nanoparticles, $r = 5$ nm. For example, the total number of gold atoms present in a nanoparticle of an average size 10 nm is about 35,000. For nanoparticles of an average size 10 nm, 15% of the gold atoms are considered on the surface of the particles. Therefore, gold atoms present on the surface of nanoparticles are only 15% of 417 nmol, which is 62.6 nmol gold or atoms per nanoparticles is about 5,300. It is expected partial thiol exchange takes place only on surface of nanoparticles. Therefore, thiol is present only on the surface of AuNPs.

Different amount of thiol was exchanged under similar conditions using the same amount of bilayer AuNPs solutions (1 mL) of an optical density 1.2 (417 nmol), i.e., 62.6 nmol surface gold atom. The percentage of thiol present on the surface gold atoms is calculated as shown below.

For 1 nmol thiol exchange, 1% of 62.6 nmol surface gold atoms = 0.62% surface covered with thiol.

For 5 nmol thiol exchange, 5% of 62.6 nmol surface gold atoms = 3.13% surface covered with thiol.

For 20 nmol of thiol exchange, 20% of 62.6 nmol surface gold = 12.5% surface covered with thiol.

After thiol exchange the various types of phospholipid-coated hybrid bilayer AuNPs were tested for their stability. The following section presents the stability of hybrid bilayer AuNPs in KCN.

2.4.4 Stability of Phospholipid-Coated Hybrid Bilayer Gold Nanoparticles in KCN

The stability tests for various types of phospholipid-coated bilayer as well as hybrid bilayer AuNPs in KCN were performed, following the procedure as described previously.¹³⁶ Hybrid bilayer AuNPs, formed after partial thiol exchange for different concentrations of thiol (1 nmol, 5 nmol, 20 nmol), were obtained by the addition of 1-decanethiol to bilayer AuNPs of an optical density 1.2. The stability tests of various types of phospholipid-coated hybrid bilayer AuNPs was performed without purification.

2.4.4.1 Stability of Different acyl chain Phospholipid-Coated Hybrid Bilayer Gold Nanoparticles in KCN

For the case of 20 nmol 1-decanethiol-exchange in POPC-coated bilayer AuNPs, the hybrid bilayer AuNP was found to be more soluble, and λ_{\max} of the plasmon resonance shifted from 542 nm to 534 nm. The “absorbance vs time” graphs of the POPC-coated bilayer and the hybrid bilayer AuNPs of an optical density 1.2 were monitored for an hour in KCN of 6 mM final concentration at their λ_{\max} as shown in Fig 2.20(A). The POPC-coated bilayer AuNP was found to

be less stable in 6 mM final concentration of KCN. On the other hand, for the 20 nmol 1-decanethiol-exchanged POPC-coated bilayer AuNPs solution of same optical density, the hybrid bilayer AuNPs showed no decomposition for one hour, indicating that the hybrid bilayer AuNPs were very stable to KCN etc.

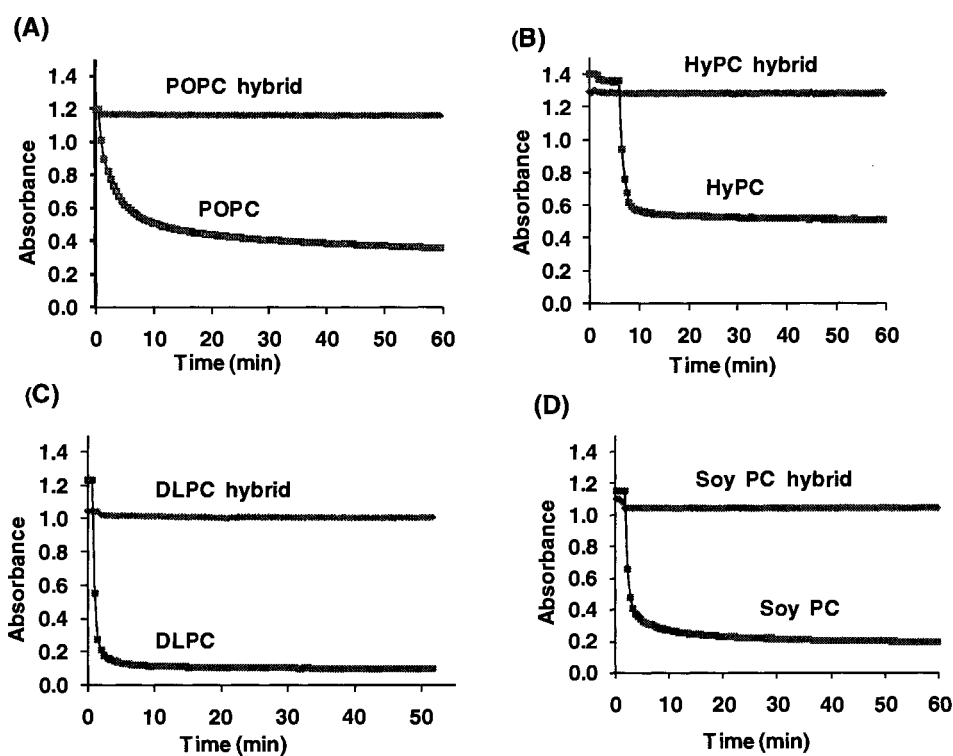


Figure 2.20 UV-vis “absorbance vs. time” experiments for 20 nmol 1-decanethiol exchanged hybrid bilayer AuNPs for one hour in KCN (6 mM final concentration) (A) POPC-coated hybrid bilayer nanoparticles (blue), POPC-coated bilayer nanoparticles (orange), (B) HyPC-coated hybrid bilayer nanoparticles (blue) (KCN added after 5 min data collection in UV-vis), HyPC-coated bilayer nanoparticles (orange), (C) DLPC-coated hybrid bilayer nanoparticles (blue), DLPC-coated bilayer nanoparticles (orange), (D) 95% Soy PC-coated hybrid bilayer nanoparticles (blue), 95% Soy PC-coated bilayer nanoparticles (orange).

The POPC-coated bilayer AuNP decomposed 67% in one hour, and complete disappearance of color took a couple of hours. The hybrid bilayer AuNPs were found to be stable for an indefinite time at a final concentration of KCN (6 mM). Since the kinetic studies of bilayer and hybrid bilayer AuNPs in KCN were carried out without purification, an excess of phospholipid present in the bilayer AuNPs solutions showed some scattering in graphs as shown by the non-zero baseline in Fig 2.20.

For the case of 20 nmol thiol exchange as shown in Fig 2.20, all hybrid bilayer AuNPs (blue traces in graph) remained stable in KCN whereas the corresponding bilayer AuNPs of these were found to be unstable (red traces in graph) under similar conditions and concentration of KCN. Fig 2.20(B) shows the case where KCN was added after 5 min of initiating the data collection in bilayer AuNPs so the graph showed decrease of absorbance only after 5 min. All hybrid bilayer AuNPs shown in Fig 2.20 were found to be stable in KCN for an indefinite amount of time. Only the DLPC-coated hybrid bilayer AuNP showed some precipitate after several days. The relative stabilities of the hybrid bilayer AuNPs in KCN are as shown in Table 2.5.

For the case of 5 nmol thiol exchange, various types of acyl chain phospholipid-coated hybrid bilayer AuNPs showed decrease in stability towards KCN compared to the case of nanoparticles with 20 nmol thiol exchanged under similar conditions. The normalized absorbance vs. time graphs for various types of phospholipid-coated hybrid bilayer AuNPs are shown in Fig 2.21(A). For normalization purposes, the absorbance of completely decomposed (after one hour

in 6 mM KCN) bilayer AuNPs of corresponding phospholipid-coated bilayer AuNP was subtracted from the hybrid bilayer AuNPs. The percentage of stable nanoparticles was calculated by using normalized absorbance of the hybrid bilayer AuNP after one hour in KCN and the absorbance of corresponding hybrid bilayer AuNP before KCN. For 5 nmol 1-decanethiol exchange, the bilayer AuNPs decomposed about 10% in an hour at 6 mM final concentration of KCN. The percentage of stable nanoparticles is as shown in Table 2.5. As compared to 20 nmol thiol exchanged, 5 nmol thiol exchanged particles were found less stable.

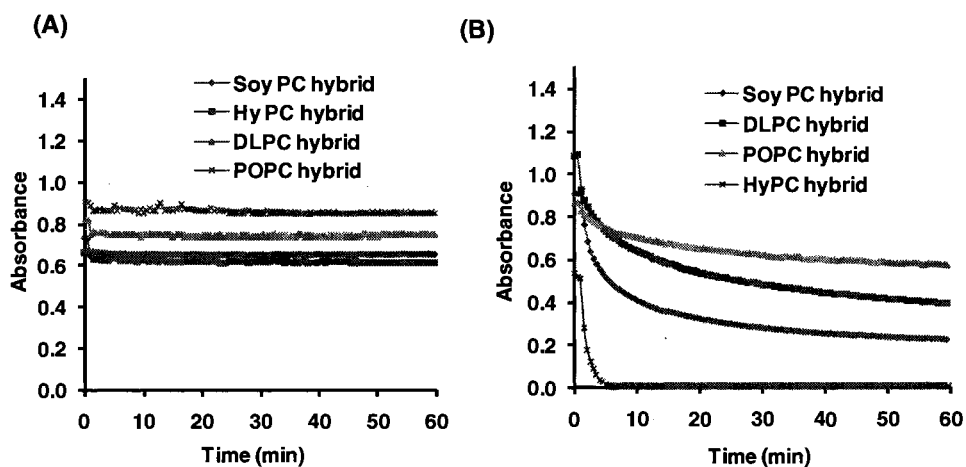


Figure 2.21 UV-vis “absorbance vs. time” experiments (normalized) of different acyl chain phospholipid-coated hybrid bilayer gold nanoparticles for one hour in KCN (final concentration 6 mM); (A) 5 nmol thiol exchanged bilayer gold nanoparticles. POPC-coated hybrid bilayer nanoparticles (purple), DLPC-coated hybrid bilayer nanoparticles (green), HyPC-coated hybrid bilayer nanoparticle (red), 95% Soy PC-coated hybrid bilayer nanoparticles (blue); (B) 1 nmol thiol exchanged hybrid bilayer nanoparticles. HyPC-coated hybrid bilayer nanoparticles (purple), 95% Soy PC-coated hybrid bilayer nanoparticles (blue), DLPC-coated hybrid bilayer nanoparticles (red), POPC-coated hybrid bilayer nanoparticle (green).

For the case of 1 nmol thiol exchange, various acyl chain phospholipid-coated hybrid bilayer AuNPs exhibited different stabilities under similar conditions and concentration of KCN (6 mM) as shown in Fig 2.21(B). Among the phospholipids, HyPC-coated hybrid bilayer AuNP was found least stable at 1 nmol 1-decanethiol exchange for the same concentration of AuNPs solution and KCN. However, all hybrid bilayer AuNPs formed after 1 nmol thiol exchange were found more stable compared to corresponding phospholipid-coated bilayer AuNPs and all 1 nmol thiol exchange hybrid bilayer AuNPs lasted from 1 day to a few days. The % stable hybrid bilayer AuNPs after 1 nmol 1-decanethiol exchange is shown in Table 2.5. When compared to the hybrid bilayer AuNPs of HyPC, the DLPC-coated hybrid bilayer AuNPs were found more stable at 1 nmol concentration of 1-decanethiol exchange. Both DLPC and HyPC are saturated phospholipids, but they differ in acyl chain lengths. The hybrid bilayer AuNPs formed by using HyPC with a long hydrophobic acyl chain was expected to have a higher stability. In contrast, DLPC-coated hybrid bilayer AuNP with a shorter hydrophobic acyl chain was found more stable compared to HyPC-coated hybrid bilayer AuNP at 1 nmol thiol exchange. One possible explanation is that the synthetic phospholipids have a higher purity when compared to natural phospholipids. HyPC obtained from eggs contains not only HyPC but also other unsaturated lipids which could have possibly affected the fluidity of the phospholipid bilayer.

At 1 nmol 1-decanethiol exchange, unsaturated phospholipids such as POPC and 95% Soy PC-coated hybrid bilayer AuNP were found to have different stabilities in KCN. 95% Soy PC and POPC differ in degrees of unsaturation in

their acyl chain. Furthermore, 95% Soy PC used in this research contains numerous other PCs and also includes PE and other lipid impurities (described in section 2.1.3). POPC-coated hybrid bilayer AuNPs were found more stable when compared to 95% Soy PC-coated hybrid bilayer AuNPs. A possible explanation of this is 95% Soy PC with various other lipid impurities could have changed packing of lipid bilayer allowing access to cyanide ions to AuNPs. Hypothetically, unsaturated phospholipids form a more ordered bilayer, and have less fluidity, whereas saturated phospholipids form a less ordered bilayer so the fluidity of the phospholipid bilayer is high, which can allow more ions to pass through the lipid bilayer. Although, acyl chain of POPC is less saturated than acyl chain of 95% Soy PC because of other lipid impurities present in 95% Soy PC, AuNPs synthesized in presence of 95% Soy PC showed low stability with KCN.

Among the phospholipids used in synthesis of AuNPs, synthetic POPC resulted in the most stable bilayer and hybrid bilayer AuNPs. On the other hand, HyPC has a long saturated tail compared to DLPC and was expected to have high stability. In contrast, DLPC-coated hybrid bilayer AuNPs were found to be more stable compared to HyPC-coated hybrid bilayer AuNPs. In particular, POPC and DLPC are synthetic phospholipids with high degrees of purity. Even though POPC is more saturated than 95% Soy PC, and DLPC has a shorter tail than HyPC, the hybrid bilayer AuNPs synthesized by using these lipids are found more stable compared to HyPC and 95% Soy PC-coated hybrid bilayer AuNPs due to other lipid impurities present in these lipids.

2.4.4.2 Stability of Different Headgroups in Phospholipid-Coated Hybrid Bilayer Gold Nanoparticles in KCN

Different headgroups of phospholipids-coated hybrid bilayer AuNPs solution at 20 nmol of thiol exchange for optical density 1.2 of bilayer nanoparticles were also tested in KCN solution. The “absorbance vs. time” graphs (Fig 2.22) of hybrid bilayer AuNPs for one hour at final concentration of KCN (6 mM) was studied.

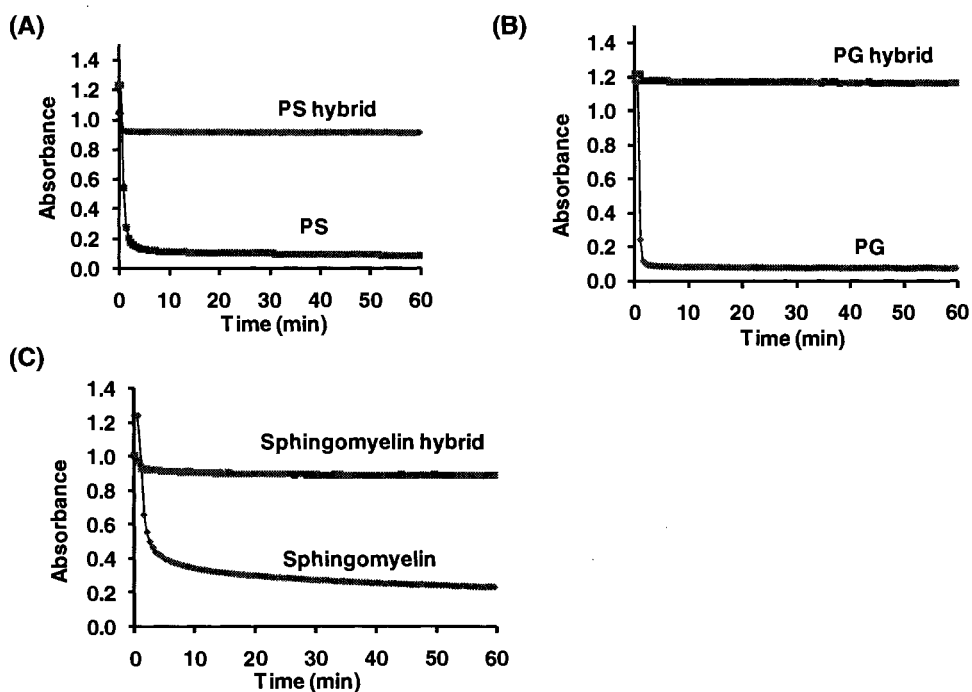


Figure 2.22 UV-vis “absorbance vs. time” experiments of different headgroups in phospholipid-coated hybrid bilayer gold nanoparticles one hour in KCN (final concentration 6 mM). Hybrid bilayer gold nanoparticles formed by exchange of 20 nmol 1-decanethiol in bilayer nanoparticles solutions of an optical density 1.2. (A) PS-coated hybrid bilayer nanoparticles (blue), PS-coated bilayer nanoparticles (orange); (B) PG-coated bilayer nanoparticles (blue), PG-coated hybrid bilayer nanoparticles (orange); (C) sphingomyelin-coated bilayer nanoparticles (blue), sphingomyelin-coated hybrid bilayer (orange).

After 10 nmol to 20 nmol 1-decanethiol exchange of an optical density 1.2, the various types of headgroup phospholipid-coated hybrid bilayer AuNPs showed the same stability. The 10 nmol thiol exchanged “absorbance vs. time” graphs for one hour in KCN were also similar to the 20 nmol thiol exchanged case (data are not shown here). All different headgroup phospholipid-coated hybrid bilayer AuNPs at 20 nmol of thiol exchanged for optical density of 1.2 were found very stable (Table 2.5).

The “absorbance vs. time” graphs of different headgroup phospholipid-coated hybrid bilayer AuNPs were also obtained at 5 nmol and 1 nmol 1-decanethiol exchange for different headgroup in phospholipid-coated bilayer AuNP solutions of an optical density of 1.2 in KCN. These graphs were normalized (Fig 2.23(A) and Fig 2.23(B)) and the percentage of stable hybrid bilayer nanoparticles was calculated. This was done in a manner analogous to that applied to the phospholipid-coated hybrid bilayer AuNPs with different acyl chain.

For the 5 nmol 1-decanethiol exchange case, various types of headgroup in phospholipid-coated hybrid bilayer AuNPs showed only a small decomposition at the final concentration of KCN (6 mM) in one hour (Fig 2.23(A)).

For 1 nmol 1-decanethiol exchange case, negative headgroup PS and PG-coated hybrid bilayer AuNPs were found less stable when compared to the neutral headgroup as shown in Fig 2.23(B). The presence of charge in the headgroup showed greater instability toward KCN.

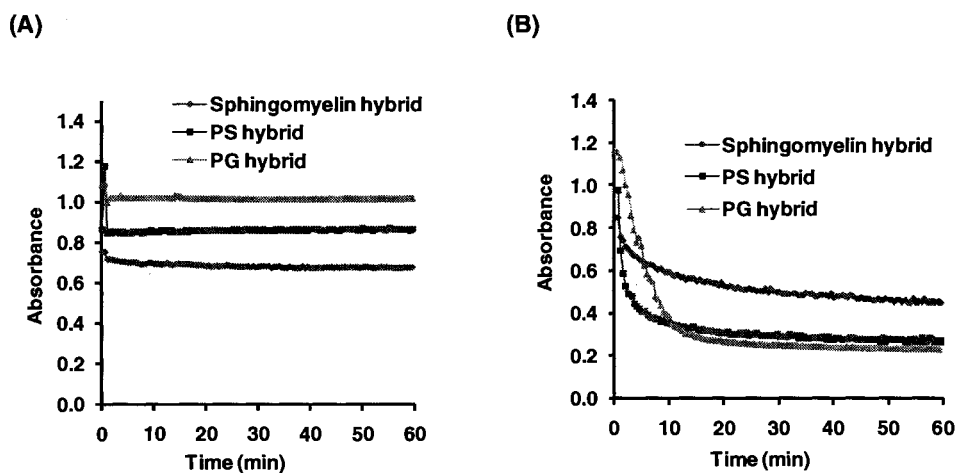


Figure 2.23 UV-vis “absorbance vs. time” graphs (normalized) of different headgroups in phospholipid-coated hybrid bilayer gold nanoparticles at final concentration of KCN (6 mM) for one hour. (A) Hybrid bilayer nanoparticles formed after 5 nmol 1-decanethiol exchanged for bilayer nanoparticle solution of an optical density 1.2; sphingomyelin-coated hybrid bilayer nanoparticles (blue), PS-coated hybrid bilayer nanoparticles (red), PG-coated hybrid bilayer nanoparticles (green). (B) Hybrid bilayer nanoparticles formed after 1 nmol 1-decanethiol exchange for bilayer nanoparticle solution of an optical density 1.2; sphingomyelin-coated hybrid bilayer nanoparticles (blue), PS-coated hybrid bilayer nanoparticles (red), PG-coated hybrid bilayer nanoparticles (green).

However, at 20 nmol and 5 nmol 1-decanethiol exchange, all different headgroup phospholipid-coated hybrid bilayer AuNPs showed similar stability in KCN. Only at 1 nmol thiol exchange sphingomyelin-coated hybrid bilayer AuNP showed higher stability compared to glycerol and serine headgroups phospholipid-coated hybrid bilayer AuNPs.

All different types of hybrid bilayer AuNPs at 1 nmol 1-decanethiol exchange were found more stable compared to corresponding bilayer AuNPs. However, when compared to neutral headgroups, sphingomyelin was found to have higher stability compared to serine and glycerol headgroup in phospholipids-

coated hybrid bilayer AuNPs. A possible explanation of this is that amide in sphingomyelin headgroup formed strong hydrogen bonding which accessed less cyanide ion compared to glycerol and serine headgroups phospholipids.

Among various types of acyl chain and headgroups phospholipid-coated nanoparticles, the POPC and sphingomyelin-coated hybrid bilayer AuNPs were found the most stable at a low concentration of 1-decanethiol exchange (1 nmol) for gold solution of an optical density of 1.2. These hybrid bilayer AuNPs were found stable for a few days. However, other various types of phospholipids-coated hybrid bilayer AuNP at 1 nmol thiol exchanged lasted from a few hours to one day.

Table 2.5 Comparative stability of various types of hybrid bilayer AuNPs at different concentrations of 1-decanethiol exchange in solution of bilayer AuNPs of an optical density 1.2 in KCN final concentration 6 mM.

Types of phospholipid in bilayer gold nanoparticle	% stable AuNPs after 20 nmol thiol exchange after one hour in KCN	% stable AuNPs after 5 nmol thiol exchange after one hour in KCN	% stable AuNPs after 1 nmol thiol exchange after one hour in KCN	% stable AuNPs in absence of thiol after one hour in KCN
HyPC	100	91.0	1.8	0
PG	100	93.0	19.8	5.7
PS	100	93.0	27.5	7.3
DLPC	100	89.0	35.7	8.0
95% Soy PC	100	86.0	24.2	16.0
Sphingomyelin	100	89.3	52.9	18.5
POPC	100	93.0	65.5	33.3

Hydrophobic thiols are rivals of small head group phospholipids, which could play crucial role in changing curvature in lipid membranes. It is expected that partial thiol exchange in a lipid bilayer lowers the density of the bilayer assembly and could possibly change the lipid curvature. This project has shown the effect of a partial thiol exchange in various types of phospholipids-coated bilayer AuNPs and the increase in stability of the nanoparticles when phospholipids are partially exchanged with hydrophobic alkanethiol. Furthermore, this research has tuned the stability of various types of phospholipid-coated bilayer AuNPs by partial thiol exchange. Hybrid bilayer with submonolayer of hydrophobic thiol at

gold: 1-decanethiol ratio of 21:1 formed stable nanoparticles for various types of phospholipids. Possible explanation for the formation of stable hybrid bilayer AuNPs is that when phospholipid was exchanged with hydrophobic alkanethiol, it decreased the density of bilayer. The presence of alkanethiol in the monolayer packed the monolayer more tightly. When 12.5% of the submonolayer consists of 1-decanethiol compared to the surface gold atoms, the nanoparticles became very stable. Possibly, 1-decanethiol changed the lipid curvature as mentioned in the prior section (2.1.3.1 Lipid Curvature) and the tightly packed lipid monolayer helped to prevent an access of cyanide ions into the AuNPs. Furthermore, at gold: 1-decanethiol ratio of 417:1, i.e., 0.62% submonolayer coverage of 1-decanethiol on surface gold atoms, and gold: 1-decanethiol ratio of 83:1, i.e., 3.13% submonolayer coverage of 1-decanethiol on surface gold atoms, the hybrid bilayer AuNPs stability increased when compared to corresponding phospholipid-coated bilayer AuNPs. To conclude, at optimum amount of alkanethiol exchange (i.e., gold: 1-decanethiol ratio of 21:1), 12.5% coverage of surface gold atoms with 1-decanethiol, all hybrid bilayer AuNPs became remarkably stable toward KCN etching and showed no drop in initial absorbance of these particles (Fig 2.20 & Fig 2.22).

2.4.5 Iodine Stability Tests of Various Types of Hybrid Bilayer Gold Nanoparticles

The stability of various types of phospholipid-coated bilayer and hybrid bilayer AuNPs was studied in presence of iodine. The “absorbance vs. time” graphs for various types of bilayer and hybrid bilayer AuNPs were obtained at their λ_{max} . Hybrid bilayer AuNPs solutions of an optical density of 1.2 formed after 20 nmol thiol exchange were tested in the final concentration of iodine (1 μM) (Fig 2.26). The addition of iodine solution changed the shape and size of the monolayer protected nanoparticles.¹³⁰ In this project, iodine (1 nmol) was added to the hybrid bilayer AuNPs (417 nmol) which is 21.4-fold in excess of AuNPs as compared to amount of iodine previously reported.¹³⁰ However, neither particle shape changed nor was particles’ aggregation observed in excess of iodine.

2.4.5.1 Iodine Stability Tests of Various Types of Acyl Chain Phospholipid-Coated Hybrid Bilayer Gold Nanoparticles

For 20 nmol 1-decanethiol exchanged case, POPC-coated and 95% Soy PC-coated hybrid bilayer AuNPs showed a decrease in absorbance in one hour at their λ_{max} in final concentration of iodine (1 μM) as shown in Table 2.6; it could be due to plasmon resonance broadening and the shift of plasmon resonance toward the red region. The addition of iodine to the unsaturated acyl chain of phospholipid could have possibly added in a double bond which could change the acyl chain structure; as a consequence changes in the packing of lipid bilayer might have

taken place. The UV-vis spectra of 95% Soy PC-coated hybrid bilayer AuNPs in the presence of iodine are shown in Fig 2.24. After the addition of iodine, scattering was observed in spectra during the first few min. During the addition of iodine, AuNP solution became cloudy and maximum scattering was observed in 2 min. When the solution was stirred for a few minutes, it became transparent, and scattering was not observed. The plasmon resonance of 95% Soy PC-coated hybrid bilayer AuNP was found to be broad and shifted to the red region after one hour in iodine (as shown in Fig 2.24).

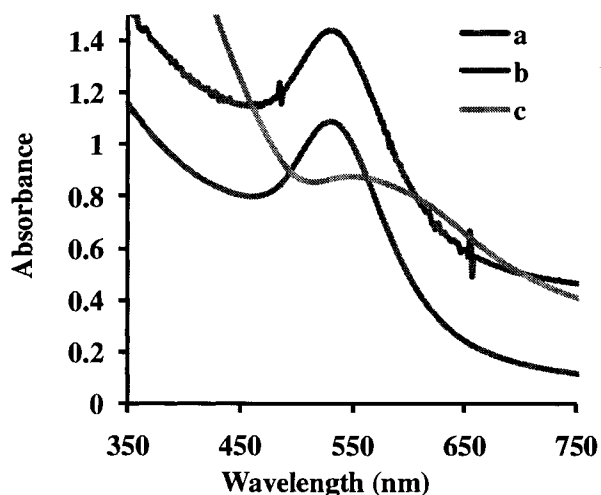


Figure 2.24 UV-vis of 95% Soy PC-coated hybrid bilayer gold nanoparticle before and after iodine final concentration 1 μM . a – 95% Soy PC-coated hybrid bilayer before iodine, b – scattering of 95% Soy PC-coated hybrid bilayer AuNP 4 min in iodine, c – 95% Soy PC-coated hybrid bilayer AuNP one hour in iodine.

TEM images of 95% Soy PC-coated hybrid bilayer AuNPs were taken after one day in the presence of iodine. The TEM images of these AuNPs in the iodine final concentration 1 μM , are shown in Fig 2.25(A). A few fields in the grid showed an aggregation of particles whereas most of the fields in the grid did not show any aggregation. Size analysis of 101 particles showed an average size of $13.6 \text{ nm} \pm 4.5 \text{ nm}$. The histogram obtained at bin size 2 nm is shown in Fig 2.25(B) displaying a broad distribution of particles similar to the previous histogram (Fig 2.11(B)) of 95% Soy PC-coated hybrid bilayer AuNPs in the absence of iodine.

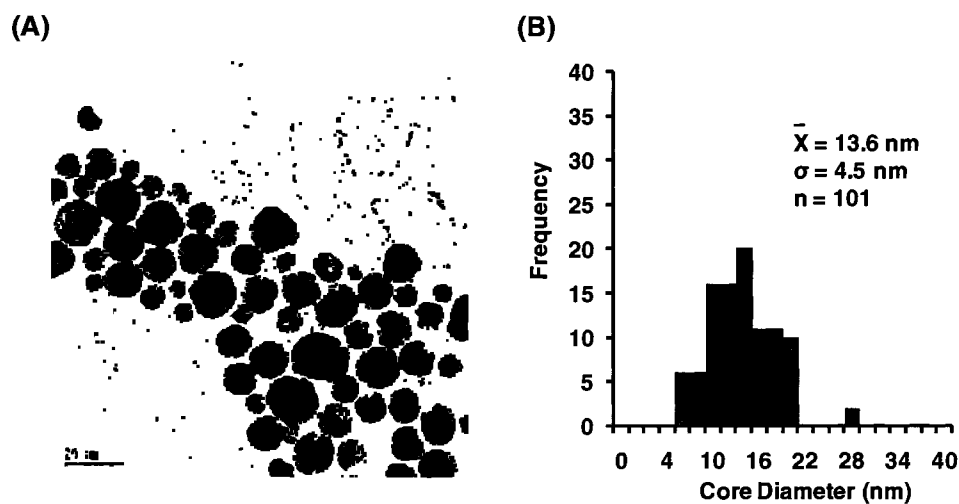


Figure 2.25 (A) TEM images of 95% Soy PC-coated hybrid bilayer nanoparticles with iodine (1 μM final concentration). Scale bar = 20 nm. (B) Histogram of 101 nanoparticles in iodine (bin size = 2 nm).

The stability of POPC-coated bilayer and hybrid bilayer AuNPs were studied under similar final concentration of iodine ($1 \mu\text{M}$) and conditions. The POPC-coated hybrid bilayer AuNP in iodine (Fig 2.26(C)) showed a very small decomposition of nanoparticles at λ_{max} 534 nm and a red shift in plasmon resonance, as in 95% Soy PC (spectra not shown of POPC). Bilayer AuNPs and

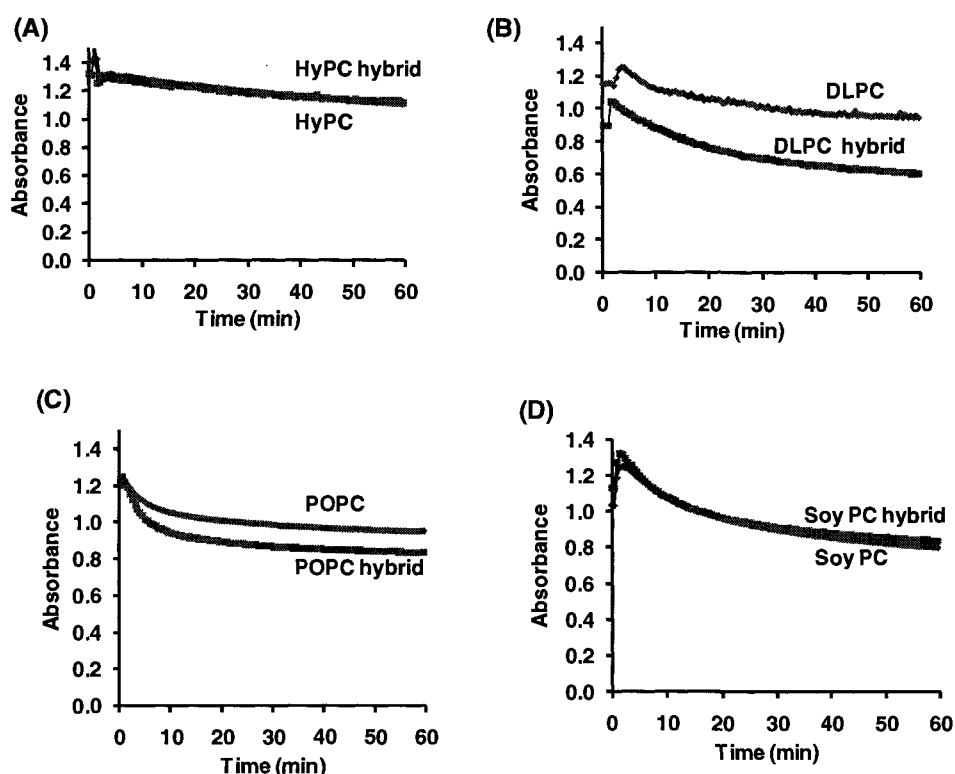


Figure 2.26 “Absorbance vs. time” graphs of different acyl chain phospholipid-coated bilayer and hybrid bilayer gold nanoparticles at $1 \mu\text{M}$ final concentration of iodine for one hour. (A) HyPC-coated hybrid bilayer nanoparticles (blue), HyPC-coated bilayer nanoparticles (red); (B) DLPC-coated hybrid bilayer nanoparticles (red), DLPC-coated bilayer nanoparticles (blue); (C) POPC-coated hybrid bilayer nanoparticle (red), POPC-coated bilayer nanoparticle (blue); (D) 95% Soy PC-coated hybrid bilayer nanoparticle (blue), 95% Soy PC-coated bilayer nanoparticle (red).

hybrid bilayer AuNP of HyPC (Fig 2.26(A)) and DLPC (Fig 2.26(B)) were stable at 1 μ M final concentration of iodine for one hour.

The UV-vis spectra of DLPC and HyPC-coated hybrid bilayer AuNPs solution before and after one hour in iodine are shown in Fig 2.27. After addition of iodine, scattering was observed in the spectra for a few minutes. The plasmon resonance of hybrid bilayer AuNPs of DLPC shifted significantly to the red region, and was found to be broad after one hour in iodine (Fig 2.27(A)). It could be due to aggregation of particles in presence of iodine. However, the UV-vis spectra of HyPC-coated hybrid bilayer AuNPs (Fig 2.27) did not show a red shift in plasmon resonance but the plasmon resonance decreased in intensity after an hour in iodine final concentration 1 μ M. As compared to other phospholipids, DLPC has a short tail so a possible reason for shift in plasmon resonance is aggregation. An iodide ion can replace a DLPC ligand much easier compared to a long tail HyPC, and can adsorb in AuNP surface which results in the aggregation of particles.

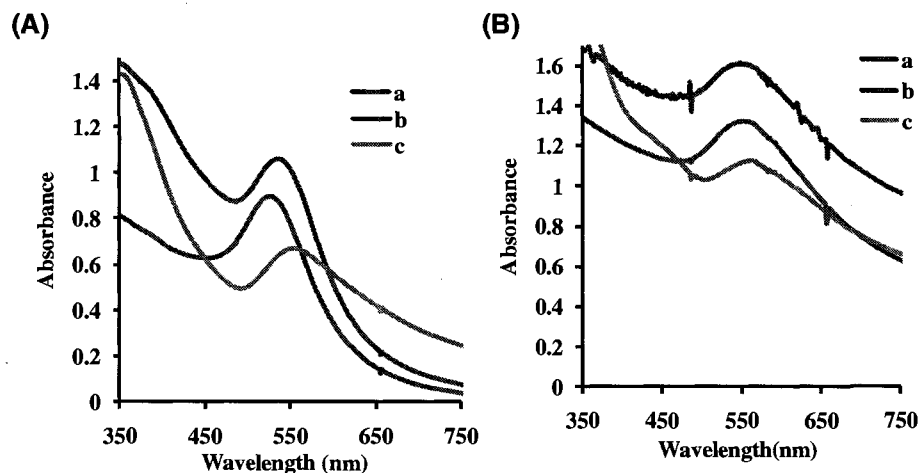


Figure 2.27 UV-vis spectra of hybrid bilayer gold nanoparticles. a – before iodine, b – 2 min in iodine, c – one hour in iodine. (A) DLPC-coated hybrid bilayer gold nanoparticles, (B) HyPC-coated hybrid bilayer gold nanoparticles.

2.4.5.2 Stability Tests of Different Headgroups in Phospholipid-Coated Hybrid Bilayer Gold Nanoparticles in Iodine

“Absorbance vs. time” graphs of bilayer and hybrid bilayer AuNPs of various types of headgroup phospholipids in the presence of iodine (1 μ M) for an hour is as shown in Fig 2.28. The absorbance at their λ_{max} was collected every 30 seconds for an hour. The initial increase in absorbance (Fig 2.28(A), Fig 2.28(C)) was due to the scattering right after the addition of iodine. However, in the serine headgroup phospholipid-coated AuNPs graph (Fig 2.28(B)), absorbance was collected after 5 min in iodine and did not show scattering in graph. The graphs (Fig 2.28) after one hour in iodine showed small drops in absorbance of AuNP

compared to the initial absorbance which could be due to the plasmon resonance shift of nanoparticles.

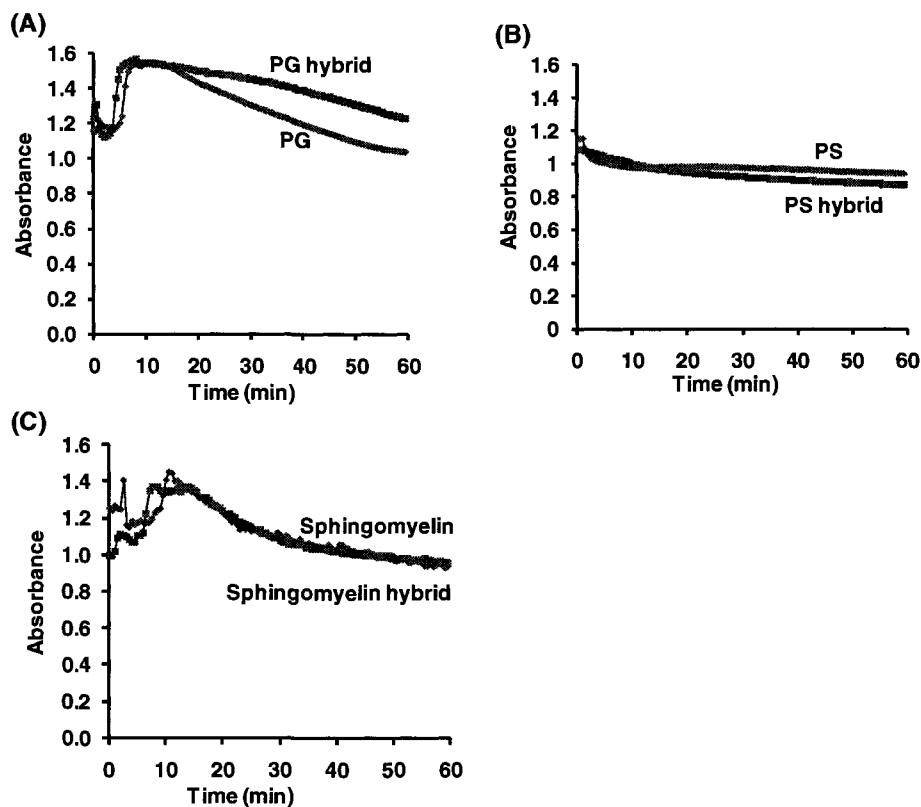


Figure 2.28 UV-vis time experiments. “Absorbance vs. time” graphs of different headgroups in phospholipid-coated bilayer and hybrid bilayer gold nanoparticles at 1 μ M final concentration of iodine for one hour. (A) PG-coated bilayer gold nanoparticles (blue), PG-coated hybrid bilayer nanoparticles (red); (B) PS-coated hybrid bilayer nanoparticles (red), PS-coated bilayer nanoparticles (blue); (C) sphingomyelin-coated hybrid bilayer nanoparticle (red), sphingomyelin-coated bilayer nanoparticle (blue).

The UV-vis spectra (Fig 2.29) of hybrid bilayer AuNPs of sphingomyelin and glycerol headgroup in phospholipids showed a small red shift of SPR in an

hour at final concentration of iodine (1 μM), but the intensity of plasmon resonance was not decreased. The spectra of PG and sphingomyelin-coated hybrid bilayer AuNPs before and after iodine are as shown in Fig 2.29(A) and Fig 2.29(C) respectively. Initial increases in absorbance in all spectra were due to scattering as discussed in the stability test of 95% Soy PC-coated hybrid bilayer AuNP with iodine. After one hour in iodine, a drop in absorbance was not observed for PG or sphingomyelin-coated hybrid bilayer AuNP at their λ_{max} . Further, the intensity of a red-shifted plasmon resonance indicated that absorbance of AuNPs did not change. In sphingomyelin, amide linkage and hydroxyl group of glycerol backbone interact to form hydrogen bond which could lead highly ordered gel phase compared to choline headgroup lipids.⁷⁸ The intramolecular hydrogen bond formed between ligands and the strength of the bond decreased as the amide functionality was moved further away from nanoparticle surface.⁷⁵ In this research, amide in sphingomyelin and hydroxyl in glycerol headgroup in phospholipid changed the fluidity of bilayer AuNP possibly by the formation of the hydrogen bond between ligands which do not allow iodide ions to adsorb on AuNPs surface.

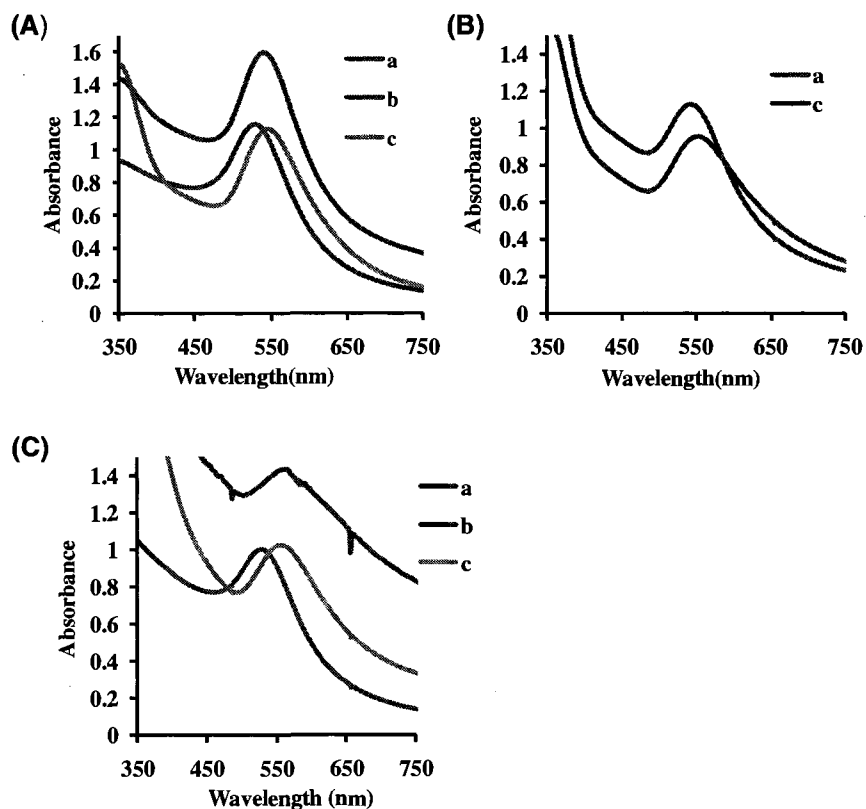


Figure 2.29 UV-vis spectra of different headgroup in phospholipid-coated hybrid bilayer gold nanoparticles formed at 20 nmol thiol exchange. a – before iodine, b – 2 min in iodine final concentration 1 μ M, c – one hour in iodine final concentration 1 μ M; (A) PG-coated hybrid bilayer nanoparticles, (B) PS-coated hybrid bilayer nanoparticles, and (C) sphingomyelin-coated hybrid bilayer nanoparticles.

Similarly, “absorbance vs. time” graphs of both hybrid bilayer and bilayer AuNPs of a serine headgroup phospholipid in the presence of iodine was measured at their λ_{\max} (Fig 2.28(C)). As compared to the serine headgroup coated bilayer AuNPs, the hybrid bilayer AuNPs showed a small drop in absorbance in an hour. The spectra of hybrid bilayer AuNPs before and after an hour in iodine are shown

in Fig 2.29(B). However, the plasmon resonance of serine headgroup coated hybrid bilayer AuNPs did not show a significant red shift as compared to other phospholipids. A serine headgroup in phospholipid has a double bond in acyl chain. Thus, iodine could possibly add on double bond. As a result, the structure of the acyl chain changes which changes lipid fluidity. But a serine headgroup in phospholipid does not have any hydrogen bond forming functional group so iodide ions could easily access the gold surface.

Table 2.6 Stability of various types of phospholipid-coated bilayer and hybrid bilayer AuNPs one hour in iodine final concentration 1 μM at their λ_{max} . Hybrid bilayer AuNP of an optical density 1.2 was formed after 20 nmol thiol exchange.

Types of phospholipid in AuNPs synthesis	Stable bilayer AuNPs after one hour in iodine	Stable hybrid bilayer AuNPs after one hour in iodine
95% Soy PC	74.0%	76.0%
POPC	66.0%	75.0%
DLPC	81.0%	66.0%
HyPC	90.0%	95.7%
Sphingomyelin	74.0%	95.0%
PS	81.7%	80.5%
PG	83.0%	100.0%

From the iodine stability study, various types of bilayer and hybrid AuNPs with submonolayer of hydrophobic alkanethiol did not show much

difference in stability with iodine in an hour. However, a small shift in SPR to the red region was observed in UV-vis spectra for 95% Soy PC, POPC, DLPC, PG, and sphingomyelin-coated hybrid bilayer nanoparticles. A decrease in absorbance was observed for HyPC and PS-coated hybrid bilayer AuNPs without a shift in SPR in presence of excess iodine.

2.5 CONCLUSIONS

In this project, seven different types of phospholipid-coated bilayer AuNPs and their corresponding hybrid bilayer AuNPs were synthesized by using both natural and synthetic phospholipids. The size of various types of phospholipid-coated hybrid bilayer AuNPs ranged from 6.9 nm to 14.4 nm. TEM image analysis showed an average size of 6.9 nm for PG-coated hybrid bilayer AuNPs and 14.4 nm for 95% Soy PC-coated hybrid bilayer AuNPs. The synthesis of POPC, DLPC, PS, and sphingomyelin-coated hybrid bilayer AuNPs resulted in an average size of 9.9 nm to 10.1 nm. The small size change of the nanoparticles was observed with variation of headgroups, acyl chain lengths, or degrees of saturation in phospholipids.

The stability of various types of phospholipid-coated AuNPs was tuned by exchanging different concentration hydrophobic alkanethiol for the same concentration of nanoparticle solutions. At the optimum concentration of thiol exchange relative to the total atoms of gold: 1-decanethiol ratio of 21:1, various types of phospholipids-coated hybrid bilayer AuNPs became remarkably stable. At this ratio both natural and synthetic phospholipid-coated hybrid bilayer nanoparticles were stable in KCN (6 mM) for an indefinite time. At a low concentration of thiol exchange, natural and synthetic phospholipid-coated AuNPs varied in stability. The synthetic phospholipid-coated AuNPs showed higher stability compared to natural phospholipid-coated AuNPs at low concentration of thiol exchange for a gold: 1-decanethiol ratio of 417:1.

Lastly, the stability of various types of natural and synthetic phospholipid-coated hybrid bilayer AuNPs was tested in the presence of excess iodine. Noticeable aggregation of stable hybrid bilayer particles was not observed in TEM images, and neither size nor shape was changed in the presence of excess iodine.

2.6 FUTURE DIRECTIONS

Having developed a method for synthesis of the stable hybrid bilayer AuNPs, the next logical step is to use them in an application, for example, micropatterning. The micropatterned fluid membrane has received increasing interests in microlithography.¹⁰⁸ The stable hybrid bilayer AuNPs can be applied in micropatterning by microfabrication or microcontact printing method. Further, protein can be tethered in micropattern for the purpose of monitoring the activities of biological membrane. Furthermore, various types of phospholipid-coated hybrid bilayer nanoparticles can be applied in the formation of the solid-supported lipid bilayer, which have potential uses in the design of biosensors. The optimum amount of 1-decanethiol, used to form stable hybrid bilayer AuNPs, could be extended to a variety of other metal nanoparticles, for example silver or magnetic nanoparticles. Moreover, thiol-modified biomolecules such as aptamers can be functionalized in bilayer AuNPs by utilizing the optimum amount of thiol calculated to obtain stable particles in this research. Additionally, the tuning of stability of various thiol-modified biomolecule functionalized nanoparticles will be an interesting area of research for their potential applications in biomedicine.

2.7 REFERENCES

1. Brugger, P. A.; Cuendet, P.; Graetzel, M. J. *Am. Chem. Soc.* **1981**, *103* (11), 2923-2927.
2. Crooks, R. M.; Zhao, M.; Sun, L.; Chechik, V.; Yeung, L. K. *Acc. Chem. Res.* **2001**, *34* (3), 181-190.
3. Takei, T.; Haruta, M. *Mater. Integr.* **2008**, *22* (1), 38-44.
4. Andreeva, D.; Tabakova, T.; Idakiev, V.; Christov, P.; Giovanoli, R. *Appl. Catal., A* **1998**, *169* (1), 9-14.
5. Haruta, M. *Catal. Today* **1997**, *36* (1), 153-166.
6. Toshima, N.; Takahashi, T.; Hirai, H. *Chem. Lett.* **1985**, *14* (8), 1245-1248.
7. Tan, M.; Wang, G.; Hai, X.; Ye, Z.; Yuan, J. *J. Mater. Chem.* **2004**, *14* (19), 2896-2901.
8. Chao, J.-I.; Perevedentseva, E.; Chung, P.-H.; Liu, K.-K.; Cheng, C.-Y.; Chang, C.-C.; Cheng, C.-L. *Biophys. J.* **2007**, *93* (6), 2199-2208.
9. Levy, R.; Wang, Z.; Duchesne, L.; Doty, R. C.; Cooper, A. I.; Brust, M.; Fernig, D. G. *Chem. Bio. Chem.* **2006**, *7* (4), 592-594.
10. Zanchet, D.; Micheel, C. M.; Parak, W. J.; Gerion, D.; Alivisatos, A. P. *Nano Lett.* **2001**, *1* (1), 32-35.
11. Cioffi, N.; Torsi, L.; Farella, I.; Altamura, D.; Valentini, A.; Quinto, M.; Sabbatini, L.; Zambonin, P. G. *Sens. Actuators, B* **2004**, *B100* (1-2), 9-16.
12. Lawrence, N. S.; Liang, H.-P. *Nanostruct. Mater. Electrochem.* **2008**, 435-457.
13. Schaadt, D. M.; Yu, E. T.; Sankar, S.; Berkowitz, A. E. *J. Vac. Sci. Technol, A* **2000**, *18* (4, Pt. 2), 1834-1837.

14. Schoen, G.; Simon, U. *Colloid Polym. Sci.* **1995**, *273* (3), 202-218.
15. Lei, Y.; Cai, W.; Wilde, G. *Prog. Mater. Sci.* **2007**, *52* (4), 465-539.
16. Takahashi, K.; Hasegawa, T.; Shinohara, H.; Ogawa, T. The magnetic material and the magnetic device. 2005-1249462006303298, 20050422., **2006**.
17. Esparza, R.; Rosas, G.; Lopez-Fuentes, M.; Pal, U.; Perez, R. *Rev. Mex. Fis. S* **2007**, *53* (5), 67-71.
18. Murphy, C. J.; Gole, A. M.; Hunyadi, S. E.; Stone, J. W.; Sisco, P. N.; Alkilany, A.; Kinard, B. E.; Hankins, P. *Chem. Commun.* **2008**, (5), 544-557.
19. Venkata, P. G.; Aslan, M. M.; Menguc, M. P.; Videen, G. *HTD (Am. Soc. Mech. Eng.)* **2005**, 376-2 (Proceedings of the ASME Heat Transfer Division--2005, Volume 2), 823-833.
20. Feldheim, D. L.; Foss, C. A., Jr.; Editors, *Metal Nanoparticles: Synthesis, Characterization, and Applications.* **2002**; 338 pp.
21. Daniel, M.-C.; Astruc, D. *Chem. Rev.* **2004**, *104* (1), 293-346.
22. Kreibig, U.; Vollmer, M., *Optical Properties of Metal Clusters. (Springer Series in Materials Science 25).* **1995**; 532 pp.
23. Link, S.; El-Sayed, M. A. *Int. Rev. Phys. Chem.* **2000**, *19* (3), 409-453.
24. Link, S.; El-Sayed, M. A. *J. Phys. Chem. B* **1999**, *103* (40), 8410-8426.
25. Thomas, S.; Nair, S. K.; Jamal, E. M. A.; Al-Harhi, S. H.; Varma, M. R.; Anantharaman, M. R. *Nanotechnology* **2008**, *19* (7), 75711-75717.
26. Orendorff, C. J.; Sau, T. K.; Murphy, C. J. *Small* **2006**, *2* (5), 636-639.

27. Yu; Chang, S.-S.; Lee, C.-L.; Wang, C. R. C. *J. Phys. Chem. B* **1997**, *101* (34), 6661-6664.
28. Malinsky, M. D.; Kelly, K. L.; Schatz, G. C.; Van Duyne, R. P. *J. Am. Chem. Soc.* **2001**, *123* (7), 1471-1482.
29. Thomas, K. G.; Zajicek, J.; Kamat, P. V. *Langmuir* **2002**, *18* (9), 3722-3727.
30. Qu, X.; Peng, Z.; Jiang, X.; Dong, S. *Langmuir* **2004**, *20* (7), 2519-2522.
31. Liz-Marzan, L. M.; Mulvaney, P. *New J. Chem.* **1998**, *22* (11), 1285-1288.
32. Mulvaney, P. *Langmuir* **1996**, *12* (3), 788-800.
33. Alivisatos, A. P. *J. Phys. Chem.* **1996**, *100* (31), 13226-13239.
34. Henglein, A. *Chem. Rev.* **1989**, *89* (8), 1861-1873.
35. Wang, Z.; Tan, B.; Hussain, I.; Schaeffer, N.; Wyatt, M. F.; Brust, M.; Cooper, A. I. *Langmuir* **2007**, *23* (2), 885-895.
36. Bohren, C. F.; Huffman, D. R., *Absorption and Scattering of Light by Small Particles.* **1983**; 530 pp.
37. Kerker, M., *The Scattering of Light and Other Electromagnetic Radiation (Physical Chemistry: a Series of Monographs, Vol. 16).* **1969**; 666 pp.
38. van der Zande, B. M. I.; Bohmer, M. R.; Fokkink, L. G. J.; Schonenberger, C. *J. Phys. Chem. B* **1997**, *101* (6), 852-854.
39. Kim, F.; Song, J. H.; Yang, P. *J. Am. Chem. Soc.* **2002**, *124* (48), 14316-14317.
40. Mohr, C.; Hofmeister, H.; Radnik, J.; Claus, P. *J. Am. Chem. Soc.* **2003**, *125* (7), 1905-1911.
41. Kato, N.; Caruso, F. *J. Phys. Chem. B* **2005**, *109* (42), 19604-19612.

42. Connor, E. E.; Mwamuka, J.; Gole, A.; Murphy, C. J.; Wyatt, M. D. *Small* **2005**, *1* (3), 325-327.
43. Frens, G. *Nature, Phys. Sci.* **1973**, *241* (105), 20-22.
44. Brust, M.; Walker, M.; Bethell, D.; Schiffrin, D. J.; Whyman, R. *J. Chem. Soc., Chem. Commun.* **1994**, (7), 801-802.
45. Zhou, J.; Ralston, J.; Sedev, R.; Beattie, D. A. *J. Collo. Inter. Sci.* **2009**, *331* (2), 251-262.
46. Isaacs, S. R.; Cutler, E. C.; Park, J.-S.; Lee, T. R.; Shon, Y.-S. *Langmuir* **2005**, *21* (13), 5689-5692.
47. Corbierre, M. K.; Cameron, N. S.; Sutton, M.; Mochrie, S. G. J.; Lurio, L. B.; Ruhm, A.; Lennox, R. B. *J. Am. Chem. Soc.* **2001**, *123* (42), 10411-10412.
48. Shimmin, R. G.; Schoch, A. B.; Braun, P. V. *Langmuir* **2004**, *20* (13), 5613-5620.
49. Sun, X.; Jiang, X.; Dong, S.; Wang, E. *Macromol. Rapid Commun.* **2003**, *24* (17), 1024-1028.
50. Itoh, H.; Naka, K.; Chujo, Y. *J. Am. Chem. Soc.* **2004**, *126* (10), 3026-3027.
51. Templeton, A. C.; Wuelfing, W. P.; Murray, R. W. *Acc. Chem. Res.* **2000**, *33* (1), 27-36.
52. Eklund, S. E.; Cliffl, D. E. *Langmuir* **2004**, *20* (14), 6012-6018.
53. Thomas, K. G.; Kamat, P. V. *J. Am. Chem. Soc.* **2000**, *122* (11), 2655-2656.

54. Gittins, D. I.; Bethell, D.; Schiffrin, D. J.; Nichols, R. J. *Nature* **2000**, *408* (6808), 67-69.
55. Prasad, B. L. V.; Stoeva, S. I.; Sorensen, C. M.; Zaikovski, V.; Klabunde, K. J. *J. Am. Chem. Soc.* **2003**, *125* (35), 10488-10489.
56. Kidwai, M.; Bansal, V.; Kumar, A.; Mozumdar, S. *Green Chem.* **2007**, *9* (7), 742-745.
57. Katz, E.; Willner, I. *Angew. Chem., Int. Ed.* **2004**, *43* (45), 6042-6108.
58. Sperling, R. A.; Rivera Gil, P.; Zhang, F.; Zanella, M.; Parak, W. J. *Chem. Soc. Rev.* **2008**, *37* (9), 1896-1908.
59. Chen, S.; Ingrma, R. S.; Hostetler, M. J.; Pietron, J. J.; Murray, R. W.; Schaaff, T. G.; Khoury, J. T.; Alvarez, M. M.; Whetten, R. L. *Science* **1998**, *280* (5372), 2098-2101.
60. Chen, S. *J. Phys. Chem. B* **2000**, *104* (4), 663-667.
61. Kim, Y.; Johnson, R. C.; Hupp, J. T. *Nano Lett.* **2001**, *1* (4), 165-167.
62. Maye, M. M.; Lou, Y.; Zhong, C.-J. *Langmuir* **2000**, *16* (19), 7520-7523.
63. Alvarez, J.; Liu, J.; Roman, E.; Kaifer, A. E. *Chem. Commun. (Cambridge)* **2000**, (13), 1151-1152.
64. Thibault, R. J.; Galow, T. H.; Turnberg, E. J.; Gray, M.; Hotchkiss, P. J.; Rotello, V. M. *J. Am. Chem. Soc.* **2002**, *124* (51), 15249-15254.
65. Zheng, M.; Huang, X. *J. Am. Chem. Soc.* **2004**, *126* (38), 12047-12054.
66. Tzhayik, O.; Sawant, P.; Efrima, S.; Kovalev, E.; Klug, J. T. *Langmuir* **2002**, *18* (8), 3364-3369.

67. He, J.-A.; Valluzzi, R.; Yang, K.; Dolukhanyan, T.; Sung, C.; Kumar, J.; Tripathy, S. K.; Samuelson, L.; Balogh, L.; Tomalia, D. A. *Chem. Mater.* **1999**, *11* (11), 3268-3274.
68. Wang, Z.; Levy, R.; Fernig, D. G.; Brust, M. *Bioconjug. Chem.* **2005**, *16* (3), 497-500.
69. Housni, A.; Ahmed, M.; Liu, S.; Narain, R. *J. Phys. Chem. C* **2008**, *112* (32), 12282-12290.
70. Mandal, S.; Arumugam, S. K.; Adyanthaya, S. D.; Pasricha, R.; Sastry, M. *J. Mater. Chem.* **2004**, *14* (1), 43-47.
71. Bhattacharya, S.; Srivastava, A. *Langmuir* **2003**, *19* (10), 4439-4447.
72. He, P.; Urban, M. W. *Biomacromolecules* **2005**, *6* (3), 1224-1225.
73. Zhang, L.; Sun, X.; Song, Y.; Jiang, X.; Dong, S.; Wang, E. *Langmuir* **2006**, *22* (6), 2838-2843.
74. Zhu, H.; Tao, C.; Zheng, S.; Li, J. *Colloids Surf., A* **2005**, *257-258*, 411-414.
75. Moon, S. Y.; Sekino, T.; Kusunose, T.; Tanaka, S.-i. *J. Cryst. Growth* **2009**, *311* (3), 651-656.
76. Mackiewicz, M. R.; Ayres, B. R.; Reed, S. M. *Nanotechnology* **2008**, *19* (11), 115601-115606.
77. Nakashima, H.; Furukawa, K.; Kashimura, Y.; Torimitsu, K. *Langmuir* **2008**, *24* (11), 5654-5658.
78. New, R. R. C.; Editor, *Liposomes: A Practical Approach*. **1990**; 301 pp.
79. Cullis, P. R.; De Kruijff, B. *Biochim. Biophys. Acta, Rev. Biomembr.* **1979**, *559* (4), 399-420.

80. Gruner, S. M. *J. Phys. Chem.* **1989**, *93* (22), 7562-7570.
81. Lundbk, J. A.; Birn, P.; Girshman, J.; Hansen, A. J.; Andersen, O. S. *Biochemistry* **1996**, *35* (12), 3825-3830.
82. Devaux, P. F. *Biochemistry* **1991**, *30* (5), 1163-1173.
83. van der Wel, P. C. A.; Pott, T.; Morein, S.; Greathouse, D. V.; Koeppe, R. E.; Killian, J. A. *Biochemistry* **2000**, *39* (11), 3124-3133.
84. Gruner, S. M. *Proc. Natl. Acad. Sci. U. S. A.* **1985**, *82* (11), 3665-3669.
85. Tate, M. W.; Eikenberry, E. F.; Turner, D. C.; Shyamsunder, E.; Gruner, S. M. *Chem. Phys. Lipids* **1991**, *57* (2-3), 147-164.
86. Kunishima, M.; Tokaji, M.; Matsuoka, K.; Nishida, J.; Kanamori, M.; Hioki, K.; Tani, S. *J. Am. Chem. Soc.* **2006**, *128* (45), 14452-14453.
87. Kirk, G. L.; Gruner, S. M.; Stein, D. L. *Biochemistry* **1984**, *23* (6), 1093-1102.
88. Seddon, J. M. *Biochim. Biophys. Acta, Rev. Biomembr.* **1990**, *1031* (1), 1-69.
89. Lundbk, J. A.; Maer, A. M.; Andersen, O. S. *Biochemistry* **1997**, *36* (19), 5695-5701.
90. Cantor, R. S. *Biochemistry* **1997**, *36* (9), 2339-2344.
91. Cullis, P. R.; de Kruijff, B. *Biochim. Biophys. Acta* **1979**, *559*, 399-420.
92. Kirk, G. L.; Gruner, S. M. *J. Phys.* **1985**, *46* (5), 761-769.
93. Allende, D.; Simon, S. A.; McIntosh, T. J. *Biophys. J.* **2005**, *88* (3), 1828-1837.
94. Salafsky, J.; Groves, J. T.; Boxer, S. G. *Biochemistry* **1996**, *35* (47), 14773-14781.

95. Sackmann, E. *Science* **1996**, *271* (5245), 43-48.
96. Groves, J. T.; Boxer, S. G. *Acc. Chem. Res.* **2002**, *35* (3), 149-157.
97. Cha, T.; Guo, A.; Zhu, X. Y. *Biophys. J.* **2006**, *90* (4), 1270-1274.
98. Castellana, E. T.; Cremer, P. S. *Surf. Sci. Reports* **2006**, *61* (10), 429-444.
99. Reimhult, E.; Hook, F.; Kasemo, B. *Langmuir* **2003**, *19* (5), 1681-1691.
100. Qi, S. Y.; Groves, J. T.; Chakraborty, A. K. *Proc. Natl. Acad. Sci. U. S. A.* **2001**, *98* (12), 6548-6553.
101. Hwang, L. Y.; Goetz, H.; Hawker, C. J.; Frank, C. W. *Colloids Surf., B* **2007**, *54* (2), 127-135.
102. Saccani, J.; Castano, S.; Desbat, B.; Blaudez, D. *Biophys. J.* **2003**, *85* (6), 3781-3787.
103. Groves, J. T.; Boxer, S. G. *Biophys. J.* **1995**, *69* (5), 1972-1975.
104. Holden, M. A.; Jung, S.-Y.; Yang, T.; Castellana, E. T.; Cremer, P. S. *J. Am. Chem. Soc.* **2004**, *126* (21), 6512-6513.
105. Johnson, S. J.; Bayerl, T. M.; McDermott, D. C.; Adam, G. W.; Rennie, A. R.; Thomas, R. K.; Sackmann, E. *Biophys. J.* **1991**, *59* (2), 289-294.
106. Boxer, S. G. *Curr. Opin. Chem. Bio.* **2000**, *4* (6), 704-709.
107. Watts, T. H.; McConnell, H. M. *Annu. Rev. Immunol.* **1987**, *5*, 461-475.
108. Ulman, N.; Groves, J. T.; Boxer, S. G. *Adv. Mater.* **1997**, *9* (14), 1121-1123.
109. Richter, R. P.; Berat, R.; Brisson, A. R. *Langmuir* **2006**, *22* (8), 3497-3505.
110. Cremer, P. S.; Boxer, S. G. *J. Phys. Chem. B* **1999**, *103* (13), 2554-2559.
111. Okazaki, T.; Morigaki, K.; Taguchi, T. *Biophys. J.* **2006**, *91* (5), 1757-1766.

112. Kam, L.; Boxer, S. G. *Langmuir* **2003**, *19* (5), 1624-1631.
113. Plant, A. L. *Langmuir* **1999**, *15* (15), 5128-5135.
114. Plant, A. L.; Brighamburke, M.; Petrella, E. C.; Oshannessy, D. J. *Anal. Biochem.* **1995**, *226* (2), 342-348.
115. Lingler, S.; Rubinstein, I.; Knoll, W.; Offenhausser, A. *Langmuir* **1997**, *13* (26), 7085-7091.
116. Steinem, C.; Janshoff, A.; Ulrich, W.-P.; Sieber, M.; Galla, H.-J. *Biochim. Biophys. Acta, Biomembr.* **1996**, *1279* (2), 169-180.
117. Elsner, L. *J. Prakt. Chem.* **1846**, *37*, 441-446.
118. McCarthy, A. J.; Coleman, R. G.; Nicol, M. J. *J. Electrochem. Soc.* **1998**, *145* (2), 408-414.
119. Paulini, R.; Frankamp, B. L.; Rotello, V. M. *Langmuir* **2002**, *18* (6), 2368-2373.
120. Boal, A. K.; Rotello, V. M. *Langmuir* **2000**, *16* (24), 9527-9532.
121. Zhu, T.; Vasilev, K.; Kreiter, M.; Mittler, S.; Knoll, W. *Langmuir* **2003**, *19* (22), 9518-9525.
122. Love, C. S.; Ashworth, I.; Brennan, C.; Chechik, V.; Smith, D. K. *Langmuir* **2007**, *23* (10), 5787-5794.
123. Liu, X.; Basu, A. *Langmuir* **2008**, *24* (19), 11169-11174.
124. Chen, Y.; Cho, J.; Young, A.; Taton, T. A. *Langmuir* **2007**, *23* (14), 7491-7497.
125. Wasileski, S. A.; Weaver, M. J. *J. Phys. Chem. B* **2002**, *106* (18), 4782-4788.
126. Finklea, H. O., *Electrochemistry*; Marcel Dekker, Inc.: New York, 1996.

127. Cheng, W.; Dong, S.; Wang, E. *Angew. Chem., Int. Ed.* **2003**, 42 (4), 449-452.
128. Rautaray, D.; Sastry, M. *Biotechnol. Prog.* **2005**, 21 (6), 1759-1767.
129. Templeton, A. C.; Hostetler, M. J.; Kraft, C. T.; Murray, R. W. *J. Am. Chem. Soc.* **1998**, 120 (8), 1906-1911.
130. Rai, A.; Singh, A.; Ahmad, A.; Sastry, M. *Langmuir* **2006**, 22 (2), 736-741.
131. Singh, S.; Pasricha, R.; Bhatta, U. M.; Satyam, P. V.; Sastry, M.; Prasad, B. L. V. *J. Mater. Chem.* **2007**, 17 (16), 1614-1619.
132. Lasic, D. D.; Editor, *Liposomes in Gene Delivery*. **1997**; 77 pp.
133. Chapman, D., *Introduction to Lipids*. **1969**; 141 pp.
134. Ansell, G. B.; Hawthorne, J. N.; Dawson, R. M. C.; Editors, *B.B.A. Library, Vol. 3: Form and Function of Phospholipids. 2nd ed.* **1973**; 494 pp.
135. Sen Gupta, K. K.; Basu, B. *Trans. Met. Chem.* **1983**, 8 (1), 3-5.
136. Sitaula, S.; Mackiewicz, M. R.; Reed, S. M. *Chem. Commun.* **2008**, (26), 3013-3015.
137. Prenner, E. J.; Lewis, R. N. A. H.; Neuman, K. C.; Gruner, S. M.; Kondejewski, L. H.; Hodges, R. S.; McElhaney, R. N. *Biochemistry* **1997**, 36 (25), 7906-7916.
138. Nerambourg, N.; Werts; Charlot, M.; Blanchard-Desce, M. *Langmuir* **2007**, 23 (10), 5563-5570.
139. Hostetler, M. J.; Wingate, J. E.; Zhong, C.-J.; Harris, J. E.; Vachet, R. W.; Clark, M. R.; Londono, J. D.; Green, S. J.; Stokes, J. J.; Wignall, G. D.;

Glish, G. L.; Porter, M. D.; Evans, N. D.; Murray, R. W. *Langmuir* 1998,
14 (1), 17-30.

TERMINAL REFERENCES

1.7 REFERENCES (CHAPTER 1)

1. Matera, M. K.; Takahashi, S.; Fujii, H.; Hong, Z.; Ishikawa, K.; Yoshimura, T.; Rousseau, D. L.; Yoshida, T.; Ikeda-Saito, M. *J. Biol. Chem.* **1996**, *271*, 6618-6624.
2. Meunier, B. *Chem. Rev.* **1992**, *92*, 1411-1456.
3. Fuller, S. D.; Darley-Usmar, V. M.; Capaldi, R. A. *Biochemistry* **1981**, *20*, 7046-7053.
4. Nam, W.; Han, H. J.; Oh, S.-Y.; Lee, Y. J.; Choi, M.-H.; Han, S.-Y.; Kim, C.; Woo, S. K.; Shi, W. *J. Am. Chem. Soc.* **2000**, *122*, 8677-8684.
5. Sono, M.; Roach, M. P.; Coulter, E. D.; Dawson, J. H. *Chem. Rev.* **1996**, *96*, 2841-2888.
6. Wagner, R. W.; Johnson, T. E.; Lindsey, J. S. *J. Am. Chem. Soc.* **1996**, *118* (45), 11166-11180.
7. Gust, D.; Moore, T. A.; Moore, A. L. *Acc. Chem. Res.* **2001**, *34* (1), 40-48.
8. Holten, D.; Bocian, D. F.; Lindsey, J. S. *Acc. Chem. Res.* **2002**, *35* (1), 57-69.
9. Wasielewski, M. R. *Chem. Rev.* **1992**, *92* (3), 435-461.
10. van der Boom, T.; Hayes, R. T.; Zhao, Y.; Bushard, P. J.; Weiss, E. A.; Wasielewski, M. R. *J. Am. Chem. Soc.* **2002**, *124* (32), 9582-9590.
11. Murakami, Y.; Kikuchi, J.-i.; Hisaeda, Y.; Hayashida, O. *Chem. Rev.* **1996**, *96* (2), 721-758.

12. Ambroise, A.; Wagner, R. W.; Rao, P. D.; Riggs, J. A.; Hascoat, P.; Diers, J. R.; Seth, J.; Lammi, R. K.; Bocian, D. F.; Holten, D.; Lindsey, J. S. *Chem. Mater.* **2001**, *13* (3), 1023-1034.
13. Hasobe, T.; Imahori, H.; Kamat, P. V.; Fukuzumi, S. *J. Am. Chem. Soc.* **2003**, *125* 14962-1496.
14. Hasobe, T.; Kamat, P. V.; Troiani, V.; Solladie, N.; Ahn, T. K.; Kim, K.; Kim, D.; Kongkanand, A.; Kuwabata, S.; Fukuzumi, S. *J. Phys. Chem. B* **2005**, *109* 19-23.
15. Collman, J. P.; Anson, F. C.; Barnes, C. E.; Bencosme, C. S.; Geiger, T.; Evitt, E. R.; Kreh, R. P.; Meier, K.; Pettman, R. B. *J. Am. Chem. Soc.* **1983**, *105* (9), 2694-2699.
16. Collman, J. P.; Bencosme, C. S.; Barnes, C. E.; Miller, B. D. *J. Am. Chem. Soc.* **1983**, *105* (9), 2704-2710.
17. Collman, J. P.; Tyvoll, D. A.; Chng, L. L.; Fish, H. T. *J. Org. Chem.* **1995**, *60* (7), 1926-1931.
18. Yu, J.; Mathew, S.; Flavel, B. S.; Johnston, M. R.; Shapter, J. G. *J. Am. Chem. Soc.* **2008**, *130* (27), 8788-8796.
19. Liu, Z.; Yasseri, A. A.; Lindsey, J. S.; Bocian, D. F. *Science* **2003**, *302* (5650), 1543-1545.
20. Wang, Z.; Li, Z.; Medforth, C. J.; Shelnut, J. A. *J. Am. Chem. Soc.* **2007**, *129* (9), 2440-2441.
21. Kanayama, N.; Kanbara, T.; Kitano, H. *J. Phys. Chem. B* **2000**, *104* (2), 271-278.
22. Rakow, N. A.; Suslick, K. S. *Nature* **2000**, *406* (6797), 710-713.

23. Zimmerman, S. C.; Wendland, M. S.; Rakow, N. A.; Zharov, I.; Suslick, K. *S. Nature* **2002**, *418* (6896), 399-403.
24. Suslick, K. S.; Rakow, N. A.; Kosal, M. E.; Chou, J.-H. *J. Porphyrins Phthalocyanines* **2000**, *4* (4), 407-413.
25. Anderson, H. L. *Chem. Commun.* **1999**, (23), 2323-2330.
26. Lin, V. S. Y.; DiMagno, S. G.; Therien, M. J. *Science* **1994**, *264* (5162), 1105-1111.
27. Screen, T. E. O.; Thorne, J. R. G.; Denning, R. G.; Bucknall, D. G.; Anderson, H. L. *J. Am. Chem. Soc.* **2002**, *124* (33), 9712-9713.
28. Wagner, R. W.; Lindsey, J. S. *J. Am. Chem. Soc.* **1994**, *116* (21), 9759-9760.
29. Park, M.; Yoon, M.-C.; Yoon, Z. S.; Hori, T.; Peng, X.; Aratani, N.; Hotta, J.-i.; Uji-i, H.; Sliwa, M.; Hofkens, J.; Osuka, A.; Kim, D. *J. Am. Chem. Soc.* **2007**, *129* (12), 3539-3544.
30. Ogawa, K.; Kobuke, Y. *Angew. Chem. Int. Ed.* **2000**, *39* (22), 4070-4073.
31. Schenning, A. P. H. J.; Meijer, E. W. *Chem. Commun.* **2005**, (26), 3245-3258.
32. Ambroise, A.; Li, J.; Yu, L.; Lindsey, J. S. *Org. Lett.* **2000**, *2* (17), 2563-2566.
33. Kozaki, M.; Uetomo, A.; Suzuki, S.; Okada, K. *Org. Lett.* **2008**, *10* (20), 4477-4480.
34. Yu, L.; Lindsey, J. S. *J. Org. Chem.* **2001**, *66* (22), 7402-7419.

35. Kuciauskas, D.; Liddell, P. A.; Lin, S.; Johnson, T. E.; Weghorn, S. J.; Lindsey, J. S.; Moore, A. L.; Moore, T. A.; Gust, D. *J. Am. Chem. Soc.* **1999**, *121* (37), 8604-8614.
36. Aratani, N.; Cho, H. S.; Ahn, T. K.; Cho, S.; Kim, D.; Sumi, H.; Osuka, A. *J. Am. Chem. Soc.* **2003**, *125* (32), 9668-9681.
37. Liu, Z.-X.; Mu, L.-J.; Shi, S.-Q.; Zhou, Y.-Q.; Shen, P.-W. *Gaodeng Xuexiao Huaxue Xuebao* **1996**, *17* (10), 1504-1508.
38. Sun, X.; Chen, G.; Zhang, J. *Dyes Pigm.* **2008**, *76* (2), 499-501.
39. Clayton, R. K., *IUPAB Biophysics Series, Vol. 4: Photosynthesis: Physical Mechanisms and Chemical Patterns.* **1980**; pp 281.
40. Nakamura, M.; Ohtoshi, Y.; Yamana, K. *Chem. Commun.* **2005**, (41), 5163-5165.
41. Flamigni, L.; Marconi, G.; Dixon, I. M.; Collin, J.-P.; Sauvage, J.-P. *J. Phys. Chem. B* **2002**, *106* (26), 6663-6671.
42. Flamigni, L.; Dixon, I. M.; Jean, J.-P. C.; Sauvage, P. *Chem. Commun.* **2000**, 2479-2480.
43. Dixon, I. M.; Collin, J.-P.; Sauvage, J.-P.; Barigelletti, F.; Flamigni, L. *Angew. Chem. Int. Ed.* **2000**, *39*, 1292-1295.
44. Sanchez-Mosteiro, G.; van Dijk, E. M. H. P.; Hernando, J.; Heilemann, M.; Tinnefeld, P.; Sauer, M.; Koberlin, F.; Patting, M.; Wahl, M.; Erdmann, R.; van Hulst, N. F.; Garcia-Parajo, M. F. *J. Phys. Chem. B* **2006**, *110* (51), 26349-26353.
45. Heilemann, M.; Kasper, R.; Tinnefeld, P.; Sauer, M. *J. Am. Chem. Soc.* **2006**, *128* (51), 16864-16875.

46. Kannan, B.; Kulkarni, R. P.; Majumdar, A. *Nano Lett.* **2004**, *4* (8), 1521-1524.
47. Eckardt, L. H.; Naumann, K.; Pankau, W. M.; Rein, M.; Schweitzer, M.; Windhab, N.; von Kiedrowsk, G. *Nature* **2002**, *417*, 286.
48. Yan, H.; Park, S. H.; Finkelstein, G.; Reif, J. H.; LaBean, T. H. *Science* **2003**, *301* (5641), 1882-1884.
49. Gao, J.; Strassler, C.; Tahmassebi, D.; Kool, E. T. *J. Am. Chem. Soc.* **2002**, *124* (39), 11590-11591.
50. Osuka, A.; Nakajima, S.; Maruyama, K.; Mataga, N.; Asahi, T.; Yamazaki, I.; Nishimura, Y.; Ohno, T.; Nozaki, K. *J. Am. Chem. Soc.* **1993**, *115* (11), 4577-4589.
51. Hoeben, F. J. M.; Jonkheijm, P.; Meijer, E. W.; Schenning, A. P. H. J. *Chem. Rev.* **2005**, *105* (4), 1491-1546.
52. Endo, M.; Fujitsuka, M.; Majima, T. *J. Org. Chem.* **2008**, *73* (3), 1106-1112.
53. Dougherty, T. J.; Kaufman, J. E.; Goldfarb, A.; Weishaupt, K. R.; Boyle, D.; Mittleman, A. *Cancer Res.* **1978**, *38* (8), 2628-2635.
54. Pullerits, T.; Sundstrom, V. *Acc. Chem. Res.* **1996**, *29* (8), 381-389.
55. Clayton, R. K., *Photosynthesis: Physical Mechanism and Chemical Patterns*. Cambridge University Press, N. Y., Ed. **1980**.
56. van Dongen, G. A. M. S.; Visser, G. W. M.; Vrouenraets, M. B. *Adv. Drug Delivery Rev.* **2004**, *56* (1), 31-52.
57. Moreira, L. M.; dos Santos, F. V.; Lyon, J. P.; Maftoum-Costa, M.; Pacheco-Soares, C.; da Silva, N. S. *Aust. J. Chem.* **2008**, *61* (10), 741-754.

58. Sternberg, E. D.; Dolphin, D.; Brückner, C. *Tetrahedron* **1998**, *54* (17), 4151-4172.
59. Ochsner, M. J. *Photochem. Photobiol. B* **1997**, *39* (1), 1-18.
60. Weishaupt, K. R.; Gomer, C. J.; Dougherty, T. J. *Cancer Res.* **1976**, *36* (7_Part_1), 2326-2329.
61. Olemick, N. L.; Evans, H. H. *Rad. Res.* **1998**, *150*, 5146-5156.
62. Triesscheijn, M.; Baas, P.; Schellens, J. H. M.; Stewart, F. A. *Oncologist* **2006**, *11* (9), 1034-1044.
63. Sharman, W. M.; Allen, C. M.; van Lier, J. E. *Drug Discov. Today* **1999**, *4* (11), 507-517.
64. Detty, M. R.; Gibson, S. L.; Wagner, S. J. *J. Med. Chem.* **2004**, *47* (16), 3897-3915.
65. Henderson, B. W.; Bellnier, D. A.; Greco, W. R.; Sharma, A.; Pandey, R. K.; Vaughan, L. A.; Weishaupt, K. R.; Dougherty, T. J. *Cancer Res.* **1997**, *57* (18), 4000-4007.
66. Hilmey, D. G.; Abe, M.; Nelen, M. I.; Stilts, C. E.; Baker, G. A.; Baker, S. N.; Bright, F. V.; Davies, S. R.; Gollnick, S. O.; Oseroff, A. R.; Gibson, S. L.; Hilf, R.; Detty, M. R. *J. Med. Chem.* **2002**, *45* (2), 449-461.
67. You, Y.; Gibson, S. L.; Hilf, R.; Davies, S. R.; Oseroff, A. R.; Roy, I.; Ohulchanskyy, T. Y.; Bergey, E. J.; Detty, M. R. *J. Med. Chem.* **2003**, *46* (17), 3734-3747.
68. Leung, S. C. H.; Lo, P. C.; Ng, D. K. P.; Liu, W. K.; Fung, K. P.; Fong, W. *P. Br. J. Pharmacol.* **2008**, *154* (1), 4-12.

69. Mallikaratchy, P.; Tang, Z.; Tan, W. *Chem. Med. Chem.* **2008**, *3* (3), 425-428.
70. Mew, D.; Lum, V.; Wat, C. K.; Towers, G. H. N.; Sun, C.-H.; Walter, R. J.; Wright, W.; Berns, M. W.; Levy, J. G. *Cancer Res.* **1985**, *45*, 4348.
71. Hamblin, M. R.; Newman, E. L. *J. Photochem. Photobiol. B* **1994**, *26* (1), 45-56.
72. Savitskii, A. P.; Lopatin, K. V.; Golubeva, N. A.; Poroshina, M. Y.; Chernyaeva, E. B.; Stepanova, N. V.; Solovieva, L. I.; Lukyanets, E. A. *J. Photochem. Photobiol., B* **1992**, *13* (3-4), 327-333.
73. Papkovskii, D. B.; Savitskii, A. P.; Egorova, S. G.; Sukhin, G. M.; Chisov, V. I.; Krasnovskii, A. A.; Egorov, S. Y.; Ponomarev, G. V.; Kirillova, G. V. *Biomed. Sci.* **1990**, *1* (4), 401-406.
74. Egorov, S. Y.; Krasnovskii, A. A.; Papkovskii, D. B.; Ponomarev, G. V.; Savitskii, A. P. *Byull. Eksp. Biol. Med.* **1990**, *109* (4), 349-351.
75. Bhatti, M.; MacRobert, A.; Henderson, B.; Shepherd, P.; Cridland, J.; Wilson, M. *Antimicrob. Agents Chemother.* **2000**, *44* (10), 2615-2618.
76. Savellano, M. D.; Pogue, B. W.; Hoopes, P. J.; Vitetta, E. S.; Paulsen, K. D. *Cancer Res.* **2005**, *65* (14), 6371-6379.
77. Goff, B. A.; Blake, J.; Bamberg, M. P.; Hasan, T. *Br. J. Cancer* **1996**, *74* (8), 1194-1198.
78. Lei, H.; Zhao, F.; Xin, H.; Zhang, F. *Huaxue Jinzhan* **2007**, *19* (4), 527-534.

79. Hasan, T.; Savellano, M. D.; Skobe, M. Photoimmunotherapies for cancer using photosensitizer immunoconjugates and combination therapies. 2002-US137762002100326, 20020501, **2002**.
80. Hamblin, M. R.; Del Governatore, M.; Rizvi, I.; Hasan, T. *Br. J. Cancer* **2000**, *83* (11), 1544-1551.
81. Bhatti, M.; Yahioğlu, G.; Milgrom, L. R.; Garcia-Maya, M.; Chester, K. A.; Deonarain, M. P. *Int. J. Cancer* **2008**, *122* (5), 1155-1163.
82. Aveline, B. M.; Hasan, T.; Redmond, R. W. *J. Photochem. Photobiol. B* **1995**, *30* (2-3), 161-169.
83. Savellano, M. D.; Hasan, T. *Clin. Cancer Res.* **2005**, *11* (4), 1658-1668.
84. Savellano, M. D.; Hasan, T. *Photochem. Photobiol.* **2003**, *77* (4), 431-439.
85. Brasseur, N.; Langlois, R.; La Madeleine, C.; Ouellet, R.; Van Lier, J. E. *Photochem. Photobiol.* **1999**, *69* (3), 345-352.
86. Hamblin, M. R.; Miller, J. L.; Hasan, T. *Cancer Res.* **1996**, *56* (22), 5205-.
87. Jiang, F. N.; Jiang, S.; Liu, D.; Richter, A.; Levy, J. G. *J. Immunol. Methods* **1990**, *134* (1), 139-149.
88. Marco Del Governatore; Hamblin, M. R.; Shea, C. R.; Rizvi, I.; Molpus, K. G.; Tanabe, K. K.; Hasan, T. *Cancer Res.* **2000**, *60* (15), 4170-4175.
89. Rakestraw, S. L.; Tompkins, R. G.; Yarmush, M. L. *Bioconjug. Chem.* **1990**, *1* (3), 212-221.
90. Missailidis, S.; Gariépy, J.; Ferreira, C. S. M. Aptamers against MUC1 and their uses in cancer diagnosis and therapy. 2006-87782437727, 20060504, 2007.
91. Baines, I. C.; Colas, P. *Drug Discov. Today* **2006**, *11* (7 & 8), 334-341.

92. Jenne, A. *Innovations Pharm. Technol.* **2005**, (16), 44-47.
93. Egli, M. *Angew. Chem. Int. Ed.* **1997**, 36 (5), 480-482.
94. Xiao, Z.; Shangguan, D.; Cao, Z.; Fang, X.; Tan, W. *Chem.--Eur. J.* **2008**, 14 (6), 1769-1775, S1769/10S1769/2.
95. Tang, Z.; Parekh, P.; Turner, P.; Moyer, R. W.; Tan, W. *Clin. Chem.* **2009**, 55 (4), 813-822.
96. Stojanovic, M. N.; Landry, D. W. *J. Am. Chem. Soc.* **2002**, 124 (33), 9678-9679.
97. Stojanovic, M. N.; Landry, D. W. *Abstracts of Papers, 222nd ACS National Meeting, Chicago, IL, United States, August 26-30, 2001* **2001**, BIOL-005.
98. Green, L. S.; Bell, C.; Janjic, N. *Biotechniques* **2001**, 30 (5), 1094-1096.
99. Shi, C.; Ma, C.; Zhang, S.; Kong, J. Method for detecting target molecules using nucleic acid aptamer and PCR. 2008-10160859101368209, 20080912, **2009**.
100. Bayer, T. S.; Booth, L. N.; Knudsen, S. M.; Ellington, A. D. *Rna* **2005**, 11 (12), 1848-1857.
101. Lin, C. H.; Patel, D. J. *Chem. Biol.* **1997**, 4 (11), 817-832.
102. Low, S. Y.; Hill, J. E.; Peccia, J. *Biochem. Biophys. Res. Commun.* **2009**, 378 (4), 701-705.
103. Ellington, A. D.; Szostak, J. W. *Nature* **1990**, 346 (6287), 818-822.
104. Tuerk, C.; Gold, L. *Science* **1990**, 249 (4968), 505-510.
105. Haes, A. J.; Giordano, B. C.; Collins, G. E. *Anal. Chem.* **2006**, 78 (11), 3758-3764.
106. Feng, H.; Hu, K.-h. *Virol. Sin.* **2008**, 23 (5), 315-320.

107. Gold, L. *Comb. Chem. Technol.* **1999**, 389-403.
108. Yang, X.; Wang, L.; Wang, K.; Tan, W.; Tang, H.; Meng, X.; Guo, Q. *Chin. Sci. Bull.* **2008**, 53 (2), 204-208.
109. Burgstaller, P.; Girod, A.; Blind, M. *Drug Discov. Today* **2002**, 7 (24), 1221-1228.
110. Burgstaller, P.; Jenne, A.; Blind, M. *Curr. Opin. Drug Discov. & Dev.* **2002**, 5 (5), 690-700.
111. Guo, K.-T.; Schaefer, R.; Paul, A.; Ziemer, G.; Wendel, H. P. *Mini-Rev. Med. Chem.* **2007**, 7 (7), 701-705.
112. Pendergrast, P. S.; Epstein, D. M. *Aptamer Handb.* **2006**, 265-279.
113. Proske, D.; Blank, M.; Buhmann, R.; Resch, A. *Appl. Microbiol. Biotechnol.* **2005**, 69 (4), 367-374.
114. Dua, P.; Kim, S.; Lee, D.-K. *Recent Pat. DNA Gene Sequences* **2008**, 2 (3), 172-186.
115. Hicke, B. J.; Stephens, A. W. *J. Clin. Invest.* **2000**, 106 (8), 923-928.
116. Cox, J. C.; Rajendran, M.; Riedel, T.; Davidson, E. A.; Sooter, L. J.; Bayer, T. S.; Schmitz-Brown, M.; Ellington, A. D. *Comb. Chem. High Throughput Screening* **2002**, 5 (4), 289-299.
117. Cox, J. C.; Hayhurst, A.; Hesselberth, J.; Bayer Travis, S.; Georgiou, G.; Ellington Andrew, D. *Nucleic Acids Res.* **2002**, 30 (20), e108.
118. Shamah, S. M.; Healy, J. M.; Cload, S. T. *Acc. Chem. Res.* **2008**, 41 (1), 130-138.
119. Chen, H. W.; Medley, C. D.; Sefah, K.; Shangguan, D.; Tang, Z.; Meng, L.; Smith, J. E.; Tan, W. *Chem. Med. Chem.* **2008**, 3 (6), 991-1001.

120. Tang, Z.; Shangguan, D.; Wang, K.; Shi, H.; Sefah, K.; Mallikratchy, P.; Chen, H. W.; Li, Y.; Tan, W. *Anal. Chem.* **2007**, *79* (13), 4900-4907.
121. Keefe, A. D.; Wilson, C.; Wang, C. Selection of oligonucleotides through SELEX. 2008-US89212009014705, 20080721, **2009**.
122. Fukusho, S.; Furusawa, H.; Okahata, Y. *Chem. Commun.* **2002**, (1), 88-89.
123. Ferreira, C. S. M.; Garipey, J. Aptamers that recognize the carbohydrate N-acetylgalactosamine for diagnosis and treatment of cancer. 2007-CA7572007128109, 20070504, **2007**.
124. Liu, Y.; Kuan, C.-T.; Mi, J.; Zhang, X.; Clary, B. M.; Bigner, D. D.; Sullenger, B. A. *Biol. Chem.* **2009**, *390* (2), 137-144.
125. Hicke, B. J.; Marion, C.; Chang, Y.-F.; Gould, T.; Lynott, C. K.; Parma, D.; Schmidt, P. G.; Warren, S. *J. Biol. Chem.* **2001**, *276* (52), 48644-48654.
126. Pietras, K.; Ostman, A.; Rubin, K.; Heldin, C.-H. Method for treatment of tumors using nucleic acid ligands to PDGF. 2001-US160782001087351, 20010517, **2001**.
127. Fang, X.; Cao, Z.; Beck, T.; Tan, W. *Anal. Chem.* **2001**, *73* (23), 5752-5757.
128. Sennino, B.; Falcon, B. L.; McCauley, D.; Le, T.; McCauley, T.; Kurz, J. C.; Haskell, A.; Epstein, D. M.; McDonald, D. M. *Cancer Res.* **2007**, *67* (15), 7358-7367.
129. Lupold, S. E.; Hicke, B. J.; Lin, Y.; Coffey, D. S. *Cancer Res.* **2002**, *62* (14), 4029-4033.

130. Diener, J. L.; Hatala, P.; Killough, J. R.; Wagner-Whyte, J.; Wilson, C.; Zhu, S. Stabilized aptamers to PSMA and their use in diagnosis and treatment of prostate cancer. 2006-US81932006096754, 20060307, **2006**.
131. Ruckman, J.; Green, L. S.; Beeson, J.; Waugh, S.; Gillette, W. L.; Henninger, D. D.; Claesson-Welsh, L.; Janjic, N. *J. Biol. Chem.* **1998**, *273* (32), 20556-20567.
132. Adamis, A. P.; Shima, D.; Wincott, F.; Calias, P. VEGF-binding aptamers capped with inverted nucleotides and sustained release compositions for use in pharmaceuticals. 2004-US254222005014814, 20040806, **2005**.
133. Daniels, D. A.; Chen, H.; Hicke, B. J.; Swiderek, K. M.; Gold, L. *Proc. Natl. Acad. Sci. U. S. A.* **2003**, *100* (26), 15416-15421.
134. Foerster, C.; Brauer, A. B. E.; Brode, S.; Schmidt, K. S.; Perbandt, M.; Meyer, A.; Rypniewski, W.; Betzel, C.; Kurreck, J.; Fuerste, J. P.; Erdmann, V. A. *Acta Crystallogr., Sect. F: Struct. Biol. Cryst. Commun.* **2006**, *F62* (7), 665-668.
135. Chen, C.-H. B.; Landgraf, R. Inhibition of heregulin signaling by aptamers to human epidermal growth factor receptor-3 and their use in cancer therapy. 2004-US230392005040339, 20040716, 2005.
136. Chen Chi-Hong, B.; Chernis George, A.; Hoang Van, Q.; Landgraf, R. *Proc. Natl. Acad. Sci. U.S. A.* **2003**, *100* (16), 9226-9231.
137. Phillips, J. A.; Lopez-Colon, D.; Zhu, Z.; Xu, Y.; Tan, W. *Anal. Chim. Acta* **2008**, *621* (2), 101-108.

138. Shangguan, D.; Li, Y.; Tang, Z.; Cao, Z. C.; Chen, H. W.; Mallikaratchy, P.; Sefah, K.; Yang, C. J.; Tan, W. *Proc. Natl. Acad. Sci. U. S. A.* **2006**, *103* (32), 11838-11843.
139. Becker, K. C. D.; Becker, R. C. *Curr. Opin. Mol. Therap.* **2006**, *8* (2), 122-129.
140. Nutiu, R.; Li, Y. *J. Am. Chem. Soc.* **2003**, *125* (16), 4771-4778.
141. Borbas, K. E.; Ferreira, C. S. M.; Perkins, A.; Bruce, J. I.; Missailidis, S. *Bioconjug. Chem.* **2007**, *18* (4), 1205-1212.
142. Lee, J. F.; Stovall, G. M.; Ellington, A. D. *Curr. Opin. Chem. Biol.* **2006**, *10* (3), 282-289.
143. Brody, E. N.; Gold, L. *J. Biotechnol.* **2000**, *74* (1), 5-13.
144. Rajendrakumar, G. V.; Sundari, N. S.; Ganesh, K. N. *Proc. - Indian Acad. Sci., Chem. Sci.* **1985**, *95* (4), 357-368.
145. Li, B. F. L.; Reese, C. B.; Swann, P. F. *Biochemistry* **1987**, *26* (4), 1086-1093.
146. Beaucage, S. L. *Methods Mol. Biol.* **1993**, *20*, 33-61.
147. Beaucage, S. L.; Iyer, R. P. *Tetrahedron* **1993**, *49* (46), 10441-10488.
148. Froehler, B. C. *Methods Mol. Biol. (Totowa, N. J.)* **1993**, *20* (Protocols for Oligonucleotides and Analogs), 63-80.
149. Reese, C. B.; Song, Q. *J. Chem. Soc., Perkin Trans. 1* **1999**, (11), 1477-1486.
150. Herdewijn, P.; Editor, *Oligonucleotide Synthesis: Methods and Applications. [In: Methods Mol. Biol. (Totowa, NJ, U. S.); 2005, 288].* **2005**; 435 pp.

151. Khudyakov, Y. E.; Fields, H. A.; Editors, *Artificial DNA: Methods and Applications*. **2003**; 417 pp.
152. Stawinski, J.; Stroemberg, R. *Trends Org. Chem.* **1993**, *4* (1), 31-67.
153. Stawinski, J. *Handb. Organophosphorus Chem.* **1992**, 377-434.
154. Kung, P. P.; Jones, R. A. *Tet. Lett.* **1992**, *33* (40), 5869-5872.
155. Froehler, B. C.; Ng, P. G.; Matteucci, M. D. *Nucleic Acids Res.* **1986**, *14* (13), 5399-5407.
156. Andrus, A.; Zon, G. *Nucleic Acids Symp. Ser.* **1988**, *20*, 121-122.
157. Stein, C. A.; Iversen, P. L.; Subasinghe, C.; Cohen, J. S.; Stec, W. J.; Zon, G. *Anal. Biochem.* **1990**, *188* (1), 11-16.
158. Grand, C. L.; Han, H.; Munoz, R. M.; Weitman, S.; Von Hoff, D. D.; Hurley, L. H.; Bearss, D. J. *Mol. Cancer Therap.* **2002**, *1* (8), 565-573.
159. Ma, H.-m.; Chen, X.; Sun, S.-t.; Zhang, L.-n.; Wu, D.; Zhu, P.-h.; Li, Y.; Du, B.; Wei, Q. *Guangpuxue Yu Guangpu Fenxi* **2009**, *29* (2), 423-427.
160. Schneider, H.-J.; Wang, M. *J. Org. Chem.* **1994**, *59* (24), 7473-7478.
161. Ward, B.; Skorobogaty, A.; Dabrowiak, J. C. *Biochemistry* **1986**, *25* (22), 6875-6883.
162. Lipscomb, L. A.; Zhou, F. X.; Presnell, S. R.; Woo, R. J.; Peek, M. E.; Plaskon, R. R.; Williams, L. D. *Biochemistry* **1996**, *35* (9), 2818-2823.
163. Mestre, B.; Jakobs, A.; Pratviel, G.; Meunier, B. *Biochemistry* **1996**, *35* (28), 9140-9149.
164. Casas, C.; Lacey, C. J.; Meunier, B. *Bioconjug. Chem.* **1993**, *4* (5), 366-371.

165. Balaz, M.; Holmes, A. E.; Benedetti, M.; Proni, G.; Berova, N. *Bioorg. Med. Chem.* **2005**, *13* (7), 2413-2421.
166. Balaz, M.; Holmes, A. E.; Benedetti, M.; Rodriguez, P. C.; Berova, N.; Nakanishi, K.; Proni, G. *J. Am. Chem. Soc.* **2005**, *127* (12), 4172-4173.
167. Balaz, M.; Steinkruger, J. D.; Ellestad, G. A.; Berova, N. *Org. Lett.* **2005**, *7* (25), 5613-5616.
168. Mammana, A.; Asakawa, T.; Bitsch-Jensen, K.; Wolfe, A.; Chaturantabut, S.; Otani, Y.; Li, X.; Li, Z.; Nakanishi, K.; Balaz, M.; Ellestad, G. A.; Berova, N. *Bioorg. Med. Chem.* **2008**, *16* (13), 6544-6551.
169. Berlin, K.; Jain, R. K.; Simon, M. D.; Richert, C. *J. Org. Chem.* **1998**, *63* (5), 1527-1535.
170. Reed, M. W.; Wald, A.; Meyer, R. B. *J. Am. Chem. Soc.* **1998**, *120* (38), 9729-9734.
171. Lukhtanov, E. A.; Kutuyavin, I. V.; Gorn, V. V.; Reed, M. W.; Adams, A. D.; Lucas, D. D.; Meyer, R. B., Jr. *J. Am. Chem. Soc.* **1997**, *119* (27), 6214-6225.
172. Robles, J.; McLaughlin, L. W. *J. Am. Chem. Soc.* **1997**, *119* (26), 6014-6021.
173. Cardullo, R. A.; Agrawal, S.; Flores, C.; Zaacetoneitrileik, P. C.; Wolf, D. E. *Proc. Natl. Acad. Sci. U. S. A.* **1988**, *85* (23), 8790-8794.
174. Walton, T. A.; Lyttle, M. H.; Dick, D. J.; Cook, R. M. *Bioconjug. Chem.* **2002**, *13* (5), 1155-1158.
175. Didenko, V. V. *Biotechniques* **2001**, *31* (5), 1106-1121.

176. Okamura, Y.; Kondo, S.; Sase, I.; Suga, T.; Mise, K.; Furusawa, I.; Kawakami, S.; Watanabe, Y. *Nucleic Acids Res.* **2000**, *28* (24), E107.
177. Okamura, Y.; Watanabe, Y. *Methods Mol. Biol.* **2006**, *335*, 43-56.
178. Eckstein, F. *Antisense Nucleic Acid Drug Dev.* **2000**, *10* (2), 117-121.
179. Major, D. T.; Laxer, A.; Fischer, B. *J. Org. Chem.* **2002**, *67* (3), 790-802.
180. Alzeer, J.; Schaerer, O. D. *Nucleic Acids Res.* **2006**, *34* (16), 4458-4466.
181. Wagner, C.; Rist, M.; Mayer-Enthart, E.; Wagenknecht, H.-A. *Org. Biomol. Chem.* **2005**, *3* (11), 2062-2063.
182. Giller, G.; Tasara, T.; Angerer, B.; Muhlegger, K.; Amacker, M.; Winter, H. *Nucleic Acids Res.* **2003**, *31* (10), 2630-2635.
183. Seela, F.; Xu, K. *Org. Biomol. Chem.* **2008**, *6* (19), 3552-3560.
184. Fendt, L.-A.; Bouamaied, I.; Thoni, S.; Amiot, N.; Stulz, E. *J. Am. Chem. Soc.* **2007**, *129* (49), 15319-15329.
185. Salon, J.; Chen, G.; Portilla, Y.; Germann, M. W.; Huang, Z. *Org. Lett.* **2005**, *7* (25), 5645-5648.
186. Li, N.-S.; Piccirilli, J. A. *J. Org. Chem.* **2004**, *69* (14), 4751-4759.
187. McGee, D. P. C.; Vaughn-Settle, A.; Vargeese, C.; Zhai, Y. *J. Org. Chem.* **1996**, *61* (2), 781-785.
188. Shohda, K.; Okamoto, I.; Wada, T.; Seio, K.; Sekine, M. *Bioorg. Med. Chem. Lett.* **2000**, *10* (16), 1795-1798.
189. Kumamoto, S.; Watanabe, M.; Kawakami, N.; Nakamura, M.; Yamana, K. *Bioconjug. Chem.* **2008**, *19* (1), 65-69.

190. Whittemore, N. A.; Mullenix, A. N.; Inamati, G. B.; Manoharan, M.; Cook, P. D.; Tuinman, A. A.; Baker, D. C.; Chambers, J. Q. *Bioconjug. Chem.* **1999**, *10* (2), 261-270.
191. Mayer-Enthart, E.; Wagenknecht, H.-A. *Angew. Chem. Int. Ed.* **2006**, *45* (20), 3372-3375.
192. Yamana, K.; Ohashi, Y.; Nunota, K.; Nakano, H. *Tetrahedron* **1997**, *53* (12), 4265-4270.
193. Henderikx, P.; Kandilogiannaki, M.; Petrarca, C.; von Mensdorff-Pouilly, S.; Hilgers, J. H. M.; Krambovitis, E.; Arends, J. W.; Hoogenboom, H. R. *Cancer Res* **1998**, *58* (19), 4324-4332.
194. von Mensdorff-Pouilly, S.; Snijdwint, F. G. M.; Verstraeten, A. A.; Verheijen, R. H. M.; Kenemans, P. *Int. J. Biol. Markers* **2000**, *15* (4), 343-356.
195. Burdick, M. D.; Harris, A.; Reid, C. J.; Iwamura, T.; Hollingsworth, M. A. *J. Biol. Chem.* **1997**, *272* (39), 24198-24172.
196. Brayman, M.; Thathiah, A.; Carson, D. D. *Reprod. Biol. Endocrinol.* **2004**, *2*, No pp given.
197. Price, M. R.; Rye, P. D.; Petrakou, E.; Murray, A.; Brady, K.; Imai, S.; Haga, S.; Kiyozuka, Y.; Schol, D.; Meulenbroek, M. F.; Snijdwint, F. G.; von Mensdorff-Pouilly, S.; Verstraeten, R. A.; Kenemans, P.; Blockzijl, A.; Nilsson, K.; Nilsson, O.; Reddish, M.; Suresh, M. R.; Koganty, R. R.; Fortier, S.; Baronic, L.; Berg, A.; Longenecker, M. B.; Hilgers, J.; et al. *Tumour Biol.* **1998**, *19 Suppl 1*, 1-20.

198. Adluri, S.; Gilewski, T.; Zhang, S.; Ramnath, V.; Ragupathi, G.; Livingston, P. *Br. J. Cancer* **1999**, *79* (11/12), 1806-1812.
199. Moore, A.; Medarova, Z.; Potthast, A.; Dai, G. *Cancer Res* **2004**, *64* (5), 1821-1827.
200. Barratt-Boyes, S. M. *Cancer Immunol. Immunother.* **1996**, *43* (3), 142-151.
201. Girling, A.; Bartkova, J.; Burchell, J.; Gendler, S.; Gillett, C.; Taylor-Papadimitriou, J. *Int J Cancer* **1989**, *43* (6), 1072-6.
202. Rowse, G. J.; Tempero, R. M.; VanLith, M. L.; Hollingsworth, M. A.; Gendler, S. J. *Cancer Res.* **1998**, *58* (2), 315-321.
203. Fujii, K.; Okamoto, S.; Sasaki, N.; Takano, M.; Kudoh, K.; Kita, T.; Tsuda, H.; Kikuchi, Y. *Trends Cancer Res.* **2005**, *1*, 133-138.
204. Swanson, B. J.; McDermott, K. M.; Singh, P. K.; Eggers, J. P.; Crocker, P. R.; Hollingsworth, M. A. *Cancer Res.* **2007**, *67* (21), 10222-10229.
205. Zhang, H.; Lu, H.; Kong, G. *Xiandai Zhongliu Yixue* **2005**, *13* (6), 756-758.
206. Jarrard, J. A.; Linnoila, R. I.; Lee, H.; Steinberg, S. M.; Witschi, H.; Szabo, . *Cancer Res.* **1998**, *58* (23), 5582-5589.
207. Nan, Z.; Ji, W. *Shanxi Yiyao Zazhi* **2007**, *36* (10), 879-881.
208. Rubinstein, D. B.; Karmely, M.; Ziv, R.; Benhar, I.; Leitner, O.; Baron, S.; Katz, B.-Z.; Wreschner, D. H. *Cancer Res.* **2006**, *66* (23), 11247-11253.
209. Yu, Y.; Li, H.; Wang, L. Recombinant fusion proteins comprising BCG heat shock protein 65 and the epitope of MUC1. 2003-6352112005031649, 20030806, **2005**.
210. Agrawal, B.; Krantz, M. J.; Reddish, M. A.; Longenecker, B. M. *Nat. Med.* **1998**, *4* (1), 43-49.

211. Berry, N.; Jones, D. B.; Smallwood, J.; Taylor, I.; Kirkham, N.; Taylor-Papadimitriou, J. *Br. J. Cancer* **1985**, *51* (2), 179-186.
212. Hilkens, J.; Buijs, F.; Hilgers, J.; Hageman, P.; Calafat, J.; Sonnenberg, A.; van der Valk, M. *Int. J. Cancer* **1984**, *34* (2), 197-206.
213. Bhavanandan, V. P.; Zhu, Q.; Yamakami, K.; Dilulio, N. A.; Nair, S.; Capon, C.; Lemoine, J.; Fournet, B. *Glycoconjug. J.* **1998**, *15* (1), 37-49.
214. Fontenot, J. D.; Tjandra, N.; Bu, D.; Ho, C.; Montelaro, R. C.; Finn, O. J. *Cancer Res.* **1993**, *53* (22), 5386-5394.
215. Ryuko, K.; Schol, D. J.; Snijdwint, F. G. M.; Von Mensdorff-Pouilly, S.; Poort-Keesom, R. J. J.; Karuntu-Wanamarta, Y. A.; Verstraeten, R. A.; Miyazaki, K.; Kenemans, P.; Hilgers, J. *Tumor Biol.* **2000**, *21* (4), 197-210.
216. Hilkens, J.; Vos, H. L.; Wesseling, J.; Boer, M.; Storm, J.; van der Valk, S.; Calafat, J.; Patriarca, C. *Cancer Lett.* **1995**, *90* (1), 27-33.
217. Sitaula, S.; Reed, S. M. *Bioorg. & Med. Chem. Lett.* **2008**, *18* (2), 850-855.
218. Syrbu, S. A.; Semelkin, A. S.; Berezin, B. D.; Koifman, O. I. *Chem. Heterocyclic Comp.* **1980**, *25*, 1149-1153.
219. Chauhan, S. M. S.; Sahoo, B. B.; Srinivas, K. A. *Synth. Commun.* **2001**, *31* (1), 33-37.
220. Stawinski, J.; Kraszewski, A. *Acc. Chem. Res.* **2002**, *35* (11), 952-960.
221. Iyer, P. C.; Yagi, H.; Sayer, J. M.; Jerina, D. M. *Chem. Res. Toxicol.* **2007**, *20* (2), 311-315.
222. Zhu, Z.; Tang, Z.; Phillips, J. A.; Yang, R.; Wang, H.; Tan, W. *J. Am. Chem. Soc.* **2008**, *130* (33), 10856-10857.

2.7 REFERENCES (CHAPTER 2)

1. Brugger, P. A.; Cuendet, P.; Graetzel, M. J. *Am. Chem. Soc.* **1981**, *103* (11), 2923-2927.
2. Crooks, R. M.; Zhao, M.; Sun, L.; Chechik, V.; Yeung, L. K. *Acc. Chem. Res.* **2001**, *34* (3), 181-190.
3. Takei, T.; Haruta, M. *Mater. Integr.* **2008**, *22* (1), 38-44.
4. Andreeva, D.; Tabakova, T.; Idakiev, V.; Christov, P.; Giovanoli, R. *Appl. Catal., A* **1998**, *169* (1), 9-14.
5. Haruta, M. *Catal. Today* **1997**, *36* (1), 153-166.
6. Toshima, N.; Takahashi, T.; Hirai, H. *Chem. Lett.* **1985**, *14* (8), 1245-1248.
7. Tan, M.; Wang, G.; Hai, X.; Ye, Z.; Yuan, J. *J. Mater. Chem.* **2004**, *14* (19), 2896-2901.
8. Chao, J.-I.; Perevedentseva, E.; Chung, P.-H.; Liu, K.-K.; Cheng, C.-Y.; Chang, C.-C.; Cheng, C.-L. *Biophys. J.* **2007**, *93* (6), 2199-2208.
9. Levy, R.; Wang, Z.; Duchesne, L.; Doty, R. C.; Cooper, A. I.; Brust, M.; Fernig, D. G. *Chem. Bio. Chem.* **2006**, *7* (4), 592-594.
10. Zanchet, D.; Micheel, C. M.; Parak, W. J.; Gerion, D.; Alivisatos, A. P. *Nano Lett.* **2001**, *1* (1), 32-35.
11. Cioffi, N.; Torsi, L.; Farella, I.; Altamura, D.; Valentini, A.; Quinto, M.; Sabbatini, L.; Zambonin, P. G. *Sens. Actuators, B* **2004**, *B100* (1-2), 9-16.
12. Lawrence, N. S.; Liang, H.-P. *Nanostruct. Mater. Electrochem.* **2008**, 435-457.

13. Schaadt, D. M.; Yu, E. T.; Sankar, S.; Berkowitz, A. E. *J. Vac. Sci. Technol, A* **2000**, *18* (4, Pt. 2), 1834-1837.
14. Schoen, G.; Simon, U. *Colloid Polym. Sci.* **1995**, *273* (3), 202-218.
15. Lei, Y.; Cai, W.; Wilde, G. *Prog. Mater. Sci.* **2007**, *52* (4), 465-539.
16. Takahashi, K.; Hasegawa, T.; Shinohara, H.; Ogawa, T. The magnetic material and the magnetic device. 2005-1249462006303298, 20050422., **2006**.
17. Esparza, R.; Rosas, G.; Lopez-Fuentes, M.; Pal, U.; Perez, R. *Rev. Mex. Fis. S* **2007**, *53* (5), 67-71.
18. Murphy, C. J.; Gole, A. M.; Hunyadi, S. E.; Stone, J. W.; Sisco, P. N.; Alkilany, A.; Kinard, B. E.; Hankins, P. *Chem. Commun.* **2008**, (5), 544-557.
19. Venkata, P. G.; Aslan, M. M.; Menguc, M. P.; Videen, G. *HTD (Am. Soc. Mech. Eng.)* **2005**, *376-2* (Proceedings of the ASME Heat Transfer Division--2005, Volume 2), 823-833.
20. Feldheim, D. L.; Foss, C. A., Jr.; Editors, *Metal Nanoparticles: Synthesis, Characterization, and Applications.* **2002**; 338 pp.
21. Daniel, M.-C.; Astruc, D. *Chem. Rev.* **2004**, *104* (1), 293-346.
22. Kreibig, U.; Vollmer, M., *Optical Properties of Metal Clusters. (Springer Series in Materials Science 25).* **1995**; 532 pp.
23. Link, S.; El-Sayed, M. A. *Int. Rev. Phys. Chem.* **2000**, *19* (3), 409-453.
24. Link, S.; El-Sayed, M. A. *J. Phys. Chem. B* **1999**, *103* (40), 8410-8426.
25. Thomas, S.; Nair, S. K.; Jamal, E. M. A.; Al-Harhi, S. H.; Varma, M. R.; Anantharaman, M. R. *Nanotechnology* **2008**, *19* (7), 75711-75717.

26. Orendorff, C. J.; Sau, T. K.; Murphy, C. J. *Small* **2006**, 2 (5), 636-639.
27. Yu; Chang, S.-S.; Lee, C.-L.; Wang, C. R. C. *J. Phys. Chem. B* **1997**, 101 (34), 6661-6664.
28. Malinsky, M. D.; Kelly, K. L.; Schatz, G. C.; Van Duyne, R. P. *J. Am. Chem. Soc.* **2001**, 123 (7), 1471-1482.
29. Thomas, K. G.; Zajicek, J.; Kamat, P. V. *Langmuir* **2002**, 18 (9), 3722-3727.
30. Qu, X.; Peng, Z.; Jiang, X.; Dong, S. *Langmuir* **2004**, 20 (7), 2519-2522.
31. Liz-Marzan, L. M.; Mulvaney, P. *New J. Chem.* **1998**, 22 (11), 1285-1288.
32. Mulvaney, P. *Langmuir* **1996**, 12 (3), 788-800.
33. Alivisatos, A. P. *J. Phys. Chem.* **1996**, 100 (31), 13226-13239.
34. Henglein, A. *Chem. Rev.* **1989**, 89 (8), 1861-1873.
35. Wang, Z.; Tan, B.; Hussain, I.; Schaeffer, N.; Wyatt, M. F.; Brust, M.; Cooper, A. I. *Langmuir* **2007**, 23 (2), 885-895.
36. Bohren, C. F.; Huffman, D. R., *Absorption and Scattering of Light by Small Particles.* **1983**; 530 pp.
37. Kerker, M., *The Scattering of Light and Other Electromagnetic Radiation (Physical Chemistry: a Series of Monographs, Vol. 16).* **1969**; 666 pp.
38. van der Zande, B. M. I.; Bohmer, M. R.; Fokkink, L. G. J.; Schonenberger, C. *J. Phys. Chem. B* **1997**, 101 (6), 852-854.
39. Kim, F.; Song, J. H.; Yang, P. *J. Am. Chem. Soc.* **2002**, 124 (48), 14316-14317.
40. Mohr, C.; Hofmeister, H.; Radnik, J.; Claus, P. *J. Am. Chem. Soc.* **2003**, 125 (7), 1905-1911.

41. Kato, N.; Caruso, F. *J. Phys. Chem. B* **2005**, *109* (42), 19604-19612.
42. Connor, E. E.; Mwamuka, J.; Gole, A.; Murphy, C. J.; Wyatt, M. D. *Small* **2005**, *1* (3), 325-327.
43. Frens, G. *Nature, Phys. Sci.* **1973**, *241* (105), 20-22.
44. Brust, M.; Walker, M.; Bethell, D.; Schiffrin, D. J.; Whyman, R. *J. Chem. Soc., Chem. Commun.* **1994**, (7), 801-802.
45. Zhou, J.; Ralston, J.; Sedev, R.; Beattie, D. A. *J. Collo. Inter. Sci.* **2009**, *331* (2), 251-262.
46. Isaacs, S. R.; Cutler, E. C.; Park, J.-S.; Lee, T. R.; Shon, Y.-S. *Langmuir* **2005**, *21* (13), 5689-5692.
47. Corbierre, M. K.; Cameron, N. S.; Sutton, M.; Mochrie, S. G. J.; Lurio, L. B.; Ruhm, A.; Lennox, R. B. *J. Am. Chem. Soc.* **2001**, *123* (42), 10411-10412.
48. Shimmin, R. G.; Schoch, A. B.; Braun, P. V. *Langmuir* **2004**, *20* (13), 5613-5620.
49. Sun, X.; Jiang, X.; Dong, S.; Wang, E. *Macromol. Rapid Commun.* **2003**, *24* (17), 1024-1028.
50. Itoh, H.; Naka, K.; Chujo, Y. *J. Am. Chem. Soc.* **2004**, *126* (10), 3026-3027.
51. Templeton, A. C.; Wuelfing, W. P.; Murray, R. W. *Acc. Chem. Res.* **2000**, *33* (1), 27-36.
52. Eklund, S. E.; Cliffel, D. E. *Langmuir* **2004**, *20* (14), 6012-6018.
53. Thomas, K. G.; Kamat, P. V. *J. Am. Chem. Soc.* **2000**, *122* (11), 2655-2656.

54. Gittins, D. I.; Bethell, D.; Schiffrin, D. J.; Nichols, R. J. *Nature* **2000**, *408* (6808), 67-69.
55. Prasad, B. L. V.; Stoeva, S. I.; Sorensen, C. M.; Zaikovski, V.; Klabunde, K. J. *J. Am. Chem. Soc.* **2003**, *125* (35), 10488-10489.
56. Kidwai, M.; Bansal, V.; Kumar, A.; Mozumdar, S. *Green Chem.* **2007**, *9* (7), 742-745.
57. Katz, E.; Willner, I. *Angew. Chem., Int. Ed.* **2004**, *43* (45), 6042-6108.
58. Sperling, R. A.; Rivera Gil, P.; Zhang, F.; Zanella, M.; Parak, W. J. *Chem. Soc. Rev.* **2008**, *37* (9), 1896-1908.
59. Chen, S.; Ingrma, R. S.; Hostetler, M. J.; Pietron, J. J.; Murray, R. W.; Schaaff, T. G.; Khoury, J. T.; Alvarez, M. M.; Whetten, R. L. *Science* **1998**, *280* (5372), 2098-2101.
60. Chen, S. *J. Phys. Chem. B* **2000**, *104* (4), 663-667.
61. Kim, Y.; Johnson, R. C.; Hupp, J. T. *Nano Lett.* **2001**, *1* (4), 165-167.
62. Maye, M. M.; Lou, Y.; Zhong, C.-J. *Langmuir* **2000**, *16* (19), 7520-7523.
63. Alvarez, J.; Liu, J.; Roman, E.; Kaifer, A. E. *Chem. Commun. (Cambridge)* **2000**, (13), 1151-1152.
64. Thibault, R. J.; Galow, T. H.; Turnberg, E. J.; Gray, M.; Hotchkiss, P. J.; Rotello, V. M. *J. Am. Chem. Soc.* **2002**, *124* (51), 15249-15254.
65. Zheng, M.; Huang, X. *J. Am. Chem. Soc.* **2004**, *126* (38), 12047-12054.
66. Tzhayik, O.; Sawant, P.; Efrima, S.; Kovalev, E.; Klug, J. T. *Langmuir* **2002**, *18* (8), 3364-3369.

67. He, J.-A.; Valluzzi, R.; Yang, K.; Dolukhanyan, T.; Sung, C.; Kumar, J.; Tripathy, S. K.; Samuelson, L.; Balogh, L.; Tomalia, D. A. *Chem. Mater.* **1999**, *11* (11), 3268-3274.
68. Wang, Z.; Levy, R.; Fernig, D. G.; Brust, M. *Bioconjug. Chem.* **2005**, *16* (3), 497-500.
69. Housni, A.; Ahmed, M.; Liu, S.; Narain, R. *J. Phys. Chem. C* **2008**, *112* (32), 12282-12290.
70. Mandal, S.; Arumugam, S. K.; Adyanthaya, S. D.; Pasricha, R.; Sastry, M. *J. Mater. Chem.* **2004**, *14* (1), 43-47.
71. Bhattacharya, S.; Srivastava, A. *Langmuir* **2003**, *19* (10), 4439-4447.
72. He, P.; Urban, M. W. *Biomacromolecules* **2005**, *6* (3), 1224-1225.
73. Zhang, L.; Sun, X.; Song, Y.; Jiang, X.; Dong, S.; Wang, E. *Langmuir* **2006**, *22* (6), 2838-2843.
74. Zhu, H.; Tao, C.; Zheng, S.; Li, J. *Colloids Surf., A* **2005**, *257-258*, 411-414.
75. Moon, S. Y.; Sekino, T.; Kusunose, T.; Tanaka, S.-i. *J. Cryst. Growth* **2009**, *311* (3), 651-656.
76. Mackiewicz, M. R.; Ayres, B. R.; Reed, S. M. *Nanotechnology* **2008**, *19* (11), 115601-115606.
77. Nakashima, H.; Furukawa, K.; Kashimura, Y.; Torimitsu, K. *Langmuir* **2008**, *24* (11), 5654-5658.
78. New, R. R. C.; Editor, *Liposomes: A Practical Approach*. **1990**; 301 pp.
79. Cullis, P. R.; De Kruijff, B. *Biochim. Biophys. Acta, Rev. Biomembr.* **1979**, *559* (4), 399-420.

80. Gruner, S. M. *J. Phys. Chem.* **1989**, *93* (22), 7562-7570.
81. Lundbk, J. A.; Birn, P.; Girshman, J.; Hansen, A. J.; Andersen, O. S. *Biochemistry* **1996**, *35* (12), 3825-3830.
82. Devaux, P. F. *Biochemistry* **1991**, *30* (5), 1163-1173.
83. van der Wel, P. C. A.; Pott, T.; Morein, S.; Greathouse, D. V.; Koeppe, R. E.; Killian, J. A. *Biochemistry* **2000**, *39* (11), 3124-3133.
84. Gruner, S. M. *Proc. Natl. Acad. Sci. U. S. A.* **1985**, *82* (11), 3665-3669.
85. Tate, M. W.; Eikenberry, E. F.; Turner, D. C.; Shyamsunder, E.; Gruner, S. M. *Chem. Phys. Lipids* **1991**, *57* (2-3), 147-164.
86. Kunishima, M.; Tokaji, M.; Matsuoka, K.; Nishida, J.; Kanamori, M.; Hioki, K.; Tani, S. *J. Am. Chem. Soc.* **2006**, *128* (45), 14452-14453.
87. Kirk, G. L.; Gruner, S. M.; Stein, D. L. *Biochemistry* **1984**, *23* (6), 1093-1102.
88. Seddon, J. M. *Biochim. Biophys. Acta, Rev. Biomembr.* **1990**, *1031* (1), 1-69.
89. Lundbk, J. A.; Maer, A. M.; Andersen, O. S. *Biochemistry* **1997**, *36* (19), 5695-5701.
90. Cantor, R. S. *Biochemistry* **1997**, *36* (9), 2339-2344.
91. Cullis, P. R.; de Kruijff, B. *Biochim. Biophys. Acta* **1979**, *559*, 399-420.
92. Kirk, G. L.; Gruner, S. M. *J. Phys.* **1985**, *46* (5), 761-769.
93. Allende, D.; Simon, S. A.; McIntosh, T. J. *Biophys. J.* **2005**, *88* (3), 1828-1837.
94. Salafsky, J.; Groves, J. T.; Boxer, S. G. *Biochemistry* **1996**, *35* (47), 14773-14781.

95. Sackmann, E. *Science* **1996**, 271 (5245), 43-48.
96. Groves, J. T.; Boxer, S. G. *Acc. Chem. Res.* **2002**, 35 (3), 149-157.
97. Cha, T.; Guo, A.; Zhu, X. Y. *Biophys. J.* **2006**, 90 (4), 1270-1274.
98. Castellana, E. T.; Cremer, P. S. *Surf. Sci. Reports* **2006**, 61 (10), 429-444.
99. Reimhult, E.; Hook, F.; Kasemo, B. *Langmuir* **2003**, 19 (5), 1681-1691.
100. Qi, S. Y.; Groves, J. T.; Chakraborty, A. K. *Proc. Natl. Acad. Sci. U. S. A.* **2001**, 98 (12), 6548-6553.
101. Hwang, L. Y.; Goetz, H.; Hawker, C. J.; Frank, C. W. *Colloids Surf., B* **2007**, 54 (2), 127-135.
102. Saccani, J.; Castano, S.; Desbat, B.; Blaudez, D. *Biophys. J.* **2003**, 85 (6), 3781-3787.
103. Groves, J. T.; Boxer, S. G. *Biophys. J.* **1995**, 69 (5), 1972-1975.
104. Holden, M. A.; Jung, S.-Y.; Yang, T.; Castellana, E. T.; Cremer, P. S. *J. Am. Chem. Soc.* **2004**, 126 (21), 6512-6513.
105. Johnson, S. J.; Bayerl, T. M.; McDermott, D. C.; Adam, G. W.; Rennie, A. R.; Thomas, R. K.; Sackmann, E. *Biophys. J.* **1991**, 59 (2), 289-294.
106. Boxer, S. G. *Curr. Opin. Chem. Bio.* **2000**, 4 (6), 704-709.
107. Watts, T. H.; McConnell, H. M. *Annu. Rev. Immunol.* **1987**, 5, 461-475.
108. Ulman, N.; Groves, J. T.; Boxer, S. G. *Adv. Mater.* **1997**, 9 (14), 1121-1123.
109. Richter, R. P.; Berat, R.; Brisson, A. R. *Langmuir* **2006**, 22 (8), 3497-3505.
110. Cremer, P. S.; Boxer, S. G. *J. Phys. Chem. B* **1999**, 103 (13), 2554-2559.
111. Okazaki, T.; Morigaki, K.; Taguchi, T. *Biophys. J.* **2006**, 91 (5), 1757-1766.

112. Kam, L.; Boxer, S. G. *Langmuir* **2003**, *19* (5), 1624-1631.
113. Plant, A. L. *Langmuir* **1999**, *15* (15), 5128-5135.
114. Plant, A. L.; Brighamburke, M.; Petrella, E. C.; Oshannessy, D. J. *Anal. Biochem.* **1995**, *226* (2), 342-348.
115. Lingler, S.; Rubinstein, I.; Knoll, W.; Offenhausser, A. *Langmuir* **1997**, *13* (26), 7085-7091.
116. Steinem, C.; Janshoff, A.; Ulrich, W.-P.; Sieber, M.; Galla, H.-J. *Biochim. Biophys. Acta, Biomembr.* **1996**, *1279* (2), 169-180.
117. Elsner, L. *J. Prakt. Chem.* **1846**, *37*, 441-446.
118. McCarthy, A. J.; Coleman, R. G.; Nicol, M. J. *J. Electrochem. Soc.* **1998**, *145* (2), 408-414.
119. Paulini, R.; Frankamp, B. L.; Rotello, V. M. *Langmuir* **2002**, *18* (6), 2368-2373.
120. Boal, A. K.; Rotello, V. M. *Langmuir* **2000**, *16* (24), 9527-9532.
121. Zhu, T.; Vasilev, K.; Kreiter, M.; Mittler, S.; Knoll, W. *Langmuir* **2003**, *19* (22), 9518-9525.
122. Love, C. S.; Ashworth, I.; Brennan, C.; Chechik, V.; Smith, D. K. *Langmuir* **2007**, *23* (10), 5787-5794.
123. Liu, X.; Basu, A. *Langmuir* **2008**, *24* (19), 11169-11174.
124. Chen, Y.; Cho, J.; Young, A.; Taton, T. A. *Langmuir* **2007**, *23* (14), 7491-7497.
125. Wasileski, S. A.; Weaver, M. J. *J. Phys. Chem. B* **2002**, *106* (18), 4782-4788.
126. Finklea, H. O., *Electrochemistry*; Marcel Dekker, Inc.: New York, 1996.

127. Cheng, W.; Dong, S.; Wang, E. *Angew. Chem., Int. Ed.* **2003**, *42* (4), 449-452.
128. Rautaray, D.; Sastry, M. *Biotechnol. Prog.* **2005**, *21* (6), 1759-1767.
129. Templeton, A. C.; Hostetler, M. J.; Kraft, C. T.; Murray, R. W. *J. Am. Chem. Soc.* **1998**, *120* (8), 1906-1911.
130. Rai, A.; Singh, A.; Ahmad, A.; Sastry, M. *Langmuir* **2006**, *22* (2), 736-741.
131. Singh, S.; Pasricha, R.; Bhatta, U. M.; Satyam, P. V.; Sastry, M.; Prasad, B. L. V. *J. Mater. Chem.* **2007**, *17* (16), 1614-1619.
132. Lasic, D. D.; Editor, *Liposomes in Gene Delivery*. **1997**; 77 pp.
133. Chapman, D., *Introduction to Lipids*. **1969**; 141 pp.
134. Ansell, G. B.; Hawthorne, J. N.; Dawson, R. M. C.; Editors, *B.B.A. Library, Vol. 3: Form and Function of Phospholipids. 2nd ed.* **1973**; 494 pp.
135. Sen Gupta, K. K.; Basu, B. *Trans. Met. Chem.* **1983**, *8* (1), 3-5.
136. Sitaula, S.; Mackiewicz, M. R.; Reed, S. M. *Chem. Commun.* **2008**, (26), 3013-3015.
137. Prenner, E. J.; Lewis, R. N. A. H.; Neuman, K. C.; Gruner, S. M.; Kondejewski, L. H.; Hodges, R. S.; McElhaney, R. N. *Biochemistry* **1997**, *36* (25), 7906-7916.
138. Nerambourg, N.; Werts; Charlot, M.; Blanchard-Desce, M. *Langmuir* **2007**, *23* (10), 5563-5570.
139. Hostetler, M. J.; Wingate, J. E.; Zhong, C.-J.; Harris, J. E.; Vachet, R. W.; Clark, M. R.; Londono, J. D.; Green, S. J.; Stokes, J. J.; Wignall, G. D.;

Glish, G. L.; Porter, M. D.; Evans, N. D.; Murray, R. W. *Langmuir* **1998**,
14 (1), 17-30.

APPENDICES (CHAPTER 1)

Appendix A: Synthesis of Mono-Carboxy Dithia Core-Modified Porphyrin (18).

Synthesis of **18** was based on literature procedure⁶⁷ with minor modifications as described below.

(a) Synthesis of 2-[1-(4-methoxyphenyl)-1-hydroxymethyl]thiophene (9)

Dry hexane (30 mL) was transferred to a two neck flask, fitted with a condenser and rubber septum under nitrogen. Then, TMEDA (4.52 mL, 30 mmol) was transferred into the flask via syringe. Subsequently, n-BuLi in hexane (18.7 mL, 1.6M in hexane, 30 mmol) was transferred into a measuring cylinder via cannula and was gradually added to the reaction flask via another cannula under nitrogen pressure. Then, the reaction mixture was stirred for an hour. Next, thiophene (2.42 mL, 30 mmol) was gradually added into the flask with a syringe. The combined reaction mixture was refluxed for 2 h and brought to room temperature. Then, the flask was cooled at room temperature. Another flask was fitted with a pressure equalizing addition funnel and rubber septum under nitrogen. Anisaldehyde (3.28 mL, 27 mmol) was dissolved in THF (20 mL) under nitrogen and transferred to a flask fitted with the pressure equalizing addition funnel and the flask was cooled at 0 °C in an ice bath. Then, the reaction mixture was transferred to the pressure equalizing funnel via cannula, and was gradually added to the anisaldehyde by the control of funnel stopper. After the addition of the reaction

mixture, it was stirred at room temperature for an hour. Subsequently, the reaction was quenched with saturated ammonium chloride (30 mL). The aqueous layer was extracted with diethyl ether (30 mL). The combined organic layers were washed with water (50 mL × 3), followed by brine (30 mL) and the organic layer was dried over MgSO₄. The solvent was evaporated in a rotary evaporator. The collected crude product was dissolved in a minimum quantity of diethyl ether. Then, hexane was added gradually to the diethyl ether solution until turbidity was seen. The crystallized compound **9** was a white solid (4.12 g) and yielded in 62.5%. ¹H NMR (90 MHz, CDCl₃): δ 3.76 (s, 3H), 6.0 (s, 1H), 6.72-7.10 (m, 4H), 7.32-7.51(m, 4H).

(a) **Synthesis of 2-[1-(4-methoxyphenyl)-1-(tert-butyldimethylsilyloxy)methyl]thiophene (10)**

Compound **9** (2.29 g, 10 mmol) in two neck flask was dissolved in CH₂Cl₂ (60 mL) under nitrogen. Then, DMAP (1.22 g, 10 mmol) and TBDMSCl (3.48, 30 mmol) were transferred to the flask. Subsequently, triethylamine (4.18 mL) was added to flask and the combined mixture was stirred at 0 °C for 2 h. Then, the flask was warmed to room temperature and the mixture was stirred for 24 h. Next day, the reaction mixture was washed with 5% NaHCO₃ (50 mL × 3), followed by water (100 mL × 3) and brine (30 mL). The crude product obtained after evaporation of the solvent was purified in a short silica column by eluting it with ethyl acetate/hexane (1:2). After column purification, a few drops of toluene was added and dried *in vacuo* overnight to get rid of the smell of triethylamine. The compound **10** (2.8 g) yielded in 83.0%. ¹H NMR (90 MHz, CDCl₃): δ 0.1-0.2

(m, 6H), 1.0 (s, 9H), 3.76 (s, 3H), 6.0 (s, 1H), 6.77-6.98 (m, 4H), 7.21-7.48 (m, 4H).

(b) Synthesis of 2-[1-(4-methoxyphenyl)-1-tert-butyl-dimethylsilyloxy]methyl]-5-(1-phenyl-1-hydroxymethyl)thiophene (11).

Dry hexane (10 mL) was added to compound **10** 2-[1-(4-methoxyphenyl)-1-(tert-butyl-dimethylsilyloxy)methyl]thiophene (334 mg, 0.99 mmol) in a flask under nitrogen, followed by addition of TMEDA (110 μ L, 1.18 mmol) and *n*-BuLi (0.73 mL 1.6M in hexane, 1.18 mmol). The reaction mixture was stirred at room temperature for 1.5 h under nitrogen. Benzaldehyde (108 μ L, 0.99 mmol) in dry THF (10 mL) was chilled on ice for 15 min in another flask under nitrogen. Then, the reaction mixture was withdrawn via syringe and added gradually to the benzaldehyde solution at 0 °C. After addition, the reaction mixture was stirred at room temperature for 1.5 h. Then, it was quenched with saturated ammonium chloride solution (25 mL) and an aqueous layer was extracted with diethyl ether (20 mL \times 2). The organic layers were combined and washed with water (20 mL \times 3), followed by brine (10 mL) and dried over MgSO₄. The crude product obtained was separated on a Chromatotron using 5% ethyl acetate in hexanes. The third band from the Chromatotron was collected and, after removal of the solvent, was dried to yield a colorless solid (148 mg, 56%). ¹H NMR (500 MHz, CDCl₃): δ - 0.045 (s, 3H), 0.051 (d, 3H, *J* = 3 Hz), 0.91 (s, 9H), 3.79 (s, 3H), 5.86 (s, 2H), 5.95 (d, 1H, *J* = 5 Hz), 6.51-6.52 (d, 1H, *J* = 5 Hz), 6.54 - 6.55 (d, 1H, *J* = 5 Hz),

6.61 (t, 1H, $J = 5$ Hz), 6.84 (d, 2H, $J = 10$ Hz), 7.30 (d, 3H, $J = 10$ Hz), 7.35 (t, 2H), 7.42 (d, 2H, $J = 5$ Hz).

(c) **Preparation of 2-(1-(4-methoxyphenyl)-1-hydroxymethyl)-5-(1-phenyl-1-hydroxymethyl)thiophene (12).**

Compound **12** (148 mg, 0.36 mmol) was dried *in vacuo* in a 100 mL flask and flushed with nitrogen. THF (3 mL) and tetrabutylammonium fluoride (TBAF) (0.45 mL, 1M in THF) were added into the flask and the reaction mixture was stirred at room temperature for 12 h. Subsequently, the reaction mixture was partitioned into saturated ammonium chloride (10 mL) and extracted with ether (10 mL \times 3). The combined ether layers were washed with water (10 mL \times 3) and brine (5 mL), dried over MgSO_4 , and the solvent was removed *in vacuo*. The crude product was purified by Chromatotron using ethyl acetate/hexanes (1:4) to yield a white solid (106 mg, 90.5%). ^1H NMR (500 MHz, CDCl_3): δ 5.96 (s, 1H), 5.92 (s, 1H), 6.69 (s, 1H), 6.80 (d, 2H, $J = 10$ Hz), 7.40 (d, 2H, $J = 10$ Hz), 7.30 (m, 5H), 3.70 (s, 3H), 2.39 (s, 1H), 2.33 (s, 1H).

(d) **Synthesis of 2,5-bis(phenylhydroxymethyl)thiophene (13)**

Dry hexane (70 mL) was transferred to a two neck flask fitted with a condenser and a rubber septum. TMEDA (3.6 mL, 24 mmol) was transferred followed by *n*-BuLi (24 mmol, 14.93 mL 1.6M in hexane) under nitrogen. The combined mixture was stirred for 30 min. Then, thiophene (0.8 mL, 10 mmol) was gradually added to the flask with a syringe. The combined mixture was refluxed for an hour, and cooled down to room temperature. Benzaldehyde (2.03 mL, 20

mmol) in THF (25 mL) was transferred to a reaction flask fitted with a pressure equalizing addition funnel. Subsequently, the reaction mixture was transferred to the addition funnel via cannula and gradually added into the reaction flask chilled at 0 °C in an ice bath by the control funnel stopper. After the addition, the reaction flask was warmed to room temperature and stirred for an hour. Next, the reaction was quenched by adding saturated ammonium chloride (80 mL). The aqueous layer was extracted with diethyl ether (30 mL) and the combined organic layer was washed with water (50 mL × 3), followed by brine (20 mL). The organic layer was dried over MgSO₄ and the solvent was evaporated in a rotary evaporator. The crude product was crystallized from chloroform, followed by recrystallization from ethyl acetate and hexane. The compound **13** (1.17 g) was yielded in 39.5%. The physical and spectroscopic properties matched to values given in literature.⁶⁷

(e) **Synthesis of 2,5-bis(1-phenyl-1-pyrrolomethyl)thiophene (14)**

Compound **13** (0.60 g, 2 mmol) in a one neck flask was dried *in vacuo* and flushed with nitrogen. Pyrrole (6 mL) was transferred into the flask and stirred at room temperature for 30 min. Then, boron trifluoride diethyl etherate (0.2 mL, 2 mmol) was gradually added to the flask with a syringe. The color of the combined mixture in the flask was changed to yellow, and it was stirred at room temperature for an hour. Subsequently, CH₂Cl₂ (50 mL) was added into the flask and the reaction mixture was quenched with 40% NaOH (12 mL). Then, the organic layer was washed with water (50 mL × 3) followed by brine (12 mL). The solvent was evaporated and crude product was purified in a silica column by eluting it with ethyl acetate/hexane (1:3). The first yellow band was collected and the solvent was

evaporated. The product was dried in vacuum and viscous yellow mass weighed (0.88 g) yielded in 97.2%. The spectroscopic properties matched to values given in literature.⁶⁶

(f) **Synthesis of 5-(4-methoxyphenyl)-10,15,20-triphenyl-21-23-dithiaporphyrin (15).**

Compound **13** (36 mg, 0.11 mmol), 2,5-bis(1-phenyl-1-pyrrolomethyl)thiophene **14** (43 mg, 0.11 mmol) and tetrachloro-1,4-benzoquinone (TCBQ) (108 mg, 0.44 mmol) were added to a two-neck 100 mL flask and fitted with a condenser. The flask was flushed with nitrogen, CH₂Cl₂ (5 mL) was injected, and the mixture was stirred for a few minutes at room temperature. Boron trifluoride diethyl etherate (7 μL, 0.05 mmol) was injected via syringe, and the mixture was stirred for an hour at room temperature. Then, the reaction mixture was refluxed for an hour. Subsequently, the mixture was concentrated on a rotavapor and the black crude product was purified over an alumina column eluting it with CH₂Cl₂. The first red band was collected. After the solvent was removed *in vacuo*, the solid was crystallized from CH₂Cl₂/methanol to yield a purple solid (18 mg, 24.3%). ¹H NMR (500 MHz, CDCl₃): δ 4.10 (s, 3H), 7.36 (d, 2H, *J* = 5 Hz), 7.80 (s, 8H), 8.18 (d, 2H, *J* = 5 Hz), 8.25 (d, 6H, *J* = 5 Hz), 8.68 (s, 3H), 8.71 (d, 1H, *J* = 5 Hz).

(g) **Synthesis of 5-(4-hydroxyphenyl)-10,15,20-triphenyl-21,23-dithiaporphyrin (16).**

Compound **15** (29 mg, 0.042 mmol) was dried *in vacuo*, dissolved in CH₂Cl₂, and chilled on ice for 15 min. Boron tribromide (0.419 mL, 1M in CH₂Cl₂) was injected into the flask and stirred at room temperature for 6 h. The solvent was evaporated from the reaction mixture and the crude product was dissolved in a minimum quantity of CH₂Cl₂. A few drops of toluene were added to induce crystallization of a purple solid (18 mg, 66.6%). ¹H NMR (500 MHz, CDCl₃) matched values reported in the literature.⁶⁷

(h) **Synthesis of ethyl-5-(4-carboxylatomoxy)-10,15,20-triphenyl-21,23-dithiaporphyrin (17).**

Compound **16** (14 mg, 0.021 mmol) was dried *in vacuo*. K₂CO₃ (116 mg, 0.84 mmol) and KI (14 mg, 0.084 mmol) were added. DMF (1.5 mL) and CH₂Cl₂ (2 mL) were added to the reaction mixture and the flask was flushed with nitrogen. 2-Chloroethyl acetate (30 μL, 0.021 mmol) was added and the reaction mixture was refluxed for 3.5 h. The reaction mixture was cooled to room temperature and CH₂Cl₂ (20 mL) and water (20 mL) were added. The organic layer was separated and washed with water (20 mL × 3) followed by brine (10 mL) and dried over MgSO₄. After evaporation of the solvent a purple solid was obtained (20 mg, crude). ¹H NMR (500 MHz, CDCl₃) data matched values given in literature.⁶⁷

(i) **Synthesis of 5-(4-carboxylatomoxy)phenyl-10,15,20-triphenyl-21,23-dithiaporphyrin (18).**

Crude **17** (20 mg, 0.02 mmol) was refluxed with 10% KOH (in 10 mL 1:1 ethanol: water) for 16 h. The reaction mixture was cooled at room temperature and ethanol was removed *in vacuo*. Water (40 mL) was added to the reaction mixture and HCl (0.1M) was added gradually with a dropper until the solution was neutral. After protonation, a purple solid precipitated. The precipitate was filtered and washed with water several times. A trace amount of unreacted compound **17** was separated on a silica column eluting it with diethyl ether/CH₂Cl₂ (1:4), followed by 10% methanol in CH₂Cl₂. The material obtained was treated with acetic acid (4 mL) in hexanes (20 mL) then ethyl acetate (30 mL) and water (30 mL) were added. The organic layer was separated, washed with water, and dried over MgSO₄. The solvent was removed *in vacuo* and a purple solid compound was obtained (9 mg, 64.2%). ¹H NMR (500 MHz, CDCl₃) matched values given in literature.⁶⁷

Appendix B: Synthesis of 2'-amino-2'-deoxyuridine (21)

Compound **19**, **20**, and **21** were synthesized by a modification of a literature procedure¹⁸⁷ as described below.

(a) Synthesis of 2,2'-O-anhydro-1-(β -D-arabinofuranosyl)uracil (**19**)

To a stirred suspension of diphenylcarbonate (3.44 g, 13 mmol), and *N,N*-dimethylformamide (DMF) (3.4 mL) in a 250 mL beaker, uridine (3.05 g, 12 mmol) was added and heated to 80 °C. Sodium carbonate (30 mg) was added and the reaction was heated to 110 - 130 °C. Once the brown reaction mixture became a sticky solid (3 - 3.5 h), the mixture was cooled to room temperature. The solid was washed with methanol (2 mL \times 3), then transferred to a flask, and methanol (15 mL) was added and refluxed for 5 h. After reflux, a white suspension in methanol was formed and filtered through a Buchner funnel. It was and dried for 16 h *in vacuo* at 90 °C to obtain a tan solid (2.103 g, 79.5%) with physical and spectroscopic properties matched values given in literature.¹⁸⁷

(b) 5'-O-(4,4'-dimethoxytrityl)-2,2'-O-anhydro-1-(β -D-arabinofuranosyl)uracil (**20**).

2,2'-O-Anhydro-1-(β -D-arabinofuranosyl)uracil (1 g, 4.7 mmol), dimethoxytrityl chloride (1.67 g, 4.93 mmol) and a catalytic amount of DMAP (4 mg) in pyridine (3.52 mL) and DMF (2.64 mL) were stirred for 16 h at room temperature. The solvent was removed *in vacuo* and the residue partitioned into CH₂Cl₂ and water. The organic layer was washed with water (25 mL), sodium

bicarbonate (0.5M, 20 mL × 2), and brine (15 mL). After drying over MgSO₄, and the evaporation of the solvent, a sticky yellow solid was obtained and it was purified over silica gel by eluting it with ethyl acetate, followed by 20% methanol in ethyl acetate. Solid white foam (1.36 g, 54.9%) was obtained. Physical and spectroscopic properties matched values given in literature¹⁸⁷

(c) Synthesis of 2'-amino-2'-deoxyuridine (21).

Trichloroacetonitrile (25.25 mL) and triethylamine (0.24 mL, 0.73 mmol) were added to **20** (13.21 g, 25 mmol), and the mixture refluxed for 16 h. The reaction mixture was cooled to room temperature and purified on a silica column by eluting it with a gradient, starting with the 10% ethyl acetate in hexanes and increasing to 20% ethyl acetate in hexanes. The second fraction was collected and, after evaporation of the solvent a sticky solid (13.195 g) was obtained. After drying overnight *in vacuo*, the material (13.20 g) was dissolved in ethanol (15 mL) and, NaOH (6 M, 50 mL) was added and refluxed for 18 h. The reaction mixture was cooled to room temperature and the solvent was removed *in vacuo*. After the evaporation of ethanol, the reaction mixture was partitioned into CH₂Cl₂ (50 mL) and saturated ammonium chloride (100 mL). The white precipitate was dissolved in ethyl acetate (100 mL), washed with water (150 mL × 2) and brine (20 mL), and then dried over MgSO₄. The crude product was eluted with 10% ethanol/ethyl acetate from a silica column. Final purification by repeated recrystallization in hot ethyl acetate resulted in a white solid (4.8 g, 25.7%). ¹H (500 MHz, CDCl₃): δ 3.38-3.49 (m, 3H), 3.6 (t, 1H), 3.79 (s, 6H), 4.24 (s, 2H), 5.42 (d, 1H, *J* = 10 Hz), 5.93 (d, 1H, *J* = 10 Hz), 6.85(d, 4H, *J* = 10 Hz), 7.24-7.32 (m, 8H), 7.38 (d, 1H, *J*

= 10 Hz), 7.8 (d, 1H, $J = 10$ Hz). ^{13}C (22.5 MHz, CDCl_3): 39.8, 42.27, 54.36, 56.42, 75.12, 77.91, 112.8, 129.5, 157.99, 173.43, 173.62, 179.98, 181.32, 188.70, 198.04, 198.23.

Appendix C: Recepte for 16% Polyacrylamide Gel (25 mL)

28% Bis-acrylamide	14.3 mL
10 × TBE	2.5 mL
Glycerol	2.5 mL
1.6% Ammonium persulfate	1.63 mL
TEMED	20-30 μ L
H ₂ O to	25 mL